COHERENT STRUCTURES AND THEIR EFFECTS ON PROCESSES OCCURRING IN SWIRL COMBUSTORS

By

AGUSTIN VALERA-MEDINA

A Thesis submitted in partial fulfilment
of the requirements for the degree of

Doctor of Philosophy
in
Mechanical Engineering

School of Engineering
Cardiff University
May 2009

ProQuest LLC
789 East Eisenhower Parkway
P.O. Box 1346
Ann Arbor, MI 48106-1346

Intellectuals solve Problems,

Geniuses prevent them.

Albert Einstein

ACKNOWLEDGEMENTS

I would like to thank Alan Griffiths, Malcolm Seabone and Paul Malpas for all their support and help to solve many technical problems that appeared during this investigation, because without their help this project would not be a reality.

To Prof. Anthony Griffiths who guided me and encouraged me to continue with the hard work. His comments and revisions increased considerably the quality of this thesis, and his dedication to this project has made it possible.

To Prof. Nicholas Syred who has been an inspiration through all this work and who has led all my steps through this thesis. His knowledge on the subject and his invaluable support have given me enough skills to develop this project with the complexity that the theme requires. His supervision and his prompt advice all this time have been the main keys for the successful conclusion of this work.

To my brother who has shown me that perseverance and hard work on an ideal may always give us the delicious fruits of victory and success. He has been an example of someone that can reach everything in life if we are capable of believing.

To my parents, Agustin Valera and Ma. de Lourdes Medina, who have always been with me, being a motivation to keep working hard day after day in the difficult tasks that the World has prepared for me. Thank you for everything that you have taught me.

To my wife, the strongest support and motivation in my life, who has joined me in this adventure of knowledge and sacrifice, and has accepted the long afternoons alone at home and hours of endless studying. Thanks for all your love.

Finally, I would like to thank God for being always with me, in good and bad times, always being the sunshine when the skies are dark, guiding me to the best that I can give. I will not fail.

Agustin Valera Medina

INDEX

Table of Contents **Page**

FIGURES INDEX

Table of Figures **Page**

TABLES INDEX

Burner Definitions

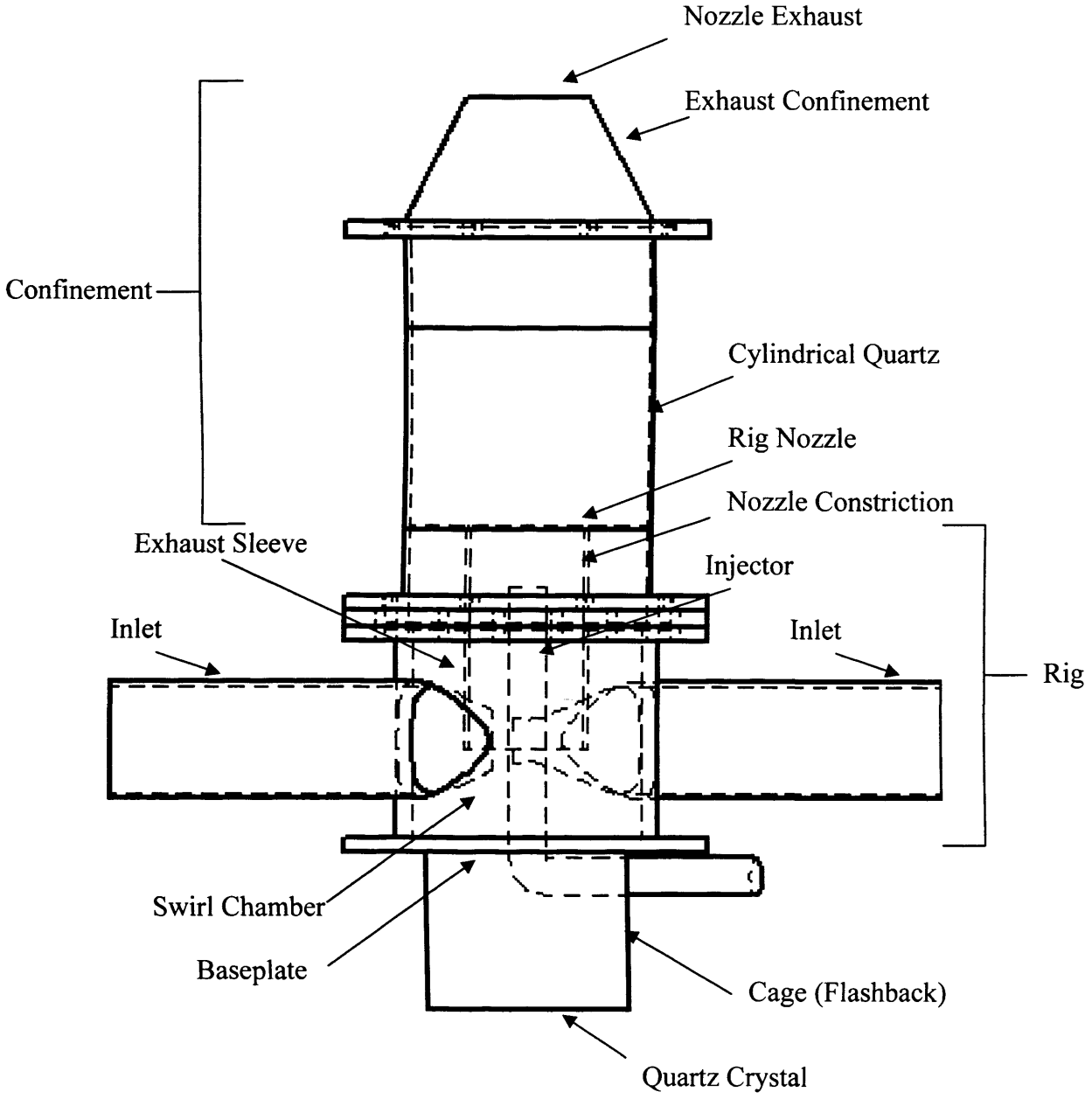

List of Abbreviations

ATS	Advanced Turbine Systems
CCD	Charge Couple Device
CCGT	Combined Cycle Gas Turbine
CCS	Carbon Capture and Storage
CFC	Chlorofluorocarbon
CFD	Computational Fluid Dynamics
CH_4	Methane
CIVB	Combustion Induced Vortex Breakdown
CO	Carbon Monoxide
CO_2	Carbon Dioxide
CPFM	Combustion Pressure Fluctuation Monitoring
CRZ	Central Recirculation Zone
DLE	Dry Low Emissions
DNS	Direct Numerical Simulation
DOF	Depth of Field
ERZ	External Recirculation Zone
ETUC	European Trade Union Confederation
EU	European Union
FFT	Fast Fourier Transform
FP	Framework Program
FTF	Flame Transfer Function
HAT	Humid Air Combustion
HCFC	Hydrochlorofluorocarbons
HCV	Higher Calorific Value
HSP	High Speed Photography
HWA	Hot Wire Anemometry
IGV	Inlet Guide Vane
Kn	Knudsen Number
LCV	Low Calorific Value
LDA	Laser Doppler Anemometry
LMC	Liquid Metal Cooling
MGC	Melt Growth Composites

NO	Nitrous Oxide
NO_x	Nitrous Oxides
Nu	Nusselt Number
PDF	Probability Density Function
PERM	Periodic Equivalence Ratio Moderator
PIV	Particle Image Velocimetry
Pr	Prandtl Number
PVC	Precessing Vortex Core
PWL	Power Level
RANS	Reynolds-Averaged Navier-Stokes
RCL	Rich Catalytic Lean Burn Combustion
Re	Reynolds Number
RFZ	Reverse Flow Zone
S	Swirl Number
SFI	Swirl Fuel Injector
SMPTE	Society of Motion Picture and Television Engineers
SO_x	Sulphur Oxides
SPL	Sound Pressure Level
Sr	Strouhal Number
SSC	Surface Stabilized Combustion
TBC	Thermal Barrier Coating
UHC	Unburned Hydrocarbons
URANS	Unsteady Reynolds-Averaged Navier-Stokes

ABSTRACT

Access to energy is fundamental to civilisation, both as economic and social development. This is fuelling a growing demand for reliable, affordable and clean energies. The current problems related to climate change have made imperative the search of technologies that can produce higher amounts of energy at lower emission rates. Therefore, technologies such as swirling flows with premixed lean injection have been characterized as one of the most reliable to achieve this objective.

However, the use of this technology implicates the appearance of phenomena that have been barely studied such as the manifestation of coherent structures that are crucial for the stability and high efficiency of the combustion process, and which have been assumed from indirect measurements. Moreover, these structures have been recognised as major players in the generation of instabilities such as pressure and heat transfer variations, internal vibrations and flashback into the mixing chambers. Therefore, a better understanding of these structures will allow the design of better burners and a greater control over the former, permitting a more efficient process.

This project is intended to reveal some of the characteristics of these structures, showing their high 3 dimensionality and high dependence on geometrical parameters, equivalence ratio, Swirl and Reynolds numbers, amongst other factors.

It is recognised how under isothermal conditions the system produces strong Precessing Vortices that are fundamental in the final shape of the flow field, while the Central Recirculation Zones are dependent on the pressure decay ratio inside of the combustion chamber. Combustion conditions showed the high dependence on the method of fuel injection used, with the appearance of stronger structures at lower equivalence ratios when high amounts of premixed gas were pumped into the system and the change in shape of the recirculation zones by using different injectors. Flashback demonstrated to be a factor highly related to the strength of the Central Recirculation Zone for those cases where a Combustion Induced Vortex Breakdown was allowed to enter the swirl chamber, whilst cases where a bluff body impeded its passage showed a considerable improvement to the resistance of the phenomenon. The use of nozzle constrictions also reduced flashback at high Re. All these results were aimed to contribute to better designs of future combustors.

CHAPTER 1

INTRODUCTION

1. INTRODUCTION

"Energy, like the biblical grain of the mustard-seed, will remove mountains."

H. Ballow, writer (1771-1852)

Access to energy is fundamental to civilisation, both as economic and social development. This is fuelling a growing demand for reliable, affordable and clean energies.

Nowadays, the most challenging factor is the price and pollution that fossil fuels have generated around the globe. After a period of low oil prices, energy security is again an issue in all political agendas. Local resources and renewable energies, together with improved efficiency throughout the whole production, supply and use chain will contribute to improving energy security all around the world (World Energy Council 2006a).

1.1. Energy Supply

The predictions for future years are based on an increase of consumption of natural gas, since it has been proved that it can generate enough energy to cope with the demand of society, as well as with the reduction of discharge of contaminants to the atmosphere. This is clearly due to the improvement of the combined cycle technology. Nowadays, numerous power plants are working with natural gas and steam, achieving production efficiencies up to 60% of thermal conversion (General Electric, 2006).

Up to the end of this decade natural gas used in the production of power has been estimated to be over 57% of the total of available electrical energy (World Energy Council, 2006b). Nevertheless, political and commercial problems such as those that happen in 2005 between the European Union and Russia, which has 26% of the total reserves of natural gas in the world (International Energy Agency, 2006), make crucial the improvement and increase of efficiency in those cycles in order to face the problems of supply during the 21st century. Figure 1.1 shows how North America and Asia have depleted almost their entire reserves, while Europe is consuming at a similar rate that will empty their own gas fields rapidly in the years to come. This

creates a scenario of instability that can only be solved with better technologies to make the best of the available resources.

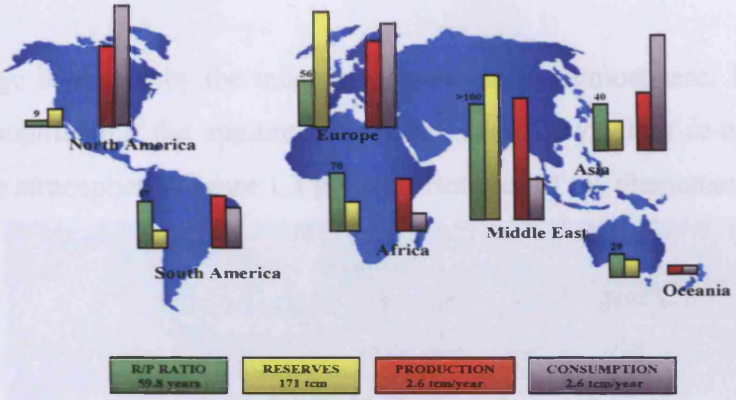

Figure 1.1. Situation of the Natural Gas in different regions (World Energy Council, 2006a).

1.2. Fossil Fuels Future

According to several authors and companies (Power Clean, 2004) the use of fossil fuels will not reduce. On the contrary, it will increase in the future years, especially with the use of coal and natural gas when the oil increases its prices. In Europe for example, an increment of 550 GW may well be necessary (Power Clean, 2004) (90% of present capacity) in the next 30 years. In figure 1.2 estimated quantities of each fuel required in the following 30 years are shown, illustrating the increasing demand for fossil fuels in the years to come.

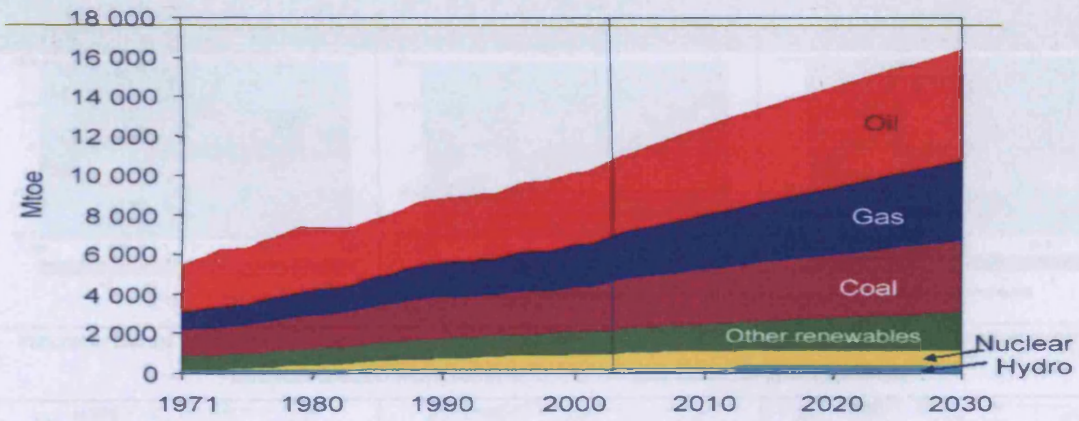

Figure 1.2. Energy demand (Buzek, 2006).

1.3. Climate Change

One of the greatest problems that the human civilization is facing is the Climate Change provoked by the emission of gases to the atmosphere. It was not until the last century that the industrial revolution created a major problem, affecting human and

animal life. Nowadays, universities and scientists around the world are trying to develop mechanisms to reduce the former, specially produced by what is known as greenhouse gases.

Climate change is caused by the increase of gases in the atmosphere. These act as a greenhouse, augmenting the amount of infrared energy, which is re-emitted by the planet into the atmosphere. Figure 1.3 gives a brief idea of the phenomenon.

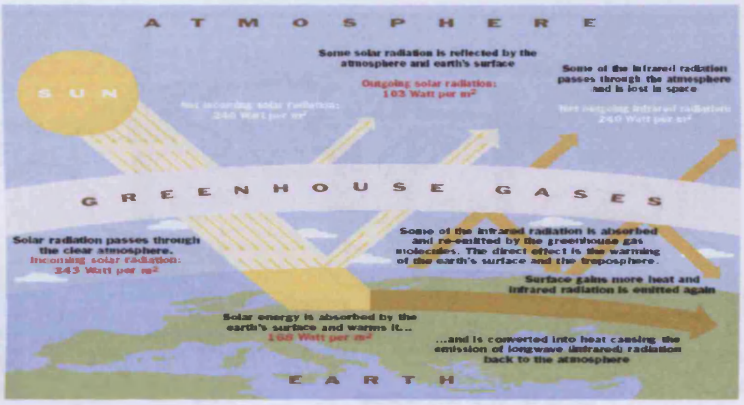

Figure 1.3. Climate change (PEW Center, 2006a).

Higher concentrations of these gases could provoke, via various mechanisms, severe temperature rises. This will generate catastrophes around the world that range from the reduction of infertile land to the increase in hurricanes and floods in the coastal areas (Belzer et al. 1996). Figure 1.4 shows some of these changes.

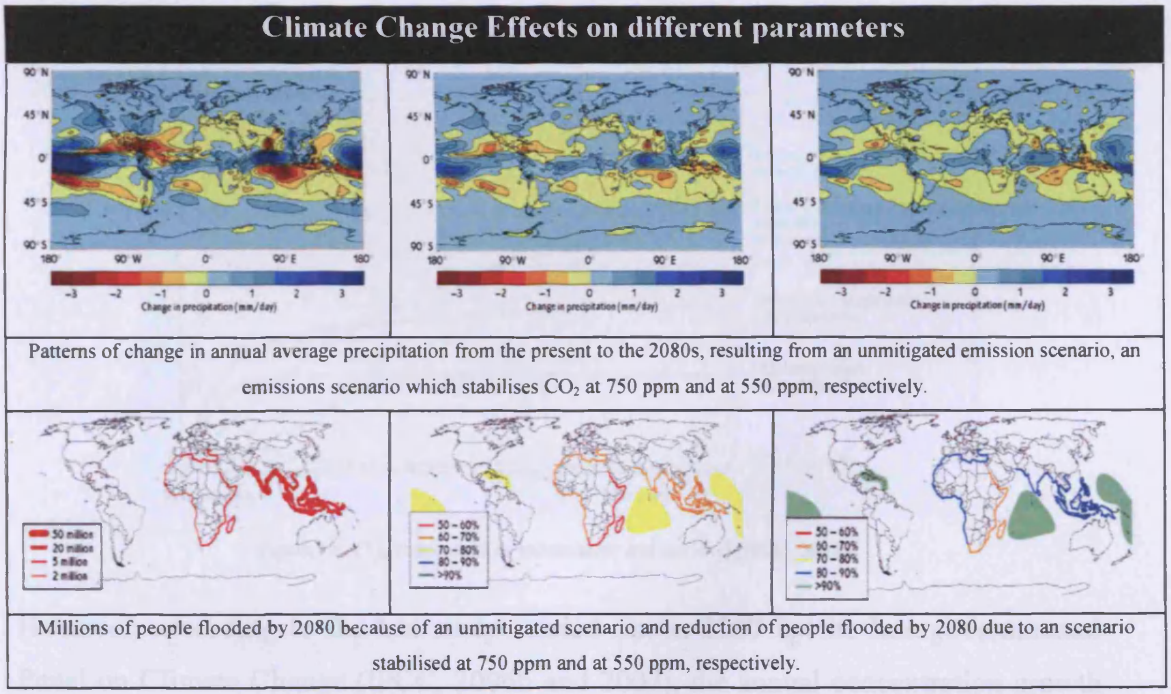

Figure 1.4. Climate change effects on different parameters (DEFRA, 1999).

The main greenhouse gases are carbon dioxide (CO_2), methane (CH_4), nitrous oxides (NO_x), chlorofluorocarbons (CFC), hydrochlorofluorocarbons (HCFC), Perfluoromethane and Sulphur hexafluoride. The most important is CO_2. Since this is generated by the consumption of fossil fuels, the objective of all alternative and zero emission technologies is to avoid as much as possible the generation of this gas, or in other cases, to sequestrate it. Figure 1.5 shows the amount of CO_2 generated in different parts of the planet and its principal source.

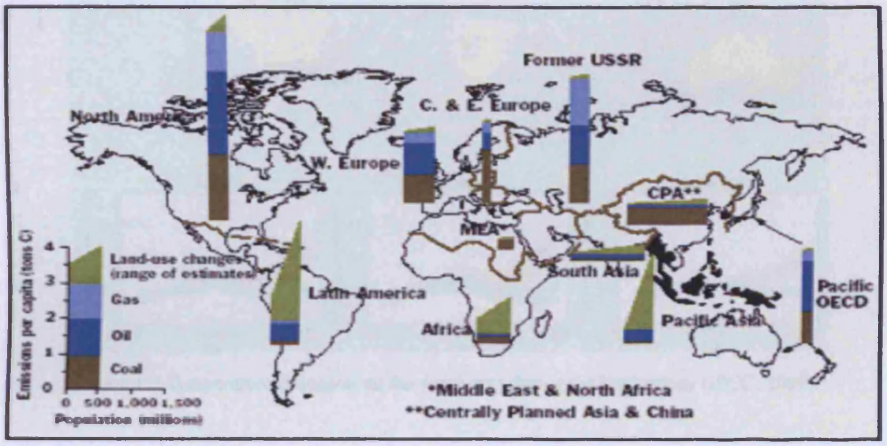

Figure 1.5. CO_2 emitted depending on the activity or fuel consumed (PEW Center, 2006b)

It has been speculated that the emissions generated in the previous century and this one will contribute to a long lived climate change phenomena due to inertia effects (IPCC, 2006a), figure 1.6.

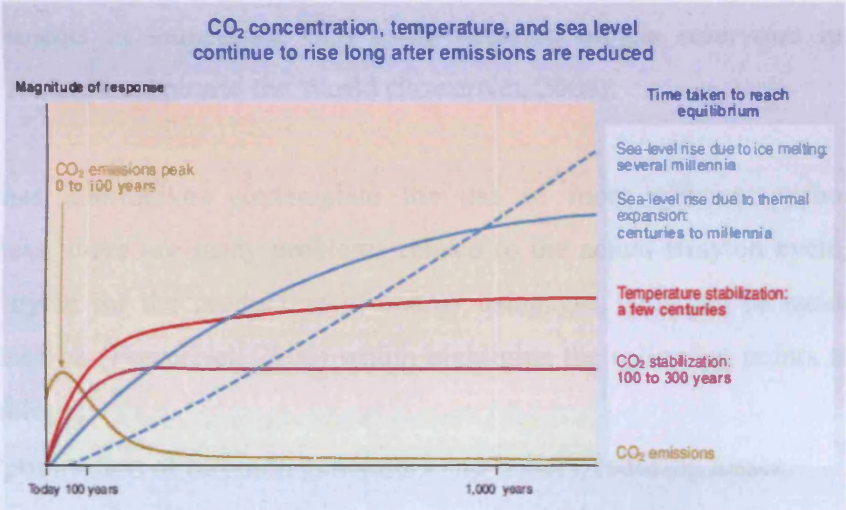

Figure 1.6. CO_2 concentration, temperature and sea level (IPCC, 2006a).

However, according to the last study carried out in 2007 by the Intergovernmental Panel on Climate Change (IPCC, 2006b and 2007), the annual concentration growth

rate of contaminants has increased in the last ten years (1995-2005) more than in all the previous years of measurements. The change in temperatures has been significant in all continents except Antarctica, figure 1.7.

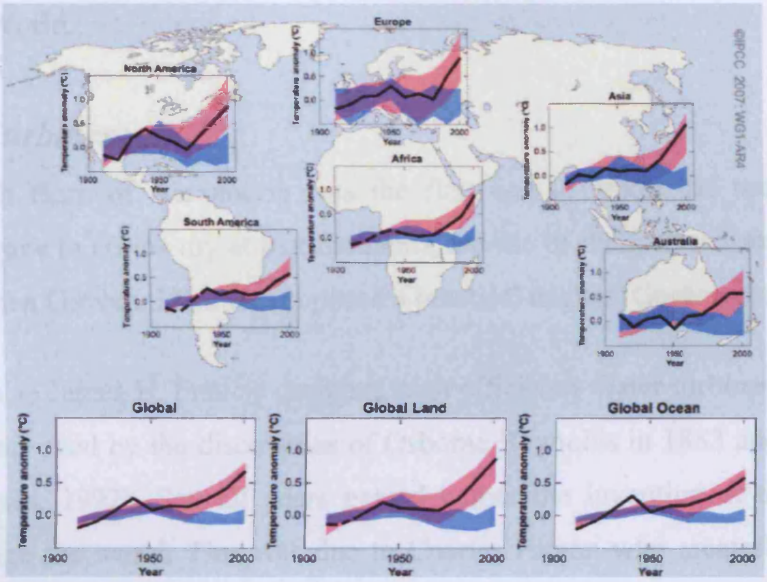

Figure 1.7.Temperature change in all the continents during the last century (IPCC, 2007).

Even though the growing concern of society about climate change and the increase of scientific understanding, there is a long way to go before the problem is mitigated and understood completely. Some of the ideas to tackle the problem that have appeared during the last decades include the use of alternative fuels such as methanol, hydrogen and enriched methane to reduce these emissions. Also, there are plans to construct several projects to sequestrate CO_2 using depleted oil/gas reservoirs in different locations around Europe and the World (PowerNet, 2006).

Some other alternatives contemplate the use of more efficient turbomachines. Nevertheless, there are many problems related to the actual Brayton cycle, which is the basic cycle for the production of energy using gas. This can be tackled by the current research (PowerNet, 2006) which highlights the following points to improve this technology,

- Optimisation of turbines, generators and boilers, reducing losses.
- Research in advance materials to resist higher temperatures and greater stresses.
- Improvement in cleaning, sealing and combustion systems.
- Analysis of alternative fuels.

Therefore, substantial work is required in this field in order to find the best way to produce energy at low cost, high efficiencies and the minimum contaminant emission from turbomachines like Gas Turbines that are increasingly being commissioned around the World.

1.4. Gas Turbines

Even though Hero of Alexandria was the first one to report the use of a steam powered engine (a curios toy at that moment), the use of the former was not practical till 1629, when Giovanni Branca proposed a practical engine (Gordon et al., 1998).

People such as James B. Francis designed high efficiency water turbines, which were promptly improved by the discoveries of Osborne Reynolds in 1883 and Rayleigh in 1892 (Shames, 1992). Several years passed before the invention of a turbine that would change the world. This was due to Charles Parson who created a multistage axial-flow reaction turbine in 1884 (Gordon et al., 1998). Since then, these devices have become increasingly dominant in the fields power production and generation.

1.4.1. Cycles and Materials

Gas turbine engines accept and reject heat to produce work. The heat input is usually in the form of fuel that is burned, and the rejected heat is either passed through a heat exchanger or boiler to make steam, or in the case of aero engines used to power large diameter cooled fans that produce most of the thrust.

A gas turbine consists of a compressor, which compresses air to a higher pressure; heaters/combustors in which the temperature of the compressed gas is raised; an expander, which expands the hot gas to a lower pressure; and a cooling system, where the heat can be recovered or "regenerated".

Turbines have certain advantages over the diesel and gasoline engines in terms of compactness, smooth running and relative simplicity. If a Gas Turbine is compared with a Diesel engine, the amount of air that the turbine suctions is 68 times that used in the engine (Gordon et al., 1998). Even though boiler steam turbine systems can produce large outputs, especially with coal firing, the relatively ease of running gas turbines, their compactness and high efficiency when operated in a combined cycle

and their costs make them a very significant player in the energy production field. Figure 1.8 shows a typical rotor and shaft in a gas turbine. It is clear that the complexity and accuracy required in this equipment can increase severely their final price.

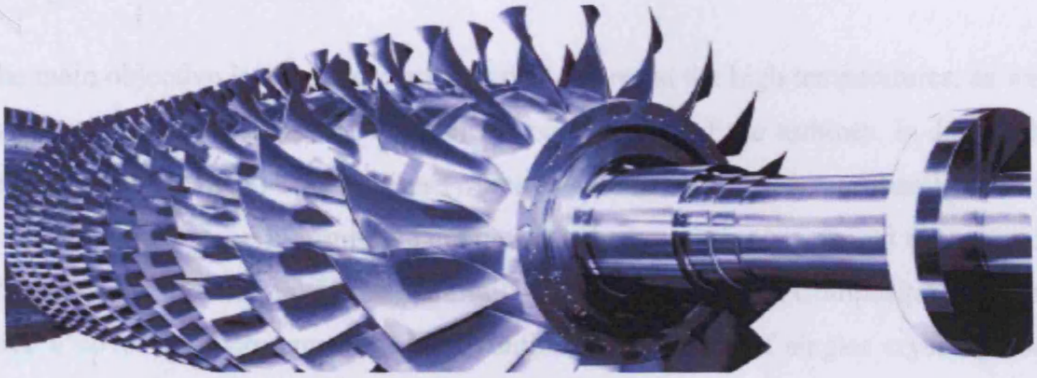

Figure 1.8 GE High Power Rotor and Shaft (General Electric, 2006a)

Figure 1.9 shows a cycle where the blue areas comprise cold air, while the red ones specify the existence of hotter gases.

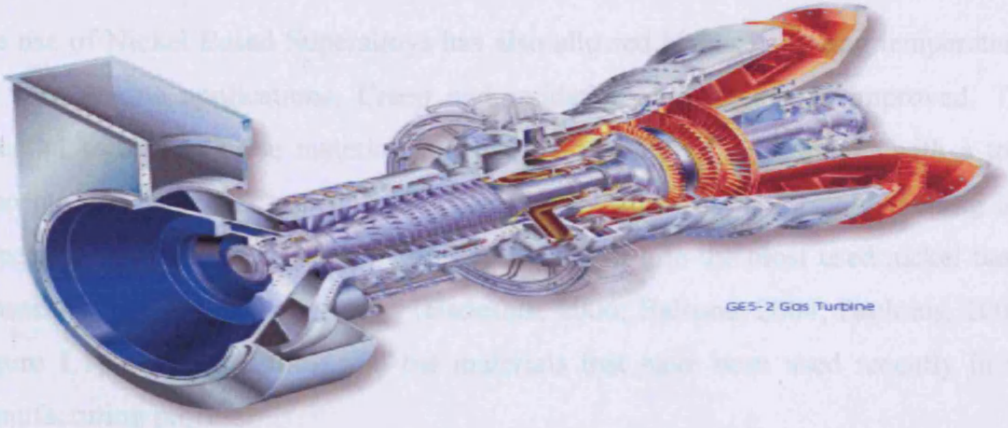

Figure 1.9 GE Gas Turbine (General Electric, 2006b)

Some technical reports claim that the higher the inlet pressure, the greater the gas turbine efficiency. This is true for aircraft engines, but not always for power cycles. Generally, the higher the turbine inlet temperature, the greater the net output and the final cycle efficiency are. Also, other constrains with the design of turbines are the operating temperatures, the atmospheric and inlet pressures, the heat exchanger, cooling systems, etc. Different manufacturers have evolved different solutions to these problems.

Another important factor that must be taken into consideration is the use of cooling technologies for the blades and stators. Previously, the lack of heat resistant materials

made difficult the design of more powerful cycles. However, nowadays the use of coated zirconia and other alloys have allowed increased performance in terms of specific power and efficiency in different cycles, as well as the design of new methods to recover energy (Gordon et al., 1998).

The main objective is to create materials that can resist the high temperatures, as well as the stress generated by the load on the components of the turbines. In Japan, the development of eutectic composites (which have a fusion point lower than the fusion point of their reactants) to improve the thermal characteristics has caught the attention of various manufacturers. These materials, named Melt Growth Composites (MGCs), have a novel microstructure in which continuous networks of singles crystal phases interpenetrate without grain boundaries. Therefore, these materials have a greater resistance to oxidation, whilst giving thermal stability and high temperature strength (Wayu et al., 2005).

The use of Nickel Based Superalloys has also allowed higher operating temperatures for aero engine applications. Creep and oxidation resistances are improved. The essential solutes in these materials are usually aluminium or titanium, with a total concentration which is typically less than 10%. Advances in forging, melting and inspection have increased its properties converting it into the most used nickel based superalloy for industrial operations (Badeshia, 2006; Balsone, 2004; Paulonis, 2001). Figure 1.10 shows a turbine and the materials that have been used recently in the manufacturing process

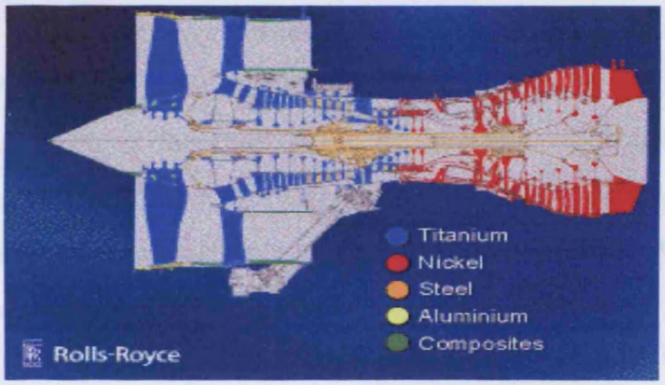

Figure 1.10. Materials used in a Rolls Royce Turbine (Badeshia, 2006).

General Electric, Pratt & Whitney and NASA have studied different alloys in order to create a super resistant material for turbomachinery applications. Lower chromium

levels, higher cobalt and rhenium levels and the inclusion of ruthenium were part of the experiment. The final material, EPM-102, had significant creep rupture and fatigue improvement, with acceptable microstructural stability. This created a 4th generation single crystal material (Walston et al., 2004).

Related to coatings, it has been demonstrated that the amount of oxides formed during the heating process is a culprit in the failure of the crystalline structures and deterioration of internal components (Ogawa et al. 2002). Even with advanced cooling systems and single crystal blades, Thermal Barrier Coatings (TBC) are used to maximise the final performance of the turbine. The Oak Ridge National Laboratory, Siemens-Westinghouse and Pratt Whitney have worked on different materials to improve the resistance of the TBCs. The most common are zirconia partially stabilized by yttria (YSZ) with a bond coating made of NiCoCrAlY (Oak Ridge National Laboratory, 2006; Herzog et al., 2006).

However, it is clear that all the previous are directly linked to the combustion system and amount of heat produced during the burning stage.

1.4.2. Combustion Systems

The fuel that is burned in the combustion systems usually is kerosene, diesel or methane (natural gas). The later has been used for decades and is gaining market share relative to other fuels due to its relative cleanliness.

Different fuels produce different flames. Nevertheless, the average speed of turbulent flames ranges from 2 to 15 m/s, whilst laminar ones are in the range of 0.1 to 2 m/s. Considering the speed of the fluid inside of the compressor and the turbine, the average value is between 125 m/s – 200 m/s (Gordon et al., 1998). Even though the speed will be reduced using diffusers in the nozzle, the reduction will only achieve a sixth of that required. Therefore, to produce a 10 m/s flame speed the fluid must be retarded using baffles, which represents an inefficient process. Also, part of the air will be used to decrease the temperature in the second zone of the combustor.

The control of emissions is achieved via a number of techniques including increased residence time of the reactants in the flame (when fuel rich) and "staged" combustion,

in which multiple fuel burners within a combustion chamber are brought into action successively as the temperature rises above that for rapid NO_x production. The use of lean pre-mixed systems is another alternative, which also increases the efficiency of the equipment. However, flashback could occur due to the prior mixing of oxygen and combustible. It is worth mentioning the use of catalytic combustors, where special catalysts are used to promote the reaction. Nevertheless, the incoming gas must be normally at least at 725 K. Therefore, the use of pre-burners is essential and the production of contaminants takes place in this area. Finally, the use of fluidized beds is another option. Recycled materials, bio-waste, coal, etc. can be utilised in this equipment. The bed is heated at temperatures where the fuel in the bed decompose and react to produce fuel gases, with components such as methane and hydrogen as well as contaminants. The contaminants are removed and the cleaned gas feed the combustor.

The use of swirl equipment is another option that is becoming much more important nowadays. These machines use a series of swirlers which mixes the air and fuel in a more effective way as well as stabilizing the flames with central recirculation zones, reducing contaminants and increasing the combustion intensity. Figure 1.11 shows the combustion system and how the hot gases access the turbine.

Figure 1.11. Combustion systems in to a gas turbine (GE Aviation, 2006)

1.4.3. Advanced Turbine Designs

Another point that must be considered is the increase in efficiency in new turbomachineries. Nowadays, a 58% in efficiency Combined Cycle Gas Turbines (CCGT) power plant produces an average of 4 MT/annum of CO_2. It has been

speculated that a 5% increase in efficiency will reduce this amount by 200,000 t/annum (CAME-GT, 2005), hence the search for new advance designs. The target in the case of the CCGT technology is to reach a 75% of efficiency by the 2020, 95% removal of CO_2 and a NO_x production to 1 ppm (CAME-GT, 2005). One of the most promising technologies is the H GE turbine, which is capable of breaking the 60% efficiency barrier using a combined cycle and more efficient heat recovery of wasted energy (General Electric, 2006; Matta et al., 2000).

One key point is the cooling system. A closed loop system increases the efficiency by 2% (International Power Generation, 2006). Also the use of Liquid Metal Cooling (LMC) has been proposed for Directionally Solidified Materials (Layne, 2000). The reduction of NO_x is achieved using a fuel premixing can-annular combustor system with 14 combustion chambers, producing a Dry Low NO_x emission flow of 25 ppm.

The injector is based on a concept that joins "swirl" and "nozzles", receiving the name of swozzle (U.S. patent number: 6438961 (Free Patents Online, 2006)). Its premixing passage uses swirl vanes to impart rotation to the admitted airflow; each of these vanes contains passages for injecting the fuel into the premixed airflow. This makes the device very resistant to flashback and flame holding, reducing stagnation spots in the mixture.

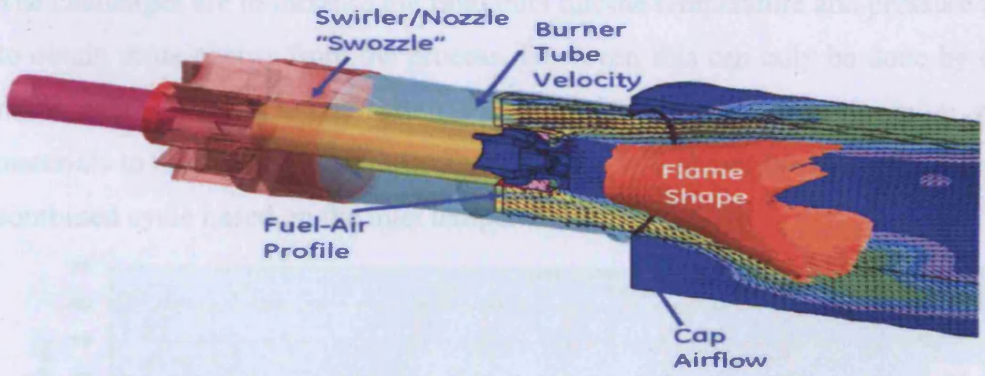

Figure 1.12. GE Swozzle and combustion Chamber (Jones, 2006).

The swirl imparted in the swozzle assembly stabilizes the flame in the combustion zone. Therefore, this equipment uses the concept of lean mixture and swirl effect to reduce NO_x without compromising the efficiency on CO and unburned hydrocarbons emissions reduction. It also provides a control of pressures and reduction of hot spots

in the combustion chamber. Another advantage is the use of other combustibles for dual fuel operations or ignition, as well as a control of natural gas into the primary and secondary holes according to the desired load. Thus, the understanding of swirling flows becomes crucial for the proper design of future prototypes.

Another key point is the materials used in this equipment, which are characterised for being light and resistant to heat and stresses. The blades are made from large single crystals airfoils, superior components and coating materials, which are capable of resisting firing temperatures (system temperature) over 1430°C (General Electric, 2006).

Other manufacturers such as Rolls Royce (Trent 60 DLE), Siemens-Westinghouse (W501ATS), Mitsubishi (M701G2) and Alstom (GT24 and GT26) are manufacturing systems capable of achieving 53-60% efficiencies. Other important firms such as Pratt & Whitney, Vericor, Ansaldo Energia, Man Turbo, MTU, Kawasaki, etc. are also interested in developing this high efficient technology. Therefore, the competition is fierce, and the better design and lower cost will be the technology chosen for new plant. Swirling flows are becoming a central part of the strategy for increase in combustion efficiencies, attracting research all around the World.

The challenges are to increase the final inlet turbine temperature and pressure in order to obtain more energy from the process. However, this can only be done by creating more efficient cycles, recovering more waste energy and using more resistant materials to tackle the high temperatures. Figure 1.13 shows the final efficiency of the combined cycle based on the inlet temperature.

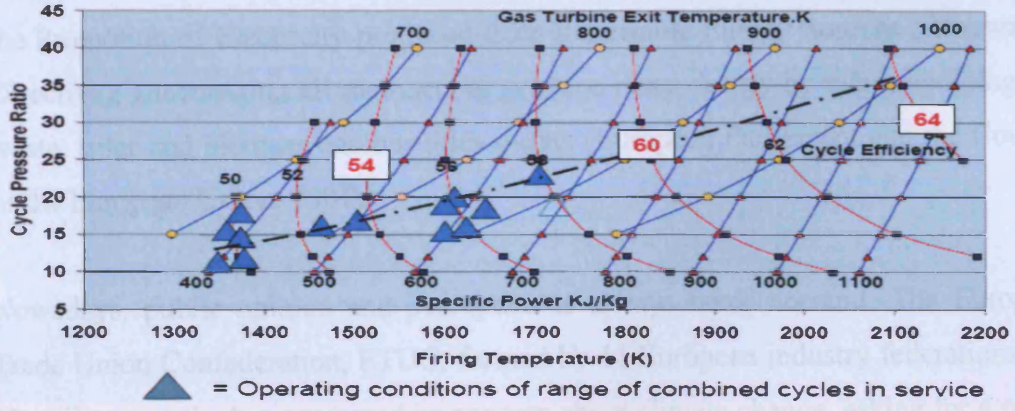

Figure 1.13. Combined cycle, the challenge (Alstom, 2006)

1.5. Government and Public Perspective

One of the major constrains in the reduction of emissions and plausible commitment is the political and public opinion. Several protocols, directives and regulations have been created to promote a friendly environmental industry. Some of them have matured from their basic concepts. A global example is the Kyoto Protocol, which has caused the creation of directives in the EU, Japan, Russia and other countries to tackle the production of greenhouse gases. This Protocol has encouraged the use of renewable and natural sources to achieve a 5% in reduction of the level of CO_2 emissions in 2008-2012 (United Nations, 1998) compared to 1990.

Concerns in the European Union are air, the water and groundwater qualities. For this reason, various Directives have been developed. Examples of these are the Air Quality Framework Directive 96/62/EC and its regulations (Commission of European Communities, 2005a). Other kind of Directives that are important and related to this field are the Framework Directive in the Field of Water Policy 2000/60/EC, which establish action in the field of water management. In the case of Carbon Capture and Storage (CCS) technologies, this law has to be developed to ensure that the CO_2 does not contaminate river basins and groundwater aquifers (Commission of European Communities, 2005b). Hence, the entire community has prioritised the search of sustainable options to avoid cross contamination and increase efficiency in the energy production.

In 1997 a White Paper named "Energy for the future: renewable sources of energy" set the use of renewables in the EU, aiming for a total contribution of 12% of the total energy consumption by 2010. By 2001, the European Union adopted a "Directive on the Promotion of Electricity produced from Renewable Energy Sources (Renewables Directive), encouraging all members to produce more energy by wind, hydrological, waste, solar and biomass combustibles means (European Parliament and the Council of the European Union, 2001).

Nowadays, public opinion and perception is always taken account. The European Trade Union Confederation, ETUC, formed by 11 European industry federations and 60 million people, has expressed its concern about climate change, asking for a major

reduction of 25% and 75% of greenhouse gases emissions by 2020 and 2050, respectively (ETUC, 2006), compared to 1990.

The UK politicians, concerned about these issues, have published a White Paper entitled "Our Future Energy – creating a Low Carbon Economy". In it, the UK will reduce its emissions of CO_2 by 60% by 2050, 50% and 20% for SO_x and NO_x by 2010, respectively (DTI, 2003).

Other types of programmes have emerged to deal with the energy problem. In the EU, the named Framework Programme (FP) has been created with the intension of supporting Research and Development. In the FD7 the main objectives are to create a contamination-free economy, using combustibles such as hydrogen, biomass, clean coal technologies, CCS, etc. (European Commission, 2006).

However, the World is conscious that the use of fossil fuels will not decrease in the short term. In fact, it will grow. Thus, the best way to tackle the obligations of the Kyoto Protocol is by increasing the energy production efficiency and reducing with advance CO_2 storage/removal systems the final emissions.

1.6. Summary

Even though some scientist have argued that Climate Change is the effect of solar sunspots, eccentricities in the earth's orbit around the sun, it is now generally accepted that man made Climate Change is contributing to the extinction of species, destruction of habitats, temperature rise and general levels of pollution (BBC, 2007). One major contribution to mitigating is the new technologies capable of reducing all the contra effects and producing a sustainable world. An important area is the subject of gas turbine combustion and swirl burners, the subject of this thesis.

1.7. Objectives

This thesis seeks to clarify the existence and form of several coherent structures that appear in swirl burners, typically used in gas turbines. Some of these structures can appear as a consequence of the process per se, like the PVC in swirling flows, or

based on the geometry and mechanic of fluids inherent of the system, such as eddies and instabilities in pre-lean mixtures such as flashback by means of vortical structures.

Therefore, it is essential to obtain more details about these structures and instabilities in order to achieve better flame stabilization, better system stability and lower emissions in combustors. At the same time, this can increase the performance of the turbomachines by for instance contributing to the development of engines with higher pressure ratios and/or turbine inlet temperatures.

Several coherent structures occurring in swirl burner flows under different conditions, geometries, pressures and temperatures have been analysed with the aim of clarifying some of the most intriguing phenomena in the combustion process. This will aid in the design of further experiments to control these structures to enhance the process and design more advanced equipments for better and more powerful systems, especially those using Alternative fuels with for instance high hydrogen content.

1.8. Hypothesis

The lack of spatial and temporal resolution experiments in the field of gas turbine combustion has led to the incorrect belief that the coherent structures that develop as a consequence of swirling flows play a secondary role in the final stability of the combustion system. The shape of these structures and the co-relation that they share has always being assumed as numerical simulations predict a scenario indirectly measured. This partial knowledge is also present in the bare understanding of how these structures can improve the combustion regime and influence the reduction in resistance to phenomena like flashback.

Thus, this thesis will recognise the extremely close interrelation between coherent structures, their high dependence on geometry and flow regimes, and their positive and negative effects on the final stabilization of the flame, with great coherence when the structures are manipulated via passive methods of suppression, decreasing the resistance to flashback at the same time. Besides, it will be demonstrated how the annihilation of the coherent structures via baffles can improve this factor, with the flashback being only affected by boundary layer and turbulent speed propagations.

1.9. Thesis Structure

This thesis is divided into a number of chapters, which are as follows,

- Chapter 1. An introduction that highlights the problem of uncontrolled emissions and energy deficit. Also, basic principles of Gas Turbines are stated.

- Chapter 2. A review of the work and basis on several structures like the Precessing Vortex Core and Recirculation Zone. The combustion process and different fuels proposed for new furnaces and turbines is mentioned as well.

- Chapter 3. A review of the techniques used to measure the structures.

- Chapter 4. Experiments using air as principal flow. Setup and Results are stated in this chapter.

- Chapter 5. Experiments using swirling flows under a wide variety of conditions under combustion. The use of different swirl numbers, injectors, constrictions and confinements are analyzed.

- Chapter 6. Experiments analyzing the effects of flashback phenomenon under a variety of combustion conditions are analyzed. The effect is characterized using different techniques.

- Chapter 7. Merge and Discussion of the results obtained under isothermal, combustion and flashback conditions in order to apply them in real industrial situations.

- Chapter 8. Conclusions and further work, providing a summary of the key findings obtained with this project, suggesting several research programmes that can be carried out for future experiments.

CHAPTER 2

DYNAMIC PROPERTIES

2. DYNAMIC PROPERTIES

"Before I die, I hope that someone will explain quantum mechanics to me. After I die, I hope that God will explain turbulence to me."

W. Heisenberg, physicist (1901-1965)

During the last decades much work to explain the behaviour of certain types of flow has been done. However, some of them still remain barely understood. In this context, large coherent structures remain as one of the most challenging aspects of many flows which need to be understood. According to the American Institute of Aeronautics and Astronautics (AIAA, 2007), the appearance of the former is often responsible for the excitation of acoustic oscillations whose coupling with the heat release distort the combustion mechanism. The Precessing Vortex Core (PVC), Central Recirculation Zones (CRZ) and Combustion Induced Vortex Breakdown (CIVB) and inner eddies are the most common of the coherent structures observed in burning process using swirl stabilization are extremely challenging in terms of recognition and theoretical explanation, since their interaction and appearance have not been explained even with the most powerful computer systems and new theories in recent years. The conceptual process of the phenomenon implies the use of the most advanced combustion aerodynamics.

2.1. Swirl Burners

Industrially, the use of swirl generators has been crucial for the design of new equipment capable of reducing emissions, improving stability, whilst extending blow off limits. The use of swirling flows is a well know technique to increase turbulent flame speed, decrease combustor size, avoid flashback and improve mixing of reactants in order to reduce emissions and increase power density (Paschereit and Gutmark, 2008; Syred, 2006; Coghe et al., 2004). For over 200 years, swirl burners have been used for combustion of fuels like pulverised coal and coke. In most countries around the world, most large combustion systems use some form of swirl combustor (Fick, 1998; Khalatov and Syred, 2005).

During the last decades many experiments have been carried out in order to gain a better understanding on the phenomenon and its applications. Some of them have been focused on the use of it in the burning of Low Calorific Value Gases (those with values as low as 1.3 to 1.4 MJ/m^3, while natural gas has 35 MJ/m^3) (Syred et al., 1974; Claypole and Syred, 1981; Avenell et al., 1996; Fick, et al., 1998). It has been proved that it is commercially possible to do this, with swirl burners capable of producing high energy output at low pressure drop.

However, some coherent vortices and large scale structures appear in the flow under particular circumstances such as the use of high swirl, high flow rates or variable equivalence ratios. Although these flows have been extensively studied for many decades (Syred, 2006; Claypole and Syred, 1981; Syred et al., 1984; Mongia et al., 2007), there are still many uncertainties concerning the occurrence of some coherent structures, their influence and their relation to the important Central Recirculation Zone, where the mixing process takes place. Details of this zone and mixing potential have been extensively investigated (Shtork et al., 2008; Chen et al., 2008), still leaving details as to their effect in the mixing process, stability and coupling with other structure still uncertain. The CRZ can be very beneficial for mixing and preheating the combustible and air (O'Doherty and Gardner., 2005), but can damage the equipment as a consequence of resonances created from the interaction of the coherent structures produced with natural system resonances and combustion induced oscillations (Paschereit and Gutmark, 2006 and 2008). The Precessing Vortex Core is one of these instabilities. This acts as a low frequency stirring mechanism, and often interacts strongly with the CRZ, which is the feature of swirling flows which give them their remarkable flame stabilization characteristics. This only occurs at levels of swirl beyond vortex breakdown.

Early work reported by Vonnegut, 1956, revealed a phenomenon described as the vortex whistle. However, the process was not fully understood. Others like Chanaud, Iionoya, etc. followed this work, until 1971, when Syred and Beer first defined the term Precessing Vortex Core.

Geometrical aspects of different burners where studied by Gupta in 1976, when he established the advantages of using multiannular swirl burners. The burner had wider stability limits, with higher heat released as a result of better aerodynamic control and

more suitable reactant distribution. All this was connected to the high turbulence levels found at the burner exit (Gupta et al., 1976). Variety of geometries have been studied recently with the aim of reducing oscillations in the system that can coupe with the heat release during the burning process. Paschereit and Gutmark (2006, 2008) have used miniature vortex generators in order to mitigate the coupling between small structures that yield to the formation of larger scales. Chen et al. (2008) have introduced inner bluff bodies to enhance the mixing of micro-particles in the central region of the combustor. General Electric (2005) like many other manufacturers have varied the geometrical characteristics of their swirl burners to produce more uniform distribution of reactants, while authors like Lieuwen et al. (1998, 2005) and Lee et al. (2000) have characterized the thermo-acoustic characteristics of such combustors under a variety of conditions. The level of swirl, the combustor geometry and the point of fuel supply have been varied. One of the predominant fluid mechanical oscillations was a PVC, regulated by feedback via the CRZ. The results allowed a better understanding of the phenomenon, giving data about the formation of the instability and other eddies in the outlet of the burner (Syred et al., 1984).

In 1980 Claypole and Syred evaluated the mechanism occurring in swirl combustors and their relation to the NO_x formation. Different swirl numbers were used in the experiment, with a variety of configurations and geometries. From the work the location of the areas of formation of the pollutant were established. The formation was attributed to primarily 2 different mechanisms: the Zeldovitch mechanism (thermal NO) and the prompt NO mechanism (due to the attack of hydrocarbons to molecular nitrogen). Fluctuations of temperature in the combustors were found to be significant, but had little effect on NO_x levels. Notwithstanding, there can be a direct connexion between the period of oscillation and the response time of the reaction, providing the period of the oscillations is greater than the reaction time to form NO_x (Claypole, 1980). Recent experiments performed by Coghe et al. (2004) showed the dependence of pollutant formation in a swirl combustion system on swirl level, with reductions of up to 30% with the slight increase in swirl number. Thus, various experiments have tried to correlate the particular system with pollutant production for different configurations. Gupta in 1991 analysed the difference between the first generation multi annular swirl burner with a new one which introduced premixed fuel and air near the centreline. Better mixing was achieved, with lower NO_x emissions.

He emphasized his work on the geometry of the combustor, assuring that all burner loadings can be obtained with that geometry combustor (Gupta et al., 1991).

In 1992, Alekseenko and Shtork carried investigation to visualize phenomena in a hydrodynamical vortex chamber seeded with small air bubbles. They identified various phenomena like the vortex core precession, the vortex filament generation, vortex breakdown and waves on vortices, double spiral, etc. Some years later, they presented a theory on the appearance of a helical vortex in swirl flows (Alekseenko et al., 1999). Shtork et al. (2008) has presented a coherent analysis of the propagation of helical structures under combustion conditions, with the definition of two different regimes (right and left handed vortices), as well as a physical analysis of the interaction of the field and the stretching of structures in the immersed flow.

Nowadays, the use of alternative fuels in lean-premixed mixing processes have contributed to the propagation of the flame upstream of the combustion zone, producing a flashback phenomenon as a consequence of the interaction of boundary layer, turbulent speed and coherent structure (CIVB) propagations. It has been recognised that this vortical structure plays a major role in this unstable phenomenon (Kroner et al., 2007), and its appearance in the system has been linked to the CRZ.

The use of novel software and laser diagnostics, in particular Laser Doppler Anemometry (LDA), High Speed Photography (HSP), CH*-OH* Chemiluminescence and Particle Image Velocimetry (PIV) have substantially contributed to the understanding of the phenomenon. Images in 2D and 3D have been taken to measure velocity in isothermal and thermal models. The usage of these techniques have allowed a deeper study of the coherent structures inside swirling flows (Yazdabadi, 1996; Fick et al.,1997; Dam, 2008).

Numerical simulation has been used to attempt to explain the complex interactions between large swirling flow coherent structures and indeed combustion (Sadiki et al., 2006; Freitag et al., 2006; Selle et al., 2006; Jochmann, 2006; Roux et al., 2005). Despite some successes, the results obtained for more intricate cases with high flow rates, high swirl and involving combustion leave much to be desired (Davison 2004, Pope 2000). Some of them seem to have appeared as a consequence of the geometry

and swirl used. Thus, more research is required in this field to be able to understand and take advantage of the phenomenon.

2.2. Swirl Characteristics

2.2.1. Characterization

According to some authors (Syred et al., 1984; Coghe et al., 2004; Al-Abdeli and Masri, 2007), swirl burners provide controllable, flexible reverse flow zones, with regions of high turbulence and shear, characteristics that give good, stable, combustion.

Consider a swirling flow. The flow is considered axisymetric until the onset of the vortex breakdown. A recirculation zone appears as an ovoid bubble of fluid that remains in the flow at a point just above the burner exit. The vortex core does not remain stable, but it starts precessing (Syred et al., 1984). Its frequency remains constant and it is determined by flow conditions and the geometry of the burner. A recirculation zone (CRZ) is formed downstream, remaining coherent at a great variety of conditions. The inclusion of this process in combustion reduces the length of the flame by the recycling of heat and active chemical species, change in density and fast mixing, especially near the boundaries of the recirculating zone.

To characterise such a flow the Swirl Number, S is used. It specifies the intensity of the swirl imparted to the flow. The value is equal to the axial flux of swirl momentum divided by the axial flux of axial momentum, non dimensionalised by the exhaust radius. Thus,

$$S \equiv \frac{G_\theta}{G_x r_e} \tag{2.1}$$

Where,

$$G_\theta = \int_0^x (\rho uw + \rho u'w')r^2 dr \tag{2.2}$$

$$G_x = \int_0^x (\rho u^2 + \rho u'^2 + (p - p_\infty r^2))dr \tag{2.3}$$

u: Axial velocity [m/s]

u': Fluctuating axial velocity [m/s]

w: Tangential velocity [m/s]

w': Fluctuating tangential velocity [m/s]

ρ: Density [kg/m^3]

r: Radius [m]

The axial flux of angular momentum, G_θ, and the axial flux of axial momentum, G_x, are assumed to be conserved in swirling flows under isothermal conditions.

$$G_\theta = \int_{r_1}^{r_2} 2\pi \cdot \rho \cdot u \cdot w \cdot r^2 dr = const. \tag{2.4}$$

$$G_x = \int_{r_1}^{r_2} 2\pi \cdot (p + \rho \cdot u^2) r dr = const. \tag{2.5}$$

However, as the flow patterns are very complicated, it is difficult to specify one specific swirl number. The changes at different heights make the estimation of the integral very complex. Thus, a more practical value is obtained from the geometric swirl number (S_g), which uses inlet conditions and hence can ignore pressure variations across the flow. For isothermal conditions, it has to be assumed that,

- The density is also constant.
- The axial velocity u can be obtained as the overall flow rate Q divided by the exit area, A_e.
- The angular velocity w is taken as the inlet velocity (Q/A_i) multiplied by an effective radius r_{eff}, located at the middle of the inlet pipe.
- The radius is the exit radius r_e.

This leads to the following equations, demonstrated somewhere else (Fick, 1998),

$$S_g = \frac{\pi \cdot r_e^{\,2} \cdot r_{eff}}{A_i \cdot r_e} = \frac{\pi \cdot r_e \cdot r_{eff}}{A_i} \tag{2.6}$$

For isothermal situations, the swirl number is only dependent on the dimensions of the burner. However, for combustion cases the momentum changes. The main effect results from the heat and expansion of the exhaust gases. The mixture inside the combustor can be approximately considered as an ideal gas. So,

$$\frac{p_1 V_1}{T_1} = \frac{p_2 V_2}{T_2} \tag{2.7}$$

The geometric swirl number is directly related to the inlet and outlet flow rates. The pressure in the process is constant, so the volume changes with respect to the ratio of absolute temperatures. As the exit volume is increased with temperature, the axial velocity at the exit is also increased, reducing the ratio of angular momentum to axial momentum. So, the geometric swirl number is reduced by a function of the average inlet and outlet temperatures (Fick, 1998). Thus,

$$S_{g,comb} = S_{g,iso}\left(\frac{T_{inlet}}{T_{outlet}}\right) \tag{2.8}$$

The combustion chemistry is also important for the swirl number. Different mixtures can have a different number of reactants, and more or less products, changing the final volume. Therefore, the swirl number will be altered. However, it is complicated to estimate a combustion swirling number in practical measurements since the temperatures in the flame tend to change according to the position of the outgoing flow and the presence of coherent structures whose behaviour alters the entire flow. Thumuluru and Lieuwen (2008) have defined the flame dynamics as a process controlled by jet fluctuations, oscillatory brush development, stabilization and fluid mechanical instabilities, making more complex the definition of an overall parameter.

Another dimensionless number that helps in the characterisation is the Strouhal Number. This dimensionless value is useful for analyzing oscillating, unsteady flows. It is defined as (John and Haberman, 1980):

$$Sr = \frac{fL}{U} \tag{2.9}$$

f: Oscillation frequency (vortex shedding) [1/s]

L: Characteristic length [m]

U: Flow velocity [m/s]

It represents a measure of the ratio of inertial forces due to the unsteadiness of the flow or local acceleration to the inertial forces due to changes in velocity from one point to other in the flow field. It represents the unsteadiness of the flow. Therefore, it is a function of the Re number. To correlate the frequency of the system with the Swirl Number, the following function is used, Sr', which is related to the Strouhal Number, Sr, by 4/Π (Syred et al., 1984),

$$Sr' = \frac{fD_e^3}{Q} \tag{2.10}$$

Where D_e is the exhaust diameter and Q the flow rate.

2.2.1.1. The Recirculation Zone

A Central Recirculation Zone (CRZ) is established in the centre of the flow due to the effect of the swirling flow. This zone, a form of vortex breakdown, serves as a flame stabilization region where the hot products and active chemical species are mixed with the incoming mixture of air and fuel. In addition, a corner, external recirculation zone (ERZ) can be formed downstream of the backward facing step (Huang and Yang, 2005).

This zone plays an important role in the stabilization of the flame and mixing process of the combustion products which are recirculated upstream. This stable region is usually formed close to or at the burner exist. According to Coghe et al. (2004), this region anchors the flame, helping to the recirculation of hot products whose time residence is increased due to recirculatory motion (Chen et al., 2008). Moreover, swirling flows reduce the combustion lengths because they encourage the mixing of components, greater rates of entrainment and reverse flow caused by the downstream tangential velocity decay. The resulting flame does not usually touch the upstream components, minimising the equipment maintenance and extending the equipment life (William, 2005).

This vortex breakdown presents an abrupt change of flow structure at some position along the axis of a vortex and is often followed by a region of vigorous turbulence. In fact, it has been shown that this phenomenon is a transition between two dynamically conjugate states of flow. This suggests that the phenomenon is a finite transition from a supercritical state to a subcritical one, similar to a hydraulic jump (Escudier et al., 1985). According to Schuermans et al. (2004), upstream of the vortex breakdown location, the velocity profile is highly jet-like with a peak velocity almost three times greater than the mean velocity. This phenomenon is said to appear under the following conditions (Mourtazin and Cohen, 2007; Serre Bontoux, 2002),

$$VB_{CRIT} = \frac{1}{u^2}\int_0^{\infty}\frac{w^2}{r}dr + \frac{gH\beta\Delta T}{u^2} \equiv S + Ri \geq 1/2 \qquad (2.11)$$

VB_{CRIT} : Vortex Breakdown critical conditions for appearance

u : Axial velocity [m/s]

w : Tangential velocity [m/s]

r : Radius [m]

g : Gravity [m/s^2]

H : Distance to the stagnation point [m]

β : Thermal expansion coefficient [1/K]

ΔT : Temperature difference [K]

Ri : Richardson number, ratio of potential to kinetic energy [-]

S : Swirl number [-]

Figure 2.1. Vortex breakdown seen from different angles (Serre and Bontoux, 2002)

Based on current theory, vortex breakdown is the large-scale disruption of the flow created by a local agglomeration of small-scale perturbations. Figure 2.1 shows such a process. This is uncannily analogous to the cascade effect of turbulence but in reverse (Dawson, 2000). This effect is the decay of larger eddies into smaller ones that dissipate turbulent energy. According to Paschereit and Gutmark (2006), the formation of coherent structures in the separating shear layer is initiated by Kelvin-Helmholtz instabilities. Thus, the exponential growth of vortices leads to the roll-up of the shear layer into larger scales, as happens in the energy cascade. Turbulent scales in the vicinity of the breakdown region must also undergo a similar effect. As turbulence itself is a direct indicator of the energy state of the flow, it stands to reason that the change in flow state (or stability criterion) would be somehow manifested in the turbulent energy spectrum (Dawson, 2000).

Recent experiments also refer to the suppression or enhancement of the Vortex Breakdown based on a temperature gradient along the downstream flow and the change of the Richardson number (buoyancy) in the field (Mourtazin and Cohen, 2007). The amount of suppression was proportional to the decrement in temperature variation. Thus, colder jets (relative to ambient fluid) would present suppression, whereas warmer would enhance the breakdown according to these findings.

2.2.1.2. The Precessing Vortex Core

Syred and Beer (1973) showed that a time dependent, hydrodynamic instability called the precessing vortex core (PVC) could be characterised by a non-dimensional frequency parameter (a form of Strouhal number which correlates eddy shedding frequencies to Reynolds number), also momentum and fluctuating pressure parameters.

According to some sources (Liewen and Yang, 2005; AIAA, 2007), the origin of instabilities arises from two factors, the fine turbulent scale structures and the large coherent structures which occur in the burning region. This also has important implications for flame stabilisation, dependent on whether or not the flames stabilise in and around the coherent structures or in other regions. Nevertheless, both the above phenomena are poorly understood, despite extensive experimentation using a variety of techniques (Syred, 2006; Lavoie et al., 2007; O'Doherty and Gardner, 2005).

Although some systems have been classified as precessing or stable swirling flows (Syred, 2006), the mechanism of manifestation of the PVC event is unclear. Some authors have studied the phenomena under isothermal conditions (Aleseenko et al., 1999), giving ideas about the movement of the core as a manifestation of the compressing-expansive mechanism in the inner part of the structure, whilst others have theorised its nature as a series of small eddies generated by the CRZ (Lieuwen et al., 2005). As specified by Paschereit and Gutmark (2006), small Kelvin-Helmholtz vortices are produced by the difference in momentum and density of the flows. These small vortices find a common path energized by the CRZ, whose exchange of momentum allows the development of larger structures such as the PVC, which starts

precessing around the system. However, this is a theory that must be corroborated by other means.

The PVC appears to be a mechanism for the rapid transport of fluid from the back wall of the generator to the downstream end of the reverse flow zone. The variation of the velocity contributes to the reduction or increase of the Reverse Flow Zone (RFZ), which is opposite to the vortex centre as observed in figure 2.2. However, the variation of velocity is not constant to the change of size of the reversal zone, thus making more complex the analysis. Figure 2.3 shows experimental results characterising the structure.

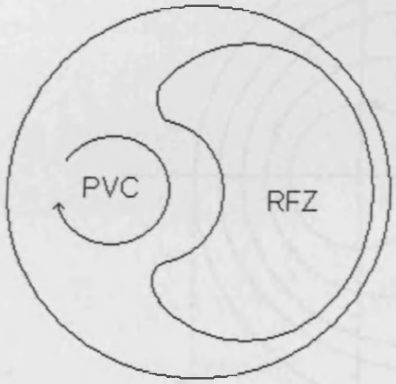

Figure 2.2. PVC and the Reverse Flow Zone (Yazdabadi, 1995)

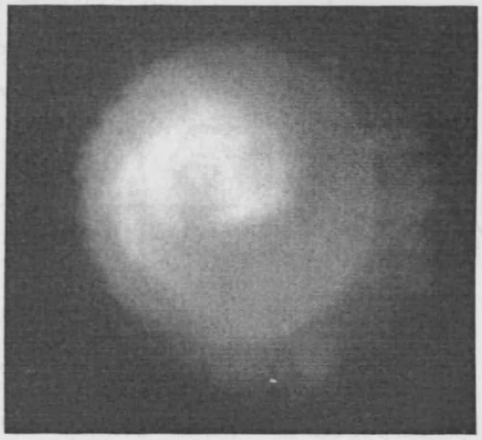

Figure 2.3. PVC and some complex eddies, external wall of the rig (Valera-Medina, 2006)

Other properties of the Precessing vortex are that it is dependent on the Re number. The velocity decays downstream, therefore the PVC is weaker in this region. However, the distance of total dissipation is sometimes very long. Yazdabadi (1996) showed that the dissipation was slow with extremely long lengths of pipes, typically 20 exit diameters in length. Syred (2006) stated that the PVC was a vortex breakdown phenomenon that was responsible for regions of turbulence and shear at the edge of the CRZ. This implied a role in flame stability and it was argued that the PVC creates 'perfectly stirred reactor' conditions in these regions (Syred et al., 1984). However, the PVC becomes significantly damped under diffusive combustion conditions and higher viscosity, being a function of Temperature. A perfectly stirred reactor, i.e. where mixing times approach zero, will have high chemical reaction times compared to characteristic flow times. Further damping effects would be supplied by non-equi-

diffusive mixture considerations caused by the asymmetry of the flow field (Dawson, 2000).

Yazdabadi (1996) showed that despite the considerable asymmetry of the exhaust flow, the angular momentum of the flow is equal on both sides of the rig, taking as reference point the centre of the PVC. Thus, the angular momentum is conserved by being squeezed through a narrow region between the precessing core and the wall. The faster the PVC, the narrower the area gets. This can be seen in figure 2.4, where the reference point is the centre of the PVC.

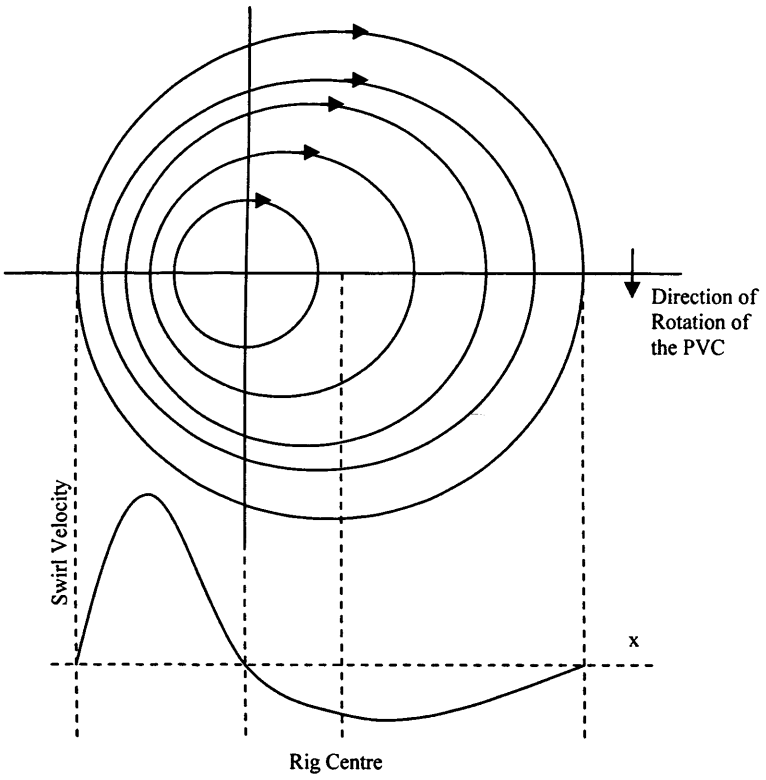

Figure 2.4. Angular Momentum flux. It is the same on both sides of the centre of the PVC (Yazdabadi, 1996)

Researchers agree on the idea of a forced vortex region (a region of solid rotational flow), which supplies the energy for the formation of the PVC. In the main part of the flow, there seems to be a flow with properties like those of a free vortex pattern (Soo and Zhou, 1990). This vortex is called Rankine vortex, and the former could be used to explain the PVC theory. For further information about the dynamics of the process, see Annex 1. Previous experiments showed that the precessing vortex is helical in nature, wrapping itself around the reverse flow zone boundary, figure 2.5 (Syred, 2006; Syred et al., 1984; Fick, 1997). However, this must be corroborated with a direct experimental approach.

Figure 2.5. Visualization of the helical nature of a single PVC (Syred, 2006; Fick, 1998)

In recent experiments using stereoscopic PIV the existence of Rankine vortices in the centre of cyclones has been confirmed, which includes an inner quasi-forced vortex and outer quasi-free vortex (Liu, 2006). These are joined by a PVC that rotates in the core of the equipment. Strong turbulence occurs inside of the inner quasi-forced vortex, especially were the PVC prevails. Therefore, 3 areas were detected in the cycle:

- Outer region ($0.35 < |r/R| < 1$) where the quasi-free vortex exists and the flow is less turbulent.
- Inner region ($0.1 < |r/R| < 0.35$) where the quasi-forced vortex exists without the influence of the PVC.
- The core of the inner vortex ($0 < |r/R| < 0.1$) where the PVC dominates producing high turbulence levels.

The fluctuating energy of the third zone consists in a chaotic turbulent fluctuation produced by the system (E_{random}) and the turbulence generated by the periodic motion of the PVC ($E_{periodic}$) (Liu, 2006).

2.2.1.3. Combustion Induced Vortex Breakdown

It has been recognized that the shape of the CRZ can influence the final stability of the system, creating other structures that can push down the flame into the mixing chamber, increasing the tendency to flashback. Some authors have observed how the recirculation zone progresses into the mixing chamber as a Combustion Induced Vortex Breakdown (CIVB) (Kroner et al., 2003; Umemura and Tomita, 2001), where they attribute the appearance of the vortex as a consequence of the combustion and air

entrance, linking the phenomenon to the CRZ which depends on pressure distribution downstream. Moreover, vortical structures can be modified by geometrical factors and flow conditions, as well as by the interaction of unburnt gases and the reaction zone, complicating even more their part in flashback occurrence and avoidance. It has been recognized that this structure plays a crucial role in the propagation of the flame, especially by a pushing effect similar to the observed by the CRZ.

2.2.1.4. Other structures

Another contribution of previous experiments was the prediction of another structure that would be found as an edge vortex, or axial/radial eddy. These kind of eddies are shed simultaneously around the walls of the system and move in an axial direction. Their formation is the result of the friction between two fields of equal density moving relative one to each other (Yazdabadi, 1995). Secondary structures thought to be linked to the principal CRZ are described as spiral arms whose dynamic mechanism interacts principally in the axial-radial plane (Stohr et al., 2008). These was confirmed in further experiments were eddies appeared in the external walls of the rig, opposite to the centre of the precessing vortex (Valera-Medina, 2006). In figure 2.6, it is possible to see that the axial velocity in the PVC passes upwards, while in the centre it decays and passes downwards, showing the existence of the CRZ. At the same time, different eddies that appear into the flow are noted, verifying unstable eddies produced by the movement of the relative flows.

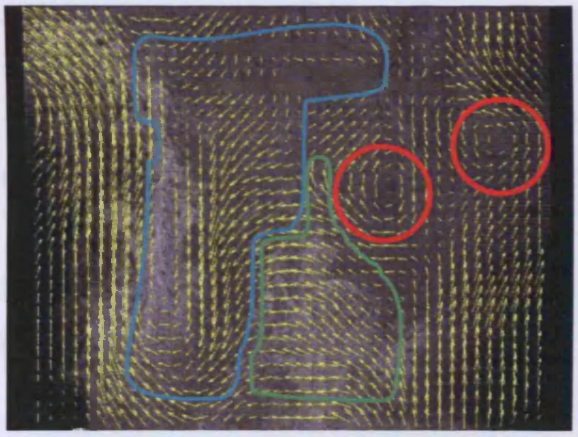

Figure 2.6. PIV axial measurement (Valera-Medina, 2006). Eddies in red, CRZ in blue and location of the PVC in green.

Recent experiments have revealed that the precession of the flow presents hysteresis under certain circumstances after increase to high S and subsequently decrease. As swirl is increased from low to high swirl a vortex breakdown is generated. Further

increasing the swirl generates a toroidal recirculation zone and the precession of the vortex. However, when S is reduced, another phenomenon named *Coanda Effect* appears, where the jet can attach to the walls of an expansion (i.e. large radius) forming a purely radial flow (Vaniershot, 2007; Vaniershot et al., 2008; Vanoverberghe, 2004). This is another instability that is beyond the scope of this thesis.

Some researchers have measured frequencies that are double that of the PVC; this has been attributed to the appearance of the vortex breakdown (Sadiki et al., 2006). However, some others have measured the existence of pairs of PVCs or the bifurcation of a single PVC into two of them (Valera-Medina, 2006; Syred, 2006).

2.2.2. Other Swirl Mechanisms

As previously mentioned, vibrations can occur at high pressures in operational equipment due to the appearance of different instabilities (Lieuwen and Yang, 2005; Paschereit and Gutmark, 2006; Syred, 2006; Lee et al. 2000). These can couple with the natural frequency of nozzles or internal mechanisms of the rig, damaging the system (Dawson, 2000). Therefore, they are undesirable problems that must be reduced. Several procedures have been developed for the reduction of these instabilities. Usually, these are divided in passive and active mechanisms of suppression. Passive mechanisms use the geometry and immobile gadgets for the suppression, whilst active mechanism use the signal response produced by pressure, velocity or temperature variations, which is fed back for vibration damping (Lieuwen and Yang, 2005). For the latter, the standard solution is to absorb the vibrations after they are produced (Guyot et al., 2008; Albrecht et al., 2008). This is in accordance with Noise Theory, where a wave can be damped using another one with a different frequency and amplitude. The only problem using this technique is that the vibration is only reduced, while the cause is not attacked.

On the other hand, realizing the importance of large scale structures as drivers of combustion instabilities, researchers have developed passive methods to control this instability by modifying geometrical and vortical conditions inside of the flow. O'Doherty et al. (1992) found that in highly swirling flows, the highest axial velocities are in the outer section of the exhaust, while in the centre the flow reverses.

Yazdabadi (1996) showed that a flow area reduction with a suitably shaped centre body would cause minimum disturbance, helping to stabilise the flow, preventing the PVC forming cyclones. Nevertheless, this could cause operational difficulties in high temperature systems, as mentioned before.

New burner configurations have been design giving successful reduction in emissions. Trapping-vortex combustors have proved to increase the recirculation of particles and combustion material when annular air is decreased and a second trapped vortex is added to the combustor via secondary after-bodies (Hsu and Goss, 1998). Elliptic burners have decreased the instabilities associated to fuel pockets due to vortical structures (Paschereit and Gutmark, 2008). The use of controlled piloted flames has improved the efficiency and reduction of emissions (Farber et al., 2008; Albrecht et al., 2008) and the generation of vortical structures inside of the system has proved to reduce the motion and strength of structures capable of coping with the natural frequency of the system such as the PVC (Paschereit and Gutmark, 2006). Counter rotating swirling flow systems have also been analysed with considerable success and are commercially employed on GE combustors (Mongia et al., 2007). Many other techniques not mentioned here have been tried in order to obtain wider operational limits, greater fuel flexibility and low emissions. However, several instabilities are still clearly a problem due to the coupling of pressure fluctuations and heat by the Raleigh criterion, where if heat fluctuations are in phase with pressure waves the instabilities augment. For these reasons a better understanding of the dynamic process that occurs in these systems and especially the formation of coherent structures.

2.2.3. Numerical Simulations and CFD

In order to solve these flows, different models can be used. The most popular are,

- The standard k-ε model relates the Reynolds stresses to the mean velocity gradients but makes the assumption of a constant viscosity.
- The Renormalization k-ε model, which also assumes an isentropic viscosity.
- The Reynolds transport model, the most accurate since it assumes anisotropic turbulences describing the anisotropic part of the stress tensor (viscous forces). However, it requires the modelling of several extra parameters (Liu, 2006).

- Probability Density Function (PDF) which represents the probability distribution in terms of integral values of the position of different structures and scales.
- Direct Numerical Simulation (DNS) which uses fundamental equations for the definition of all the scales embedded in the fluid. It has been used lately for the analysis of the equations of conservation of mass, momentum and transport of passive scalars (Warhaft, 2000).
- Large Eddy Simulation, whose filtered correlations allow the recognition of large structures, reducing both cost and time in the computational calculation (Sadiki et al., 2006).
- Reynolds-averaged Navier-Stokes (RANS). An ensemble version of the governing equations is solved, which introduces Reynolds stresses. This adds a second order tensor of unknowns for which various models can provide different levels of closure. Unsteady RANS (URANS) has been used successfully when analyzing the swirling phenomenon at lower cost than the first prediction attempts (Sadiki et al., 2006, Jochman, 2006).

Some examples of time dependent swirl computations are shown in figure 2.7 and 2.8.

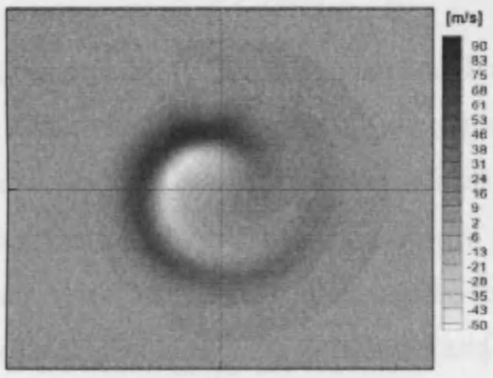

Figure 2.7. Spiraling motion of the emerging flow in a numerical simulation (Jochmann, 2006)

Figure 2.8. DNS Simulation of a Swirling Flow (Freitag et al., 2006)

2.3. Combustion

2.3.1. Combustion Principles

Combustion in a gas turbine is a continuous process, like an open fire, except that it takes place at higher pressures and temperatures above the melting point of the burner. The incoming air is slowed down and a stable flow pattern is generated to provide

adequate residence time for the process to take place. However there are still many unknowns in practical systems.

The principle of combustion is the chemical reaction between combustibles and oxidizer, commonly oxygen, to produce heat. Therefore, to consume all the fuel (f), an exact amount of oxygen must be injected. This value is known as the stoichiometric value. Nevertheless, this is rarely used, since more oxygen is required to reduce the unburned fuel. So, the equivalence ratio ϕ is used to relate a particular fuel/air ratio to the stoichiometric value. Thus,

$$\phi = \frac{(f/a)_{actual}}{(f/a)_{stoichiometric}} \tag{2.12}$$

From the reaction, available heat is obtained, which is the gross heating value minus the energy in the exhaust gases after the process. Different values correspond to different fuels based on their atomic bonds. However, to characterize a combustible it is common to use the term the lower calorific value (LCV), which is the energy released by the consumption of the fuel. Another term, the higher calorific value (HCV) is slightly greater as it includes the latent heat of the steam generated when fuel hydrogen is present.

The variety of species in the fuel and those produced by the combustion process must be taken into consideration, since they all have very different thermodynamic properties. The heavier fuel fractions take longer to break down than the lighter ones, while branched molecules take longer than straight-chain ones. The reaction takes place at different stages, breaking the long molecules into smaller ones, and so until the process is finished. The radicals and products can be seen in the flame colours. A blue one indicates combustion of low molecular weight, fairly simple, components, white or yellow show the formation of soot and green the existence of radicals.

The combustion process is based on breaking of atomic bonds, with some that give out energy (exothermic) and some others that absorb it (endothermic). To characterise this behaviour, the following formula is useful,

$$\Delta H^0{}_{RT} = \sum_P m_p \Delta h^0{}_{fT_p} - \sum_R m_R \Delta h^0{}_{fT_R} \tag{2.13}$$

This represents the reaction enthalpy at temperature T and 1 atmosphere. P and R are the products and the reactants, respectively (Baukal, 1998).

High values of temperature and pressure increase the energy and frequency of collision between reactant molecules. Even though some of them do not react, the chance of having a reaction is increased with these collisions. As the combustion continues, the reactant concentration reduces exponentially while the temperature rises, with a rate of reaction proportional to $e^{-E/RT}$ where E is the activation energy of the substance, T the temperature and R the Universal gas constant (Harman, 1981).

When the reaction is complete, the final products are low energy, inert gases. However, sometimes the combustion is not completed, so residues of hydrocarbons or contaminants appear in the flue gases. Even if the combustion is complete, some residues may appear due to the interaction of different compounds in the flame. Some of these are Nitrogen Oxides and CO, considered to cause some of the major emission problems. Various manufacturers have designed a great variety of burners to reduce contaminants and improve the final combustion efficiency (Tuthill, 2002; Syred, 2006; Khalatov and Syred, 2006; Lieuwen and Yang, 2005).

Different modes of combustion are often used. The first mode is the laminar diffusion flame, which forms as a "sheet" between separate supplies of fuel and air. Thus, this kind of combustion occurs when fuel and air mix and burn simultaneously. This process permits better control of the flame and the avoidance of flashback into the system (Baukal, 1998), but can give high NO_x emissions.

In contrast, the premixed laminar flame occurs where the fuel and air are already mixed in a combustible form. The flame front velocity falls to a low value if the equivalence ratio goes below unity (lean mixture) or above unity (a rich mixture). The use of turbulences can create laminar flames due to relaminarisation, since the turbulence mixes rich and lean, hot and cold eddies continuously to maintain stable combustion (Harman, 1981), whilst the Reynolds Number reduces due to kinematic viscosity effects.

In a secondary zone of the burner, air is introduced to provide an excess of oxygen for the remaining molecules. The equivalence ratio here is about 0.5. The temperature in this area is less than in the primary zone where combustion occurs, but still too high for the turbine blades. So, a tertiary zone is used where more compressed air is injected to dilute the combustion products and cool them to a safe temperature.

The ignition is another part of the process, where a spark or a torch igniter can be used into the primary zone to start the combustion. The heat raises the temperature of a local pocket of the mixture to above its spontaneous ignition temperature. This pocket enlarges to heat and ignite the whole primary zone.

To visualize this concept, observe figure 2.9. A hot plate (darker line) is located across the fluid flow. The flow (thinner line) gets hotter as it passes through the plate. However, there is a point where the fuel reaches its ignition energy necessary to start the combustion process and self sustain it. Thus, if the plate is large enough, the fuel will ignite. The same happens with a torch or spark, which give the energy necessary to combust the first particles of fuel (Panduranga et al., 2006). However, care must be taken to steer clear of flashbacks.

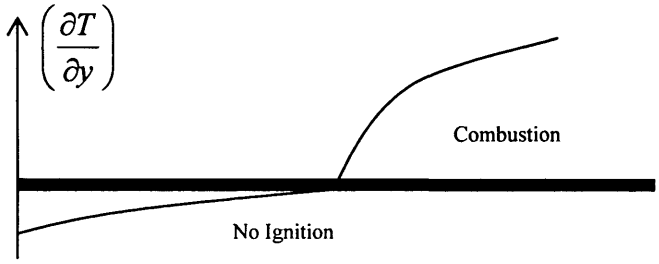

Figure 2.9. Forced Ignition on a hot plate (Panduranga et al., 2006)

There are different forms of ignition, so the designer must be aware of them to avoid further complications. The previously mentioned one is of the forced type. There are also the chemical and the spontaneous ignitions. The first one refers to an induced combustion between different chemicals at room conditions. The second is produced after the mixture of oxygen and fuel has taken place, and the temperature is high enough to start the process. In practice, this is an unwanted situation, since it can damage the equipment and the people working on them, unless one is in the area of diesel combustion.

To understand the implications of turbulence effects on the combustion process it is beneficial to note the tacit assumptions surrounding laminar burning. In laminar flames the flow conditions alter neither the chemical kinetics nor the rate of heat release. Turbulence changes this dependence (Dawson, 2000).

In turbulent combustion, chemical species are mixed at the molecular level as a result of small-scale turbulence. This induces fluctuations in velocity and pressure as well as in temperature, density and concentration. This is due to the influence of turbulence on the whole flow field including the flame structure and rate of heat release and vice versa. Turbulence also increases the system's susceptibility to instability, for example the formation of vortex breakdown phenomena in isothermal and combustion conditions, flame shape and stability, reactant mixing times, flashback, etc. In general, turbulence promotes better mixing of the reactants which increases their rate of consumption (burning velocity or flame speed) and, in turn, energy release rate (O'Doherty and Gardner, 2005).

Current research indicates that the thickness of premixed turbulent flame zones is related to turbulent length scales. As premixed flames generally have steep velocity and density gradients between the cold reactants and hot products they are strongly influenced by small-scale turbulence. Turbulence cascades through a distribution of length and time scales defined as l_o (largest eddies, integral length scale), l_λ (average eddy size, Taylor microscale) and l_k (smallest scale, Kolmogorov scale) and describe the size of eddies in descending order of magnitude. The cascade describes the transfer of energy from the largest scales to the smallest scales where the energy of the eddies dissipate as heat (Regunath, 2008; Davidson, 2004). These length scales with the turbulent intensity can be combined to form three different Reynolds numbers, one for each regime:

$$R_{l_o} = \frac{U' l_o}{\upsilon}, \quad R_\lambda = \frac{U' l_\lambda}{\upsilon} \text{ and } \quad R_k = \frac{U' l_k}{\upsilon} \tag{2.14}$$

The orders of magnitude between the length scales are approximately $R_{lo} \approx R_\lambda^2 \approx R_k^4$ but cannot be directly correlated.

Thus the nature of the turbulent flow has considerable effects on flame structure, and different regimes are observed according to their length scale due to differences in chemical to flow time scales (Vanoverberghe, 2004; Dawson, 2000). Wrinkled flames, thin reaction sheets, Flamelets (laminar) in eddies and Distributed reactions are the different regimes observed in combustion and defined in the Borghi diagram (Vanoverberghe, 2004). Their appearance is correlated to the scale growth progression in the system.

The influence of turbulence on the propagation of a combustion wave was first studied by Damkhöler in 1940. He suggested that a combustion wave will wrinkle into peaks and troughs under the influence of large-scale turbulence. The wave may then break up or remain continuous under the influence of the distortion. This results in a flame that is significantly larger in surface area than it would normally be under laminar conditions resulting in an increase in the overall burning rate. This showed that the turbulent flame speed S_T, must exceed the laminar flame speed, S_L (Dawson, 2000). Quantifying S_T proves difficult as one must determine the surface area and thickness of a turbulent flame (Vanoverberghe, 2004). Usually, the effect of turbulence on a combustion wave is measured in terms of the ratio of turbulent mixing time, τ_m, and the chemical reaction rate, τ_c. This gives a non-dimensional parameter known as the Damkhöler number and is defined as follows:

$$Da = \frac{\tau_m}{\tau_c} = \frac{l_0 S_L}{U' \delta_L} \tag{2.15}$$

The turbulent mixing time, τ_m, is defined as the integral turbulent length l_o divided by the turbulence intensity, U'. S_L is the laminar burning velocity and δ_L is the laminar flame thickness and describes the reaction time over a flame thickness (τ_c). Large Da numbers describe a fast reaction and give 'perfectly stirred reactor' conditions implying that spatial variations in temperature or concentration are absent as the mixing is considered instantaneous. This would give a very thin reaction zone. For small Da numbers the reaction is slow and non-equi-diffusive, thus thicker flames will occur (Dawson, 2000).

Karlovitz in 1953 was the first to introduce the concept of flame stretch. Unlike the Da number, which characterises flame thickness, the Karlovitz stretch factor measures

the area increase a flame undergoes in the midst of velocity gradients. The number is defined as:

$$K_a = \frac{\delta_l}{U}\frac{dU}{dy} = \frac{\delta_l}{S_L}\frac{U'}{\lambda_t} \tag{2.16}$$

In the case of turbulent flames, the turbulence intensity and characteristic lengths must in the Taylor microscale, λ. The turbulent Ka number basically describes a ratio of chemical to eddy (flow) lifetimes. In this way it is similar to the Da number but acts along a different plane relative to the flame front, i.e. Da number acts normal to the flame surface (flame thickness) whilst the Ka number acts along its length (Law,1988).

In diffusion flames, flame response also critically depends on preferential diffusion processes which are generally characterised by the Lewis number, Le. The Lewis number is defined as,

$$Le = \frac{\alpha}{D} \tag{2.17}$$

Where is α is the thermal diffusivity and D is the mass diffusion governed by Fick's law. When Le=1 the combustion process is said to be diffusionally neutral and adiabatic as total energy conservation is maintained. When Le<1 the mass transport exceeds heat loss resulting in an increase in combustion intensity. When Le>1 the heat loss exceeds mass transport and the combustion intensity decreases accordingly.

2.3.2. Combustion Instabilities

The main problem with the combustion processes is the variety of instabilities that appear in the system. Large structures in the flame cause many of them. These can produce low frequency/high amplitude oscillations that can cause resonation in the equipment (Lieuwen and Yang, 2005). Also, it can cause pressure fluctuations capable of damage to the burner shell by problems of fatigue (Paschereit and Gutmark, 2006). The principal mechanism of acoustic oscillations is amplification by the Rayleigh criterion, where pressure oscillations interact with the heat release, which is distorted by the former, producing pressure variances that feedback the first oscillations. The position of the flame, geometry of the burner and fluid mechanics

(such as vortices in the combustion chamber and flame speed) into the system are basis of the noise and vibrations generated.

To analyse the different types of instabilities in burners and combustion processes, different authors have characterise the principal forms of instabilities that can be found in these systems (Gupta, 1979),

- Chamber Instabilities: Specific to the geometry and acoustic character of the system chamber.
- System Instabilities: Involve the interaction between the dynamics of the combustion and the components of the system. They are responsible for the low frequency noise in the range of 20 – 400 Hz.
- Intrinsic Instabilities: Instabilities that involve only the reactants. These are dependent on the combustion kinetics. Usually found in places where the levels of combustion are very high (like rockets).

The periodic nature of swirling flows can lead to different modes of periodic combustion instabilities, called fluid dynamic instabilities, which is associated to vortex shedding mechanisms. Among the combustion chamber different instabilities can appear such as acoustic, shock or fluid dynamic ones. The acoustic instabilities are characterised by the propagation of acoustic waves in the chamber, being determined by the geometry of former and the speed of sound in the medium.

The fluid dynamic instabilities are related to vortex shedding mechanisms. Where vortices appear at frequencies that are multiple of the chamber acoustic frequency, resonance can occur. If the former is sensitive to pressure changes, coupling can increase the final amplitude of the oscillation. The most predominant fluid dynamic instability in swirling flows is the PVC, which can be augmented by different eddies that have been mentioned previously.

It has been demonstrated that the PVC is detrimental for isothermal systems (Yazdabadi, 1996). Due to the precessing core, the reverse flow zone rotates about an axis displaced from the central axis of the system, contributing to the instability of the system and inefficiency of cyclones or mixing systems. In fact, the RFZ changes its

shape to that of a distorted ovoid due to the PVC. The greatest velocities levels of the flow occur at the front of the RFZ. It has also been stated that in premixed situations, the PVC can cause a feedback mechanism with acoustic modes, resulting in flashback of the flame into the nozzle (Freitag et al., 2006).

Stretching caused by large coherent scales is also a problem of instability, since the system suffers heat losses and changes of velocity that will influence the pressure field. The argument follows that if a flame is subjected to aerodynamic strain (with Le=1) then the surface area of the flame will increase, increasing heat loss. This in turn will reduce the burning velocity until extinction occurs. Thus a complete description of flame extinction needs both Da and Ka numbers, which describe the thinning of the flame as well as its expansion in surface area, respectively (Dawson, 2000). If thin flames match long shapes, heat loss will occur. Thus, large Da with small Ka must be avoided.

Finally, flashback produced as a consequence of the stretching of the CIVB and its influence in the pushing of the flame upstream the combustion chamber may also be considered as an unstable phenomenon, especially nowadays that the use of alternative fuels make imperative its avoidance in new gas turbines.

2.3.3. Contaminants

As mentioned in the previous chapter, different contaminants are emitted by combustion processes. However, the most important at this moment are those related to the greenhouse effect, acid rain and smog formation, namely CO_2, CO, NO_x and SO_x.

2.3.3.1. Carbon Dioxide

It is present in the atmosphere at 0.04%, but this value is rising steadily due to the increasing use of fossil fuels. Concentrations of 6 to 10% can cause health problems (Baukal, 1998).

2.3.3.2. Carbon Monoxide

Carbon monoxide is another important gas that is formed after incomplete combustion of fossil fuels. It is a flammable gas that can act as a toxic, asphyxiating chemical

when it is combined with haemoglobin, since it has 240 times more affinity to blood (IPCS, 2006). Therefore, it is regulated by specific emission guidelines depending on its application and geographic location.

2.3.3.3. Oxides of Nitrogen

NO_x are poisonous to human and can create a lot of health problems such as irritation, nauseas, headaches and asphyxiation. Also, these contaminants are very undesirable since they promote the formation of smog and increase the greenhouse effect. Another problem is their corrosive properties when they mix with water to produce acids that in conjunction with sulphuric acids in acid rain corrode metal and concrete.

The problem with NO_x is that they are often produced from the high temperatures of furnaces combined with long residence times (thermal NOx).

There are 3 different ways NO_x may be formed (i.e. Claypole, 1980),

- Thermal mechanism (Zeldovich), where the contaminant is formed under high temperature conditions by reaction between nitrogen and oxygen, especially at temperatures greater than 1600°C. The appearance of hot spots in the combustion chamber contributes to the formation of these contaminants and the aim of engineers is to minimize their formation.
- Prompt NO_x are formed by the relatively fast reaction between nitrogen, oxygen and hydrocarbon radicals. The number of reactions in this process is vast, thus making difficult to predict and control them as well.
- Fuel NO_x are those concerning to the nitrogen compounds in the fuel. A direct oxidation or the later creates high variety of species. The main concern here is coal or solid fuel combustion; this thesis is focus on gaseous combustion.

2.3.3.4 Sulphur Oxides

Sulphur oxides, SO_x, are of particular importance in the combustion process. These unwanted contaminants can interact with the water of the atmosphere to form sulphuric acids that can corrode and damage structures and concrete. Also, their presence in the upper layers of the atmosphere can promote the greenhouse effect, with its well known consequences.

2.3.3.5. Other contaminants

Other contaminants that appear in the combustion process are Dioxins and Furans (from chlorine containing wastes), with their carcinogenic effects; unburned and partially burnt fuel and volatile organic compounds, especially when oil and biomass are used; methane from incomplete processes and leaks of storage tanks, etc. All these contaminants are subject to control by legislation now in major industrialised countries.

2.3.4. Advanced Industrial Combustors

With the increasing use of fossils to produce energy during the 21st century, the research has become focused on the improvement of their emission performance, blow off limits, high turndown and general stability. Since natural gas and gasified coal are seen as very major contributors to the energy markets, new combustion processes will have to achieve all the above; this thesis is a contribution.

As part of the Advanced Turbine Systems (ATS) project in the USA, the National Emissions Technology Laboratory in conjunction with Universities all over the country has started to achieve ultra low emissions with the use of new processes. The most promising are (Layne, 2000),

- Surface Stabilized Combustion (SSC): producing less than 2 ppm of NO_x in laboratory tests, this technology is based on the use of a thin, compressed and sintered porous metal fibre matrix (Pyromat) at the burner inlet to stabilize combustion. The stable combustion is maintained by the presence of a high temperature surface in the fuel air flow path.
- Dry Low Emissions (DLE): DLE combustors use high excess of air in order to reduce the flame temperature and thus NO_x emissions, but have associated stability problems.
- Humid Air Combustion (HAT): Water saturated air is introduced along with gaseous fuels into the combustion chamber, and some steam is directly generated at the high pressures and temperatures found in gas turbine combustors. Advances are the reduction of NO_x and the increase in power, since the mass flow rate has been increase through the turbine. The use of

steam cooled combustion liners and turbine blades allow higher turbine inlet temperatures, hence higher cycle efficiency.

- Dual Fuel Combustion: System used to utilize liquid and gaseous fuels. A novel dual fuel pre-mixer has been developed. It has been created by "macrolamination", a technique that allows complex internal flow channels to be formed by etching them into thin substrates and bonding the substrates together to form fuel injector arrays. Diesel and natural gas performance were almost equal using this device.
- Periodic Equivalence Ratio Moderator (PERM): Methods to measure acoustic and combustion responses are essential to achieve a better response of the equipment. Knowing these phenomena, adjacent injectors alternately inject fuel at a modulated frequency. This modulation is used to damp pressure pulses from any injector, maintaining a desired equivalence ratio. This mechanism has proved to have eliminated a 3 psi peak-to-peak pressure oscillation.
- Catalytic Combustion: This technology serves to stabilize flame formation by enhancing oxidation under lean firing conditions. A piloted ring combustor will replace the standard diffusion flame pilot burner with a catalytic pilot burner. The only problem is that the flow must be at high temperatures to be activated by the catalytic material, thus forming pollutants. Catalyst contamination is the main problem.

2.3.4.1. Surface Stabilized Combustion

The use of surface stabilized fuel injectors has been developed by Alzeta, an American company located in California. These injectors use a patented technique to form interacting radiant and blue-flame zones immediately above a selectively perforated porous metal surface. This allows stable operation at low reaction temperatures. These devices have proved to emit ultra low NO_x quantities at different pressures. By 2003, the emissions were at 3 ppm of NO_x and 10 ppm of CO at pressure from 0.18 MPa to 1.68 MPa and temperatures between 340 and 670 K. The adiabatic flame temperature was from 1740 to 1840 K (Greenberg et al., 2005).

2.3.4.2. Dry Low Emissions Combustion

Many companies use this technique. One of them, Siemens Westinghouse Power Corp. has designed and advanced system for its W501F series turbines. The design is based on the concept that homogeneous fuel/air mixtures burn with less NO_x production than poorly mixed designs. Therefore, to improve the mixing a swirl fuel injector (SFI) is used to achieve this objective (Miller, 2004).

A major problem that can appear arises from the tight tolerances used in gas turbines; when operating at a single digit NO_x emission small changes can dramatically affect the entire system. Oscillations that occur create pressure changes that can affect the final performance of the equipment, producing more pollutants (Goldmeer et al., 2005). Some research centres, such as EPRI (Angello et al., 2004), are leading experiments to classify and characterise dynamic oscillations in ultra low NO_x premix combustors that can produce instabilities which can affect the final performance of the equipment. Multi task programs to map the operating regime for stable combustion in modern DLE combustors are taking place to identify key parameters of the instabilities. Thus, dry low emission systems will be monitored and improved based on the noise and instabilities features.

Some improvements to this technology are the so called self-tuning Combustion Pressure Fluctuation Monitoring systems (CPFM). These typically apply different setting according to different frequency bands, so the system pressure fluctuations can be analysed and automatic systems adjust several parameters to control the former. Some companies like Mitsubishi have created advanced systems that can adjust by-pass valves, pilot ratios and Inlet Guide Vane position in order to give a quick response to stabilize the system (Koeneke, 2004).

General Electric has designed and patented its DLN 2.6+ Combustion System, which has guaranteed as low as sub-15 ppm NO_x, with a proved sub-9 ppm. It increases the efficiency, reducing fuel cost in $1.5 million per year, maintaining flexibility with different fuels. European and American facilities are starting to use this equipment in order to achieve their environmental compromises (General Electric, 2006).

Other companies are working on DLE technologies are Alzeta Corporation, Power Systems Mfg. LLC, Precision Combustion Inc., Power Tech Associates, etc. (Shelly, 2006).

2.3.4.3. Humid Air Combustion

In the Humid Air Turbine (HAT) cycle, as the absolute humidity of the moist combustion gas increases, the performance of the turbine will also change and design changes will be needed. However, this has proved to reduced CO_2 and increase efficiency in certain circumstances.

It has been found that moisture addition can lead to a reduction in combustor temperature, a more uniform distribution of temperature and a drastic lowering of NO concentration in the combustor as well as a reduction in the length of a return flow zone (Zhou, 2004). A simulation has been carried on using a swirl combustor where different humidity values were used. The aim was to recognise the contribution of humidity to the reduction of NO, change in temperature and velocity, and stabilities associated to the process. Different inlet conditions were analysed at different pressures. The effects show that with the increase of inlet pressure, the dimension of the reverse flow zone becomes smaller while its centre moves forward, peak temperatures increases and NO formation increases as well. With the addition of moisture, the reverse flow region becomes smaller while its centre moves further ahead, peak temperature drops greatly and NO formation is reduced drastically. Thus, humid air combustion is helpful to reduce pollution and to shorten the axial length of the combustor.

Nevertheless, this technology has some problems. Temperature distributions within and at the exit of the combustor, some pollutant emissions (CO and unburned hydrocarbons, UHC) and the stability of the combustion were affected by the change in humidity (Fang, 2005).

2.3.4.4. Duel Fuel Combustion

The use of different fuels to run advanced turbines has increased in recent years, especially because of the need for cleaner combustibles. The versatility of using more than one fuel has always being a concern for designers. Therefore, Duel Fuel Injectors

have been developed over many years in order to use liquids or gaseous fuels in the same turbines. This enabled more flexible usage and the possibility of switch over from one combustible to another, based on prices, deployment, ecological factors, etc.

Some manufacturers, like General Electric, have created duel pre-mixers capable of using either natural gas or distillate oil as fuel for combustion, or a mixture of the two of them. Also, the turbines are capable of switching over from 100% one fuel to 100% another fuel, avoiding the lack of combustible for future scenarios (Global Energy Equipment, 2006).

In order to construct this equipment, a novel manufacturing technique called "macrolamination" has been developed. A spatially distributed injection strategy is used to enhance fuel placement, distribution and mixing inside the premixer. Different parameters have been studied and analyzed in these devices, showing a considerable reduction of contaminants thanks to the generated mixing. Also, numerous fuels have been studied, making a special emphasis on Diesel and natural gas (Mansour et al., 2001).

2.3.4.5. Periodic Equivalence Ratio Moderator

Also named "Pulse Combustors", these equipments have proved to reduce NO emissions during several lab tests. The concept is based on an equipment that reduces the instabilities generated in gas turbines. The device employs a control system that rapidly detects the presence of sound waves and then modifies the fuel injection scheme in a manner that instantaneously dampens the instability. This equipment has been proved in a low emission Westinghouse gas turbine, giving very low NO_x levels (Georgia Institute of Technology, 2006).

The reduction in emissions occurs because the residual products leave the chamber with lower temperature due to the increase in heat transfer, with the Zeldovitch NO_x being reduced (Keller et al., 1990). Another variant of this process is the use of the concept of "antisound" to suppress the instabilities. This method uses external acoustic excitation by loudspeakers to suppress the oscillations of the flame (Lang et al., 1987).

In other experiments, combinations of small quantities of fuel and imposed oscillations have been shown to ameliorate combustion oscillations in ducted flows of premixed methane and air with equivalence ratios from the lean limit to the stoichiometric. The added fuel enhanced stability and reduced the amplitude of low frequency oscillations associated with high strain rates and their tendency to modulate acoustic frequencies at high equivalence ratios. The imposed oscillations at harmonics of the acoustic frequencies moderated the latter (Emiris and Whitelaw, 2003).

2.3.4.5. Catalytic Combustion

The principle of this method is to use a catalytic material to enhance the combustion reaction. Therefore, there is no need to use sparks or other energies to start the process. Thus, the generation of contaminants is very low. However, the inlet parameters required for the catalysis are those that produce the final emissions, since the material must be at high temperatures to work efficiently and during the process of warming up the pollutants are emitted.

In order to tackle the emissions of contaminants and NO_x, the use of catalytic combustion has been extended to the industrial sector. These systems also have the advantage of reducing the vibrations induced by the combustion, producing low NO emissions and small fluctuations in the flame temperature.

Some materials used have been palladium, platinum, copper, iron, etc. Palladium and platinum have showed good performance at different pressures. Copper and iron molecules have increased the efficiency of the material. However, their performance is a function of the inlet temperature and the final pressure. Very small NO_x concentrations have been achieved using the last materials (Kuper, 1999). They are all, however susceptible to catalyst poisoning.

Another system, the Rich Catalytic Lean Burn Combustion (RCL) has been developed to work with natural gas, providing advantages for fuel flexible operation on non methane fuels. Also, fuel rich operation limits the extent of catalyst stage reaction based on available oxygen, regardless of the fuel's intrinsic reactivity on the catalyst, obtaining similar performances for different fuels. This enables the use of low heating value fuels and other fuels, with low NO_x emissions (Smith et al., 2006).

The basis of this technology is the injection of ammonia into the exhaust gas stream of the turbine. This compound reacts with the nitrogen oxides in the presence of the previously mentioned catalysts, forming water and nitrogen. However, it has been proved that this technology only is capable of reducing NO_x when these are produced from natural gas. The inclusion of oil or liquid fuels can damage the catalyst (Schorr et al., 1999). In the case of CO, this is reduced using potassium carbonate coated on a platinum catalyst surface which reacts with the CO to form CO_2. However, this is out of the scope of this project.

Nevertheless, the main problem with this technology is that, even though it generates NO_x levels less than 3 ppm, the amount of ammonia required and the solid waste produced to capture the contaminants become an important environmental issue. Therefore, the disposal of the former can be more expensive and more detrimental to the environment that the nitrogen oxide emissions.

2.4. Summary

The use of swirl flows to reduce the contaminants and stabilise combustion processes is very widespread globally. There are still many aspects of these systems that are poorly understood, especially in the area of the important coherent structures, flashback behaviour and overall stability. Current technologies use the advantages of premixing, lean mixtures, swirling flows and alternative fuels. However, the instabilities associated to all these factors can compromise the final efficiency of the system and the amount of emissions generated by each technology. Therefore, this thesis is intended to make a contribution to understanding the processes occurring in these systems, especially in the area of gas turbine combustors.

CHAPTER 3

MEASUREMENT TECHNIQUES

3. MEASUREMENTS TECHNIQUES

"The camera introduces us to unconscious optics as does psychoanalysis to unconscious impulses."

Walter Benjamin (1892-1940)

Different techniques were tested to measure different rig configurations to try to visualize the PVC, Recirculation Zones and Flashback. The need of fast acquisition and high accuracy lead to the use of Phase Locked Particle Image Velocimetry (PIV) triggered by Hot Wire Anemometry (HWA) and Acoustic Condenser Microphones. Spontaneous emission spectroscopy, or Chemiluminescence spectroscopy, was also used to define boundaries of high combustion intensity and rapid reaction in the flame regime. The use of Laser Doppler Anemometry (LDA) was investigated, but its utilization to measure more than 40 planes in more than 20 different experiments made it unjustifiable due to the time required for data processing. Moreover, the new equipment and systems used for the PIV systems allowed faster and different techniques to measure recirculation, flow velocity, field shapes, etc., making it the best system to reconstruct phase locked instabilities in these kinds of flows. Finally, other techniques such as High Speed Photography (HSP) were employed to observe the development of large coherent structures in the vicinity of the nozzle as well as flashback. This proved to be an excellent qualitative and quantitative method for structural and length definition, although poor for quantitative planar intensity analysis. The results obtained with the latter allowed the recognition of special cases for deeper study.

3.1. Hot Wire Anemometry

Hot Wire Anemometry has the necessary frequency response, in the range of kHz, and sensitivity at low flow velocities for measurements in the high turbulence levels encountered in swirling flow systems.

3.1.1. Calibration of Hot Wires for Velocity Changes

All the instruments related to the measurement of fluid velocities and heat transfer are linked to several non-dimensional parameters and geometrical factors such as the Nusselt (Nu), Reynolds (Re), Prandtl (Pr), Knudsen (Kn), etc. In the context of a cylindrical thermal anemometer, the equation can be expressed as follows,

$$Nu = f(Re, Pr, Kn, \ldots \text{ geometrical factors}) \tag{3.1}$$

In 1914, King derived a solution for the heat transfer from an infinite cylinder in an incompressible low Reynolds number flow that may be written as:

$$Nu = A' + B'Re^{0.5} \tag{3.2}$$

A' and B' are constants. Knowing that the heat loss is equal to the electrical power delivered by the sensor (V^2/R, where R is constant), the geometrical parameters of the wire and the fluid characteristics are constants, then the expression can be reduced to (University of Cambridge, 2005),

$$V^2 = A'' + B'' U^{0.5} \tag{3.3}$$

Where the new values A'' and B'' are constants. V_0^2 can be replaced by A'' when the velocity of the fluid is equal to zero. In practice, the voltage registered at the anemometer output is the electro-mechanical force E that is applied to the top of the bridge, where the two arms act as potential dividers. So, a more general expression can be written as,

$$E^2 = A'' + B'' U^{0.5} \tag{3.4}$$

However, this expression has shown to be unsatisfactory when used over a large cooling range. So, higher order polynomials provide curves that fit to the experimental calibration curves E vs U. The equation commonly used is,

$$E^2 = A + BU^{1/2} + CU \tag{3.5}$$

However, the value of U is comprised of 3 different velocity components, so the instantaneous cooling velocity is given by,

$$U^2 = u^2 + G^2w^2 + K^2v^2 \tag{3.6}$$

Where u, w and v represent the 3 velocity components and G and K are values dependent on the wire characteristics (Syred, 2005). For flows where turbulence intensities are less than 10% and where one main flow direction predominates, the mean velocity is obtained from the mean voltage level, and the turbulence intensity form the R.M.S. voltage,

$$U = \left(\frac{E^2 - A}{B}\right)^2 \quad \text{and} \quad \frac{(U'^2)^{1/2}}{U} = \frac{4(E'^2)^{1/2}E}{E^2 - E_0^{\,2}} \tag{3.7}$$

Where U' and E' are instantaneous values. Typically six different measurements are taken at a given point to obtain the 3 components of the velocity U and their mutual relation.

3.1.2. Equipment Selection

Probes are selected on basis of (Jorgensen, 2005):

- Fluid Medium
- Number of velocity components to be measured (1, 2 or 3)
- Velocity Range
- Quantity to be measured (velocity, wall shear stress, etc)
- Required Spatial Resolution
- Turbulence intensity and fluctuation frequency in the flow
- Temperature variations
- Contamination Risk
- Available space around measuring point

The way of selecting one or other can be as follows,

- Miniature Wires: First choice when analysing air flows with turbulence intensities up to 5-10%. These wires have the highest frequency response and can be repaired easily. These wires are the most affordable.
- Gold plated Wires: These can be used when turbulence intensities are up to 20-25%. However, their frequency response is inferior to miniature wires. They can also be repaired.

- Fibre-film sensors: These can be used for application in air, with a lower frequency response than wires. They are more rugged and can be used in less clean air. They can be repaired. If a Heavy-quartz coating sensor is used, this can function for applications in water.
- Film-sensors: These can be used for applications in air at moderate to low fluctuation frequencies, if they are thin-quartz coated. They can be used in less clean air than fibre-sensors. If the coated is a heavy-quartz one, they are more rugged than fibre sensors and can be used in application in water. However, they cannot be repaired.

3.1.3. Anemometer Setup

For the hardware, the setup consists on an overheat adjustment (static bridge balancing) and a square wave test (dynamic balancing). When a signal conditioner is part of the array, the hardware setup also includes low pass filter and optional gain settings. The overheat adjustment determines the working temperature of the sensor. The overheat resistor in the system is adjusted so that the wanted sensor operating temperature is established when the bridge is set into Operate. The cold and warm resistors are related by the following equation,

$$a = \frac{R_W - R_0}{R_0} \tag{3.8}$$

a: Overheating Ratio

R_W: Sensor resistance at operating temperature T_W

R_0: Sensor resistance at ambient temperature T_0

So,

$$R_W = R_0(1 + a) \tag{3.9}$$

The recommended value for a is 0.8 in air (over temperature approx 220 °C) and 0.1 in water (over temperature 30 °C). So the value can be setup to measure the values with the correct resistance at the desired temperature.

The over temperature $T_W - T_0$ can be calculated as:

$$T_W - T_0 = \frac{a}{\alpha_0} \tag{3.10}$$

Where α_0 is the sensor temperature coefficient of resistance at T_0, which is given by the manufacturer. The probe leads resistance and the resistance of the support and cable are provided by the manufacturer (DISA, 1995).

This value is adjusted only once and left untouched during calibration and data acquisition. Only if more accurate measurements are required this can be done every time that the equipment is turn on.

3.2. Noise in Combustion. Pressure Measurement.

Instabilities that appear in the flow due to the precessing behaviour of the swirling flows produce vibrations that can couple the natural frequency of the equipment, damaging it. However, these vibrations and pressure oscillations can be used for triggering purposes as well under combustion conditions, since the use of seeding material can damage any hot wire inserted in the flow.

Sound travels in the form of very slight pressure fluctuations in the air or medium. Thus, the appearance of a wave may generate a difference in pressure in the system of interest, with high and low pressure areas that can be measured. The audible range of sound pressure and intensity is too wide to be displayed on a simple scale. Thus, a logarithmic scale of sound pressure level (SPL) is used to relate the intensity of the signal to a datum value (0 dB at $p_0 = 2 \times 10^{-5}$ Pa). The SPL is defined as,

$$SPL = L_p = 20\log_{10}(p/p_0) \text{ [dB]} \tag{3.11}$$

Being P the pressure to analyze. While the SPL indicates the intensity of sound, the power level (PWL) is used to indicate the acoustic energy emitted from the source. With the reference value at $P_0 = 10^{-12}$ W,

$$PWL = L_W = 10\log_{10}(p/p_0) \text{ [dB]} \tag{3.12}$$

The turbulence generated due to all the flow passages and processes in a combustor generates a broad band white noise (random signal at constant power) of a moderate level. Some other processes generate lower frequency noises, like those related to the delay between fuel entry and its combustion. Also, if there is a momentary air pressure drop, this will increase the fuel flow. Thus, the increased heat release may increase the pressure in an organ pipe cycle at a frequency of a few hundred hertz. This self sustained phenomenon can be avoided by changing the fuel nozzle pressure. Another problem is generated by temperature fluctuations, causing a wave that can be reflected from the turbine to the nozzles. High frequency noises are related to afterburners where vortex, expansions and contractions cause resonance. The mechanism of acoustic signal generation for combustion is a monopole, where the noise is radiated equally in all directions (Baukal, 2003), making possible its recognition with adequate pressure transducers or Acoustic Condensers.

In jets, the noise is produced by the turbulent mixing of the jet with the atmosphere. Two zones can be defined: the primary zone in which the flow continues as it leaves the nozzle, and the turbulent mixing zone. The noise is generated at the shear zone with the atmosphere, where the randomness of the turbulence generates noise over a wide frequency spectrum. The spectrum shifts to lower values with distance, from a high value to a lower one downstream, with a potential function shape (Baukal, 2003).

Factory regulations have been implemented by the government. The use of pipes, channel diffusers, acoustic liners, etc. has decreased any potential risk to employees, as well as the use of protective equipment. Notwithstanding, the cause is not eradicated, and the problems still exists in the system. Therefore, more studies must be done to eliminate this kind of problems, especially in swirling flow systems. The pressure gradients caused by the swirling movement can aid in the triggering of the process based on the cyclic nature of the phenomenon, phase locking different periodic signals.

3.3. Particle Image Velocimetry (PIV)

Particle Image Velocimetry (PIV) bases its applications on the simple formula velocity = distance/time. Velocity and distance are both vectors.

Since the air or the water are transparent, the behaviour of the fluid elements can not be observed. Thus, seeding particles are needed to analyze the movement. Typical seeding are smoke, fog, water droplets or metal dioxides in air. The seeding plays an important role because it must allow its visualization with the use of light and it must follow any pattern of the fluid. The light for visualization can be provided by different sources such as a candle light, bulb, etc. In order to maintain coherence, intensity and monochromatic advantages, Lasers are used to emit light as sheets that then will be scattered. Thus, the scattered light can be gathered using a camera place perpendicularly to the light sheet.

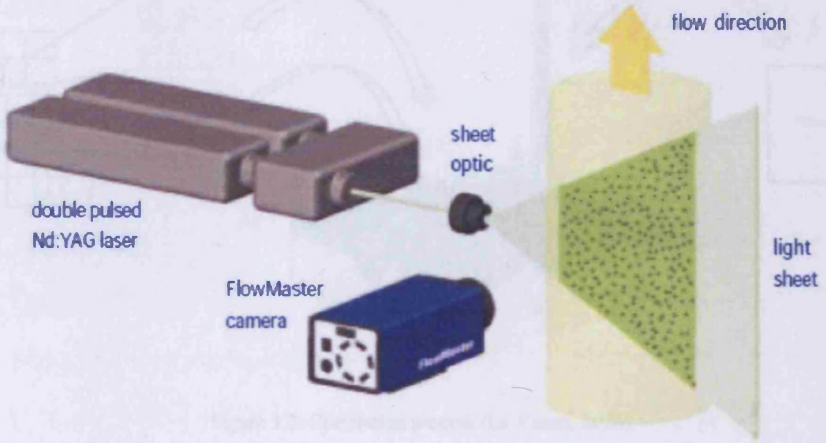

Figure 3.1. PIV Technique (La Vision, 2006)

The light sheet is quickly pulsed for a very short time. A photographic frame can be taken, freezing the position of the particles at that instant moment. A second light sheet is emitted, and another frame recorded, showing the position of the particle at that moment. Knowing the time between both pulses, with the initial and final position of the particle, velocity and displacement vectors are obtained.

The program divides the whole frame into small areas called *interrogation regions*. In each one, the displacement of groups of particles between frame 1 and frame 2 is measured. This is repeated for every region until the whole field is built up.

To find the displacement, the process is called *cross correlation*, applicable to 2 frames PIV. This only denotes the form of the pattern/relationship. In PIV, the pattern is the common displacement between many pairs of particles in an interrogation area.

The correlation plane is found by processing the randomly distributed seeding particles, identified as bright grey scale in a dark background, using a mathematical algorithm based on Fourier Transforms. The former distinguishes the common displacement between pairs of images as a peak. After multiple peaks are detected, especially the first and second highest, a subpixel interpolation is carried out to define where is located the highest of them. Finally, a velocity vector is displayed in less than 0.38 ms for a cross-correlation.

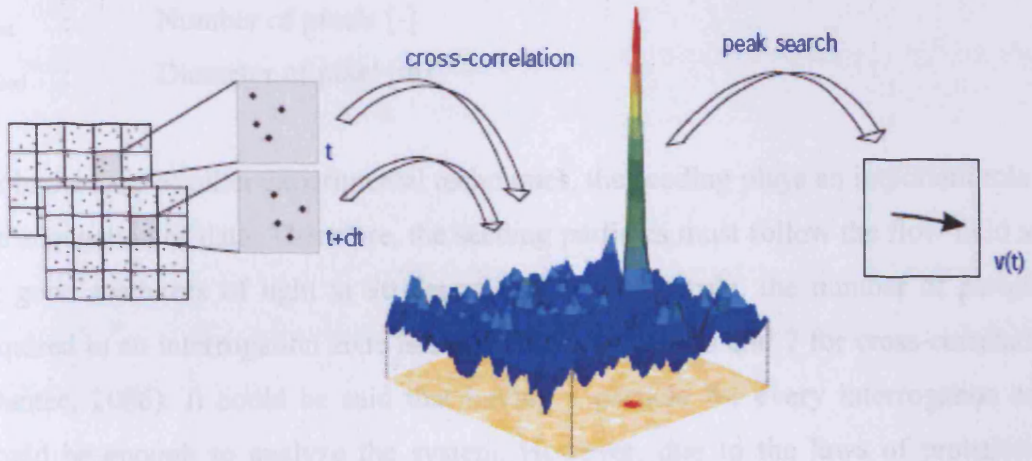

Figure 3.2. Correlation process (La Vision, 2006)

The number of vectors is also important, since they are related to the number of results that we can get from the analysis. This number is dependent on the number of pixels in the camera array and the size of the interrogation region. An interrogation area typically has a size of 32 pixels in cross-correlation and 64 in auto-correlation.

It is highly probable that if a particle has an image near the outer edge of its interrogation area, its pair may be in a neighbouring interrogation area. Therefore, the best way to deal with the problem is to overlap interrogation areas, maximizing the use of available information (Dantec, 2006).

Since the technique measures velocity, the term resolution focuses on the smallest velocity structure in the flow field, which is defined by the size of the interrogation area. Also, the time between pulses must be so small to allow "instant" velocity vectors instead of average ones.

Therefore, with the following equation we can define the maximum distance that can be measured with any equipment (Dantec, 2006),

$$d_{max} = Mv_{max}t \leq 0.25N_{int}d_{pixel} \tag{3.13}$$

d_{max} : Maximum distance between particles [m]

M : Magnification factor [-]

v_{max} : Maximum velocity [m/s]

t : Time [s]

N_{int} : Number of pixels [-]

d_{pixel} : Diameter of pixel [m]

As in the case of other experimental techniques, the seeding plays an important role in the acquisition of data. Therefore, the seeding particles must follow the flow field and be good scatterers of light at 90 degrees. In a thumb rule, the number of particles required in an interrogation zone is 12 for auto-correlation and 7 for cross-correlation (Dantec, 2006). It could be said that having 1 particle for every interrogation area would be enough to analyze the system. However, due to the laws of probability, there will be areas with 2 particles and some other with zero, presenting a problem.

Other characteristics that the particles must have are good efficiency to scatter the light, a good particle size distribution with a well defined average (so the light can be uniformly scattered) and spherical surfaces (so the scattered light will not depend on the position of the particle (Dam, 2008)). The scattered light could be analyzed using the Mie-Lorenz Theory. However, the multiple scattering effect does not allow us to use this solution, since it only relates to perfect spherical particles. Thus, another approach must be used where the scatting efficiency is proportional to the diameter squared of the particle. For that reason, the particles must be as large as possible, without affecting their capacity to follow the flow. Fading of the image can also represent a problem. If there are many seeding particles between the plane and the camera, the consequence can be the re-scatter of light, so the final image can be distorted, producing an unpleasant signal-to-noise effect.

The need of powerful Lasers is recommended Double cavity Nd-YAG (solid state) lasers are generally used for air flows. In PIV, these Lasers are Q-Switched. That is,

instead of emitting the lasing energy for the entire duration of the exiting flash lamp, the cavity is closed for the majority of this time and it is allowed to open for a brief period. The mechanism that quickly opens the cavity is called a Q-Switch. This builds up the lasing energy, and so a high energy beam is released. These mechanisms have a pulse duration of 5-10 ns. Because there is a trade-off between the energy to build up and the natural dissipation of the cavity, the Q-Switch must be fired for about 150-200 microseconds. Thus, the short duration beam will illuminate the seeding particles virtually instantaneously. However, almost all YAG lasers emit infra red light. Thus, the laser must be frequency doubled with a second harmonic generator, which doubles the frequency of the laser light (to 1064 from 532 nm).

Because it is unpractical to use a pulse every 0.1 s in most of the PIV applications, another way is to double the number of beams that the equipment can generate. The way to do this is using Double-Q-Switches. This allows the emission of 2 laser beams with a single flash lamp.

In the double cavity lasers, the use of 2 separate lasing cavities allows 2 beams independent one from each other, with independent time intervals to analyze the PIV images accordingly to the needs of the experiment.

However, it is important to move the equipment close to the measurement, because if the distance between camera and light sheet is doubled, the amount of light will be decreased by a quarter (inverse square).

Even though this technique is quite accurate, there are some sources of error that can affect the final data. Some of them are,

- Random correlation noise: This is when the program can not identify the particle in the second frame, and correlates its position to another particle. This can create inaccuracies in the final results. To avoid it, several filters of noise have been incorporated into the PIV programs (Dantec, 2006). Nevertheless, they are not infallible, and there is noise in the measurements that can not be eliminated. Therefore, size, amount of seeding particles and size of the interrogation zone must be set up in order to reduce as much as possible this problem.

- Particles straddling interrogation boundaries: When particles in the second frame are in the boundary of the interrogation zone. This can be solved by overlapping the frames. This can create confusion when analyzing the data.
- Unpaired particles: Some particles may appear in the first frame, but not in the second due to their movement to another interrogation zone. This can be solved by overlapping the frames.
- Badly scattered light: This occurs when particles scatter the light inefficiently, emitting a very small amount of reflected light. These particles will not contribute in the final result. This can reduce the accuracy of the data.

According to Raffel et al. (1998) and Schreel (2008), the settling velocity of the particles and the flow must be comparable, ensuring the visualization of the flow correctly. If the settling velocity is negligible compared to the flow velocity, the particles are suitable. Thus, the settling velocity of the particle can be defined by,

$$u_{\infty} = \frac{g d_p^2 (\rho_p - \rho_f)}{18\mu} \tag{3.14}$$

Where d_p and ρ_p are the particle diameter and density respectively, μ and ρ_f are the fluid viscosity (dynamic) and density respectively and g is the acceleration due to gravity.

PIV in the combustion community has been widely accepted for the resolution of a great variety of problems. The combination of this technique with other measurement systems such as PLIF, Chemiluminescence Spectroscopy, High Speed Photography, etc. can be able to reveal a deeper understanding of the primary phenomena developing during the burning process (Van der Meer, 2008).

3.4. High Speed Photography

High Speed Photography (HSP) is based on taking pictures of very fast phenomena. It has been defined by the Society of Motion Picture and Television Engineers (SMPTE) as photographs captured at rates higher of 128 frames per second.

Digital cameras have been used for a long time. The technology has been evolving for the last decades, with the principle based in the context of pixels of a Charge-couple

device (CCD) camera which is an analogue shift register that enables analogue signals to be transported through successive stages controlled by a clock signal, digitalizing them in the camera. These can be used as a form of memory or for delaying sampling signals. Usually they are placed in arrays as photoelectric light sensors. Digitalization often occurs at 8 bits, which is related to the number of colours (or gray levels) perceptible by the device (2^8 = 256 colours or tones). Since there is no analogue protocol to which one must adhere to images can be taken randomly or triggered (Schreel, 2008). The introduction of the CCD camera in 1980 allowed higher resolution. The scanning artefacts were eliminated by the use of the sensors. The addition of image intensifiers allowed the capture of thousands of frames per second (Pendley, 2002).

HSP is based on the use of extremely fast cameras. Such equipment can acquire a large succession of images in a very short time. However, their use in flow visualization is limited to the tracking of a low number of particles because of their limited resolution, sacrificing resolution for frame rate.

The storage of digital images has also allowed the acquisition of large number of frames per second, filling the main memory of the computer often in less than a second. Modern cameras can operate at more than 3000 frames/s resulting in a massive stream of data ~6 GBtyes/s.

3.4.1. Optics

The use of different devices during the acquisition of images with CCD cameras is required for the appropriate magnification and quality of the images obtained. Some of the most used optical diagnostics are the optical lenses and bandwidth filters, whose properties permit the selection of a proper volume of study with magnification/reduction of the latter, spatial resolution of the system where one wishes to carry out the experiments of interest and selection of wavelengths for the correct correlation of images based on the desired scalar or vector parameter to be analyzed.

Optical lenses have different parameters that must be considered when performing an experiment such as the focal ratio, depth of field, focal length, etc. This information must be documented in order to establish the appropriate conditions for the study.

- Focal length is a basic parameter defined by the geometrical characteristics of the lens of interest. It defines how strongly it converges (focuses) or diverges (diffuses) light. The point where light converses (or diverges behind the plane where diffusion is produced) is known as the focal point.
- The F-number. Sometimes called focal ratio, f-ratio, or relative aperture of an optical system, it expresses the diameter of the entrance pupil in terms of the effective focal length of the lens; in simpler terms, the f-number is the focal length divided by the aperture diameter.
- The depth of field (DOF) is the portion of a scene that appears sharp in the image. Although a lens can precisely focus at only one distance, the decrease in sharpness is gradual on either side of the focussed distance. DOF of camera lens is given by Adrian (1991) as,

$$\delta = 4(1 + M_f^{-1})^2 (F)^2 (\lambda) \tag{3.15}$$

Where M_f refers to magnification of the lens, whilst λ is the frequency of the laser used for any flow visualization technique.

These parameters are used for the correct definition of the setup used in the present study.

3.4.2. Interference Filters

Such optical filters reflect one or more spectral bands or lines and transmit others, while maintaining a nearly zero coefficient of absorption for all wavelengths of interest. An interference filter may be high-pass, low-pass, band-pass or band-rejection, allowing different wavelengths to be transmitted according to their optical properties.

An interference filter consists of multiple thin layers of dielectric material having different refractive indices. There also may be metallic layers. Interference filters are

wavelength-selective by virtue of the interference effects that take place between the incident and reflected waves at the thin-film boundaries.

If a thin transparent spacer is placed between two semireflective coatings, multiple reflections and interference can be used to select a narrow frequency band, producing an interference filter. If the spacer is a half wavelength for the desired wavelength, then other wavelengths will be attenuated by destructive interference (figure 3.3). Commercial filters are available with a half-power width of about an angstrom. If the back layer is totally reflective, then the arrangement is called a dichroic mirror, reflecting only the selected wavelength. Figure 3.4 shows different transmitted wavelengths using different filters. The percentage of transmission refers to the amount of light in the specific wavelength that crosses the array.

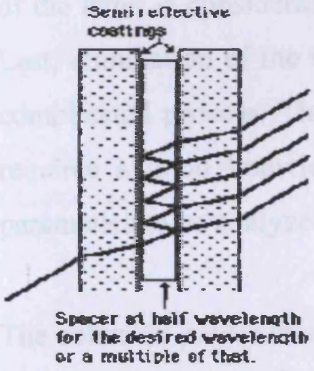

Figure 3.3. Interference filter concept (Nave, 2008).

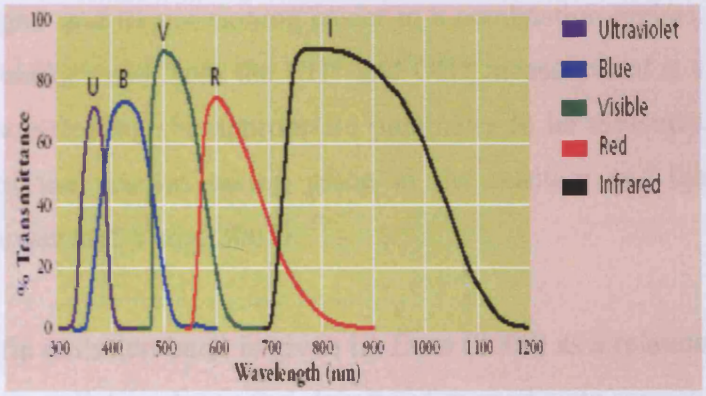

Figure 3.4. Different transmitted wavelengths using different filters (Andover Corporation, 2008).

3.5. Chemiluminescence Spectroscopy

Spontaneous emission spectroscopy or Chemiluminescence Spectroscopy is the most straightforward technique for combustion diagnostics (Dam, 2008). Lenses collect the light emitted by part of the flame onto the entrance of a CCD camera, monochromator or spectrograph. The latter spectrally disperses the incident light, decomposing it in individual components that can be detected by a photomultiplier or a digital camera.

This technique is sensitive only to chemical species that are present in electronically excited states such as CH*, C_2*, CO_2* or OH* radicals that produce visible and ultraviolet emissions in typical hydrocarbon-air flames (Nori et al., 2008). These have an efficient radiative decay channel, so the emitted light is powerful enough to be recorded. The decay of the excited state to lower energy levels is responsible for the

emission of light. In theory, one photon of light should be given off for each molecule of reactant, or Avogadro's number of photons per mole. However, this is never the case. The excited molecules must be present in sufficient quantities to overcome the background luminosity (Lieuwen and Yang, 2005). Emitted light normally presents different frequencies, which makes the use of filter optics very effective.

Chemiluminescence emission from CH* (431 nm) and OH* (309 nm) occur at distinctly different and relatively narrow wavelength intervals (a few nanometres), whereas the CO_2* chemiluminescence lies over a broad wavelength (350-600 nm), overlapping the CH* and OH* spectra. Thus, several considerations must be keep in mind when selecting one specie. CO_2* can be significantly increased by using broad filters, whilst OH* requires ultraviolet optics for the analysis. However, the intensity of the latter is considerably higher and its positioning easier in a combustion regime. Last, elimination of the CO_2* background from the CH* and OH* measurement is a complicated process. Therefore, selecting the appropriate parameter to be measured requires a good knowledge of the process taking place in the reaction and the parameters to be analyzed (Lieuwen and Yang, 2005).

The collected power in a specific emission band is given by Dam (2008) as a relation between the detection efficiency, radiative decay and density of excited state species. Even though the emitted power is proportional to the density of species, this technique is very difficult to calibrate. Moreover, there is a risk of spectral interference, the spectral resolution typically limited by the resolving power of the spectrometer if any is used, making this technique more qualitative than quantitative (Dam, 2008). The spatial resolution is determined by the lenses used for experimentation.

Chemiluminescence imaging is employed to detect flame position, shape and structure in combustors. For combustion dynamic studies, it is often used as a measure of heat release fluctuations, both temporally and spatially. However, the results have to be interpreted and calibrated according to their nature, pressure strain, preheat temperature, equivalence ratios and recirculation, amongst some other factors that have to considered (Nori et al., 2008). Models have been attempted to simulate the presence of the excited specimens under different regimes. However, this is dependent on the reliable kinetic mechanism of fluctuation of the former to achieve

coherent results comparable to experimental findings (Nori et al., 2008). Figure 3.3 and 3.4 show some results obtained using this technique.

Figure 3.3. Chemiluminescence applied to combustion analysis (Paul Schrrer Institut, 2002)

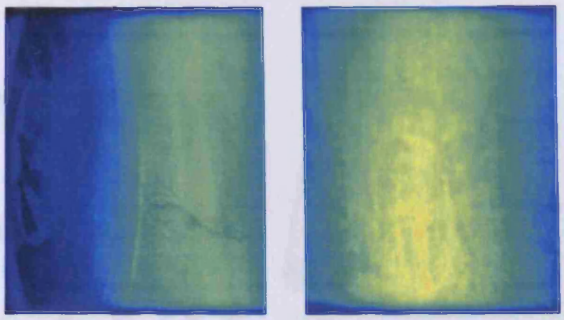

Figure 4.4. Influence of piloting on chemiluminescence for equivalence ratio 0.5 (Faber et al., 2008)

3.6. Summary

In summary, these techniques vary considerably. However, all of them give different parameters important in the definition of coherent structures and analysis of instabilities inside the combustion region. The aid of PIV allows the location of the PVC, CRZ and other recirculatory zones, whilst Chemiluminescence and HSP permit the recognition of regions of high combustion intensity where the exchange of energy and mass takes place, allowing a more complete characterization of the system. The triggering of the system can be achieved via flow speed or pressure fluctuation, depending on the conditions of the experiment to be analyzed.

CHAPTER 4

ISOTHERMAL EXPERIMENTS

4. ISOTHERMAL EXPERIMENTS

"A theory is something nobody believes, except the person who made it. An experiment is something everybody believes, except the person who made it."

Albert Einstein, physicist (1879-1955)

The objective of this experiment was to analyze different coherent structures and their evolution in space under different conditions. The use of techniques such as PIV and HWA allowed the reproduction of tomographies of the former by recording different planes. Phase Locking the PIV system with high peaks of velocity produced by the high momentum compressed region between the wall and the PVC, was used. A special Camera recorded the phenomenon under a quasi stable condition in space.

4.1. Experimental Setup

A 100 kW Perspex swirl generator was used to investigate the phenomenon. This was based on a quarter scale model of a 2MW industrial scaled swirl burner/furnace system. Figure 4.1 and 4.2 show the prototype and geometry drawing, respectively. Two tangential entries together with variable inserts allowed the measurement of different swirl numbers and their effects on the PVC. The system was fed by a centrifugal fan providing air flow via flexible hoses and a bank of rotameters to measure the airflow rate.

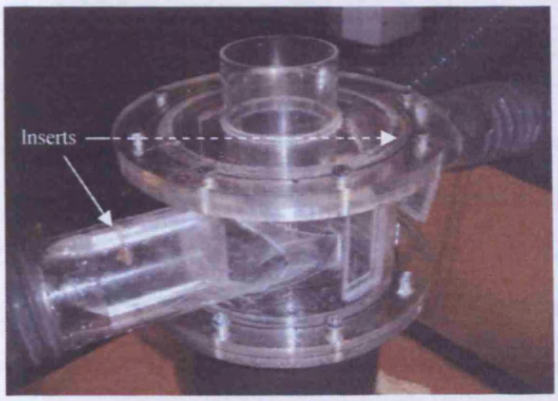

Figure 4.1. Experimental Rig.

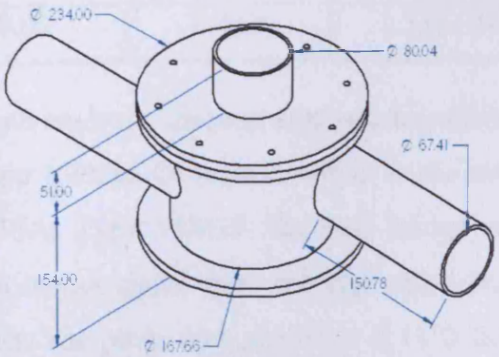

Figure 4.2. Geometry of the Rig.

Each inlet had an insert, figure 4.1, that could be changed to alter the swirl number. Two different widths of inserts could be used, a pair of 50% of the diameter of the inlet and a pair of 25%. Also, the configuration with no insert (0%) could be analysed.

According to previous experiments (Valera-Medina, 2006), some insert combinations at different Re showed the existence of bifurcations and even trifurcation based on the number of strong harmonics recorded. Therefore, various configurations were especially studied to elucidate the underlying mechanisms. Configurations investigated are shown in Table 4.1. The objective was to recreate 3D bodies of the structures to characterize their shape and behaviour. The condition selected was [25-25], i.e. 25% blockage in each inlet, at a flowrate of 1,400 l/min. This has been shown by Fick (1998), Syred (2006) and Valera-Medina (2006), to be a very stable condition. In order to present a proper comparison between cases, other configurations at different flowrates were also selected (PVC2). Other chosen conditions enabled comparison of the stability of the coherent structures and the flame when asymmetry of the flow occurred at the same swirl number (i.e. See configurations PVC2 and PVC3, Table 4.1). Finally, PVC4 was analyzed in order to distinguish the type of flow occurring close to vortex breakdown.

Table 4.1. Different insert combinations

No. of Combination	Inserts Used (%)	Flowrate (l/min)	Swirl number ( )	Re number ( )
PVC1	25 – 25	1400.00	0.985	2.67E+04
PVC2	25 – 25	800.00	0.985	1.53E+04
PVC3	50 – 0	1600.00	1.059	3.05E+04
PVC4	0 – 0	800.00	0.659	1.53E+04

Once the rig and inserts were in place for each analysis, the next step was to calibrate the Hot Wire Anemometer that would trigger a Pulse Generator, which at the same time would trigger the PIV system. A DISA, Type 55M10 Standard bridge was utilized with 55P16 Hot Wires to obtain an output signal from the high momentum region near the vicinity of the burner exhaust. The probe was placed at -0.12 D from the outlet, positioned orthogonally to the tangential axis and 1.00 D from this radially. Greater sensitivity was found when orienting the probe in the tangential direction. To calibrate the Hot Wire, its initial values must be setup to zero. Using a dummy probe

the calibration resistance was found. Plugging in the Hot Wire to be used, the previous value must be multiplied by the factor (1+*a*) to obtain the sensor resistance at the operating temperature (DISA, 1995). This value, 1.8, gave the final resistance of the sensor, 6.58 Ω.

A *Dantec DISA 55D26* Signal Conditioner was used with a Low Pass Filter configuration, filtering frequencies up to 125 Hz. In order to improve the outgoing signal, a gain of 10 provided a stronger data for triggering purpose. The system was monitored using a *Tektronic DS2024B* Oscilloscope at 2 Gsamples/s, 200 MHz and four channels. The former was used to trigger a *BNC Model 500 Pulse Generator* which would produce a TTL digital signal every time that the filtered signal reached a designated level of 90% of the highest peak recorded after 5 minutes. This value is recognised to be arbitrary but consistent within all the measurements.

This lead to a Phase Locked Particle Image Velocimetry (PIV) system locked by the filtered signal. The pulse was then redirected to a Nd: YAG Litron Laser of 532 nm, 5 Hz and to a Hi Sense MkII Camera model C8484-52-05CP, with 1.3 MPixel resolution at 8 bits. A 60mm Nikon lens was used for resolution purposes, with a depth of view of 1.5 mm. The system was seeded by a water Nebulizer. Figure 4.3 shows the system with all the output signals.

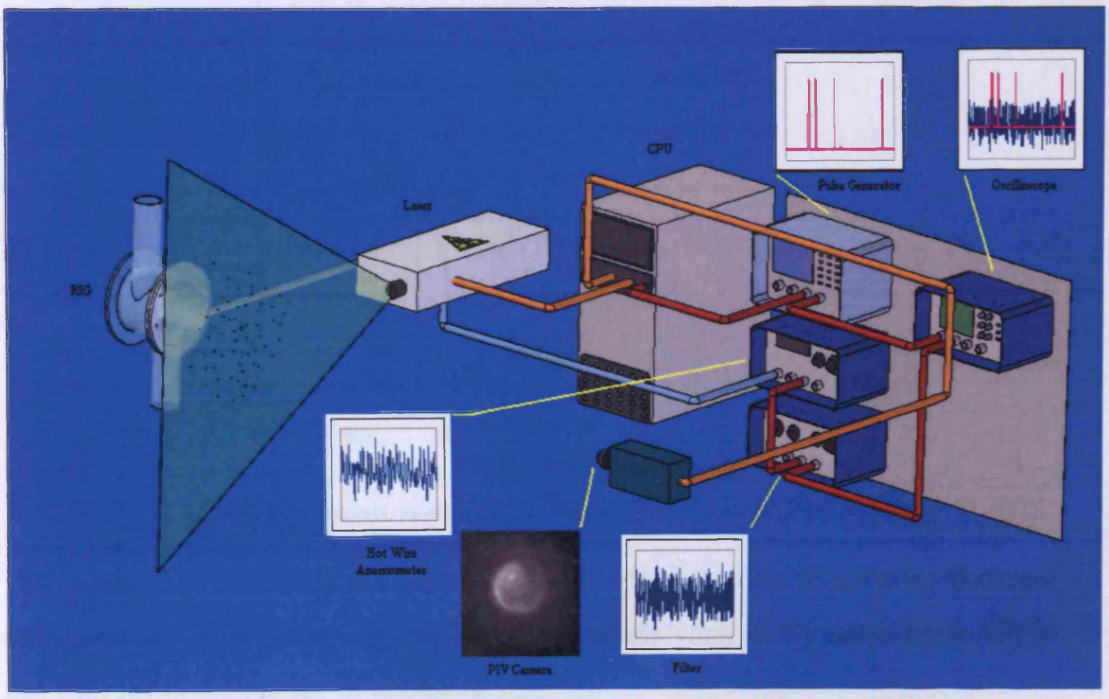

Figure 4.3. Experiment Setup

4.2. Experimental Approach

4.2.1. Preliminary reconstructions

PVC1 gave a very consistent signal at the oscilloscope. The highest level was established at 2.50 V, with a triggering point of 2.25 V in the Pulse Generator. Figure 4.4 shows the output signals and how the system was triggered at the highest velocity values.

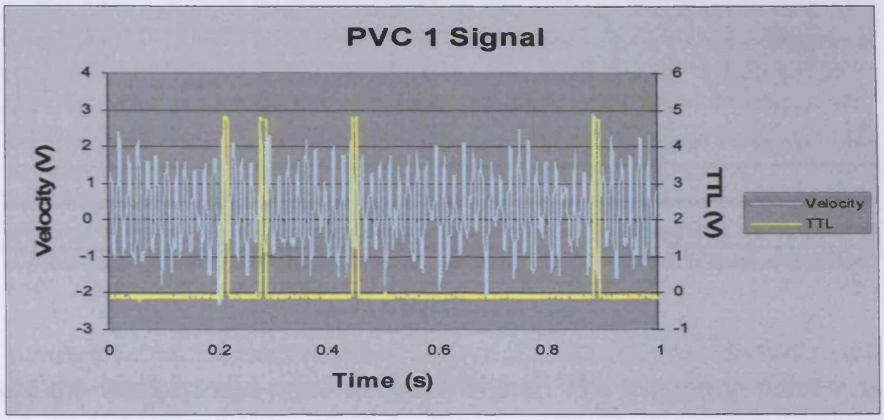

Figure 4.4. PVC 1 Output Signal.

The results obtained and the periodic shape of the signal made evident the existence of a precessing movement. Figure 4.5 shows the FFT data with the first harmonic at 55 Hz. High coherence was expected from further analysis.

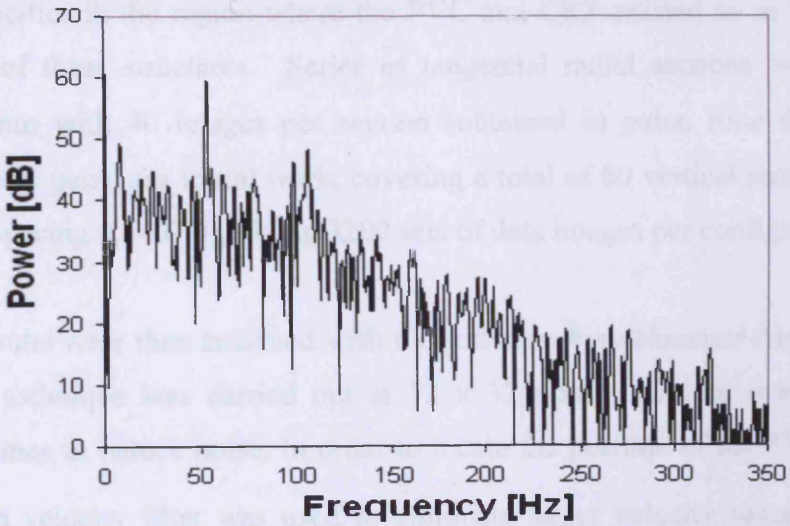

Figure 4.5. FFT Analysis, showing the presence of strong harmonics at 55.0 and 110.0 Hz.

PVC2 had less stability and presented various small peaks and frequent fluctuations, even with the filter. However, the strongest levels were of the same order of PVC1, but with lower frequency of appearance.

PVC3 was more irregular but of higher frequency than the previous cases, due to the higher flowrate. As in previous cases, the highest value was set at 3.00 V with a triggering point of 2.70 V, as observed in figure 4.6.

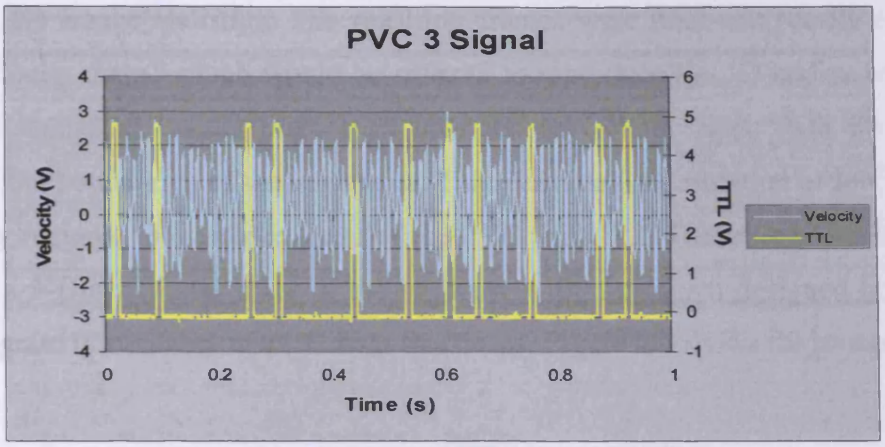

Figure 4.6. PVC 3 Output Signal.

PVC4 gave the weakest and more irregular signal. The triggering point was found to be 1.90 V, 15% less than in previous cases, doubtless related to the weak swirl and low Re used, as well as nearness to the onset of the vortex breakdown phenomena.

Experimentally a series of measurements were obtained at different positions with these TTL signals. In the tangential plane, the objective was to recognise the position of zero velocities in the region where the PVC and CRZ existed so as to define the boundaries of these structures. Series of tangential radial sections were analyzed every 3.25mm with 40 images per section (obtained in pairs, time delay 20 μs between image pairs) for initial work, covering a total of 80 vertical sections (from 0 to 3.175D, spacing 0.0407D), giving 3200 sets of data images per configuration.

The PIV results were then analyzed with the software *FlowManager* from Dantec. A correlation technique was carried out at 32 x 32 pixels, with an overlap of 50% between frames to reduce noise. In order to locate the position of the PVC and other structures, a velocity filter was used to eliminate larger velocity values ($\sqrt{U^2+V^2}$, where U and V are radial and tangential velocities, respectively) beyond 0.000 and 3.000 m/s, to initially define structure boundaries, being based on the contour distribution in the images. Another second filter was also used to move the average of the vectors and align them to follow their closest neighbours, compensating errors in

correlation. An average of 31.66% and 21.27% of total elimination was obtained using the first filter for small and high Re, respectively. The second filter substituted 6.70% of the remaining vectors. This made clear that more frames were needed to improve the image statistics. The resulting frames were used statistically to create mean velocity maps, which would be utilized to reproduce the 3D bodies whilst the vectorial statistical results were then changed to contour maps with 30 colours defining the boundaries of the structures. This permitted the isolation of low velocity boundary regions, for instance those of the PVC and CRZ. These were overlapped to recreate a 3-Dimensional body of the structure with a program designed in *Matlab*. This program is available in a CD with this thesis. Figure 4.7 shows the procedure.

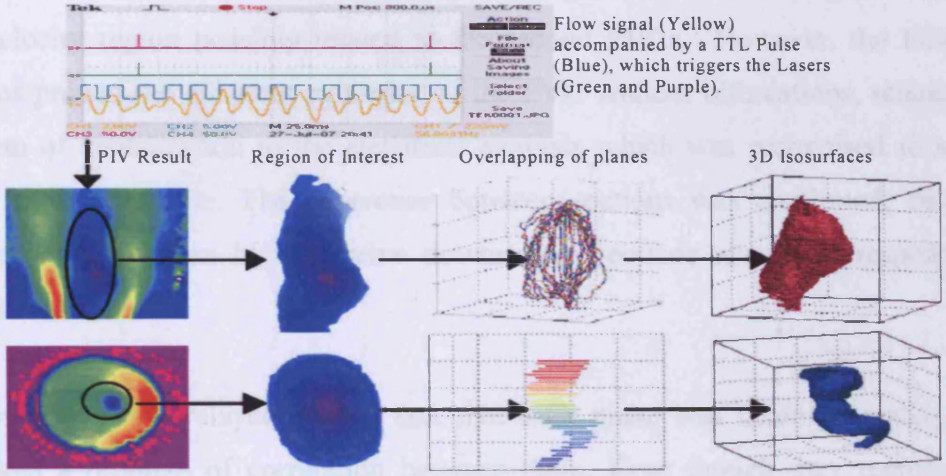

Figure 4.7. 3D reconstruction.

Figure 4.8 shows one of these maps at 0.00 D for PVC1. The purple and navy blue areas are zones of very low velocity in the range of 0.000 to 0.372 m/s. Although they effectively show the PVC boundary, the location of the Crescent moon shaped region of high velocity that is triggering the system is not completely visible due to the filter used to eliminate higher disturbances. The irregular shape of the outer region of the PVC is related to the image statistics. 12,000 frames (since the fourth case only had 60 planes) were used to re-construct the 3 dimensional body of all the PVCs.

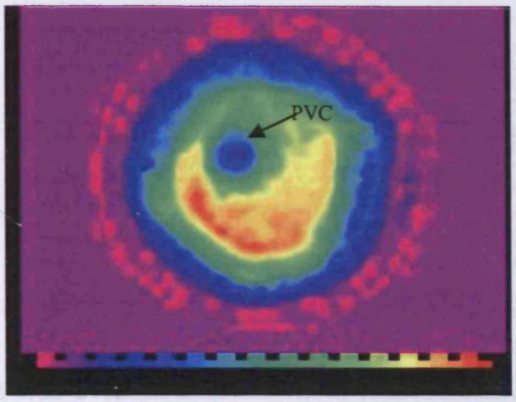

Figure 4.8. Contour map of plane 0.00 D for PVC 1.

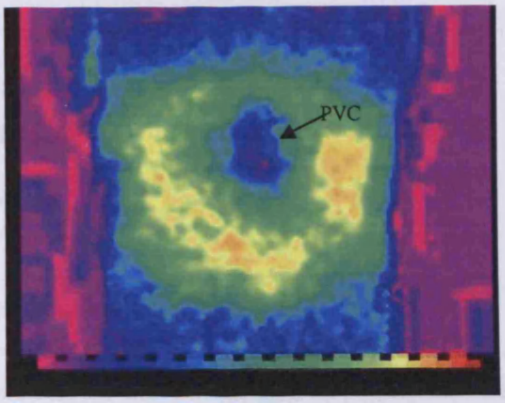

Figure 4.9. PVC1, apparent bifurcation in the Vortex, plane 0.31 D. Following section corroborates no bifurcation.

Some of the results showed the existence of complex bifurcations (Figure 4.9) in the low velocity region possibly related to the second PVCs. However, the following sections proved the coherent existence of the PVC without bifurcations, relating this problem of visualization to the statistical analysis which was recognised to require more frames per case. The coherence between sections was confirmed, since the position of the vortex in successive downstream sections always corresponded to those below them.

The main problem relayed on the fact that each plane was taken separately. This provoked a problem of correlation between them. Even though they represent the same instability in space, they belong to different bodies in time. Therefore, an interpolation technique was used to smooth the graph for the PVC analysis. The correlation was performed using 2 planes separated by another one, which will become the "new plane". The idea was to take several points from plane "1" and plane "3" measured from each centre of mass to form pairs, generating radiative lines between points. The angle of these lines would be the correlation factor between different planes. The distance between each pair of points would be interpolated at the middle to give the position of the point in the "new plane". The new centre of mass would be placed between the centres of mass of the known slices. The "new plane 2" will become plane "1" in the following cycle. A scheme is shown in figure 4.10. However, it only functions with elliptical/oval shapes and high correlation between sections, as found for the PVC.

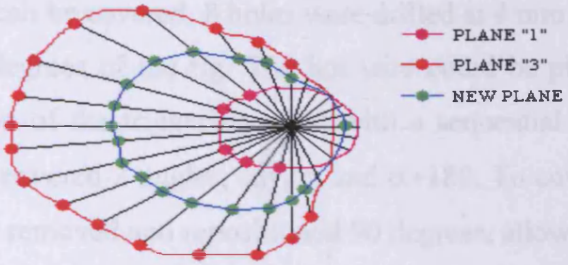

Figure 4.10. Correlation technique between planes.

It was evident that the most representative portion of the vortex lies between the first 40 slices after the first analyses. Thus, the smoothing analysis was only done for these planes, which represents 1.67 D downstream the nozzle. The resulting 3D bodies can be seen in Figure 4.11 to 4.14.

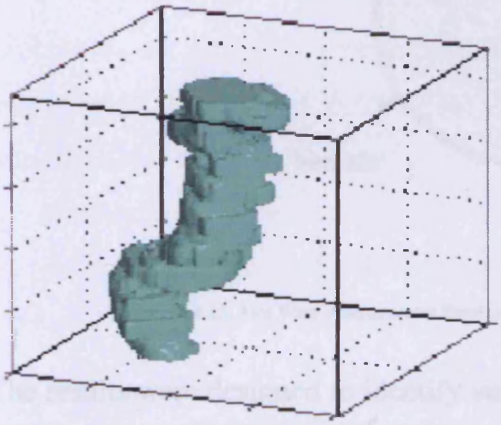

Figure 4.11. 3D Reconstruction of PVC1.

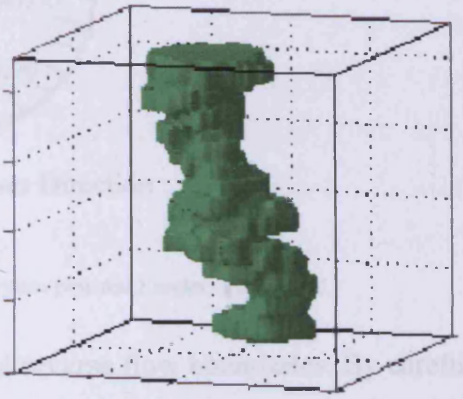

Figure 4.12. 3D Reconstruction of PVC2.

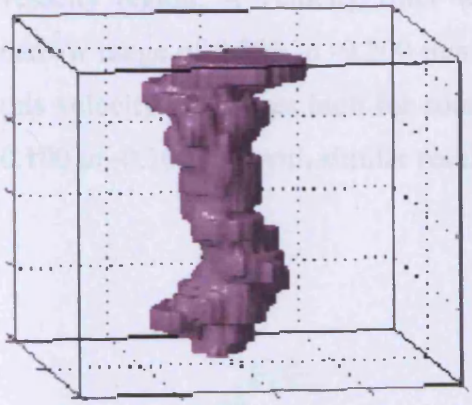

Figure 4.13. 3D Reconstruction of PVC3.

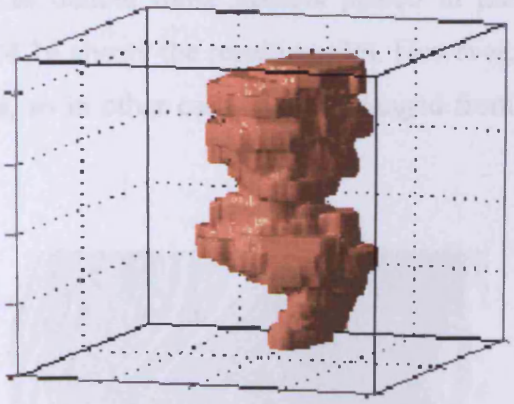

Figure 4.14. 3D Reconstruction of PVC4.

These experiments showed the precessing vortex core but only traces of the central recirculation zone. Therefore, the only manner to visualize the recirculation zone was to perform an axial-radial analysis in a similar manner. The difference relayed on taking images of the axial at various radial positions so the whole range of 360

degrees of the outlet can be covered. 8 holes were drilled at 4 mm upstream the outlet, only in the first 90 degrees of the rig. The hot wire could be placed in all of them diphasing the position of the triggering point with a sequential increment of 11.25 degrees. Each frame covered 2 angles, say, α and α+180. To cover the entire range, the top of the rig was removed and repositioned 90 degrees, allowing the triggering of 16 different sections and 32 different views of the field. Figure 4.15 shows the positions of the HWA during the experimental trial.

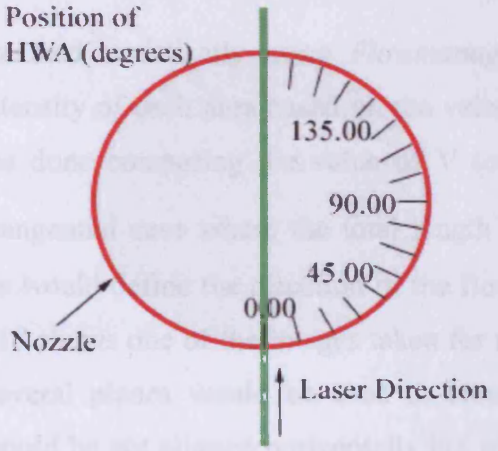

Figure 4.15. Hot Wire Anemometer Position. Each axial plane provided 2 angles, α and α+180.

The results were designed to identify vortices and reverse flow boundaries. By careful analysis of the data, a quantitative boundary for the CRZ was defined via the zero velocity region. A velocity filter was used to denote those vectors placed in the narrow range of 0.200 to -0.200 m/s. Figure 4.16 shows the resulting plot. However, this velocity range was high for some images, so in other cases it was changed from 0.100 to -0.100 m/s with similar results.

Figure 4.16. Vector map from 0.200 to -0.200 m/s. PVC1 at 90 degrees.

Figure 4.17. Streamlines of the flow, PVC1.

The correlation between particles could be matched by using streamlines. The results gave information about the appearance of eddies inside of the CRZ, which were related to the Richard's cascade theory of energy between different length scales in turbulent flows. However, this is only a qualitative interpretation of the data. Flows inside of the CRZ and PVC have not been quantified here; indeed the concept of a streamline in this complex flow becomes very difficult to analyze, with 3D flow paths extremely intricate to define. Figure 4.17 shows the latter.

Colour maps were obtained statistically using *Flowmanager*. The former gave a precise location and intensity of each area based on the velocity and direction of the flow. The analysis was done comparing the value of V (or the axial velocity), in contrast to the radial-tangential case where the total length ($\sqrt{V^2+U^2}$) was taken into consideration. This would define the direction of the flow showing the CRZ and other eddies. Figure 4.18 shows one of the images taken for the reconstruction. As in the horizontal case, several planes would be used to create a volumetric matrix. However, the planes would be not aligned horizontally but placed at different angles, changing the algorithm of the final program.

These images were used to capture the areas with velocities between zero and negative values, figure 4.7. In the software, the boundaries of the CRZ are used to create the "skeleton" of the 3 dimensional body (Figure 4.19).

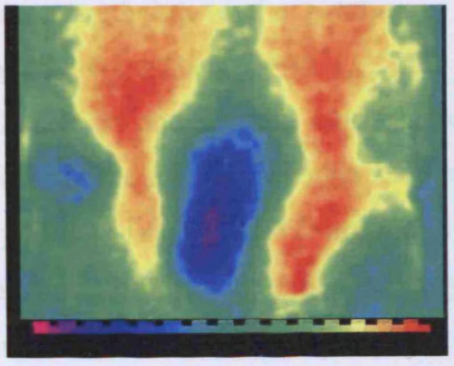

Figure 4.18. Colour map of the Recirculation Zone.

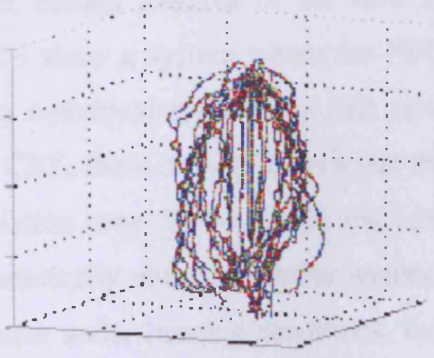

Figure 4.19. Skeleton to create the 3D body.

To extract as much information as possible, 40 pictures were taken of each section as in the radial-tangential case. With a total of 2,560 pictures, these would be used to match the results of the PVC analysis, defining the position and possible co-dependence under isothermal conditions. Each point in the skeleton was linked to its

neighbour (if any; if not to the centre of the array) to create the body. The shape of the CRZ for the first three cases, PVC1 to PVC3, is that of an elliptical lobbed shape close to the burner exit, being located at some distance from the hot wire. This is in agreement with finding of Syred (2006). Analysis of numerous images show that the shape of the CRZ is similar to a light bulb where the middle region presents a convoluted, more voluminous shape, with an upper slimmer, contracted zone. The latter is attached to the rig for PVC1, PVC2 and PVC3. However, PVC4 showed a lifted unattached behaviour, with a very unstable PVC wobbling with periods of expansion and contraction. Since this is the configuration where the vortex breakdown has just taken place, this behaviour is attributed to the unstable nature of the phenomenon with substantive periods of intermittency.

Despite the use of only 40 images per section the structure of the CRZ can be defined, confirming the use of the technique. The CRZ can be seen to be elliptical in shape, whilst in certain sections it extends back into the burner exit. The length of each CRZ could also be compared, being 0.96D (PVC1) and 1.18D (PVC2). This is obviously an effect of Re as the configurations are otherwise the same.

The results from the analysis of the velocity sections in the tangential-radial and axial-radial planes were amalgamated to produce 3D bodies of the PVC and CRZ in all the four cases investigated, figures 4.20-4.23. The relationship between both structures was smeared due to the resolution. However, certain features of the flow are as expected, for instance, PVC1, PVC2 and PVC3 show a system where the PVC and CRZ coexist and interact closely. Contrary to numerical simulations that predict a helical shaped PVC that winds itself about the CRZ, these results showed that there is only little twist of the PVC around the recirculation zone. Syred (2006) and Lieuwen and Yang (2005) have experimentally and numerically obtained similar results for a minimum twist in the lower regions of the flame under burning conditions. Initially the PVC diameter is quite small, followed by an expansion at some downstream sections. There is also a region where the precession stops and the vortex core expands. The PVC and the reverse flow zone appear to rotate together, with the latter being distorted by the former into a more elliptical shape.

The length of the CRZ for a given S can be changed by variations in Re. Even though the pattern followed by the PVC remains constant with a little twist, the elongation of the recirculation zone seems to be a function of the velocity of the flow, which is linked to the increment of radial pressure caused by the phenomenon per se. Also, the case of PVC3 is more compact, with less twist than in previous cases and a more compact CRZ. This suggests that the strength of both structures has increased to the point of avoiding dominance of any of them in the field.

Finally, figure 4.23 shows the appearance of each structure immediately after the vortex breakdown takes place. However, the relation between structures is not clear, with a very irregular shape for the PVC which develops into an expansion-contraction process, whilst the CRZ remains weak and inconsistent in space, lifted well out of the burner exit.

Figure 4.20. Dimensional interaction of the PVC and CRZ, case PVC1, top, left and right views respectively.

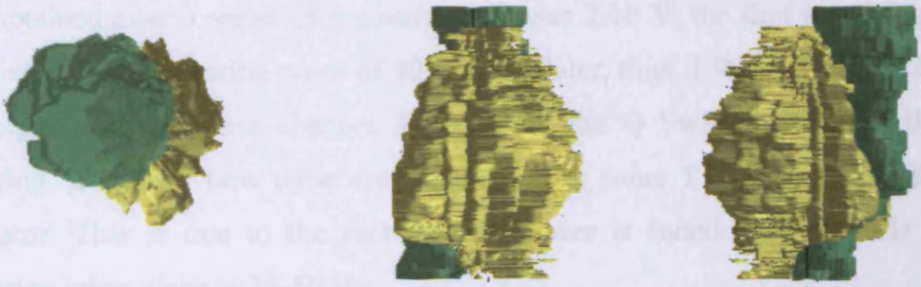

Figure 4.21. Dimensional interaction of the PVC and CRZ, case PVC2, top, left and right views respectively.

Figure4.22. Dimensional interaction of the PVC and CRZ, case PVC3, top, left and right views respectively.

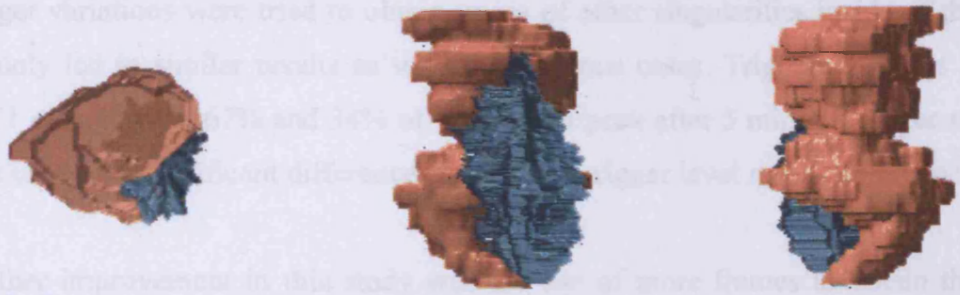

Figure 4.23. Dimensional interaction of the PVC and CRZ, case PVC4, top, left and right views respectively.

4.2.2. Trigger and Statistical variations

Even though the previous experiments show the complete flow under different conditions, all of them were done using the maxima of the signal from the Hot Wire. Therefore, any change or condition at different triggering points is unknown.

Another set of experiments was carried out using variable triggering levels. The objective was to recognise if there was any change in the vortex, projection or inconsistency during visualization of the sections. One hypothesis suggests the existence of double PVCs (Syred, 2006; Valera-Medina, 2006), since the final strength of the phenomenon allows the split of the main core into two or even three vortices.

The case used was PVC1 since this proved to be the most stable of all. The highest level obtained after a series of measurements was 2.10 V, the first set of frames was obtained using a triggering point of 90% of the later, thus, 1.90 V. Figure 4.24 shows the output signals, where channel 3 and 4 are the Q Switch pulses for the Laser triggering. It is clear how these are triggered after some TTL pulses from the Pulse Generator. This is due to the fact that the Laser is functioning at 5 Hz and the precession takes place at 35-50 Hz.

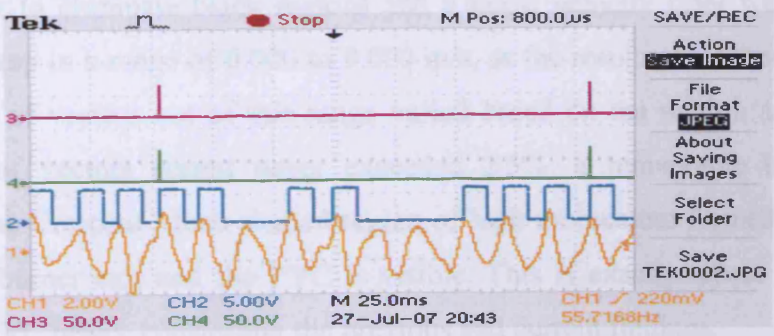

Figure 4.24. Triggering Point at 90% of the highest peak.

Trigger variations were tried to obtain traces of other singularities inside of the flow but only led to similar results as with the previous cases. Triggering points for the PVC1 case at 90%, 67% and 34% of the highest peak after 5 minutes of free running were used. No significant differences to the 90% trigger level results could be found.

Another improvement in this study was the use of more frames to obtain the final sections. In the previous experiment, 40 images per section were used. However, some of the results were blurred or showed poor resolution. Therefore, 150 pictures were used to recreate each section. The statistical analysis denoted a highly improved quality. Knowing that the structures were located in the first 40 planes, the 3D bodies consisted of 6,000 frames. The same methodology was used for the experiments.

The better resolution allowed the avoidance of a second filter to orientate irregular vectors. The same correlation was used as in the previous analysis with 32 x 32 pixels and 50% overlap between frames. Figure 4.25 shows one of the sections obtained with this method. If compared to figure 4.8 the resolution improvement is clear.

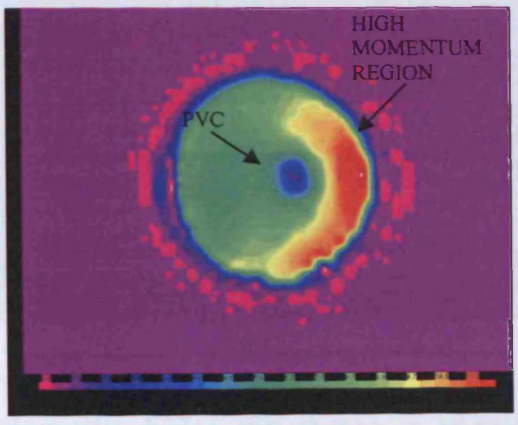

Figure 4.25. 150 frames/section, PVC1, section 0.00 D.

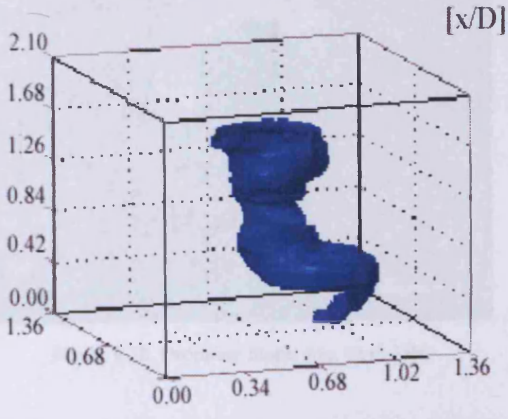

Figure 4.26. Detailed PVC, configuration PVC1. 67% triggering level.

Only a mask to eliminate black regions and a range velocity filter were used. The latter was setup in a range of 0.000 to 9.000 m/s, as the results were more consistent. The number of vectors out of this range varied based on the section analyzed. The percentage of vectors erased never exceeded 2.5%, a remarkable improvement. Moreover, the Crescent Moon shaped region of high momentum formed between the wall of the burner exit and the PVC is visible. This is exactly where the hot wire locates the PVC peaks, confirming the previous and current findings.

A 3D representation of the PVC using the 67% triggering results can be observed in figure 4.26. The PVC behaves as before. The twist is only seen up to 0.60 D from the outlet, spiralling for some 70-90 degrees from its origin, then straightening. If these results are compared to figure 4.10 with poorer statistics, the same trend is noticeable. Since little filtering was used, this gives considerable confidence in the results. Scaling of the structure was more accurate and definition of the real shapes more accurate.

No bifurcations or projections were observed. Confidence on the results and triggering variations can be observed in figures 4.27 and 4.28, where the flow was visualized using signals from opposite sides of the burner. As expected, the structures are opposed to each other. Thus, a statistical analysis changing the triggering value or position is not the best manner to characterize sporadic manifestations such as double PVCs, since they are eliminated in the mathematical process.

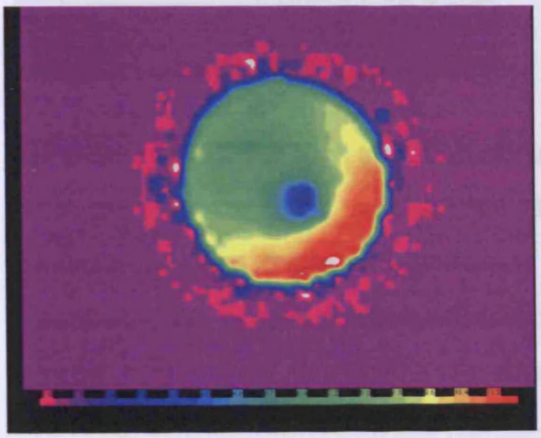

Figure 4.27. Rising Slope, trig. level 34%

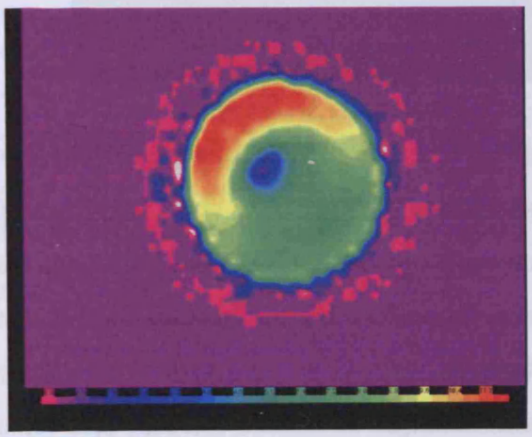

Figure 4.28. Dropping Slope, trig. level 34%

However, during the change in triggering values another process was found. The higher resolution showed that the region where the PVC stopped spiralling was where enlargement of the PVC section occurred at ~0.45-0.60 D. The PVC appeared to keep rotating up to ~0.45 D without any constraint. At this point, two smaller vortices appeared inside of the PVC envelope. They then increased their size and strength to a point where they dominated the flow. At this point, both vortices joined and merged as a single stronger vortex. This vortex then went straight upwards with considerable coherence. Figure 4.29 to 4.32 show the development of both structures until they merge as a single stronger vortex.

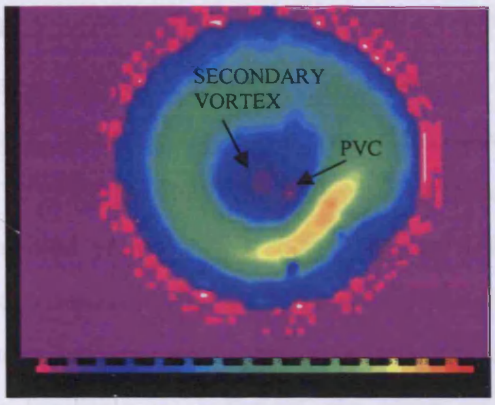

Figure 4.29. Plane 11, trig. Level 67%.

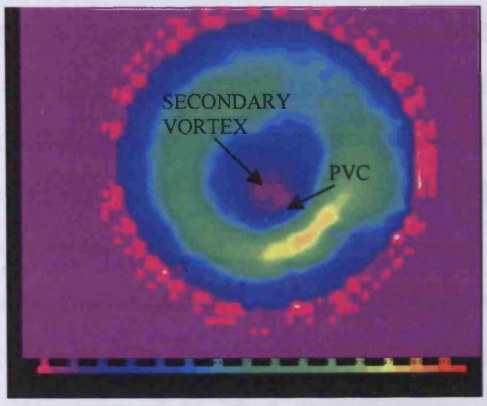

Figure 4.30. Plane 12, trig. Level 67%.

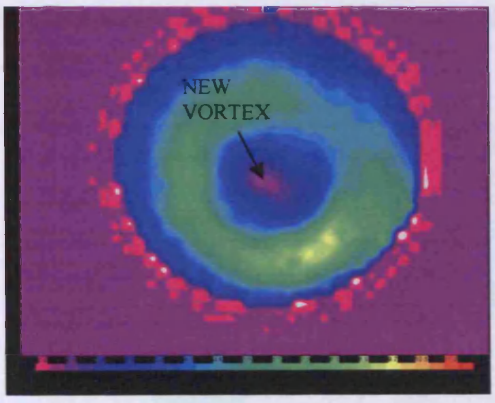

Figure 4.31. Plane 13, trig. Level 67%.

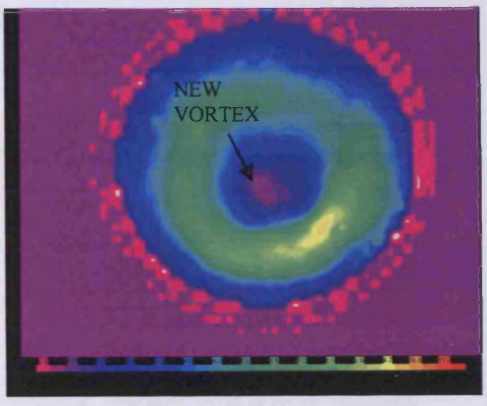

Figure 4.32. Plane 14, trig. Level 67%.

The axial analysis for such configurations using different triggering levels was carried out in the same way. The total number of pictures per body was 2,400. The enhanced resolution allowed better recognition of the shape of the CRZ. Since the flow was unconfined, no Corner Recirculation Zones (ERZ) were observed. Although some external eddies were detected, their appearance was attributed to Kelvin-Helmholtz instability in which the difference in viscosity and velocity of two co-adjacent flows generates these structures. The latter were not considered in the current study. Figure 4.33 shows one of the images obtained from the statistical analysis performed using 150 frames/section.

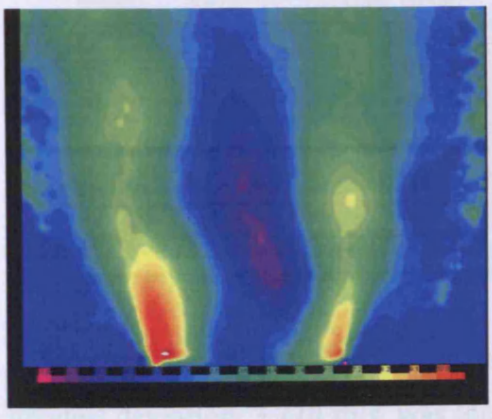

Figure 4.33. Plane 4, triggering Level 90%.

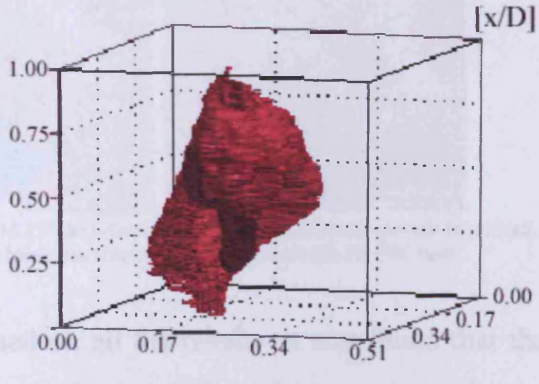

Figure 4.34. Recirculation Zone. Canal highlighted.

Data were again obtained every 11.25° for comparison purposes. The velocity filter range used was set between -3.000 and 11.000 m/s, giving a percentage substitution of only 1.5%. Better definition of the zero boundary region was immediately achieved. The CRZ is coherent and well defined, of lobed shape, similar to those previously derived. The lowest region of the CRZ passes back into the swirl burner exit. A convoluted region with a contraction was found in the middle of the CRZ, creating an intermediate canal, ending with a sudden contraction at the top, figure 4.34. Darkened to facilitate its location, the canal at the middle seemed to be a manifestation of another structure associated/linked with it, i.e. the PVC.

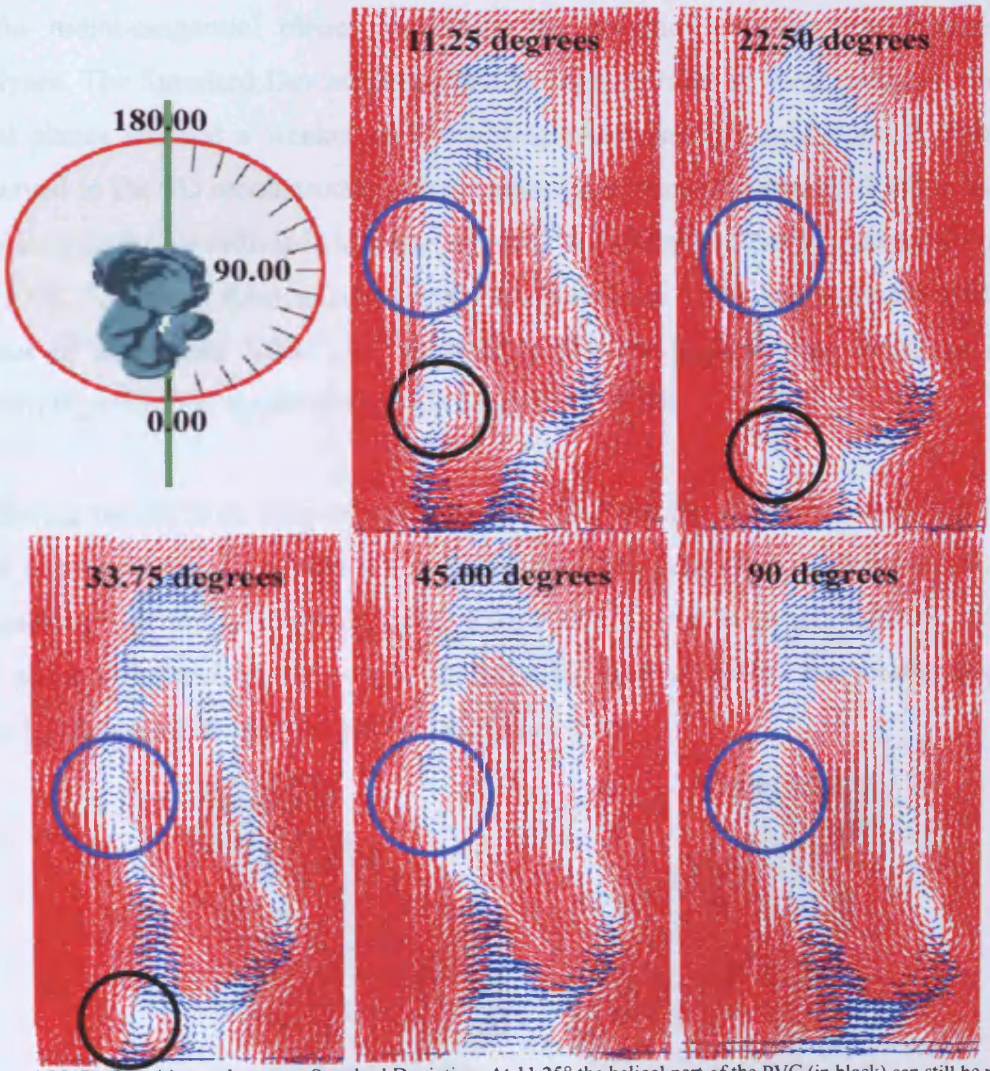

Figure 4.35. PVC position and greatest Standard Deviation. At 11.25° the helical part of the PVC (in black) can still be noticed. However, at 90.00° only the remaining straight part (in blue) was noticed, as expected from the 3D PVC body.

A standard deviation analysis was performed on all the results. It was found that the greatest deviation, 3.214 m/s, was located in the lowest region of the structure where a

vortical entity appears, figure 4.35. This is thought to be linked to the presence of the PVC. The lowest values were 0.959 m/s, located at the top of the CRZ. The rest of the boundaries showed a standard deviation in the range of 1.200 to 1.800 m/s. Although it is considered that the structure is highly coherent, a flapping movement is revealed by these measurements. Moreover, it also showed that there is considerably interaction between the PVC and CRZ in only specific localized regions (marked in black), suggesting greater coherence in the remaining boundaries.

First axial planes of figure 4.35 showed a very strong precessing vortex (highlighted in black) which moves upstream and disappears according to the 3D results obtained in the radial-tangential plane, confirming the accuracy between both independent analyses. The Standard Deviation reached its highest value in these positions. Further axial planes showed a weaker and wobbling recirculation (highlighted in blue). As observed in the 3D reconstruction, these planes are where the straight PVC is located, thus confirming its reduced exchange of mass in comparison to the twisting section of the PVC. However, these points are still places where the standard deviation reaches values of more than 2.000 m/s, confirming that the highest mass exchange in the system is performed by the interaction of the PVC-CRZ.

Gathering results from both experiments, the CRZ and the PVC were matched. Figure 4.36 shows the real flow with the appearance of two very strong, coherent structures. From the triggering level results of 90% for PVC1, it is evident that the PVC matches the portion defined by the canal in the CRZ and confirms the relationship and interdependence between the structures, figure 4.36.

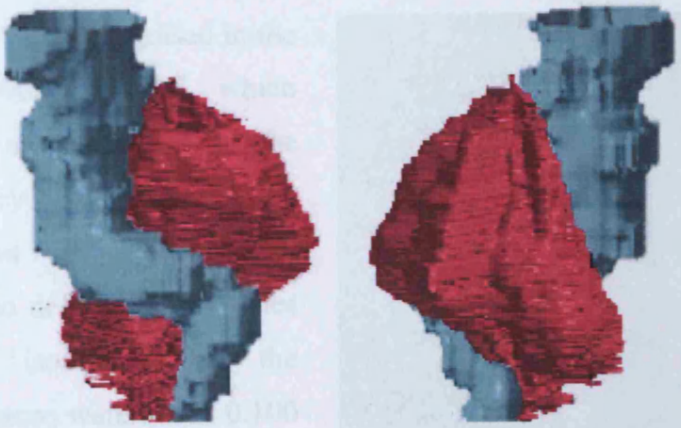

Figure 4.36. The flow. 90% triggering level, PVC1 configuration.

4.2.3. Confined Conditions. Square Case.

The effect of burner exhaust confinement on the system was the next step in the investigation. Square and circular confinements were studied with different outlets since these configurations are extensively studied and analyzed (Farber et al., 2008; Selle et al., 2006).

The first confinement had a square transversal area of 2.00x2.00 D^2. Its total length was designed to be larger than the total visualized length of the CRZ under unconfined conditions, 1.67 D. Hence, the confinement was designed to be 2.50 D (200 mm) long, this being typical of industrial practice (Syred et al., 1984). Three types of confinement exhaust were used,

- Completely open.
- Pyramidal exhaust with length of 1.00 D and square transversal open area of 1.00x1.00 D^2.
- Sudden flat obstruction at the end of the burner with a circular 0.50D hole.

Based on results for PVC1 (unconfined), experiments were performed taking 150 frames/section. The range of velocity acquisition was 0.000 to 10.000 m/s and -5.000 to 8.000 m/s for the tangential and axial analysis, respectively. The percentage of substitution was 2.8% and 2.2% for each case.

4.2.3.1. Completely open.

First, the configuration without obstruction was analyzed, figure 4.37. The objective was to have a starting point of comparison between other configurations in this project and other studies. The system was analyzed first via the axial plane.

Several structures were recognised in the field. The first was the CRZ, which seems to appear at the bottom of the burner. Consistency between sections in the axial position was evident. The threshold values to define the velocities to create the isosurface of the recirculatory structure were set at 0.100 and -5.000 m/s.

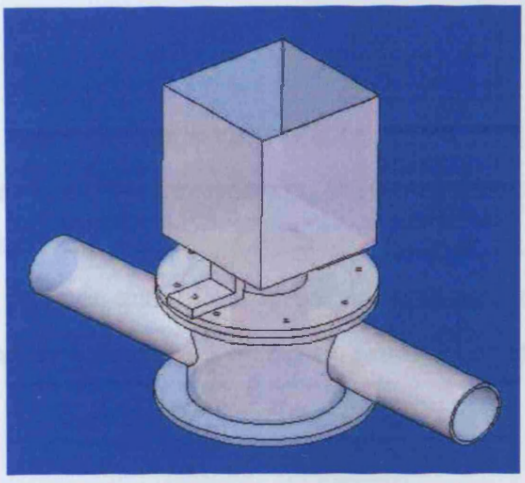

Figure 4.37. Experimental Setup.

However, opposite to the CRZ another CRZ developed, being lifted out from the burner exit completely. The structure not only appeared in some of the planes, but was also coherent between them, growing and increasing its size to the point of eliminating the main recirculation zone attached to the outlet of the rig in some of them. The progression can be seen in figure 4.38.

At first sight, this new CRZ seemed to be a toroidal structure which arises from the central recirculation zone, increasing in size at further sections. However, this assumption was soon discarded after a closer analysis of the vertical images was performed, figure 4.39. Relevant eddies in the flow are emphasized. A large central reverse zone is formed, as in previous cases.

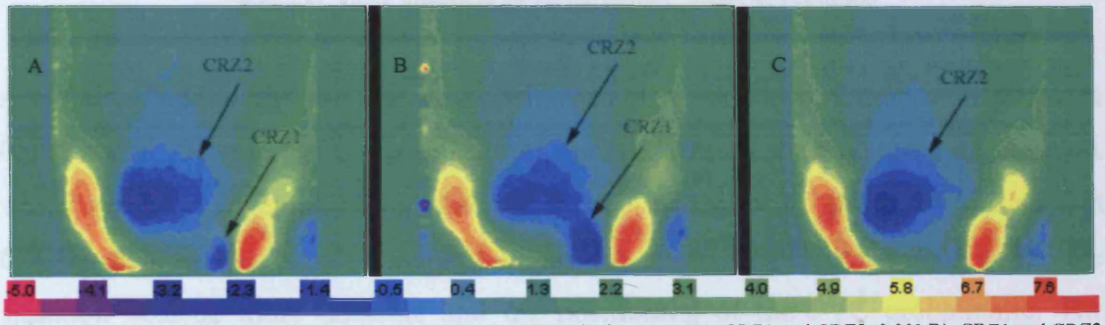

Figure 4.38. Different Phase angle sections with CRZ1 and CRZ2 in Case 4.A. A) CRZ1 and CRZ2, 0.00° B) CRZ1 and CRZ2 attached, 146.25°; C) CRZ2 only, 22.50°.

However, two sets of eddies are noticeable both external and internal to the shear layer flow, figure 4.39. The external eddies are well known, toroidal in nature and arise from the sudden expansion. Indeed they can be largely eliminated by using a quarl on the burner exit (Dawson et al., 2005). The other set of eddies is located in between the shear flow and the CRZ and is indicative of an initially separate spiral vortex, often of intermittent nature. Similar structures were also found by Yazabadi (1996) in the exhaust of a cyclone separator.

There is also evidence that the former recirculation zones (CRZ1 and CRZ2, respectively) reach a level were they merge. The 3D representation shows initially a small gap before these CRZs join. This has been mentioned by others (Ibas et al., 2006; Syred, 2006; Valera-Medina, 2006) but not quantified before, as well as the large size of CRZ2 relative to CRZ1. Moreover the centralised location of CRZ1 has changed to an off centered location close to the confinement outlet.

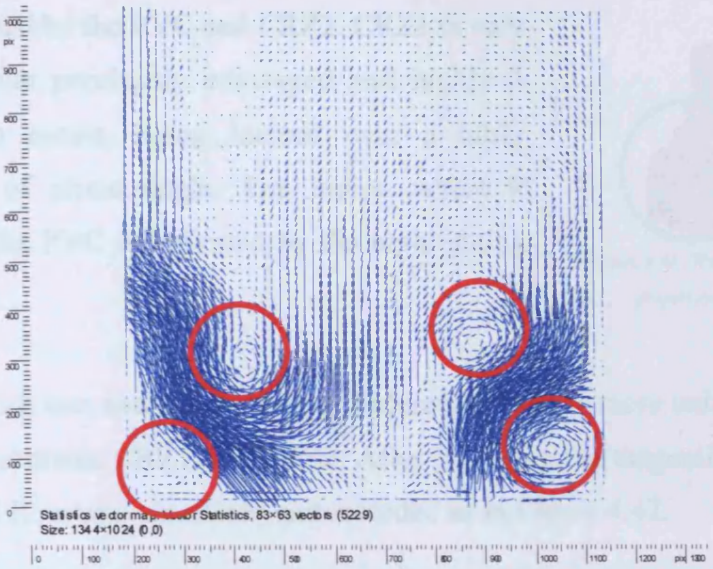

Figure 4.39. Vector Analysis of the vertical sections. Eddies are highlighted.

A radial tangential analysis was next performed. The boundary velocities chosen were 0.000 and 0.330 m/s for the definition of the PVC. In the first planes a PVC/vortex was observed. Tangential radial analysis showed evidence of a strong PVC at section 0.00D, next to the burner exit and persisting up to 0.30D. After this point, the situation became more unstable and the positioning of the PVC problematic. The radial sections showed the movement of flow close to the wall, while the centre remained almost empty of flow or at very low velocities. The flow initially expanded from the burner into the confinement, hitting the walls, whilst creating an initial ERZ.

After 0.28D the vortex had completely joined another region of low velocity, disappearing completely in the following sections. It was also evident how weak the vortex was, causing visualization troubles. To confirm that the vortex passed over the CRZ, the images at section 0.00D (tangential) and section 90° (axial) were compared, figure 4.40. This axial section was selected as both are sections where the triggering takes place.

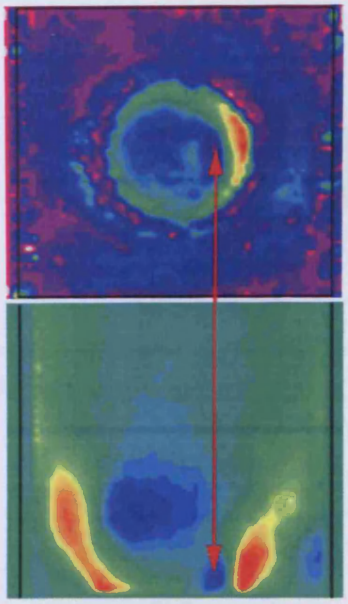

Figure 4.40. Comparison of planes. Position of the PVC.

In the unconfined case the existence of the canal confirmed the relationship between structures. Figure 4.41 shows the resulting 3D visualisation of CRZ1 and

how it is distorted by the PVC and CRZ2. CRZ1 is very much larger than previously envisaged and highly 3 dimensional in nature, being located over a fairly narrow range of phase angle. The region where it interacts with the PVC is indicated by the highlighting circle.

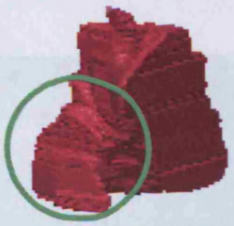

Figure 4.41. Recirculation Zone. The projection is highlighted.

The PVC is much less noticeable, the circumferential flow is more uniform, whilst the central region contains CRZ1 and CRZ2. After gathering the tangential and axial 3D results, the real flow was visualized and recorded as in Figure 4.42.

A small gap between the CRZ1 (in purple) and the CRZ2 (Yellow) represents the position where both structures join. Since the 3D body was assembled from data from numerous sections, this region was difficult to apportion, indeed possibly there is intermittent overlap or merging of the structures.

The PVC is represented by a blue structure, which was observed only up to 0.30D. It must be recognised that some problems of visualization arose due to the use of the perspex. Reflections and diffraction caused by the material produce scattered light in the regions close to the walls, making characterization here difficult. Better materials and manufacturing processes are needed for future work.

Figure 4.42. Real Flow. CRZ1 (purple), CRZ2 (yellow) and PVC (blue). The first image (top view) shows the continuity problem between structures. The PVC is extremely weak.

4.2.3.2. Pyramidal Obstruction

Figure 4.43 shows the case. The velocity boundaries selected for the axial isosurface were the same as in the previous case, 0.100 to -5.000 m/s. As observed in the open case, CRZ2 appeared in the system. It had a toroidal eddy shape as well. The same coherence between sections made evident the existence of this body and its evolution, as well as the similar problem of continuity between the CRZ1 and the former. Figure 4.44 shows one of the planes of interest.

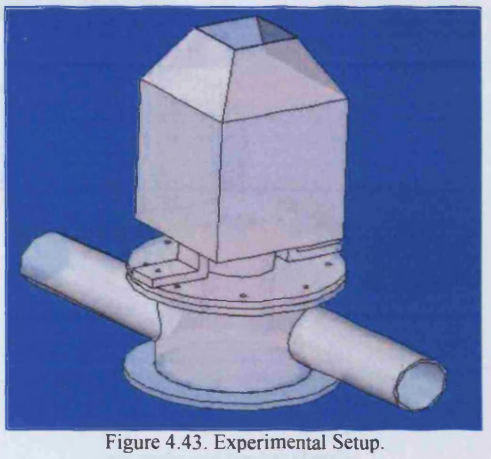

Figure 4.43. Experimental Setup.

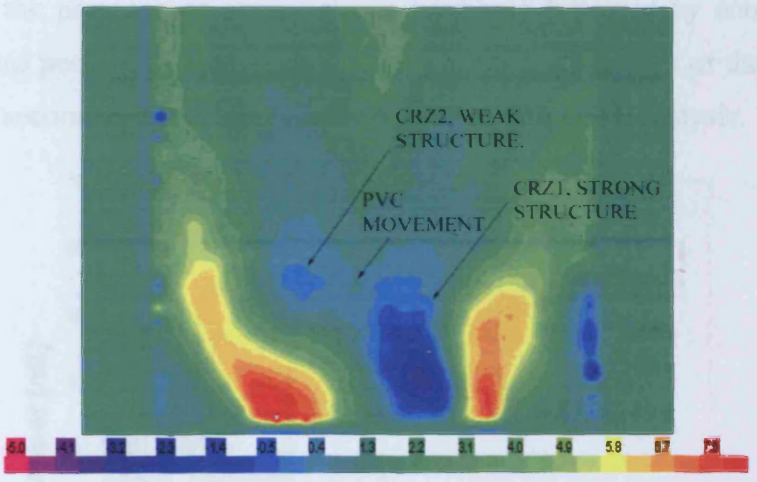

Figure 4.44. Strong CRZ apparently split into a strong and weak structure, 0.00°.

CRZ1 seems to be dominating the field in the lower part of the burner. At higher sections downstream, a stronger vortex forms associated with the confinement exhaust. A feature observed in several of the axial sections was the splitting of the CRZ into a strong and weak structure, possibly caused by a stronger PVC, in contrast to the case with the open exhaust to the confinement.

Marked differences between the open case and this confinement were evident. Variations of the HWA signal were noticed and it was found that the signal of the PVC had changed. Figure 4.45 and 4.46 show the phenomenon. The first signal was obtained with the open confinement and it was more homogeneous and regular. The

second signal, figure 4.46, was weaker and more unstable. This was not a problem for triggering, but clearly is a manifestation of changes in the PVC.

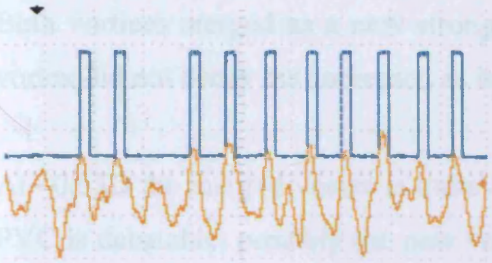

Figure 4.45. Open Confinement Case signal.
Similar to unconfined conditions.

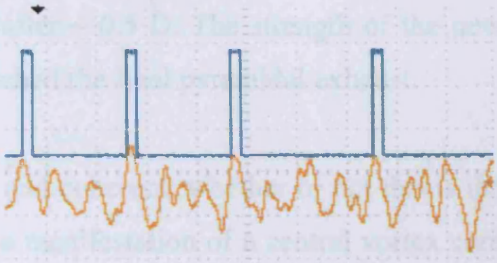

Figure 4.46. Pyramidal Case signal.
Less peaks and weaker signals.

Although there is a difference between cases, the frequency of the system was very similar, with the presence of a very strong harmonic followed by another 2 strong harmonics. This peculiarity was a consequence of the confinement of the flow and the interaction of secondary structures. Figure 4.47 shows the FFT analysis.

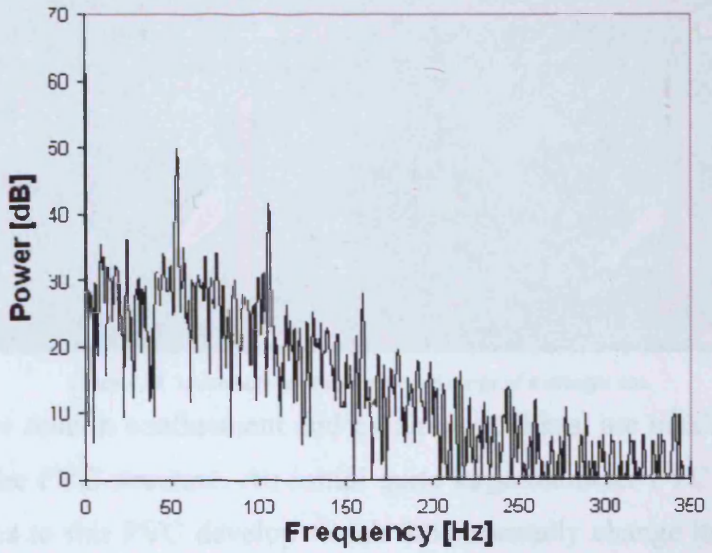

Figure 4.47. FFT Analysis of Open, Cylindrical and Conical cases. Three harmonics at 55.0, 110.0 and 165.0 Hz.

The tangential radial analysis denoted the existence of the PVC. Contrary to the open case, the system tended to split into two regions. Even though the presence of a very slow flow was observed downstream, the region of the confinement close to the pyramidal confinement exhaust was more complex in the sense of having what appeared to be an anchored vortex produced by the outgoing flow passing through a narrow orifice.

Figures 4.48 shows the existence of a large off centred low velocity vortex region at ~0.40 D with the presence of at least two separate weak, but distinct, vortex structures. Both vortices merged as a new stronger one after ~ 0.5 D. The strength of the new vortex did not decay but increased as it approached the final pyramidal exhaust.

At ~0.53D the merged vortex is quite evident and coherent; whether or not this is the PVC is debatable, possibly the new vortex is a manifestation of a central vortex core which is merely wobbly, a phenomena noted by Dawson (2000) and Syred (2006). Figure 4.48 also shows evidence in the vortex core of other weak structures, possibly some of the higher harmonics noted earlier.

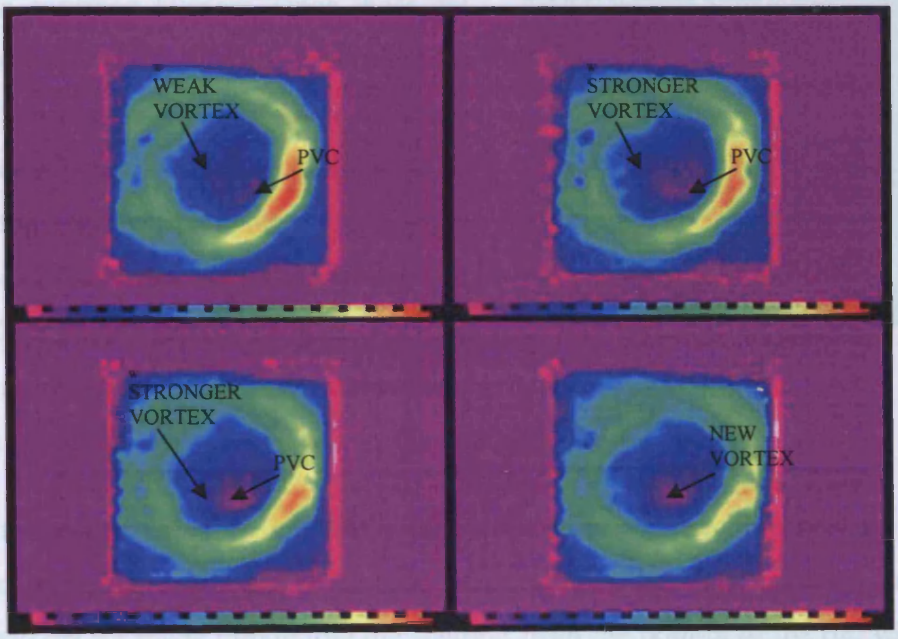

Figure 4.48. Union between two vortex and merge of a stronger one.

Thus the square section confinement and pyramidal exhaust are making fundamental alterations to the PVC structure. An initial quite large diameter PVC forms. Internal secondary flows to this PVC develop which fundamentally change its structure after 0.4D. The whole flow structure is reconstructed in figure 4.49.

Figure 4.49. Real flow under confinement. A pyramidal obstruction has been used on the top of the burner. The flow is composed by CRZ1 (purple), CRZ2 (yellow) and PVC (blue).

As observed in figure 4.49 the PVC passes through CRZ2 and then merges with other structures with a main central wobbling vortex core. CRZ1 is located in the exit of the swirl burner and clearly extends well upstream into the burner exhaust. It is highly asymmetric here as shown by the lobe by the PVC in the middle diagram. Similar problems of visualization close to the wall were observed.

4.2.3.3. Sudden Obstruction

Some simulations (Selle et al., 2006) use a sudden contraction to corroborate their results in confined burners, since these are common in the field. The formers use LES and DNS programs to asses their accuracy and practical use. Many of them tend to make the analysis under combustion conditions. Therefore, this experiment was intended to obtain results using isothermal conditions to show the main differences between processes. Figure 4.50 shows the experimental set up.

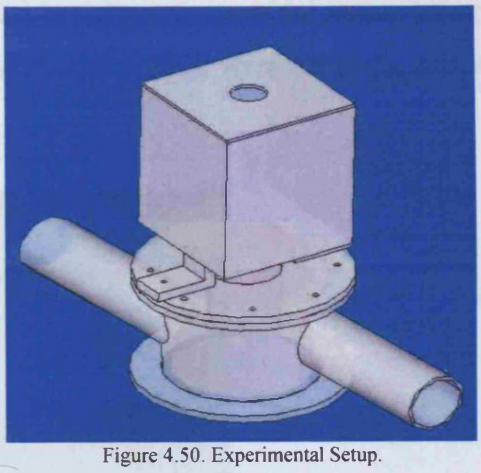

Figure 4.50. Experimental Setup.

During the experimental procedure a problem arose. The seeding process used in previous experiments did not work with this configuration. The pressure inside the burner and the rig made impossible the seeding from the bottom of the rig, which had always been the preferred method in order to avoid large particles and extra kinetic energy from the water nebulizer spray. In fact, the whole configuration operated at much higher pressure than the other configurations due to the small confinement exhaust nozzle. It was found that the centre line pressure inside of the system remained almost unchanged for the first two confined cases, ~10 Pa, rising to ~100 Pa for the sudden exhaust, due to the

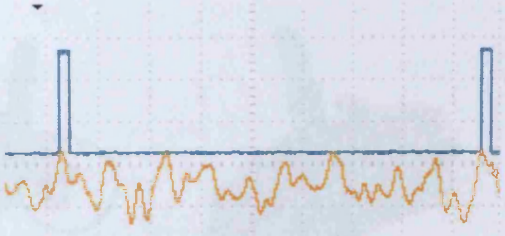

Figure 4.51. Sudden Exhaust Case signal.

small area of the final exit. Therefore, a direct seeding 50 cm downstream into the tangential inlet hoses was used.

Axial analysis was carried out first to reveal the existence of important vertical vortical structures. Again the shape of the HWA signal changed becoming weaker and more unstable, with fewer peaks and more irregularity, figure 4.51. Phase locked results could still be obtained. This was again related to the change in strength and behaviour of the PVC. The axial sections, figure 4.52, showed a CRZ located at the swirl burner exit, but obviously high asymmetrical in nature, the toroidal nature being evident. The velocity boundaries selected for the reconstruction were set at the same values as previously.

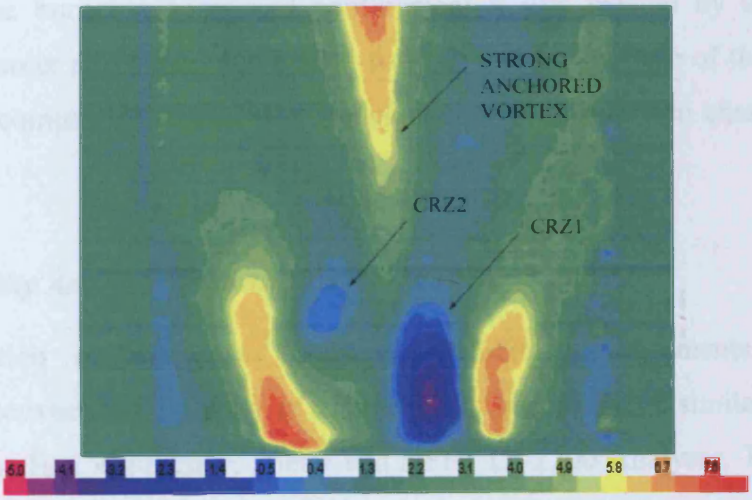

Figure 4.52. CRZ1 is anchored in the swirl burner exit, case 4.C, 45.00°.

CRZ1 dominates here and CRZ2 was suppressed to such an extent that only small traces appeared in 3 sections. Therefore, CRZ2 was left as part of CRZ1, highlighted in the visualization of the entire flow, figure 4.53.

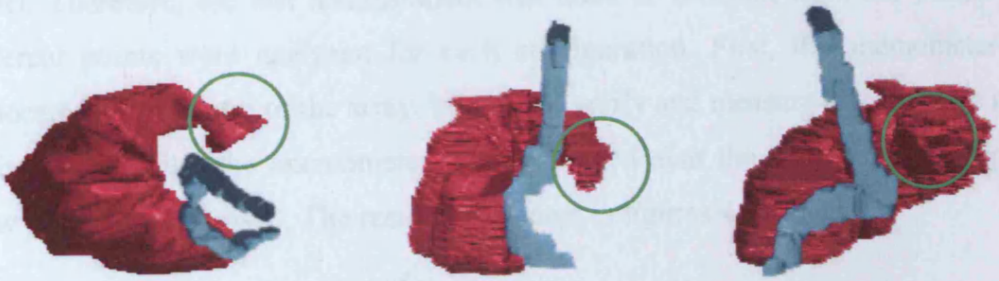

Figure 4.53. Total Flow seen from three different views. CRZ1 (purple) and PVC (blue). CRZ2 is ringed.

The existence of an extremely powerful vortex was observed in the tangential radial analysis. The PVC always started from the burner exit with a spiralling movement,

stopping its precession at ~0.40D suddenly. No second internal vortex was observed, probably because in the previous experiment this was only a manifestation of the decrease of the precessional movement and realignment of the vortex towards the central axis. The similar movement of the PVC indicates that the mechanism is similar to the pyramidal case, where a new vortex is developed as the merging of two independent structures. Their interaction generated a new strong structure which was mainly dominated by PVC behaviour at lower sections and the centred vortex further downstream.

A general feature observed in all the experiments was an eddy formed in the vicinity of the burner exhaust, the ERZ. With a toroidal shape that fitted into the corners formed by the burner exhaust and confinement it was created by the shear flow leaving the burner and hitting the burner wall. The square section of the confinement increased its complexity and three dimensionality; it has not been characterised here to any extent.

4.2.3.4. Velocity Analysis from the HWA signals

The recognition of harmonics from the velocity measurements allowed the comparison between the stability of different configurations. A similar analysis was done using the Hot Wire Anemometer and a FFT DI-2200 Analyser. The aim was to locate powerful harmonics in the flow, which are related to inherent frequencies of the signal from the anemometer.

The measurements were done every 20 mm upstream starting at 10 mm above the outlet. Therefore, the last measurement was done at 190 mm from the outlet. Two different points were analyzed for each configuration. First, the anemometer was collocated at the centre of the array, in order to verify and measure any structure in the vicinity. Secondly, the anemometer was positioned near the wall, so any intriguing flow could be recognised. The results are shown in figures 4.54 to 4.57.

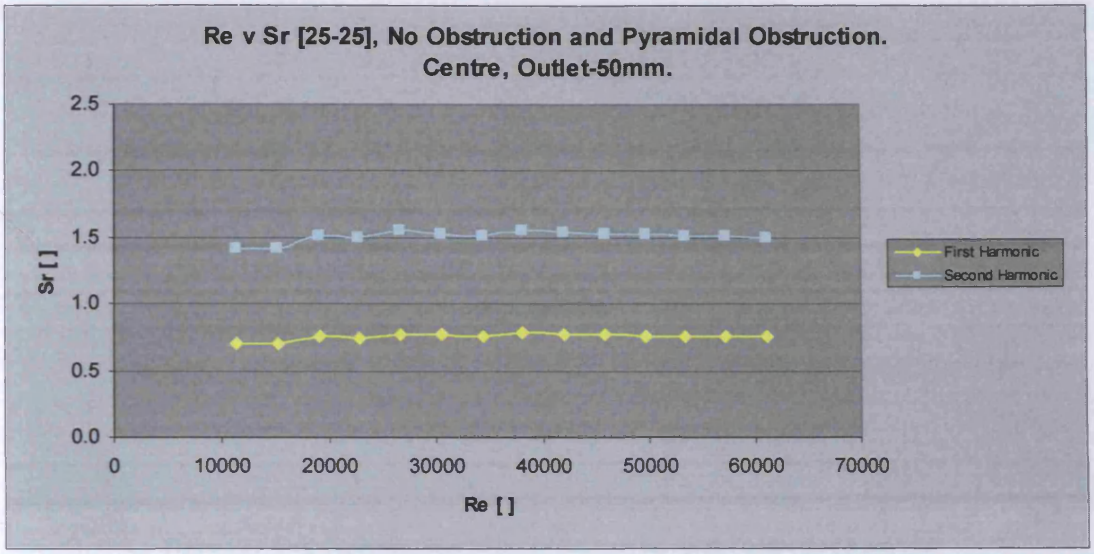

Figure 4.54. First and Second Harmonic, up to 50 mm from the outlet. No obstruction and Pyramidal obstruction cases.

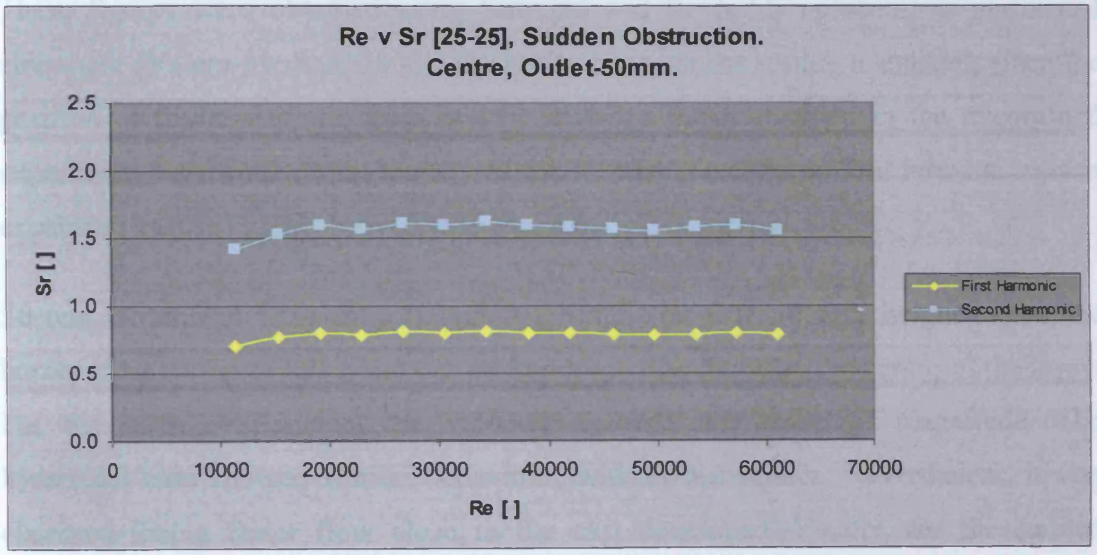

Figure 4.55. First and Second Harmonic, up to 50 mm from the outlet. Sudden obstruction case.

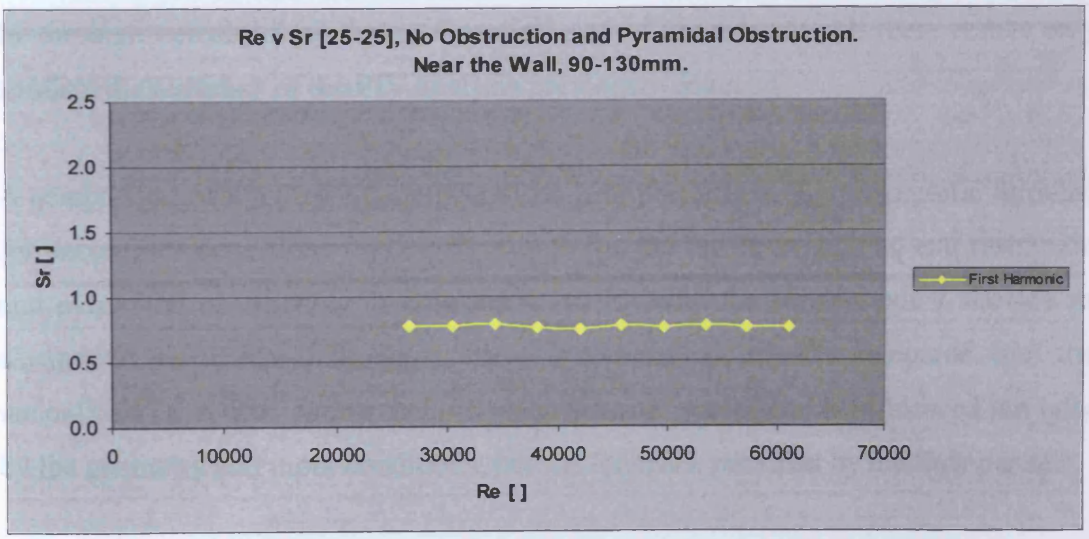

Figure 4.56. First Harmonic, from 90 to 130 mm from the outlet. No obstruction and Pyramidal obstruction cases.

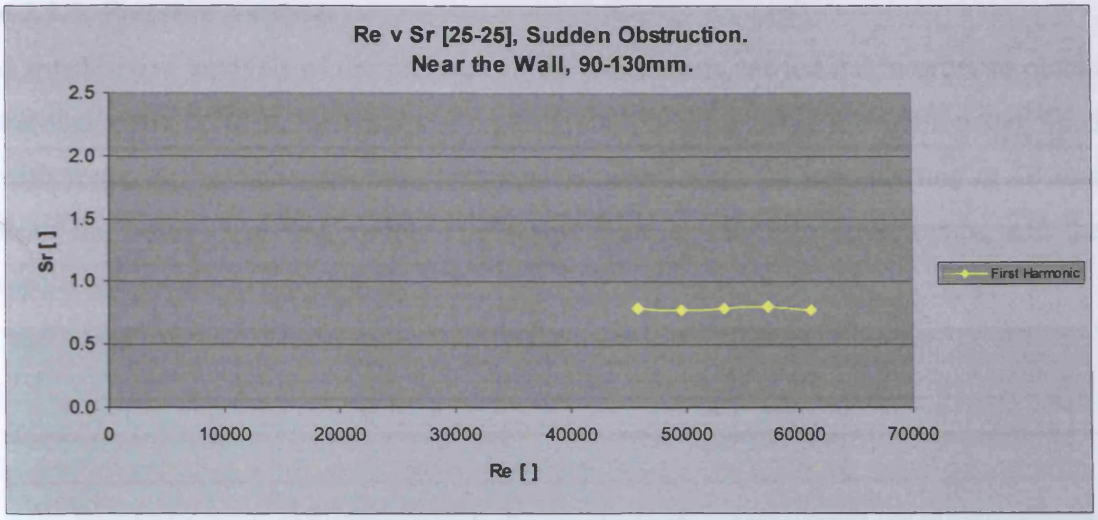

Figure 4.57. First Harmonic, from 90 to 130 mm from the outlet. Sudden obstruction case.

These figures were obtained using Strouhal and Reynolds numbers, as performed elsewhere (Valera-Medina, 2006). Similarity between the results is evident, since the position of the asymptotic lines is very close to those obtained in the unconfined experiment, confirming the accuracy of the former. It can be noticed how the sudden expansion case is slightly moved to higher Sr.

Second harmonics were only obtained through the first 50 mm height above the burner exhaust. From this point on, no harmonic was found in the centre of the array. For the open confinement the velocity decayed one order of magnitude. The Pyramidal case showed similar behaviour, with no harmonics. Nevertheless, it was observed that a faster flow close to the exit developed. Finally, for the sudden obstructed confinement case no secondary harmonics were observed, possibly caused by the high velocity flow due to the small size of the exhaust. All these results only confirm the accuracy of the PIV analysis previously done.

A comparison of the Strouhal numbers was also performed. The asymptotic Strouhal for unconfined conditions was ~0.83 at high Re; for the cases with no exit restriction and pyramidal obstructions it dropped to ~0.75; with the sudden exit it showed an asymptotic value of ~0.78. Thus, there is a variation of ~8% compared with the unconfined case. This shows that the mechanism of precession is influenced not only by the geometry and input conditions, but the feedback provided by the flow per se.

4.2.3.5. Pressure Analysis

A quantitative analysis of the pressure in the burner was carried out in order to obtain the scalar and confirm the results. The analysis was done using a U manometer filled with water at the walls. Measurements were taken every 20 mm, starting at 10 mm from the outlet. The last measurement was done at 190 mm downstream, and the results are shown in figure 4.58.

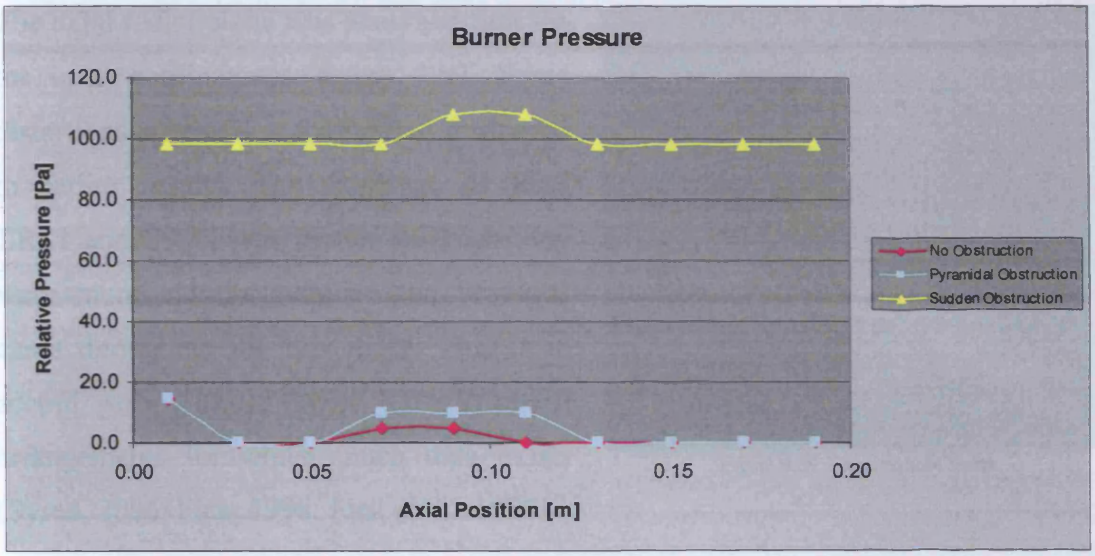

Figure 4.58. Pressure analysis at the burner wall.

It is noticed how the wall pressure in the open and pyramidal cases is scarcely higher than the atmospheric pressure; however this is not true in the central region where tangential velocity decays caused substantial pressure gradients which lead to the formation of CRZs and other structures (Syred, et al., 1984; Syred, 2006).

The sudden exhaust to the confinement, coupled with its reduced diameter produced much higher wall pressures, doubtless lower pressure gradients in the confinement and burner exhaust, thus virtually eliminating CRZ2.

4.2.4. Confined Conditions. Circular Case.

A circular confinement was next used to allow the recognition of structures in a more common type of burner/furnace arrangement. Thus, this experiment used a circular confinement of 2.00D diameter, the length of the burner was kept at 2.50D (200 mm). Hence, to match results with the previous cases, three similar exhausts for the confinement were used. An open case, a conical obstruction similar to the pyramidal case, and a sudden flat sharp 0.5D exit were studied. The quasi-stable PVC1 case was

used for comparison purposes. The range of validation for the velocity vectors was set at 0.000 to 9.000 m/s and -3.000 to 8.000 m/s for the tangential radial and axial radial analysis, respectively. The percentage of substitution was 1.5% and 2.1%, confirming that the results were satisfactory.

4.2.4.1. Completely open.

The axial radial plane was analyzed first for the open confinement, figure 4.59. Some distortions appeared in the system compared to earlier results. The existence of both CRZ1 and CRZ2 was found, although they were more closely merged than previous cases throughout the flow field. This is in accord with similar swirl burner/furnace arrangements for which much data exists (Syred, 2006; Fick, 1998; Fick et al., 1998).

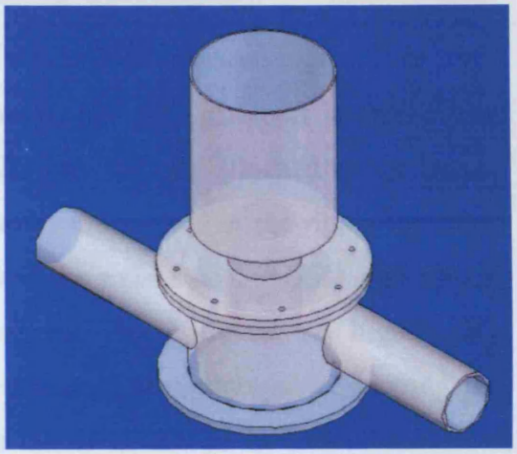

Figure 4.59. Experimental Setup.

Following the development of the flow, CRZ1 detaches from the burner exit, moving upwards in a more pronounced manner than with the square confinement. In the first section both CRZ1 and CRZ2 could be identified. However, those sections in the phase angle range between 90° and 135° are more complex than before due to a process of body unification that seems to take place. CRZ1 is being lifted to a point where it joins CRZ2; this is then the only structure in the system for a couple of sections. Moreover, the region of reversed flow has increased in size considerably compared to that in the square confinement. Figure 4.60 shows the progression of the structures. The position of the CRZ1 is antiphased between the first and last picture because of the rotation required for the analysis. It is thus confirmed that the same merging process between structures occurs, even though both CRZs appear to be independent in nature as in the previous case. However, the CRZs are much larger, doubtless due to the circular nature of the confinement.

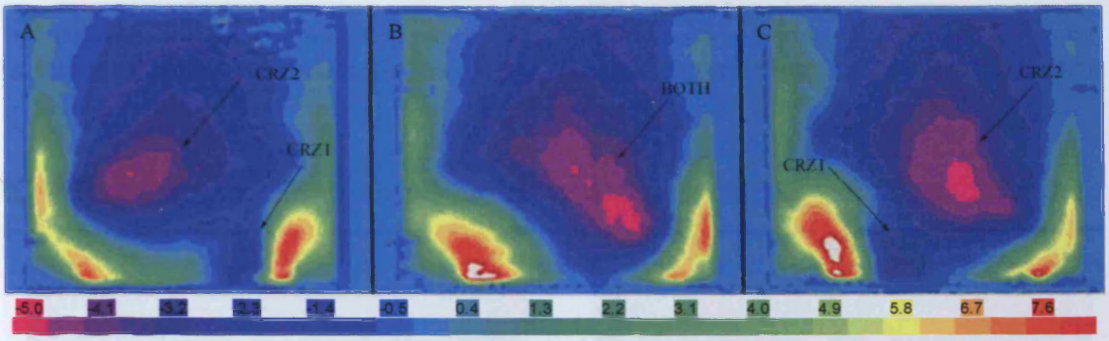

Figure4.60. Different sections showing the evolution of both structures. A) CRZ1 and CRZ2 0.00°; B) Union between both structures, 135.00°; C) CRZ1 and CRZ2, 168.75°.

The process is similar to the square confinement, but with different intensity. The merging of CRZ1 with CRZ2 is evident. CRZ1 was initially attached to the burner exit and then mixed with CRZ2 which was always unattached to the rig, being lifted during the process. Thus, some sections showed the existence of CRZ1 and CRZ2, whilst others showed traces of a merging mechanism. The results were of high quality and allowed the recreation of the 3D bodies for both structures, also showing the existence of the small indentation, doubtless the manifestation of the PVC.

As in the square confinement, CRZ1 and CRZ2 showed similar trends overall in terms of positioning and relationship. However, it is evident how the negative velocity region has increased substantially, creating a larger CRZ. More flow close to the recirculation region is being entrained, re-entering into the structure, something that was less evident than in the previous experiment.

The tangential radial analysis showed the existence of the PVC for the first sections, similar to the square case. A negative reverse flow region close to the PVC has developed, CRZ1, which also extends back into the burner exit Moreover, the strength and definition of the region is better than before, showing that the symmetry of the confinement has created a more stable process, figure 4.61, section 0.00D.

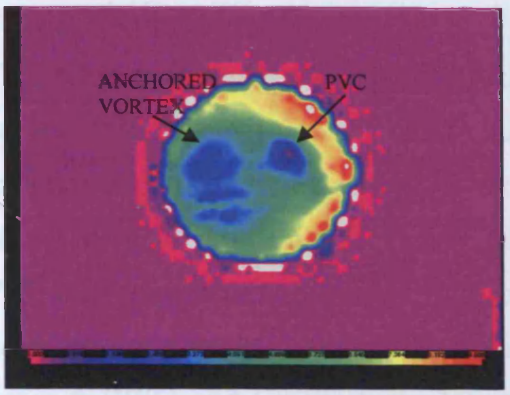

Figure 4.61. PVC and the 3 dimensionality of CRZ1, section 0.00D

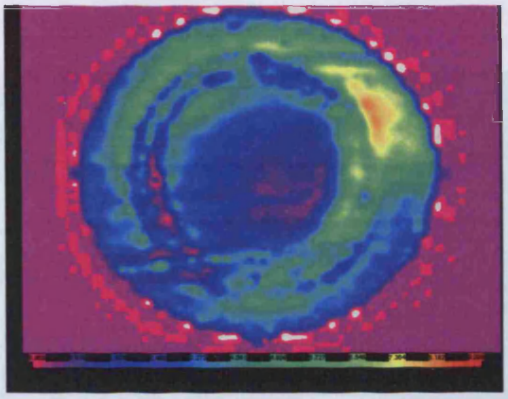

Figure 4.62. PVC stops precessing and expands to central vortex core, section 10 at 0.407D.

However, the PVC virtually disappeared after a couple of sections, not being found after 0.41D, suggesting that the vortex had entered into the region of the CRZ2 whose strength overcomes the vortical movement of the vertical structure, as observed in the square case. It was recognised that the PVC was likely to exist in the system after this point, since the strength of the structure was very consistent downstream. Figure 4.62 shows how the flow has returned to a near symmetrical form with a large central core, which is wobbling slightly at 0.407D.

Some visualization problems were encountered. Due to the concave outer surface, reflections and diffraction caused by the powerful laser light caused a serious problem for the camera. Thin flat surfaces were manufactured for the entrance and exit of the laser sheet, reducing the optical problems. Also, opaque black sheets were used to avoid undesirable reflections, making impossible the visualization of the flow near the walls. Thus, no boundary layer recognition was possible due to the intensity of the laser and properties of the material used, encouraging the use of better materials for further experiments. As in previous cases different hot wire signals were observed. Figure 4.63 shows the derived flow.

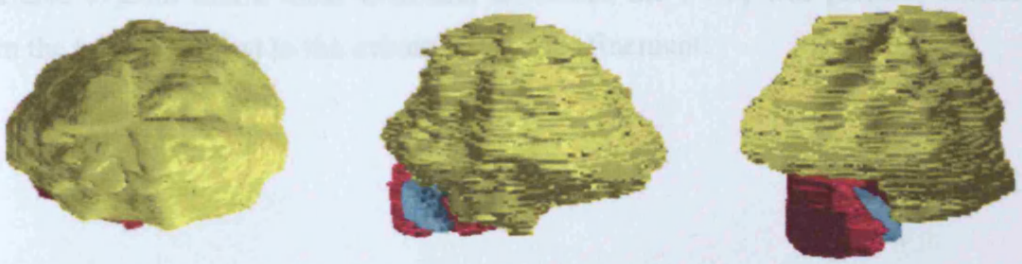

Figure 4.63. Total Flow seen from three different views. CRZ1 (purple), CRZ2 (yellow) and PVC (blue).

4.2.4.2. Conical Confinement

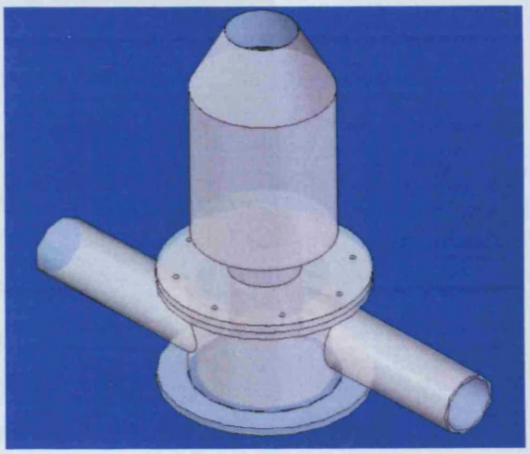
Figure 4.64. Experimental Setup.

The same technique was used for the conical case, figure 4.64. The axial radial experiments showed traces of a very strong vortical structure. Previously, the PVC interacted with CRZ1 and CRZ2, but here a considerable separation exists between CRZ1 and CRZ2. A similar split as in the square case was observed under these conditions. The strength of CRZ2 has decreased whilst it has been deformed into a toroidal shape. Figures 4.65 show the progression of the flow. The toroidal and complex nature of the CRZs is clear, requiring a full 3 dimensional holographic analysis again. The deformation of the shear flow leaving the swirl burner exhaust is also noticeable in both figures. As has been discussed elsewhere (Syred et al., 1984; Beer et al., 1974; Syred et al., 1978) the formation of CRZs is a function of the axial decay of tangential velocity, hence axial decay of centrifugal pressure gradient. With a circular confinement and a confinement/burner exit diameter ratio of 2 (similarly for the confinement exhaust) the rate of decay of tangential velocity is reduced and other structures appear in the system, as has been observed with the pyramidal exhaust.

Hence centrifugal pressure gradients, which are the drivers for the formation of CRZs, change. This gives rise to very complex CRZs as described by Syred and Dahmen (1978). After observing the progression, it was evident how the system splits a main CRZ into two independent structures, leaving one attached to the rig, with a central position whilst the other was lifted substantially inside of the burner, figure 4.65. It was also evident that a third structure, doubtless the PVC, was present, extending from the burner exhaust to the exhaust of the confinement.

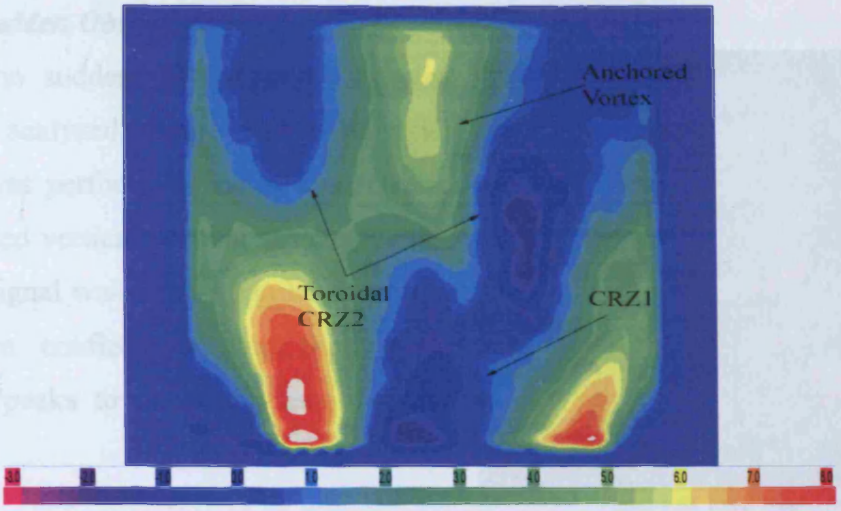

Figure 4.65. Section 146.25°, conical confinement exhaust.

During the radial tangential study, the PVC was found to extend up to ~0.49D, stopping its precession and changing to a centrally located compact vortex core, again wobbling, figure 4.66 at 1.50D downstream. The consistency of the structure within all the sections remains constant, and it was possible to reconstruct the 3D body with high accuracy.

The total flow pattern obtained is thus shown in figure 4.67, again CRZ1 and CRZ2 are evident and the two eddies eventually merge. Thus this type of confinement clearly affects the CRZ formation as well as the extent of the vortex core precession. As previously observed in other cases, the transition of the PVC at the burner exhaust into a stable vortex core is a phenomenon which may be important with combustion as it could improve the system stability.

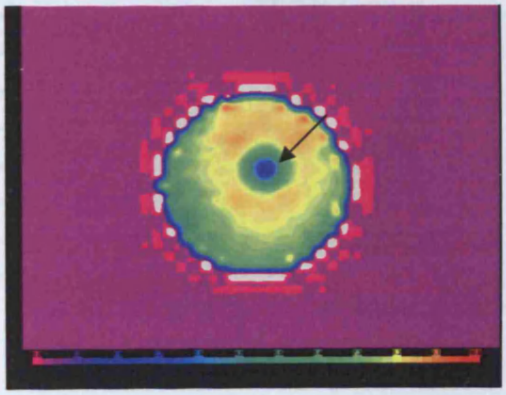

Figure 4.66. Coherence of the anchored vortex at section 36, via radial tangential analysis, 1.50D downstream of the burner exit.

Figure 4.67. Total Flow seen from three different views. The CRZ1 (purple), CRZ2 (yellow) and PVC (blue).

4.2.4.3. Sudden Obstruction

Finally, the sudden confinement exhaust case was analyzed, figure 4.68. The axial analysis was performed first to characterize the expected vertical vortical structures. The hot wire signal was more irregular than with the square confinement, but there were sufficient peaks to allow the use of phase locking.

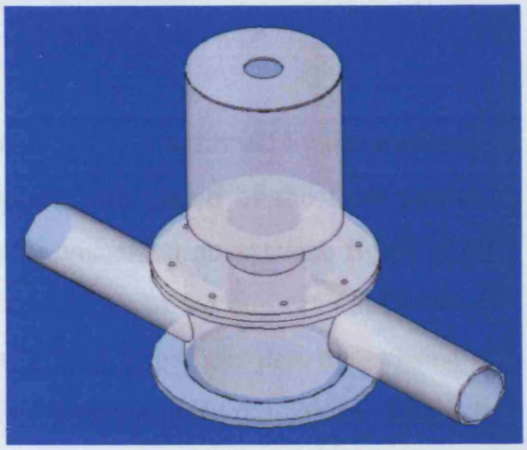

Figure 4.68. Experimental Setup.

Some similarity with the square case was evident. An even stronger but off centred CRZ1 appeared close and extending well inside the burner exit. However, this CRZ is much stronger than with the square confinement. Figure 4.69 shows one of the axial radial sections, denoting the CRZ and the existence of a central forward flow on the central axis.

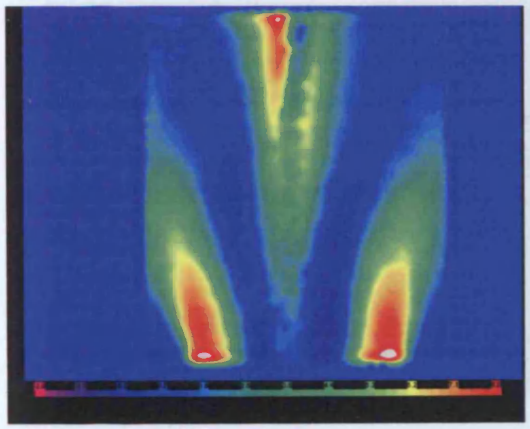

Figure 4.69. Section 112.25°, circular confinement, sudden exhaust to confinement.

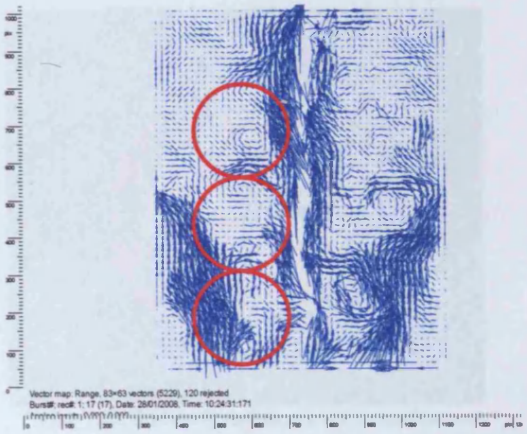

Figure 4.70. Vectorial analysis in the axial radial direction. Large eddies highlighted.

This mechanism has been observed before (Syred et al., 1978) and is caused by the small diameter exhaust of the confinement and associated effects on the centrifugal pressure gradients. A vector axial radial plane, figure 4.70, shows that the bottom of the annular CRZ is irregular, being broken up by families of eddies down near the burner exhaust, similar comments apply to the central forward flow. According to O'Doherty et al. (2005), these eddies are responsible for a better mixing in the vicinity of the recirculation zone, improving the burning process. Moreover, the system is

functioning as a reversed energy cascade, proving energy to the smaller eddies for their re-integration into larger scales.

Vortex core precession has been suppressed considerably, confirmed by the weakened hot wire signal and the straightened vortex found over much of the flow section, which could be observed even without the laser visualization system, figure 4.71; PVC precession seemed to virtually disappear very close to the burner exit. However it has been shown that this vortex core can easily start to precess past the exhaust of the confinement, providing there is an appropriate expansion (Syred, 2006). This is in agreement with findings of Paschereit et al. (2006), whose distributed vortex generators reduced considerably the acoustic disturbances produced by large vortical precessing structures. Thus, it is confirmed that controlled anchored structures with enough energy can merge with the main PVC to alter its dynamics. The length of CRZ1 now extends to 1.04D axially, being stable and uniform in shape; CRZ2 is not evident.

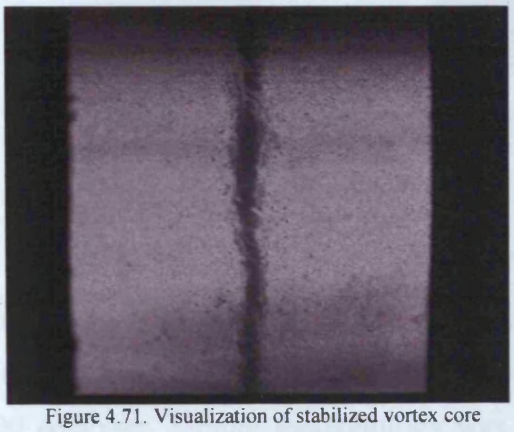

Figure 4.71. Visualization of stabilized vortex core downstream of burner exit.

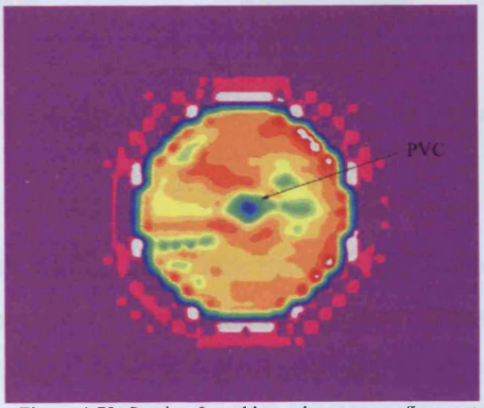

Figure 4.72. Section 0, sudden exhaust to confinement. Vortex core precession has almost stopped.

In the tangential radial analysis, the existence of a strong central vortex was confirmed with its reduced precession. The spiralling movement of the PVC was barely seen. The positioning of the low velocity region that denotes the vortex core was near centrally located in the flow, contrary to all the other cases where the latter was off centered and pushed back by the high momentum Crescent Moon shaped flow region (figure 4.25). The 3D representation showed little movement in the vicinity of the burner exit, figure 4.72, in accord with the signal analysis showing very little precession.

This is completely different from previous cases where vortex core precession was high and indeed this shows ways to suppress the PVC. There is a cost of course in terms of higher pressure drop and the annular shape of the CRZ. Comparison with the square section confinement results is interesting as the losses inherent in firing a swirling flow into a square section give a faster rate of decay of swirl velocity, hence centrifugal pressure gradients and more vortex core precession. Figure 4.73 gives details of the total flow, with CRZ1 and a PVC with little precession. Despite the suppression of most of the vortex core precession the CRZ is still highly 3 dimensional in nature. The secondary recirculation zone has been completely suppressed as observed in the square confinement, likely a product of the increased pressure inside of the system and reduced pressure gradients due to the small diameter confinement exhaust.

Figure 4.73. Total Flow seen from three different views. The CRZ1 (purple) and PVC (blue). CRZ2 has not been defined.

4.2.4.4. Velocity Analysis

As in the square case, the recognition of harmonics and definition of the Strouhal Number, Sr, from the HWA velocity measurements allowed the comparison between cases. A similar analysis was done using the Hot Wire Anemometer and a FFT DI-2200 Analyser. Similar methodology was followed to recognise the first and second harmonics of the flow. Data were obtained from the centreline, since the results near the wall were not so coherent. Moreover, the modes of the sudden exhaust did not show strong harmonics, probably due to the sensitivity of the equipment and the reduced amplitudes of any PVC effect caused by smaller exhaust to the confinement. Figure 4.74 and 4.75 show the Open and Conical cases from the outlet to 50mm downstream.

Asymptotic values were ~0.78 for the open case and ~0.80 for the conical case, representing an increment of 4% and 7% respectively, again due to the reduced decay of tangential velocity due to the nature of the confinement. PVC amplitudes were

generally reduced (most significantly with the sudden exhaust); no higher harmonics could be clearly distinguished.

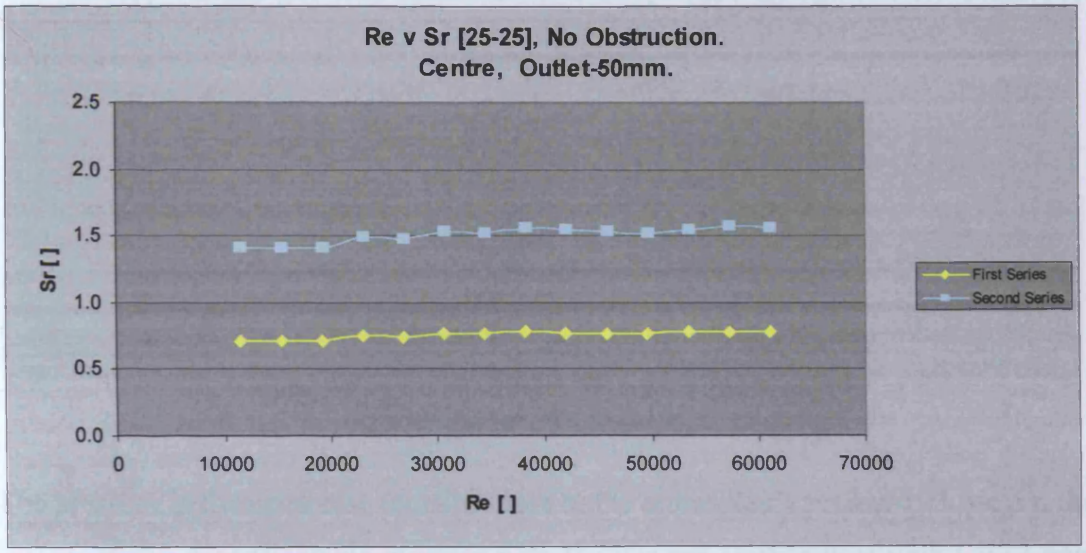

Figure 4.74. First and Second Harmonic, up to 50 mm from the outlet. No obstruction case.

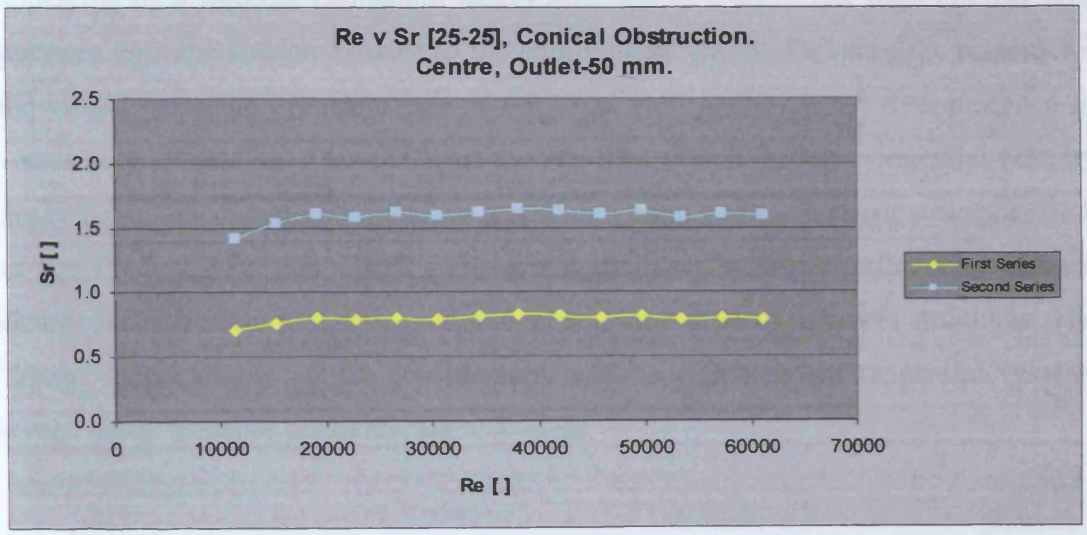

Figure 4.75. First and Second Harmonic, up to 50 mm from the outlet. Conical obstruction case.

4.2.4.5. Pressure Analysis

Pressures were recorded inside of the burner to obtain the scalar, confirm the results and previous asseverations about the influence of pressure in the development of the structures. The same methodology was used as in the square case. Figure 4.76 shows the comparison of all cases, including those obtained with the square confinement.

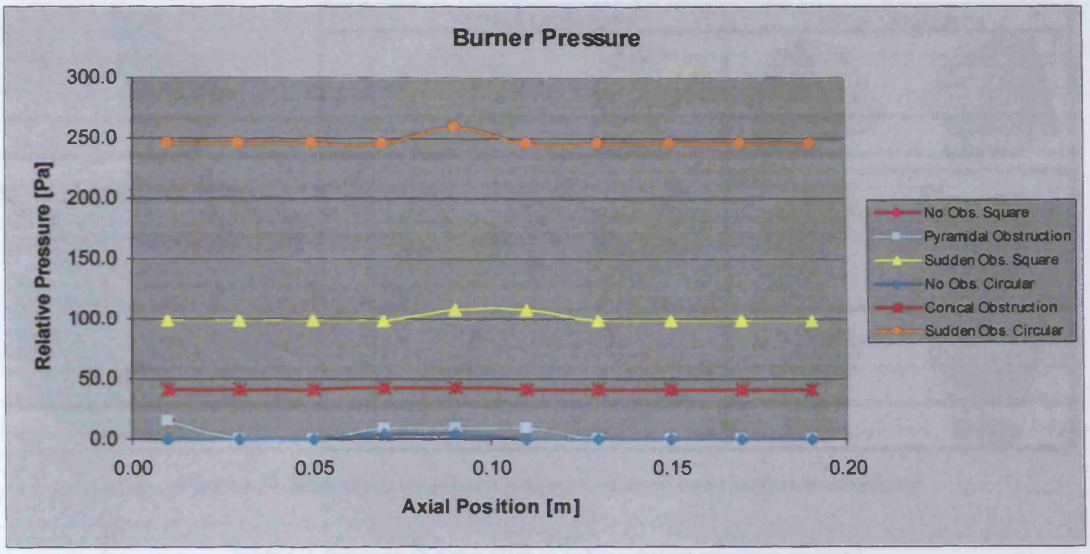

Figure 4.76. Pressure analysis inside the burner.

The pressure in the open case remains close to the atmospheric pressure. However, the system shows a considerable increase with the conical confinement with CRZ2 now appearing as a toroidal elongation barely attached to CRZ1. The high internal wall pressure with the sudden exhaust to the confinement clearly indicates the reasons for the virtual complete disappearance of CRZ2 as well as the virtual disappearance of vortex core precession. This confirms the previous assertion about tangential velocity decay being associated with pressure gradients giving rise to coherent structures such as the PVC, CRZ1 and CRZ2. The small diameter sudden confinement exhaust clearly reduces these pressure gradients, hence formation of coherent structures. The "lossy" nature of the square confinement and the effect on the tangential velocity levels, hence pressure gradients, are also clear.

4.3. Summary

Different coherent structures were observed under different conditions. The use of different tangential inserts and confinements showed the development of a variety of coherent structures, especially the PVC and two CRZs. The progression and behaviour of each structure was linked to the geometry, swirl number, Re, pressure in the system and secondary vortices that interact with them. The shape and dimensions of each case are denoted in table 4.2 and figure 4.77 and will allow a quantitative comparison between combustion and isothermal conditions.

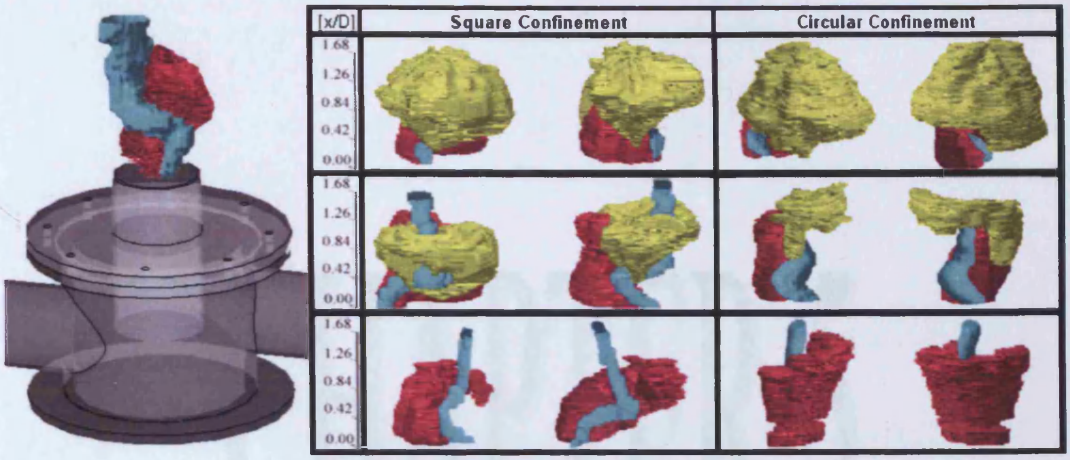

Figure 4.77. Summary of all different structures observed under isothermal conditions.

Table 4.2. Summary of dimensions of all the coherent structures observed.

Analyzed Case	*CRZ1*	*PVC*	*CRZ2*	*Anchored Vortex*
PVC1				
- Shape	Lobbed	Semi helical		
- Location	Centered	Off centered		
- Size (length x width [D])	0.96 x 0.36	1.62 x 0.16		
PVC2				
- Shape	Lobbed	Semi helical		
- Location	Centered	Off centered		
- Size (length x width [D])	1.18 x 0.51	1.62 x 0.16		
PVC3				
- Shape	Lobbed	Little helicity		
- Location	Centered	Off centered		
- Size (length x width [D])	0.88 x 0.39	1.62 x 0.16		
PVC4				
- Shape	Prismal	Little helicity		
- Location	Centered	Off centered		
- Size (length x width [D])	1.26 x 0.49	1.62 x 0.14		
PVC1 Square Open				
- Shape	Lifted	Helical	Toroidal	
- Location	Near wall	Off centered	Middle Burner	
- Size (length x width [D])	0.53 x 0.34	0.30 x 0.23	0.78 x 0.78	
PVC1 Square Pyramidal				
- Shape	Lifted	Semi helical	Toroidal	Straight
- Location	Near wall	Off centered	Middle Burner	Centered
- Size (length x width [D])	0.43 x 0.40	0.44 x 0.21	0.57 x 0.68	1.23 x 0.09
PVC1 Square Sudden				
- Shape	Lifted	Semi helical	Projection	Straight
- Location	Near wall	Off centered	Middle Burner	Centered
- Size (length x width [D])	0.61 x 0.28	0.40 x 0.17	0.27 x 0.16	1.27 x 0.06
PVC1 Circular Open				
- Shape	Lifted	Helical	Toroidal	
- Location	Near wall	Off centered	Middle Burner	
- Size (length x width [D])	0.49 x 0.31	0.41 x 0.17	0.94 x 1.13	
PVC1 Circular Conical				
- Shape	Lifted	Semi helical	Toroidal	Straight
- Location	Near wall	Near center	Top Burner	Centered
- Size (length x width [D])	0.82 x 0.24	0.49 x 0.21	0.84 x 0.29	1.18 x 0.12
PVC1 Circular Sudden				
- Shape	Lifted	Straight	Toroidal	Straight
- Location	Near wall	Centered	Middle Burner	Centered
- Size (length x width [D])	1.04 x 0.33	Unknown	Unknown	~1.60 x 0.07

Strong
Weak
Very weak
Null

Note: For the PVC and Anchored vortex, the width is based on the dimensions of section 0 and last measured, respectively.

CHAPTER 5

COMBUSTION EXPERIMENTS

5. COMBUSTION EXPERIMENTS

"Mr. Speaker, high natural gas prices and the summer spike in gasoline prices serve as a stark reminder that the path to energy independence is a long and arduous one."

Judy Biggert, U.S. House of Representatives (1937-)

Large scale coherent structures play an important role in combustion and heat release processes by controlling the size and shape of the recirculation zone in diffusion and premixed flames (Paschereit and Gutmark, 2008). The most important contribution to the turbulent momentum transport and considerable mass and heat transfer are attributed to large coherent structures, therefore often making it a defining parameter in engineering applications (Kuhn et al., 2006). Not only complex geometries, but also variation in wall surface configuration can increase the number of modes in certain regimes, changing the structures in the flow (Kuhn et al., 2006). This indicates the lack of understanding of the phenomenon and the real interaction between the flow and its surroundings.

Therefore, it is crucial to obtain a better understanding of such structures, to understand flame stabilization processes, whilst reducing instabilities that can cause damage and increase emissions. According to Bradley et al. (1998), some instabilities in swirl combustors are explained as a periodic extinction of the flame produced in the outer recirculation zone by stretching fluctuations due to periodic vortex shedding. Lee et al. (2000) has observed a high correlation between heat release and pressure fluctuation in the recirculation zones of their systems, confirming their importance in the combustion mechanism. However, their dynamic behaviour is poorly understood, as is their mutual correlation and real mixing mechanisms; these can tend to change the mixing patterns producing zones of unmixedness which can drive instabilities. Premixed technologies where fuel and air are mixed shortly before entering the combustion chamber often lead to a significant degree of unmixedness (Sadanandan et al., 2008). This generates a complex process that creates thermoacoustic instabilities which would feedback into the mixing-reaction process of combustion (Meier et al., 2007). O'Doherty and Gardner (2005) have suggested that the

appearance of vortices such as the precessing vortex core (PVC) improve the mixing due to the turbulent mechanism capable of creating larger scales which in the dissipation range of the energy cascade augment the interaction between particles. Moreover, recent studies by Bouremel et al. (2008) attribute high mixing levels to the interaction between large structures, their boundaries acting as the region for major exchange of mass and energy. However, these studies lack information on the direct definition and interaction between the large coherent structures that dominate the flow field, posing questions about the real nature of such phenomena.

Since the increase in instabilities in the system is linked to pressure fluctuations, heat release and strength of swirl (Malalasakera et al., 2008), and such mechanisms are correlated to large structures, the production of emissions such as NOx from such variances (Lieuwen and Yang, 2005; Lafay et al., 2006) and the damaging coupling of the latter with natural frequencies of the combustor (Huang and Yang, 2005) could be more efficiently tackled with the better understanding of the phenomenon involved.

During combustion, swirling flows are capable of recycling hot chemically active reactants to enable excellent flame stability to be achieved coupled with wide stability limits for diverse fuels (Lieuwen and Yang, 2005; Lafay et al., 2006; Al-Abdeli and Masri, 2007). Combustion may also occur in and around these structures (Khalatov and Syred, 2006) causing fundamental changes of flame stabilization mechanisms owing to changes in length scales, turbulent flame speed, flame stretch and other related parameters. Simultaneously or alone combustion may occur in flame fronts which engulf these coherent structures again giving rise to different flame stabilization mechanisms (Syred et al., 1984). Combustion may also suppress some time dependent coherent structures, although evidence is that acoustic coupling may well re-introduce them (Syred, 2006).

According to Lafay et al. (2006) and work at the International Flame Research Foundation (IFRF) (Morgan et al., 1995), the intensity of combustion has a low impact on the mean flow structure characteristics. Lafay et al. based his conclusions on the radius of the Inner Central Recirculation Zone (CRZ), which at different equivalence ratios did not showed variations in shape. However, this was only carried

out in a 2 dimensional analysis. The scaling trials at the IFRF with swirl burners, fired on natural gas, ranging in size from 250kW to 12 MW, (hence in power density) showed consistent non-dimensionable combustion aerodynamics above 1 to 2 MW sized burners. Many authors (Syred 2006; Khalatov and Syred, 2006) have found that the process of combustion changes the flow field compared to the isothermal state, roughly in line with the change in swirl number caused by combustion. Equivalence ratio, φ, is thus an important parameter as well as Re, as experience shows that changes in φ, depending on the mode of fuel injection, can completely change the structure of the important central recirculation zone (CRZ), indeed under some circumstances completely eliminating it (Syred 2006; Khalatov and Syred, 2006).

Despite some modeling successes, the results obtained for more intricate cases with high flow rates, high swirl and involving combustion leave much to be desired (Davidson, 2004; Pope, 2000). Therefore, systems that use high swirl numbers require extensive and expensive experimentation for optimization.

The CRZ is the phenomenon which is used so extensively in combustion systems for extending flame holding and stability (whilst keeping the hot flame away from the walls) as well as minimizing emissions via staged combustion techniques. Malalasekera et al. (2008) have shown that combustion products inside the CRZ continuously provide an ignition source, thereby stabilizing the flame. In the combustion state the associated PVC can often be damped with diffusion controlled combustion, but premixing is well known to excite the amplitude of the PVC to the detriment of the system (Syred, 2006), whilst acoustic coupling can make the PVC reappear even with diffusion controlled combustion. Thus, some authors (Shtork et al., 2007) have found that the release of heat in combustion situations does not affect severely the PVC structure, which can be attributed to the balance of energy; moreover, the strength of the structure decays at 0.6 D, with an increase of the mixing rate upstream (Shtork et al, 2007). The vortex breakdown phenomena typically occurs in swirl burners at around swirl numbers of 0.5, but is also strongly dependent on Re (Syred, 2006; Khalatov and Syred, 2006), low Re flows with high swirl numbers do not necessarily give CRZs, this can give problems with scaling burners.

Realizing the importance of large scale structures as drivers of combustion instabilities, researchers have developed passive and active methods to control these instabilities by modifying geometrical and vortical conditions inside of the flow. New configurations have been designed with successful reduction in emissions and efficiency increases. Trapping-vortex combustors have proved to increase the recirculation of particles in the combustion process when annular air is decreased and a second trapped vortex is added to the combustor via secondary after-bodies (Hsu and Goss, 1998). Elliptic burners have decreased the instabilities associated with fuel pockets due to vortical structures (Paschereit and Gutmark, 2008). The use of controlled piloted flames has also improved efficiency and reduced emissions (Farber et al., 2008) whilst the generation of vortical structures inside of the system has proved to reduce the motion and strength of structures capable of coupling with the natural frequency of the system as well as the PVC (Paschereit and Gutmark, 2006). Counter rotating swirlers have also been analysed with success (Mongia et al., 2007).

Thus, this chapter explains the experimental approach used to characterise large coherent structures in swirl burners under combustion conditions so as to reveal the effects of swirl, Re and φ in a number of geometries. Aided by different techniques such as High Speed Photography (HSP), CH* Photo Chemiluminescence (CH* CL) and Particle Image Velocimetry (PIV), the recognition of several structures was achieved.

5.1. Experimental Setup

Experiments were performed in a 100 kW Steel versions of a 2 MW Swirl burner under combustion conditions. Two tangential inlets were used together with variable width inserts in order to change the swirl number for each case. Three different configurations were utilized during the procedure. These are reported as [50-50], [50-0] and [25-25]. The system was fed by a centrifugal fan providing air flow via flexible hoses and two banks of rotameters for flow rate control and a further bank for the injection of natural gas. The inclusion of a stainless steel mirror 0.8 m from the outlet (and rotated by 45°) allowed the radial-tangential visualization of the system when flames were present, figure 5.1.

Two different modes of natural gas injection were utilized for the prototype; a diffusive mode with fuel injected along the central axis from the burner bottom and a premixed mode with entry in one or both tangential inlets, located before the inserts used for varying the swirl number. Premixed gas injectors, extending across the inlet ducts, were located just before the inlets. Overall equivalence ratio φ is reported as well as the fuel proportion injected diffusively by the fuel injectors mounted along the axis followed by that injected as premixed in the tangential inlets. The format (25-80) here refers to 25 l/min diffusive natural gas injection, the 80 l/min to that injected as premixed. Due to the high temperature variation, the Re is defined from the nozzle diameter and isothermal conditions.

Figure 5.1. Experimental Setup

Pressure fluctuation measurement was made with a EM-1 Yoga Electret Condenser Microphone, with a frequency response of 20 Hz-16 kHz and sensitivity of -64±3 dB. Its resolution allowed the determination of high pressure peaks attributed to the existence of a crescent shaped high momentum region linked to the PVC. Even thought the signal was obtained successfully, combustion processes created a more unstable signal and filtering was needed. The signal was analyzed using the Tektronic DS2024B Oscilloscope at 2 Gsamples/s, 200 MHz and four channels.

No Phase Locked measurements were tried during the first part of the experiment, so free runs were allowed for the recording of the phenomenon with the aid of a High

Speed Photography system. A Fastcam High Speed Camera model Apx RS of 250,000 frames/s maximum speed was used with a 105mm, 1:2.8 Nickon Lens. The camera was setup at only 4,000 frames/s to avoid resolution problems and increase the visual field, since the frequency of the large coherent structures has been observed to lie on the range of 100-200 Hz (Valera-Medina, 2006; Vaniershot et al., 2008). The resulting images were analyzed using the PFV version 2.4.1.1 software. The radial-tangential characterization of the system from the mirror could be simultaneously matched with the axial-radial results.

Aided by a 429 nm wavelength filter of 10 nm bandwidth (at 50% of transmissivity), the intensity of the flame was also analyzed with a CH* chemiluminescence emission technique, the camera being set to 60 frames/s due to light intensity considerations and required exposition time.

Different equivalence ratios were investigated, from very lean conditions at 0.151 to near stoichiometric values at 1.050. A wide variation in the airflow and gas flow rates was also made to visualize the progressive development of the coherent structures. Different modes of fuel injection were used, as other authors (Syred, 2006; Farber et al., 2008) have shown that various structures, flames types and stability conditions can be achieved with the tuning of fuel injection positions and their relative position with respect to the burning zone.

Three different systems were used to change the diffusive fuel injector, all extended from the burner baseplate to near to the rig nozzle, detailed below. This study is carried out as a consequence of the problems related to the injection system (Brundish et al., 2007). High momentum injection within the swirler shows less sensitivity to pressure variations than those observed in air. Fluctuations in air supply can thus produce significant variation of equivalence ratio, creating gas pockets of varying equivalence ratio inside of the system. This represents the first step of a feedback loop known as oscillating fuel supply combined with a convective time delay (Meier et al., 2007; Dhanuka et al., 2009).

- Narrow injector, 9.9 mm diameter. Positioned 0.9 mm upstream of the burner exhaust.
- Wide injector, 23.4 mm diameter. Positioned 47.5 mm upstream of the burner exhaust.
- Perforated injector of 27.5 mm diameter, with 8 perforated holes of 1.7 mm each. Positioned 11.6 mm downstream of the burner exhaust.

A graphic representation of the system is shown in figure 5.2.

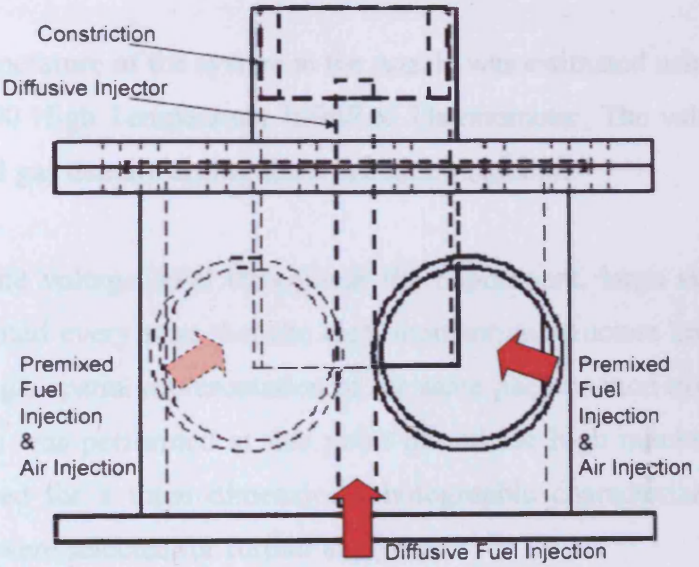

Figure 5.2. Diagram of the System, Fuel and Air injections. No constrictions were used for this part of the experiment.

Follow on experiments were made using a Phase Locked PIV system. This technique has proved to be consistent with the results of different experiments under a variety of approaches (Valera-Medina, et al. 2008b) as well as for the use of advance filters for the characterization of large coherent structures (Vaniershot et al., 2008).

The use of Condenser Microphones has been used by others for acoustic measurements (Schuermans et al., 2004; Krebs et al., 2002; Paschereit and Gutmark, 2008). Its signal was conditioned to obtained low-frequency parameters related to large scale structures. This signal was redirected to a BNC Model 500 Pulse Generator, whose TTL signal was sent to a Dantec PIV system. The latter consists of a Nd: YAG Litron Laser of 532 nm at 5 Hz and a Hi Sense MkII Camera model C8484-52-05CP, with 1.3 MPixel resolution at 8 bits. A 60mm Nikon lens was used

for resolution purposes, with a depth of view of 1.5 mm. The inlet air was seeded with aluminium oxide Al_2O_3 by a Venturi system positioned 2.0 m upstream of the burner inlets. 250 l/min of air were used to fluidize the seeding material; this was accounted for the determination of the final flowrate. The entire system was triggered at 90% of the highest peak observed after 5 minutes of free run. It is recognised that this empirical value was arbitrary, yet consistent with all the measurements and previous experiments, enabling a quantitative comparison between cases. The entire system is depicted in figure 5.3.

The average temperature of the system at the nozzle was estimated using a Kane-May Ltd Infratrace 800 High Temperature InfraRed Thermometer. The value was used to define the air and gas density during the combustion reaction.

Being at the same voltage level throughout the experiment, large structures of the system were framed every time that the high momentum structure crossed the same position, allowing a spatial representation of the same phenomenon every cycle. Only a planar analysis was performed at this point due to the high number of cases that could be analyzed for a three dimensional holographic characterization; the most intriguing cases were selected for further analysis.

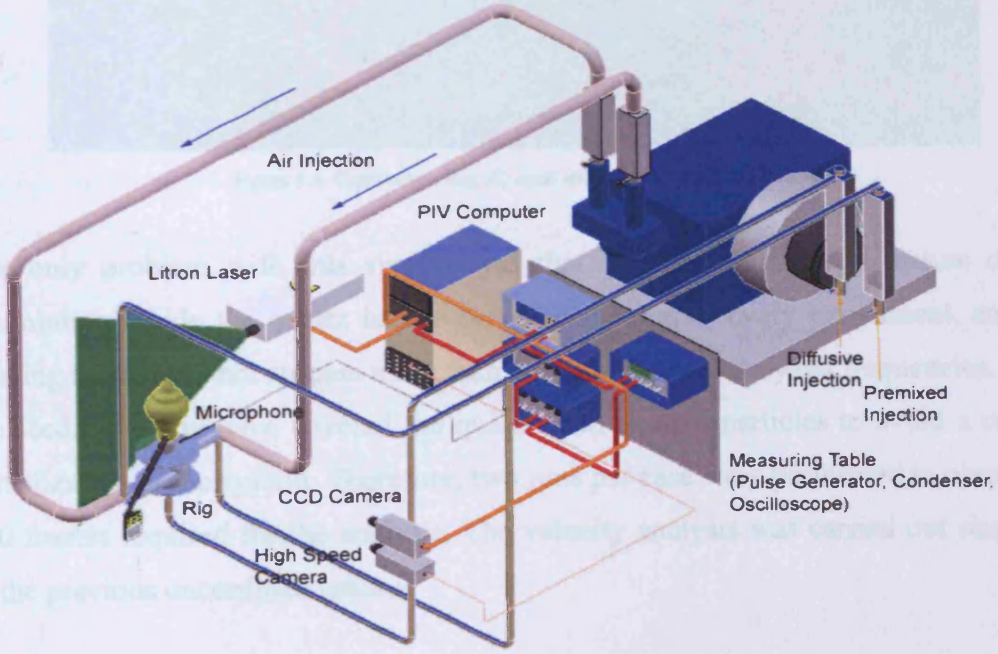

Figure 5.3. Setup of the Entire System, including HSP and PIV.

The experiment was expanded to the study of confined flames in two different geometries. Since interesting results were obtained using a circular confinement, the analysis was done using this geometry, with open and conical shapes, the latter being the most representative of combustors and burners. For the flame analysis, the Phase Locked PIV system was used. Therefore, access to the inner system was performed using a cylindrical cylinder quartz of 154 x 6 x 130 mm, with a cone of 2Dx1Dx1D, as shown in figure 5.4. Due to reflection caused by the cylindrical shape of the quartz, white panels were placed in front of the CCD camera in order to avoid burning its sensors. This reflection only occurred at the walls of the system, making impossible the visualization of the latter. Moreover, a small amount of light was observed in the posterior wall, making mandatory covering it with black, high temperature resistant paint. After some trials, it was found that this was the best option, giving very good results without noise.

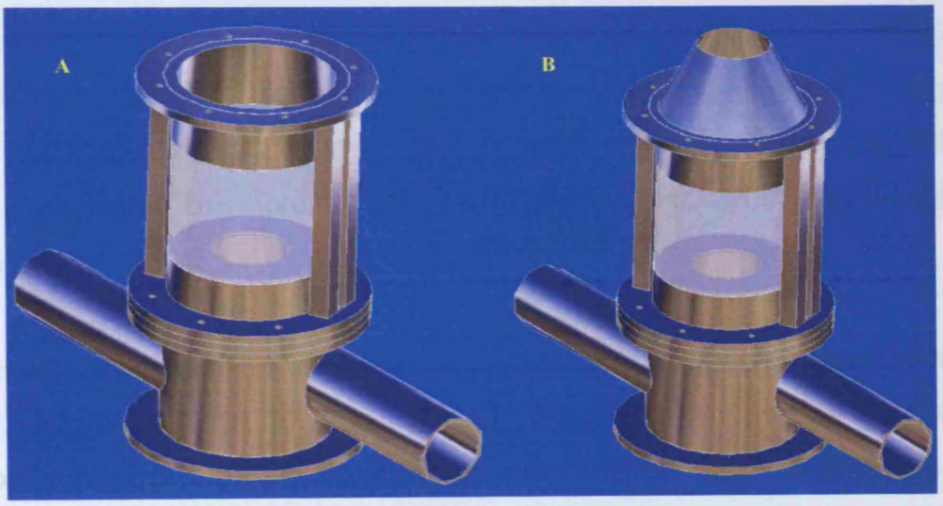

Figure 5.4. Combustion Rig, A) open and B) confined geometries.

The only problem with this system was that due to the corrosive nature of the Aluminium Oxide the quartz had to be cleaned up after every experiment, and the running time could not surpass more than 80 frames at the analyzed frequencies, since the seeding would have covered the quartz with enough particles to avoid a correct visualization of the system. Therefore, two runs per case were performed to obtain the 150 frames required for the analysis. The velocity analysis was carried out similarly to the previous unconfined cases.

A fixed air and gas flows condition would be used for the reconstruction of 3D bodies. The conditions would be selected from experiment where more efficiency in creating the CRZ was observed, at safe-stable conditions (moderate flowrates). To allow complete visualization in 3D space, the laser was moved circumferentially around the outlet lip every 11.25°, as in the isothermal case. Each section will be referred according to the position where the Laser was placed during their acquisition. It must be remembered that this is only a spatial correlation between sections, since each of them is time locked. The objective was to recognise the position of zero velocities where the CRZ existed so as to define the boundaries of the structure.

5.2. Experimental Approach. Open Combustion.

5.2.1. High Speed Photography

Three different isothermal Swirl Numbers, S, were used for the series of experiments here presented. These are; case [50-50], S=1.86; case [50-0], S=1.06; case [25-25], S=0.98. Although the swirl number is expected to change due to the increase in temperature (equation 2.8) the great variance at the outlet made difficult the definition of a unique value. Therefore, the cold isothermal number was kept as the reference number.

First results showed the existence of the Precessing Vortex Core, figure 5.5 and 5.6. Some configurations not only showed traces of a single core, but the existence of a pair of vortices that spiraled opposite to each other for some milliseconds. Syred (2006) and Valera-Medina (2006) have earlier noted the phenomenon. Figure 5.5 shows the progression of the phenomenon, which was obtained at S = 1.86, low Re ~ 12,000 and φ = 0.39. The phenomenon is visualized as a rich burning flame in the central region of the burner, the low density fuel being entrained into the PVC, burning on its boundary. Low density reactants and products are trapped inside the PVC, which evolves as a semi-helical structure, doubtless wrapped around a CRZ.

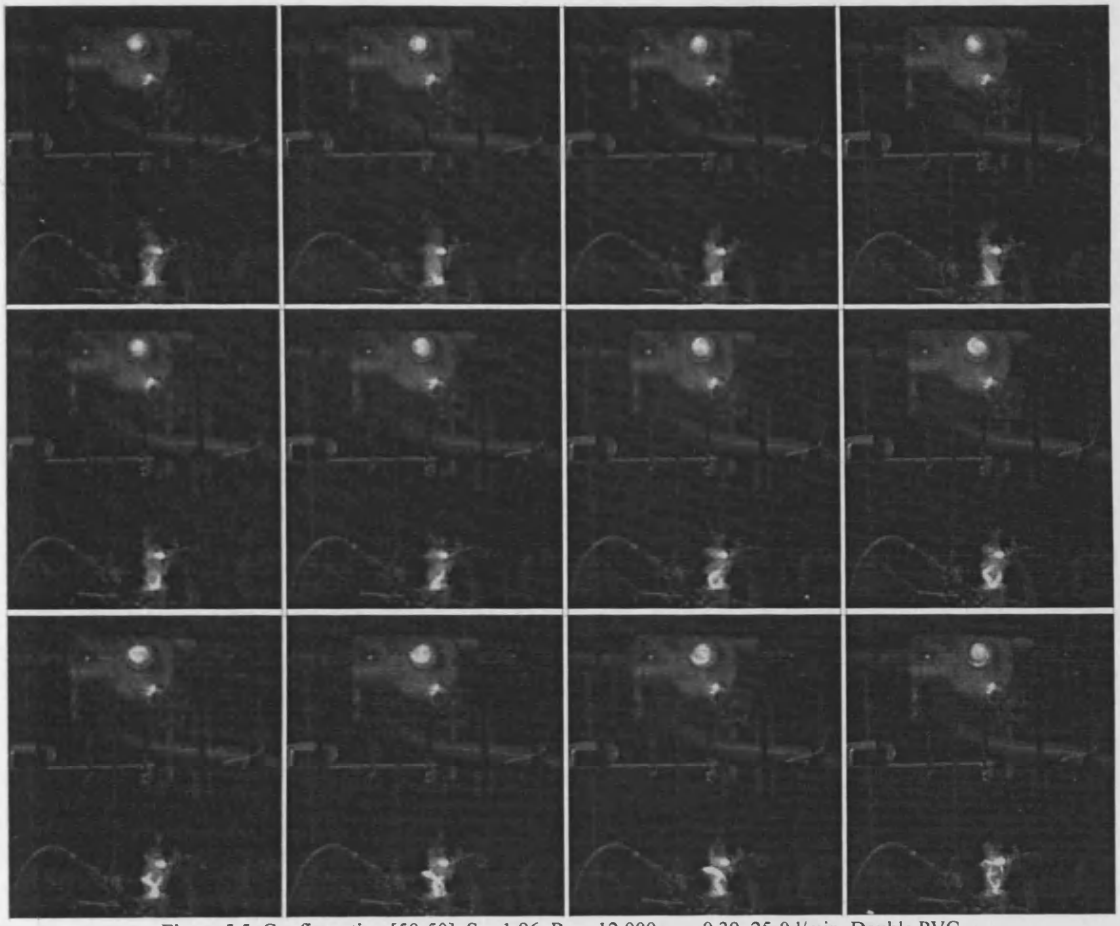

Figure 5.5. Configuration [50-50]. S = 1.86, Re ~ 12,000, φ = 0.39, 25-0 l/min. Double PVC.

Figure 5.6. S = 1.86, Re ~ 15,700, φ = 0.29, 25-0 l/min.
Single PVC.

After ~0.012 s the main vortex splits in two parts, and the largest is expelled to a more radial position due to centrifugal forces; this forces the remaining structure to also move radially, forming a twin PVC structure which only remains stable for a couple of milliseconds, followed by their collapse into a merged vortex, which subsequently dislocates from the burner; the isolated structure remains visible for

several milliseconds. The entire process from the creation of the main vortex to the disappearance of the isolated structures takes ~0.046 s. It is thought that the PVC is stretched to a point of annihilation by the CRZ.

Different methods of fuel injection resulted in different flame types. According to Vanovergerghe (2004) and Vaniershot (2007), certain flames can only be obtained after transition from a specified flame has occurred. This proved to be the case, where the PVC could only be obtained after a laminar flame is strained by the swirling flow. When the flame was reignited in an already strained field with high swirl, the PVC did not developed, forcing the shut down of the system in order to generate the latter. This phenomenon was observed several times, confirming that the vortex core could only develop after going through this flow transition, probably related to the appearance of the vortex breakdown in the field. However, this is left for future works.

Increasing Re and decreasing φ, the double PVC disappeared, and a more stable single system developed. This was correlated to a more stable CRZ. The increase in tangential inlet flow and velocity has caused a compact, well defined recirculation zone to appear as shown by the isothermal experiments and Dawson (2000). The higher flow velocity stretched the vortex, creating a larger structure whose life time is ~0.13 s, somewhat higher than the previous case. The system collapses afterwards, with the creation of an isolated vortex which disappears downstream. Figure 5.6 shows the PVC.

The PVC is a structure that is born at the baseplate of the rig when there is no fuel injector; it can be a stable structure or is periodically shed from the burner baseplate under unstable flow conditions, especially at low Re. A process of compression and expansion caused by the straining of the inner flow could be responsible for the movement and long life expectancy of the vortex in the vicinity of the CRZ and the shedding flow, as discussed by Alessenko et al. (1999). Although the roughness of the baseplate was not considered for the experiments, it is recommended an expansion on this topic, specially due to the changes in thickness of the boundary layer which will alter the pressure in the vicinity of the baseplate, probably causing changes to the PVC.

Isothermal experiments performed in chapter 4 confirm that the helical shape of the PVC only occurs just downstream of the burner exhaust, it then straightens whilst continuing to precess as it decays. This contradicts numerical and theoretical predictions that claim a complete helical movement around the CRZ, at least in this type of swirl system.

Increasing Re and decreasing φ, the PVC decreases in size somewhat. The signal obtained presents more features of an isothermal case due to the reduced temperature and lower position of the flame. This can be observed in Figure 5.7, where various conditions at the same gas flow rate and diffusive conditions were investigated.

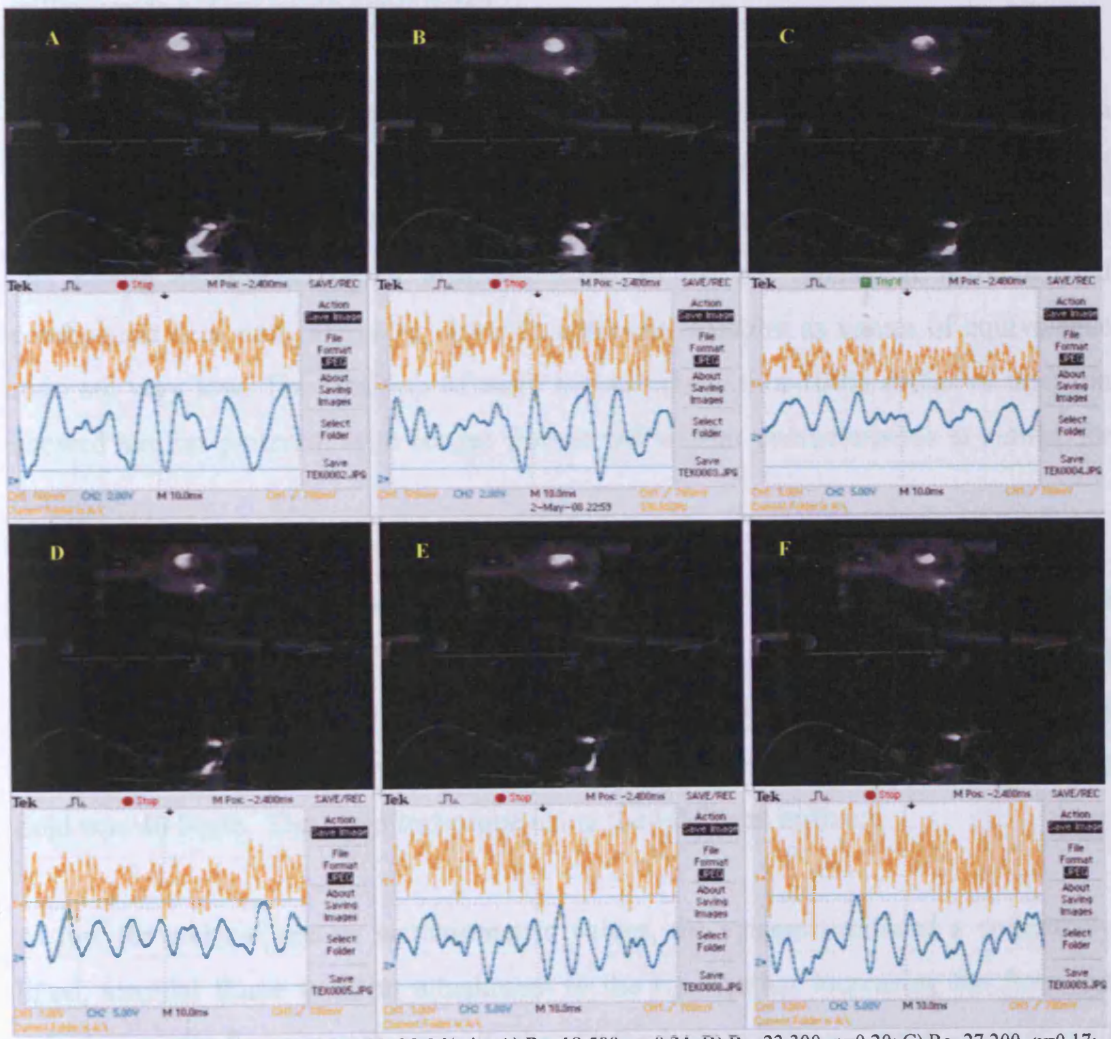

Figure 5.7. Configuration [50-50]. S=1.89, 25-0 l/min. A) Re~19,500, φ=0.24; B) Re~23,300, φ=0.20; C) Re~27,200, φ=0.17; D) Re~31,000, φ=0.15; E) Re~38,600, φ=0.12; F) Re~42,500, φ=0.11. Notice the change in signal scale for the last 4 cases.

Keeping the same configuration [50-50], the gas was increased to 30 l/min. This produced an unstable double PVC at low Re and lean conditions, whose wobbling structure lasted up to 0.18 s. The associated CRZ is weak and unstable. Increasing the air flow rate further, a single more stable PVC system develops, followed by the previously observed reduction at higher Re and lower φ.

Augmenting the gas rate to 35 l/min, the flow patterns changed. First, no PVC was observed at very low Re, not even the single PVC. Only a lifted blue flame was noticed, with no clear attachment to the burner exhaust. Increasing the flow rate further, the flame moves back into the burner and a blue envelope starts to form. At this moment, a very weak and unstable PVC develops, which lasts only a few milliseconds before being annihilated.

This tendency continues as flowrates are increased, with a stronger PVC. After a quasi-stable regime, the PVC then starts to compact. From this point, the stability of the PVC decreases and its life time is reduced considerably. However, the vortex is still strong enough to reach locations close to the rig nozzle. It is recognized combustion here only serves to visualize coherent structure as values of equivalence ratio are very low. The addition of more natural gas with a 100% diffusive injection showed similar patterns, with longer flames but similar characteristics at similar Re numbers.

In order to confirm the existence of helical structure with different cases, premixed gas injection was studied. Two different techniques of injection were used, with both two and a single inlet, in order to observe the stability of the flame. The diffusive gas was left at 25 l/min to ensure flame stability. The total premixed gas injected into the field was 40 l/min. The same technique using the HSP was utilized.

At low Re and φ close to stoichiometric values, the system produced a completely lifted, toroidal flame with no attachment to the rig. Further increasing the flow and reducing φ, the flame envelope reattached to the burner exhaust, but it was not until Re~28,000 and φ=0.43 that a sporadic, weak PVC was observed, gaining strength when increasing the flow. However, at higher Re and lower φ the unstable, intermittent PVCs reoccurred, never reacquiring its pseudo-stability. Similar

tendencies were observed for the single inlet fuel injection case, with no visual differences.

A fluctuating pressure intensity analysis was performed for all cases in order to compare their signals. The results would allow the definition of structures with higher stability based on smoother signal behaviour. Figure 5.8 shows the results. The first cases using 100% diffusive injection (25-0: 30-0: 40-0 l/min) all showed very stable trends over the whole flow range tested, indicative of a stable CRZ and associated structures. Partial premixed combustion (25-40, 2 inlets: 25-40 1 inlet) gave more irregular curves, indicative of changing flame stabilization patterns and coherent structures as the Re was changed as well as the level of premixing. However, higher equivalence ratios showed similar pressure fluctuations to the observed at lower φ with 100% diffusive injection, confirming higher stability with premixing.

The use of 100% premixed injection was also studied, but the unstable mechanism of combustion did not allow the complete development of the flame, collapsing all structures at moderate flow rates.

Blow off was observed at high Re and flashback at low Re, making impossible comparison with previous cases. Therefore, some level of diffusive fuel injection was required to achieve stability in the combustion process (Syred, 2006; Farber et al., 2008).

Configuration [50-0] was also analyzed to compare results. First, 25 l/min of 100% diffusive gas were injected. Some noticeable differences were that the PVC at the lowest Re and low φ did not appear as a compact well-formed structure, but more like a vortex with a centralized position and various bifurcations, which gave the impression of double structures.

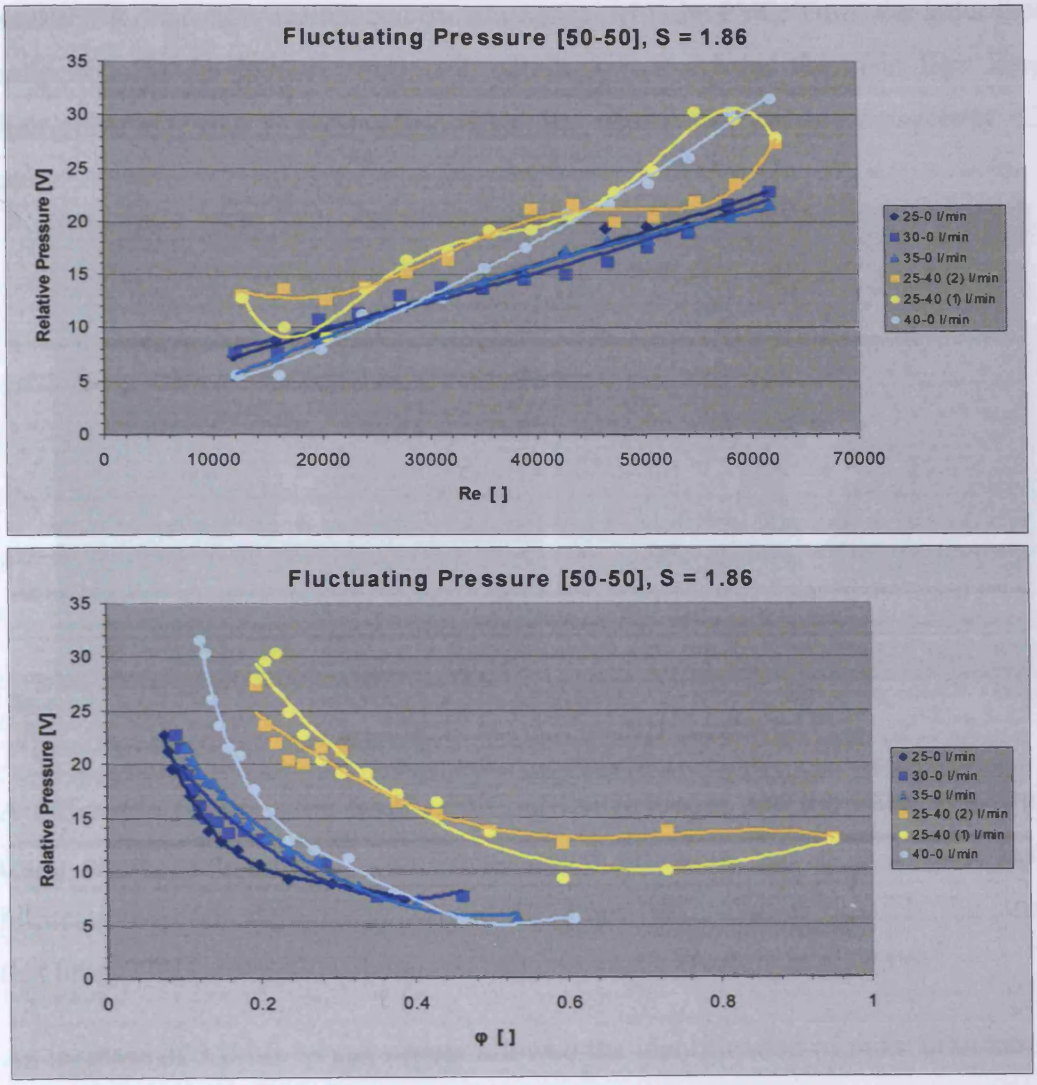

Figure 5.8. Fluctuating Pressure between different cases using configuration [50-50] v Re and Equivalence Ratio, respectively.

The latter were long enough to twist around the PVC, completing several cycles around it. It was verified that each of the twisting projections emanated from the main vortex, eliminating the hypothesis of helical double vortices for this case. Increment of flow rate stabilized the structure, but bifurcations were still present. A more stable PVC was observed at higher Re, even though the life expectancy never surpassed the 0.09 s, the time that the core would remain coherent and bifurcated. This sporadic structure was observed several times, although it appeared only after long periods of running the experiment. The latter was thinner than previous cases, although it was still coherent. Life expectancy dropped to 0.05 seconds. Finally the PVC disappeared from the visual range. It is evident that the structure is still forming inside the rig, before the nozzle. The flame was more elongated with apparently a narrower and

weaker CRZ strongly influenced by interaction with the PVC. Thus, the latter created projections as the contact continued, which then re-entered the main flow keeping their coherence due to momentum exchange whilst disappearing completely 0.28 s later.

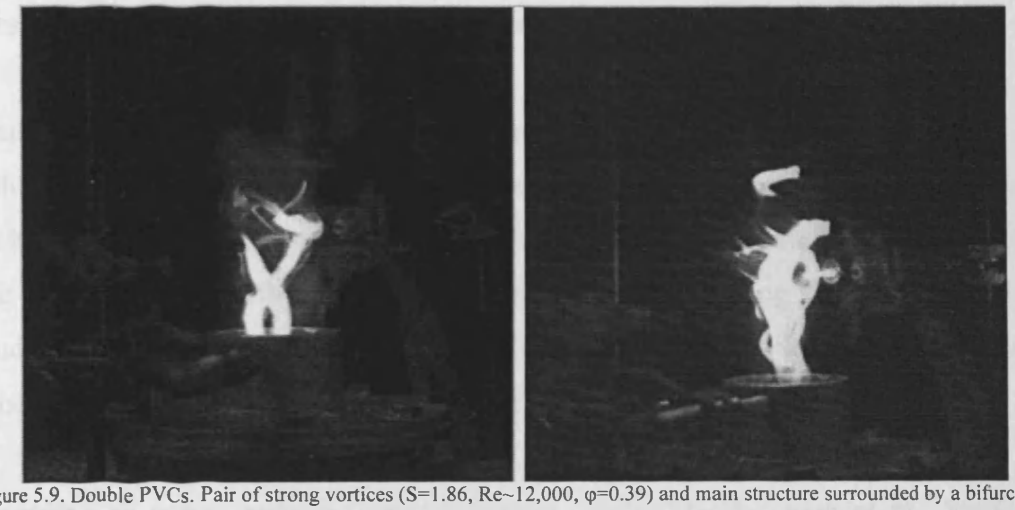

Figure 5.9. Double PVCs. Pair of strong vortices (S=1.86, Re~12,000, φ=0.39) and main structure surrounded by a bifurcating vortex (S=1.06, Re~12,000, φ=0.39), respectively.

A difference between the double PVC of the first case and the bifurcated structure using configuration [50-0] can be observed in figure 5.9. It is evident that the bifurcation spirals completely around the inner PVC. This is possibly the structure that many CFD simulations have tracked previously (Freitag et al. 2006).

An increase of 5 l/min in gas supply allowed the identification of more bifurcations in the flow, with some that were larger and twisted even more than the preceding case. The higher energy output fed the system, creating structures with life expectancies over 0.35 s.

The first case at low flow rates showed the existence of a flame whose envelope was wobbling, re-attaching to the rig sporadically. As the Re was increased and φ decreased, the bifurcations diminished and the PVC stability increased. However, after a stable range the vortex decreased its size and was again confined to inside of the rig.

Following the same methodology, 35 l/min of diffusive natural gas showed different results to the uniform [50-50] condition. Different to any other case, some isolated vortices appeared in the wide lean flame. These vortices had a relatively high life

expectancy of 0.12 s. Due to the reduced straining force of the CRZ, these vortices evolved gradually and slower than their counter parts at higher S, thus living longer. A higher air flow rate created longer structures that bifurcated into several eddies which last up to 0.08 s. Only small and intermittent flashes were observed at low flow rates, with no coherent structure in the burner exhaust vicinity.

Finally the case 40 l/min of diffusive gas was investigated. For the first low Re, only a blue envelope was observed downstream of the burner exhaust. This re-attached to the burner at higher air flows, creating a very weak and sporadic PVC at Re~20,000. The stability of the PVC increases slightly when increasing the flowrate, giving structures whose life fluctuates between 0.08 and 0.10 s. No PVC can be observed since the flame and flow is totally confined inside of the rig at elevated Re.

According to some authors (Vanoverberghe, 2004; Malalasakera et al., 2008) the appearance of the lifted flame is a consequence of the interaction of the flame, inner and external recirculation zones. Since the flame speed is lower than the velocity of the flow at the nozzle, the flame is lifted with some recirculation zones providing both fresh and hot reactants that stabilize the system. However, this must be corroborated by other work.

Premixed injection was used as before at 40 l/min with 25 l/min of diffusive gas. Two cases were analyzed. The first case, with both premixed gas inlets open, gave a lifted bluish flame. Its emissivity was higher than any previous case. No PVC was observed, not even with increase of the air flow rate. However, the flame moved back into the rig nozzle at 1,000 l/min creating instabilities that were possibly the manifestation of the PVC. The tendency continued during the entire experiment, with no coherent PVC(s) being observed. The case with only one tangential inlet open [0], i.e. one inlet without insert, showed the same behaviour as the case with both inlets.

In order to compare all cases and estimate the stability of each one a fluctuating pressure comparison was made. Only the first 6 cases were analyzed, since all structures were completely confined inside of the rig at higher Re. Figure 5.10

presents the results and demonstrates how the diffusive flames at higher Re are more stable than the premixed-diffusive.

The final configuration used for this geometry used the [25-25] inserts. Previous experiments (Dawson, 2000; Valera-Medina, 2006) showed this to be the best configuration for the formation of coherent structures. Using 25 l/min of diffusive gas the peaks of the signal disappeared. No PVC was observed, instead a blue attached flame envelope was found near the rig nozzle. When increasing the flow rate only sporadic vortices occurred. These were elongated unattached concurrencies that showed some patterns reminiscent of the PVC. Their signal continued to be very small in magnitude.

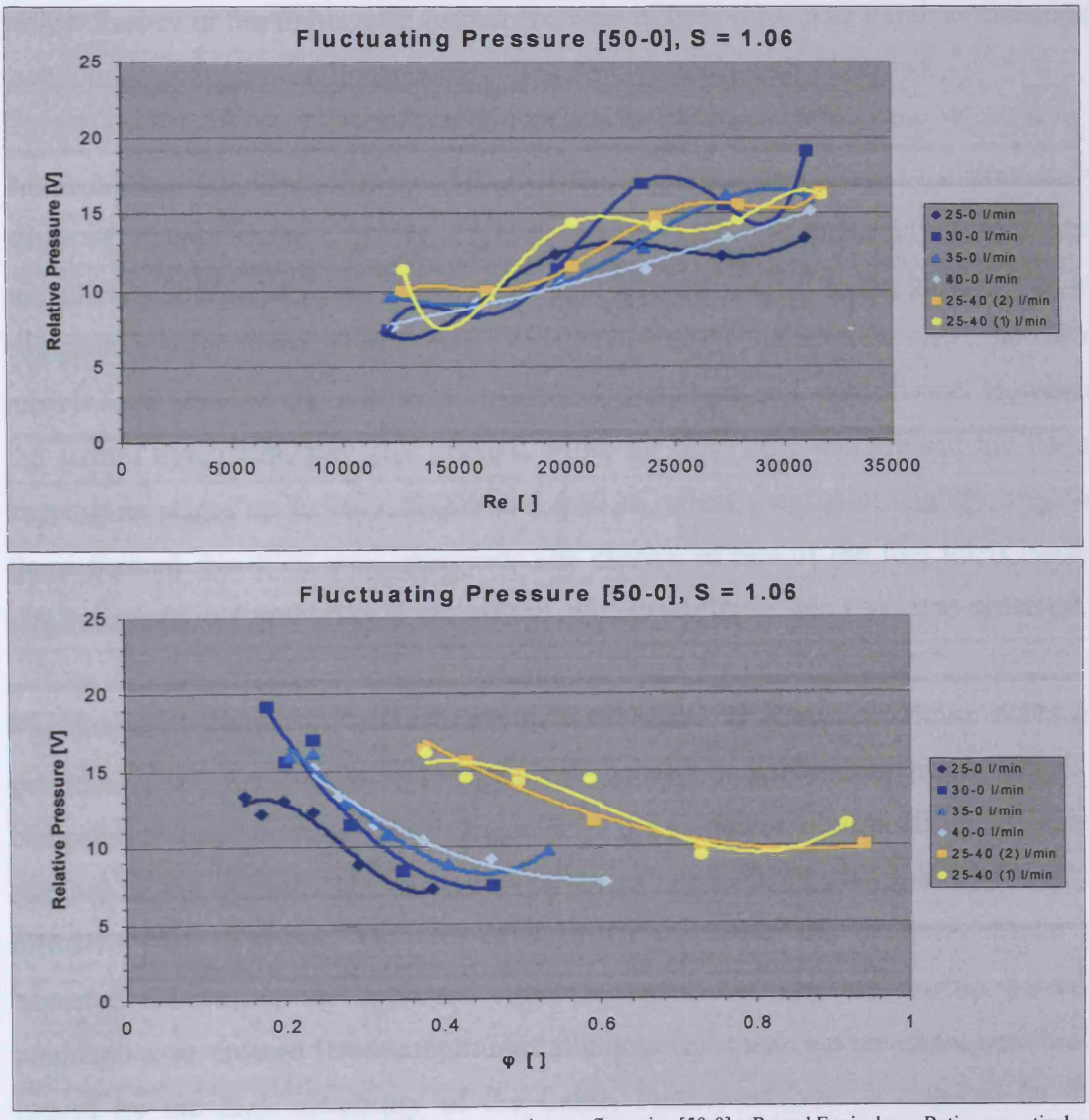

Figure 5.10. Fluctuating Pressure between different cases using configuration [50-0] v Re and Equivalence Ratio, respectively.

At higher Re, the typical PVC signal was observed and sporadic, intermittent vortices of 0.04 s duration were observed. These increased their life expectancy to ~ 0.06 s at higher flow rates, but reduced their length. Finally, higher Re compressed the flame completely.

Although the well known PVC signal was present, the maximum voltage obtained was reduced in comparison with other cases. Increasing the gas supply by 5 l/min only slightly altered the amplitude of the signal, size and shape of the flame envelope.

Further increase of natural gas to 35 l/min gave a long blue attached flame envelope, swirling around the nozzle at very low Re and lean conditions, followed by a series of yellow flashes in the flame with further increase in flow rate. The trend continued up to 40 l/min, with no clear appearance of the PVC as previously observed.

Premixed fuel addition with the diffusive fuel significantly changed the previously observed flame shape. At Re~12,700 and φ=0.87, an extremely large, blue sporadically lifted flame envelope developed, toroidal shaped at the bottom with an elongated central flame, similar to an elongated hat. At higher flow rates, the flame moved back into the rig, and the toroidal shape changed to a conical one. However, the central elongation was still present. More air flow only compressed the flame, keeping its shape up to Re ~24,000 and φ=0.36, when a compact slightly irregular flame formed. No PVC was observed. The closure of one of the fuel inlets caused size variations and wobbling to the central, elongated flame. No PVC was observed.

The fluctuating pressure comparison between cases is shown in figure 5.11. As previously, the first cases at low gas rate present a polynomial trend, which if compared to configuration [50-0], figure 5.10, are smoother, corroborating the higher stability of the system. The system experiences more stability with the increase of diffusive fuel injection. The use of premixing reduced the pressure change as expected. However, the pressure curve measured for the asymmetric partially premixed case showed lower amplitudes at higher flowrates, a phenomenon probably caused by the high instability of the flame. Further analysis is required on this exception.

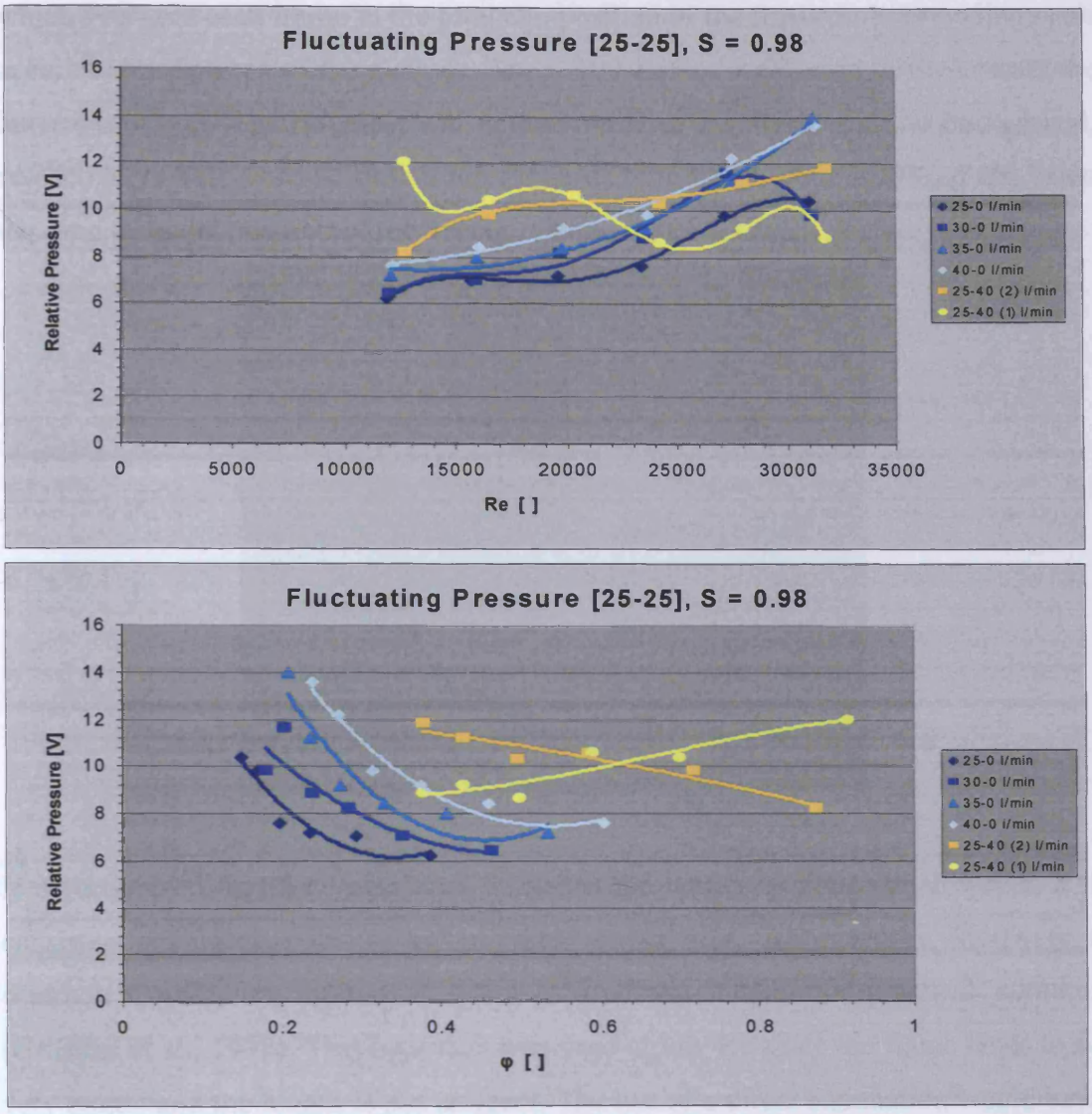

Figure 5.11. Fluctuating Pressure between different cases using configuration [25-25] v Re and Equivalence Ratio, respectively.

The results with only one premixing inlet used clearly showed greater irregularity and the importance of proper premixing. Flames tended to develop inside of the rig since the diffusive injection is at the baseplate. Hence three extended fuel injectors were used to push the flame past the rig nozzle so as to be able to identify the positions of the different coherent structures that interact in the system.

Experiments were run both to obtain the fluctuating pressure generated for each configuration, also to measure flame length and size. When the flame was extremely random in size, especially for the lowest Re cases, a computational algorithm was used to determine the average shape and position of the flame. Different to others (Griebel, 2007) who have used the summation of all images, an algorithm was used

which averaged each frame in the total composition of the final result, providing more accurate descriptions of the average flame. 500 frames were used to reconstruct the latter (Annex 2). The brightest and darkest point of the flame and the background, respectively, were used to define the range of luminosity, with a 90% of the value defining the axial position of the average flame, figure 5.12.

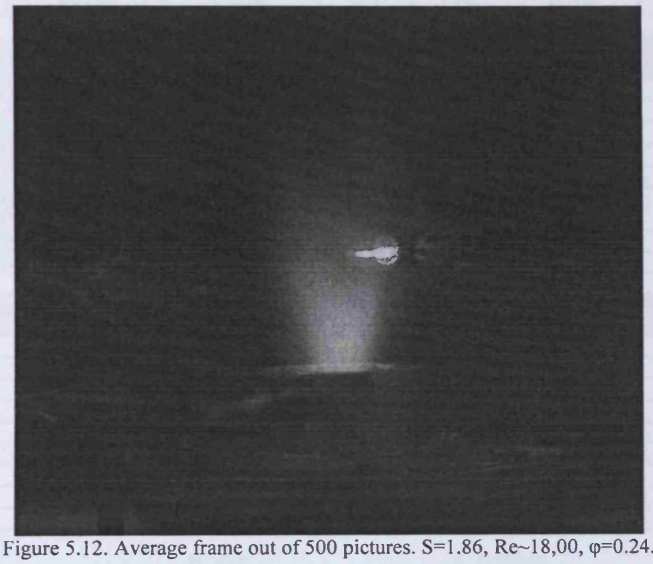

Figure 5.12. Average frame out of 500 pictures. S=1.86, Re~18,00, φ=0.24.

It is recognized that the value used to define the length is arbitrary. However, it is consistent among experiments and provided a good analytical response. Moreover, a common Confidence Interval of 90% is used statistically for practical purposes (Griffiths et al., 1998). This approach was used at low Re since the flame tends to be very erratic and the length is not uniform. The use of a direct summation would have led to longer flames whose position would be only defined by few pictures out of hundreds, an incorrect assumption. This problem was not observed at higher Re, where the flame was highly stable, especially for diffusive-premixed flames.

Due to the high number of independent variables in the system, the number of cases considered was reduced to 100, where shape, color, flame type and coherent structures were analyzed. Table 5.1 shows an example for configuration [25-25], 25-0 l/min, with a Wide Injector. Here the presence/absence of the PVC was not noted as this would have involved extensive probing, PIV or similar techniques. The degrees of freedom were vast enough to give thousands of points and features for all the flames.

Table 5.1. Example of Experimental Table required for Complete Analysis of the Flame.

Airflow (l/min)	Re Isotherm. []	Vel (m/s)	Temp °C	Temp K	Length (m)	Rel. Pres. (V)
600	10993	2.072	213	486	0.65	0.680
800	14511	2.736	222	495	0.52	0.760
1000	18028	3.399	225	498	0.40	1.040
1200	21546	4.062	226	499	0.30	0.880
1400	25064	4.725	222	495	0.28	0.880
1600	28582	5.388	220	493	0.22	1.080
1800	32099	6.051	219	492	0.21	0.520
2000	35617	6.714	218	491	0.19	0.720
2200	39135	7.378	227	500	0.18	1.000

Gas density	Air density	Gas Used	Air used	Equivl. Rat.	Flame Characteristics		
kg/m3	kg/m3	l/min	g/s	[]	Emission	Gas smell	Type
0.402	0.727	25.000	7.270	0.396	H	N	C
0.395	0.714	25.000	9.520	0.297	R	N	C
0.393	0.709	25.000	11.817	0.238	R	N	C
0.392	0.708	25.000	14.160	0.198	R	N	C
0.395	0.714	25.000	16.660	0.170	S	N	C
0.397	0.716	25.000	19.094	0.149	S	N	F
0.398	0.718	25.000	21.540	0.132	S	N	F
0.398	0.719	25.000	23.967	0.119	S	N	F
0.391	0.706	25.000	25.887	0.108	S	N	F

Flame Characteristics							
Note	Top Colour	Top Shape	Bottom Col.	Bottom Shp.	Entrance Burner	Recirculation	PVC
----		T		L	N	N	N
----		T		L	N	N	N
Medium Stagnation		W		L	N	N	N
Diluted bottom		W		L	Y	Y	N
Diluted bottom		W		L	Y: 1-2 cm	Y	N
Diluted bottom		W		W	Y: 1-2 cm	Y	N
Diluted bottom		W		W	Y: 1-2 cm	Y	N
Diluted bottom		W		W	Y: 1-2 cm	Y	N
Diluted bottom		W		W	Y: 1-2 cm	Y	N

Yellow flame	H: High	C: Concave	D: Double ring flame
Yellow projection- Thin Blue brush	R: Regular	F: Flat	Prj: Only projections
Blue flame	S: Small	Sp: Sparkling at the top	Lif: Lifted flame
Blue flame-yellow sparks	T: Turbulent, with projections	P: Pulsating	
Blue flame-yellow Inner projection	W: Wrinkled	N: Not observed	
Flashback limit	L: Laminar, Swirling	Y: Observed	

Each case possessed different parameters according to the diffusive fuel injector extension, Re, S and φ used. A system map based on shape and stability was constructed, similar to those obtained by Lafay et al. (2006) and Bradley et al. (1998). Figure 5.13 and 5.14 show the maps for configurations [50-50] and [25-25] using a narrow fuel injector extension.

Different flow/flame regions were recognized during the experiment, as follows:

A) Unstable, very long flames. They could be lifted and unattached; very close to the flashback point.

B) Stable, wrinkled, long flames. All flames were attached to the burner exhaust. Swirl was evident at the bottom and wrinkled elongations at the top.

C) Stable, conical, medium length flames. These flames were not as compact as those at higher Re. For 100% premixed flames, only remnants of the PVC were observed. Large stable recirculation zones expected.

D) Stable, flat, small flames. Strong recirculation causing flame quenching and poor combustion, leading to blow off for 100% premixed flames at higher Re.

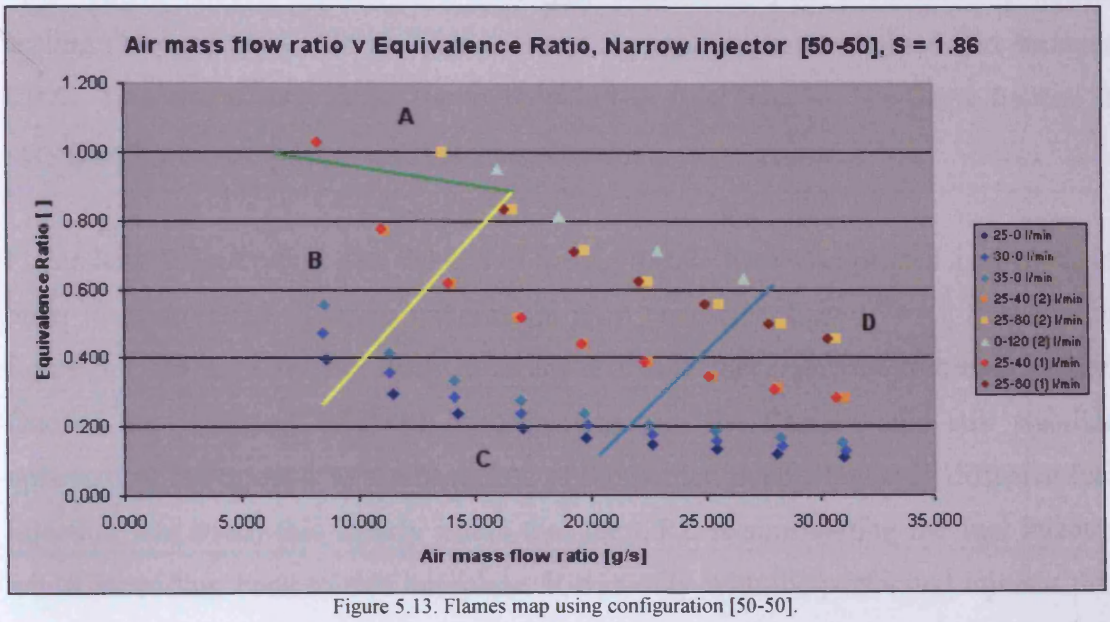

Figure 5.13. Flames map using configuration [50-50].

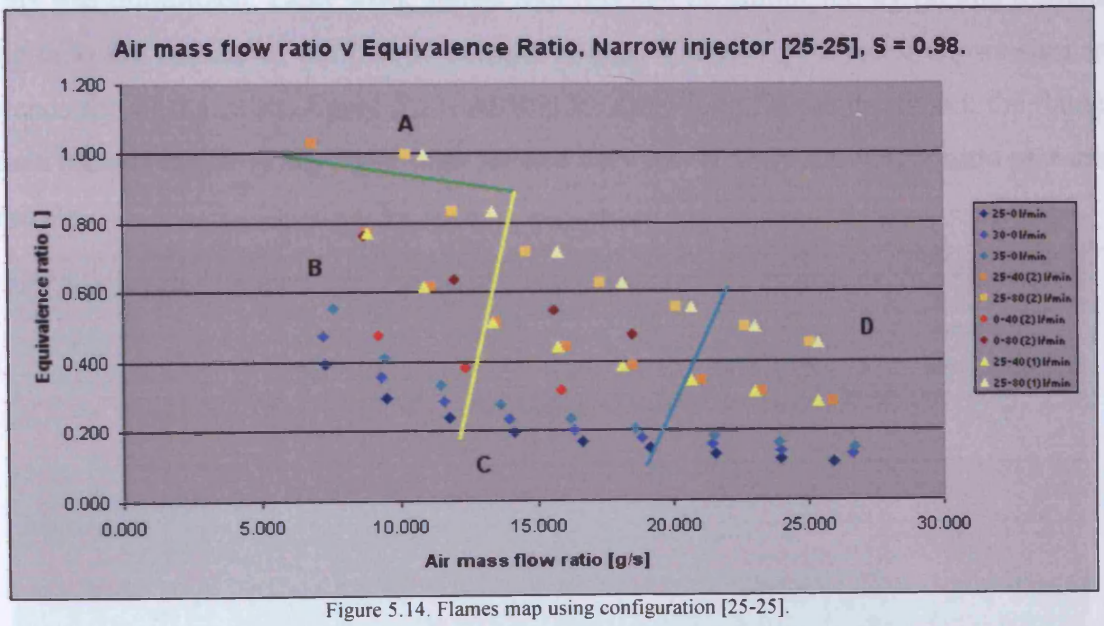

Figure 5.14. Flames map using configuration [25-25].

These 4 regions were consistent with all the experiments. The only differences between cases were the boundaries between each region. As is observed in figure 5.13 and 5.14, the position of the limits between region B and C change considerably. This is due to the intense swirl produced by the [50-50] case, whose strength creates a more compacted flame at moderated Re. Thus, the squeezing of the flame is achieved earlier. This is observed between the C and D boundaries as well. However, region A remains almost invariant among the experiments. Therefore, it is not only the swirl

but a combination with the Re number and φ that produces different recirculation zones, whose strength is highly dependent on these parameters, controlling the behavior of the field. Again this is consistent with work by the IFRF on swirl burner scaling (Morgan et al., 1995). Higher S and Re produce better defined and stronger CRZs. This also compacts the flame, reducing its final length. The flame flattens at very high Re as combustion intensity increases.

Flame lengths extending past the end of the rig nozzle were also plotted against Re in order to observe the different patterns for each condition. Case [50-50] is shown in figure 5.15 to 5.17 for the three different diffusive fuel injectors described earlier. One of the problems of these injectors was that the flame would still stabilize upstream of the injector to the baseplate of the burner, even when only diffusive fuel injection was used; this clearly infers that the CRZ is surrounding the fuel injector whilst extending back to this baseplate. It was only with the perforated injector that this was minimized. Later work shows that this can be eliminated by putting a small lip onto the outside of the burner exhaust nozzle. The narrow injector shows similar trends for all the cases, figure 5.15. At low Re quite long flames are found, the flame then retreats inside of the rig at high Re and very low φ, only showing a little past the nozzle.

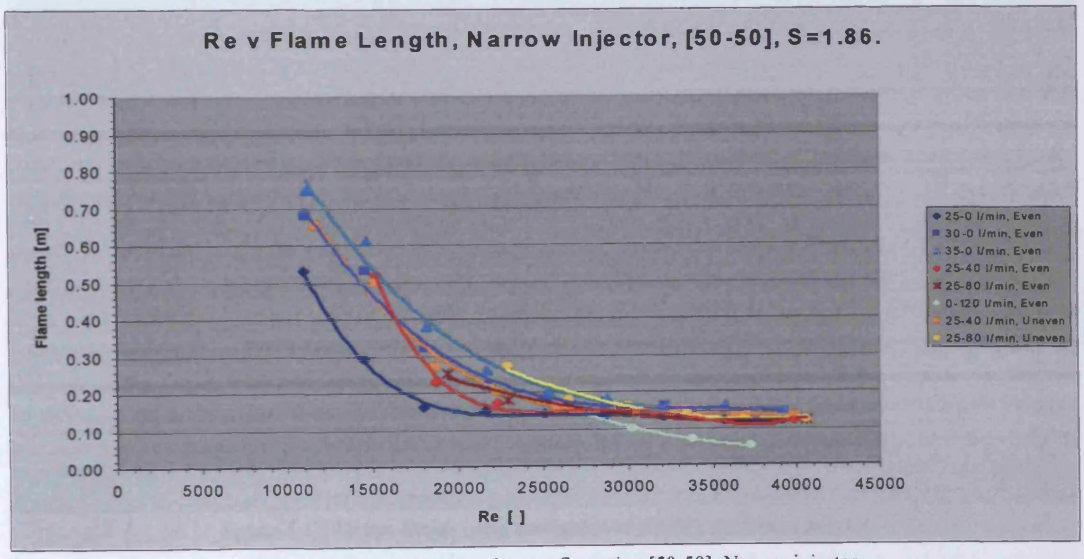

Figure 5.15. Flames length using configuration [50-50], Narrow injector.

The 23.4 mm diameter, wider injector, figure 5.16, showed a generally similar behaviour to the narrow one, except for the totally premixed cases where the flame more rapidly retreated inside of the rig.

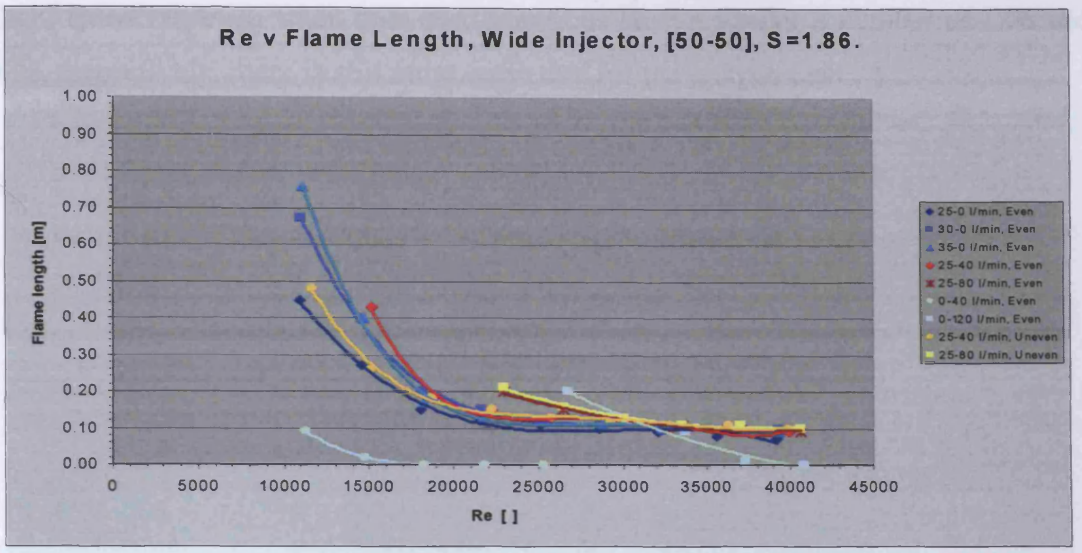

Figure 5.16. Flames length using configuration [50-50], Wide injector.

With the radial fuel injector the natural gas is forced in and towards the annular, swirling shear layer leaving the rig, although some gas is entrained by the CRZ which does extend someway upstream into the rig and around the fuel injector at moderate Re. Figure 5.17 shows that several of the flames cannot exist at low Re, although behaviour at high Re and very low φ is similar to the other injectors. The fully premixed cases are similar to that of figure 5.16. Since the shape of both injectors is similar, no great difference was expected using an entirely premixed gas injection.

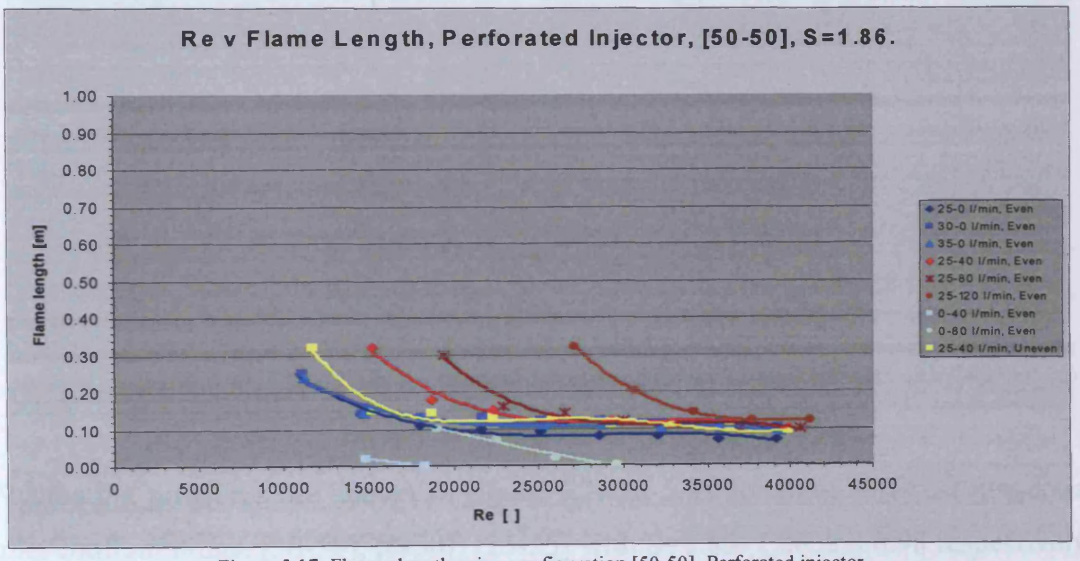

Figure 5.17. Flames length using configuration [50-50], Perforated injector.

Length comparison between different configurations was performed. Figure 5.18 and 5.19 show the cases using the Narrow injector for configuration [50-0] and [25-25], respectively. The systems show fewer inflexions than the [50-50] configuration. This is attributed to the smaller S, which now produces lower radial pressures with weaker

CRZ. However, even when both configurations have a similar S number of 1.06 and 0.98, respectively, there is still more curvature for the uneven case.

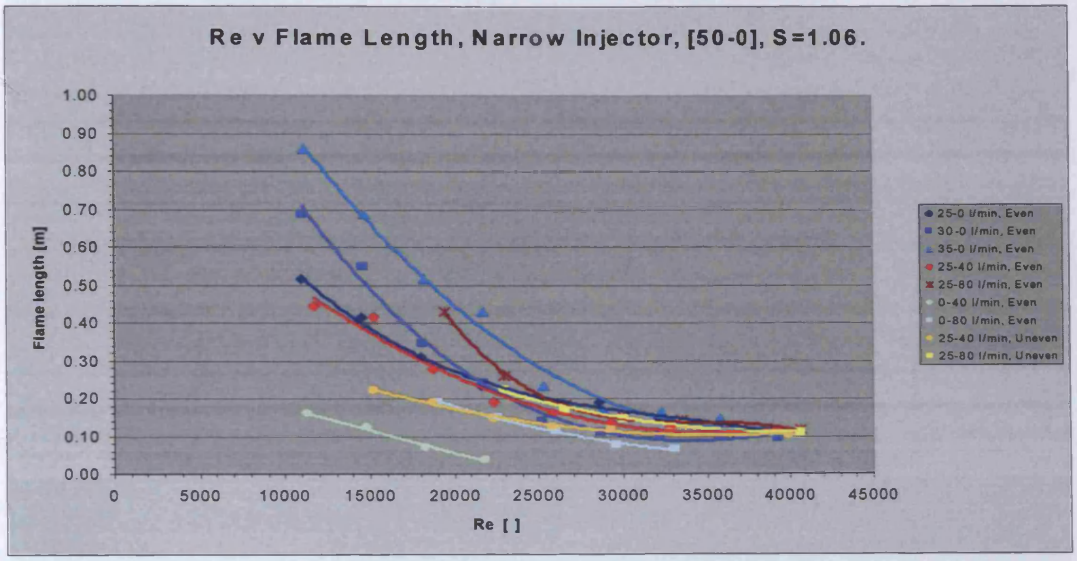

Figure 5.18. Flames length using configuration [50-0], Narrow injector.

At certain point the flame is flattened and the system reaches a constant length faster than its [25-25] counter part.

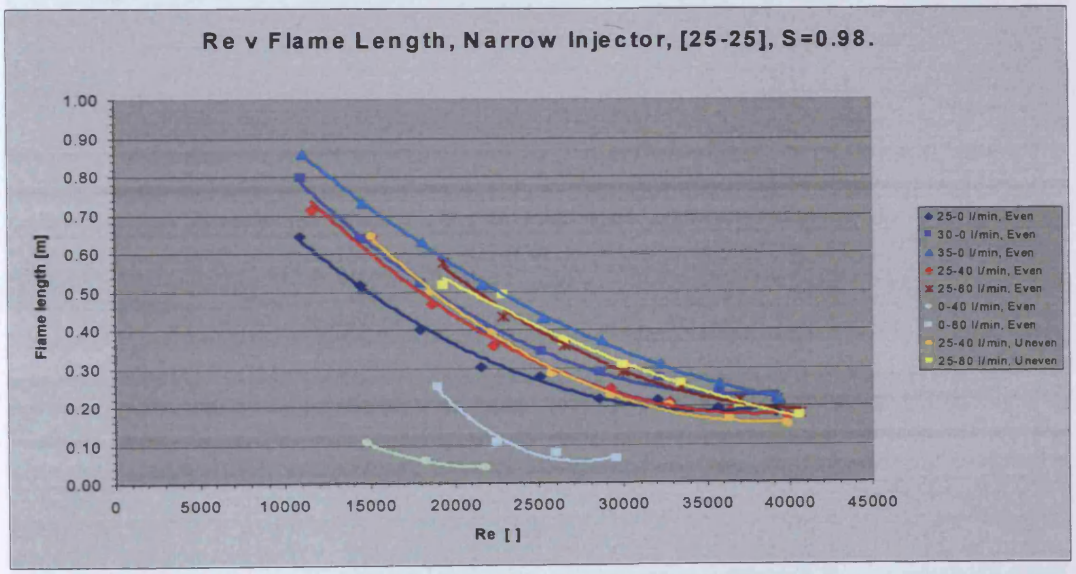

Figure 5.19. Flames length using configuration [25-25], Narrow injector.

Fluctuating pressures are shown in figure 5.20 to 5.22 for three different tangential inlet configurations, [50-50], [0-50], [25-25] with S=1.86, 1.06 and 0.98 respectively. The [50-50] case, Figure 5.20, shows an expected increase of amplitude with Re, apart from one premixed case, where clearly changes in flow structure are occurring at Re~30,000.

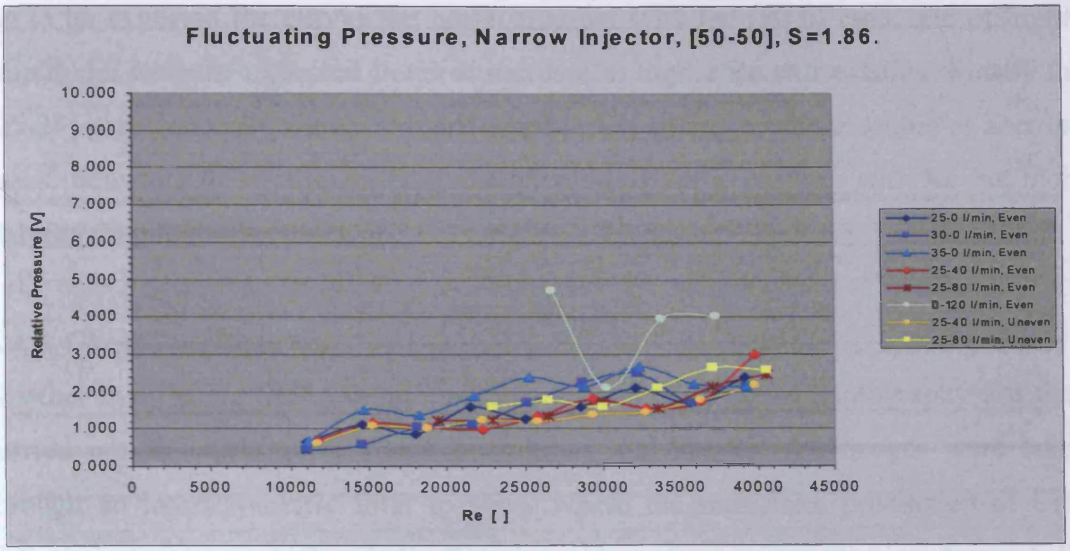

Figure 5.20. Fluctuating pressure analysis using configuration [50-50], Narrow injector.

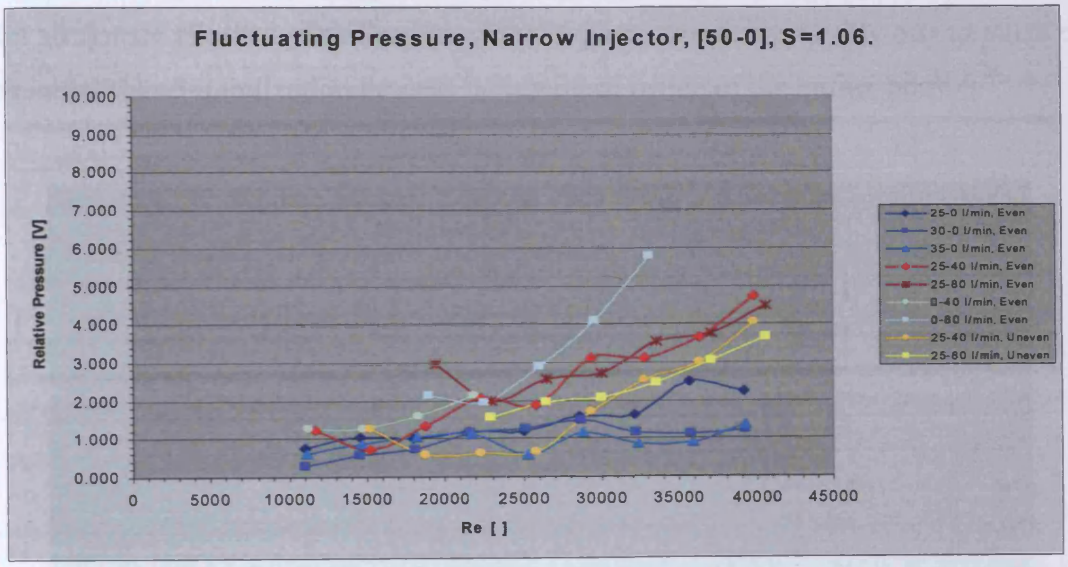

Figure 5.21. Fluctuating pressure analysis using configuration [50-0], Narrow injector.

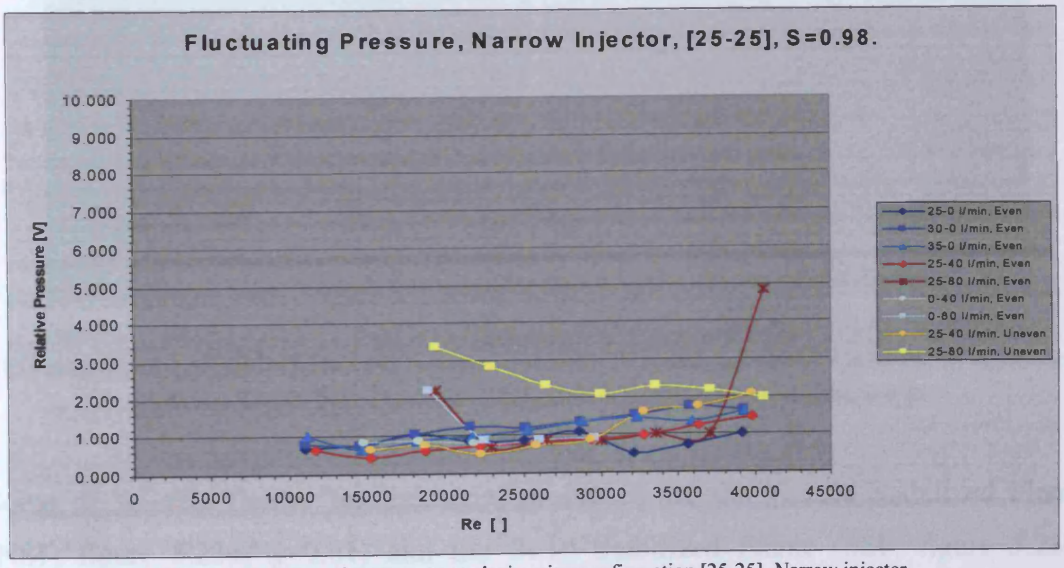

Figure 5.22. Fluctuating pressure analysis using configuration [25-25], Narrow injector.

As to be expected the curves are more irregular with the [50-0] case, and of higher amplitude, with the expected trend of increase at higher Re still existing. Finally the [25-25] case generally shows reduced amplitudes, although with a couple of aberrant cases indicative of significant combustion aereodynamic changes with Re but more stability than the other cases.

5.2.2. Chemiluminescence

Another study using CH* Chemiluminescence and High Speed Photography was then carried out to characterize flame boundaries and shapes. All images were taken through an interferometric filter to show where the maximum production of CH* radicals was occurring, thus indicating the region of the initial reaction, figure 5.23. Not all flames allowed visualization of this region; this was probably due to much of the initial flame stabilization process taking place inside of the burner body.

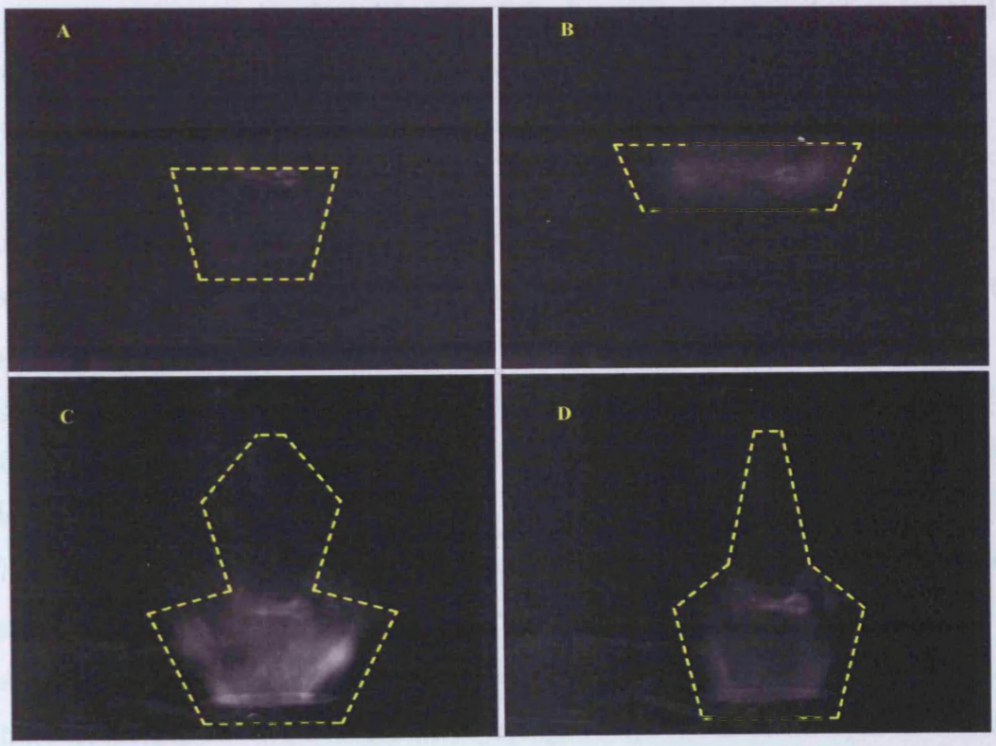

Figure 5.23. Four cases using CH* chemiluminescence. A) Configuration [50-50] at Re~12,200, 40-0 l/min, φ=0.61; B) Configuration [50-50] at Re~12,700, 25-40 l/min even case, φ=0.95; C) Configuration [25-25] at Re~12,700, 25-40 l/min even case, φ=0.87; D) Configuration [25-25] at Re~16,500, 25-40 l/min even case, φ=0.72.

Some of suitable flames for industrial processes are the Nozzle Stabilized Flame (NSF, figure 5.23a, φ=0.61) and the Swirl Stabilized Flame (SSF, figure 5.23b,

φ=0.95), which have been used to create high emissivity flames with reduced NOx emissions. The SSF was observed at near stoichiometric equivalence ratios, high swirl and low Re numbers. The flame was stable and extremely emissive before re-attaching to the burner exit at higher Re and leaner equivalence ratios, then becoming more stable and uniform but less emissive, probably due to the development of the CRZ and faster shear flows.

Figure 5.23 shows other structures such as a hat shaped flame, expanded in regions close to the burner, compressed and jet-like at the inner enlarged centre. This shape evolves into a complete jet-like form at higher Re and lower equivalence ratios. The transition between cases has been documented but not assessed. Some workers (Vanoverberghe, 2004; Malalasekera et al., 2008) believe that the phenomenon is based on the swirl number, but these experiments confirm their evolution based also on Re and equivalence ratios. The reaction of the flame is attributed to the strength of the coherent structures developed inside of the burning region including internal and external recirculation zones. Nevertheless, this can only be corroborated with visualization techniques such as PIV.

5.2.3. Particle Image Velocimetry

Phase Locked Particle Image Velocimetry was used for the analysis of all these structures and flames in each of the four different regions previously mapped. The triggering value selected was in the range of 90% of the highest peak detected in 5 minutes of free running of the system. Unfortunately, some flames in the A region could not be detected, as they collapsed in a couple of seconds from an unstable flame to flashback. However, for those flames with higher stability the triggering values ranged between 0.50 and 0.82 V, lower than the isothermal studies. This is a consequence of the decrease in gas density, thus fluctuating pressures produced by the high temperatures of the flame. The average temperature of the system of the non burning shear flow at the rig nozzle was estimated to be around 120 and 203 °C.

Phase locking of successive images was achieved with a TTL pulse, whilst seeding with Al_2O_3 showed good and clear results. Due to the high reflection an interferometer filter with a centered wave length of 532 nm was used to extract the

required information. 150 frames per configuration were obtained, with a 32 x 32 pixels correlation technique and 50% overlap between frames to reduce noise. Only the axial-radial plane velocity was measured, and only 1.15% of vectors out of the ranged specified were eliminated, showing good quality of results. Pairs of images were obtained every 20 μs, and a statistical analysis was performed to obtain the average structures. Velocities were filtered in the range of 9.00 and -2.00 m/s.

Figure 5.24 shows the results using the perforated fuel injector under different regimes for configuration [25-25]. It is observed how the case at 600 l/min of air and 35-0 l/min of gas, figure 5.24a, has barely developed a CRZ (denoted by a blue navy zone of low velocity). Since the structure is very weak and the Re very low, this produces a very long wrinkled flame. On the other hand, the case at 2200 l/min of air and 35-0 l/min of gas, figure 5.24d, has created a more defined and stronger CRZ, enabling better flame stabilization.

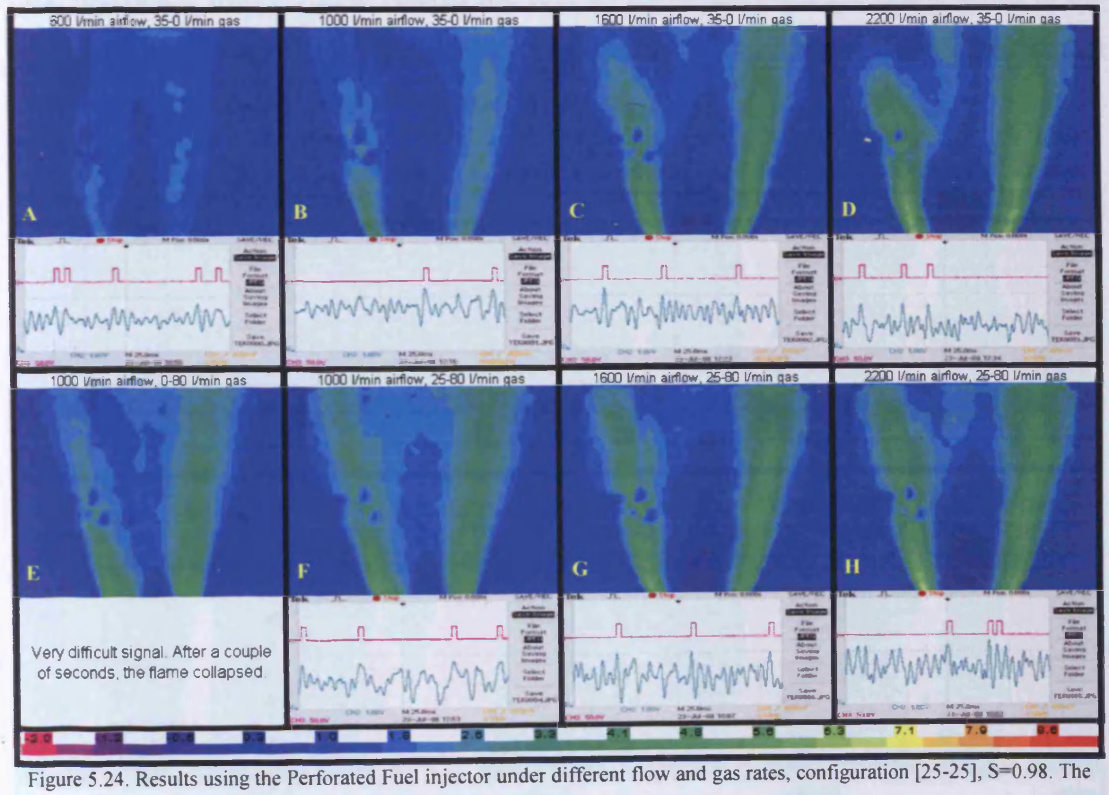

Figure 5.24. Results using the Perforated Fuel injector under different flow and gas rates, configuration [25-25], S=0.98. The conditions for these experiments were: A) Re~11,100, φ=0.55; B) Re~18,200, φ=0.33; C) Re~28,800, φ=0.21; D) Re~39,300, φ=0.15; E) Difficult Flame, no measurement; F) Re~19,400, φ=0.99; G) Re~30,000, φ=0.62; H) Re~40,500, φ=0.45.

When the system is run solely in the 100% premixed condition, the CRZ appears extremely small and weak, being intermittent and periodically collapsing, figure

5.24e. Thus some diffusive fuel injection is normally required to aid flame stabilization.

The combination of premixed and diffusive gases, i.e. the cases 25-80 natural gas flows and 1000, 1600 and 2200 l/min air flowrates, figure 5.24f to h, show especially at high air flowrates a large, stable, well developed CRZ and more uniform surrounding shear flow, giving more uniform combustion.

Figure 5.25 shows the results with the 23.4 mm diameter fuel injector. The first image at 600 l/min of air and 35-0 l/min of gas, figure 5.25a is of a lifted flame similar to the observed in figure 5.23b. This SSF flame seems to be formed as the fuel jet fires through the initially weak recirculation zone.

As the airflow is increased successively to 2200 l/min the size and strength of the CRZ increases, figure 5.25d, retards the fuel jet more and pulls the flame down to the burner exhaust. There is some evidence of complex flow motions in the CRZ at high air flowrates, visible as yellow internal flamelets.

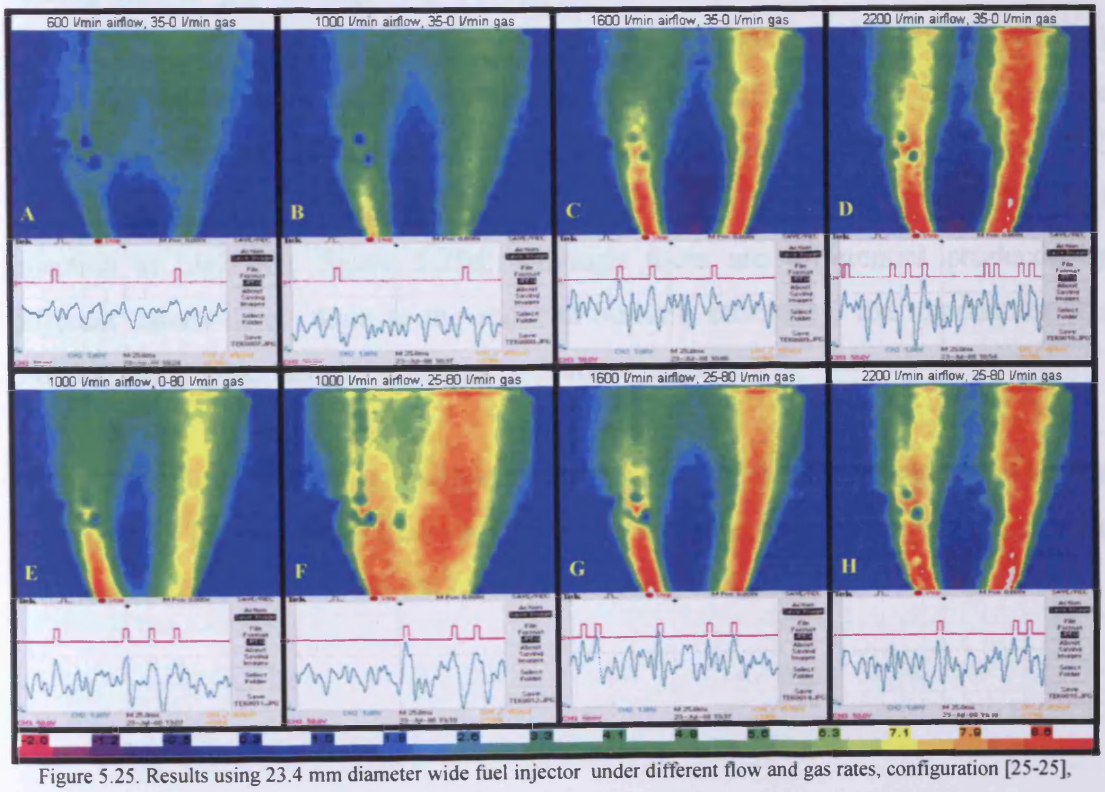

Figure 5.25. Results using 23.4 mm diameter wide fuel injector under different flow and gas rates, configuration [25-25], S=0.98. The conditions for these experiments were: A) Re~11,100, φ=0.55; B) Re~18,200, φ=0.33; C) Re~28,800, φ=0.21; D) Re~39,300, φ=0.15; E) Re~19,000, φ=0.77; F) Re~19,400, φ=0.99; G) Re~30,000, φ=0.62; H) Re~40,500, φ=0.45.

The initial pure premixed flame (0-80 gas, 1000 l/min air), figure 5.25e, shows a lifted, wobbling CRZ, indicative of conditions close to the Vortex Breakdown.

This is a Swirl, Re number and Equivalence Ratio effect and occurs because the increased burning inside of the rig has caused an increment in the axial flux of axial momentum, reducing the swirl number at the exit and hence the formation of the CRZ. At higher air flowrates and hence Re, and with some diffusive gas, more of the flame moves past the burner exhaust, the swirl number increases, a large CRZ is established and a large stable flame results, figure 5.25f to h. Blow off limits and stability for premixed flames, as in figure 5.24e and 5.25e, are not so good as for ones with some diffusive fuel entry. Visual observation shows that premixed flame boundaries inside the burner body and close to the burner exhaust are generally located at larger radii than their diffusive counterparts, thus being in a much higher velocity shear layer region. Diffusive gas added on the central axis feeds directly to the CRZ boundaries where it ignites and directly feeds the CRZ with the desirable very hot gases and active chemical species necessary for flame stabilization.

Adding natural gas through the central diffusive injector to the premixed flame produced a separate central jet flame, as shown in figure 5.25f, (overall φ=0.99) destroying the weak CRZ. This central jet shows very little swirl. As the air flowrate is increased to 2200 l/min, figure 5.25h, φ decreases to 0.46 and a strong CRZ becomes established; this has similarities to the one produced by diffusive fuel injection at high Re, figure 5.25d, although there are differences produced by different values of φ. Due to the reduced burning efficiency, the temperature has dropped with higher densities, increased S and stronger CRZ.

Figure 5.26 shows the results obtained with the narrow 9.9 mm diameter fuel central diffusive fuel injector. Here for solely diffusive fuel injection, figure 5.26a to d, there is a clear conflict between the CRZ and the entering fuel jet.

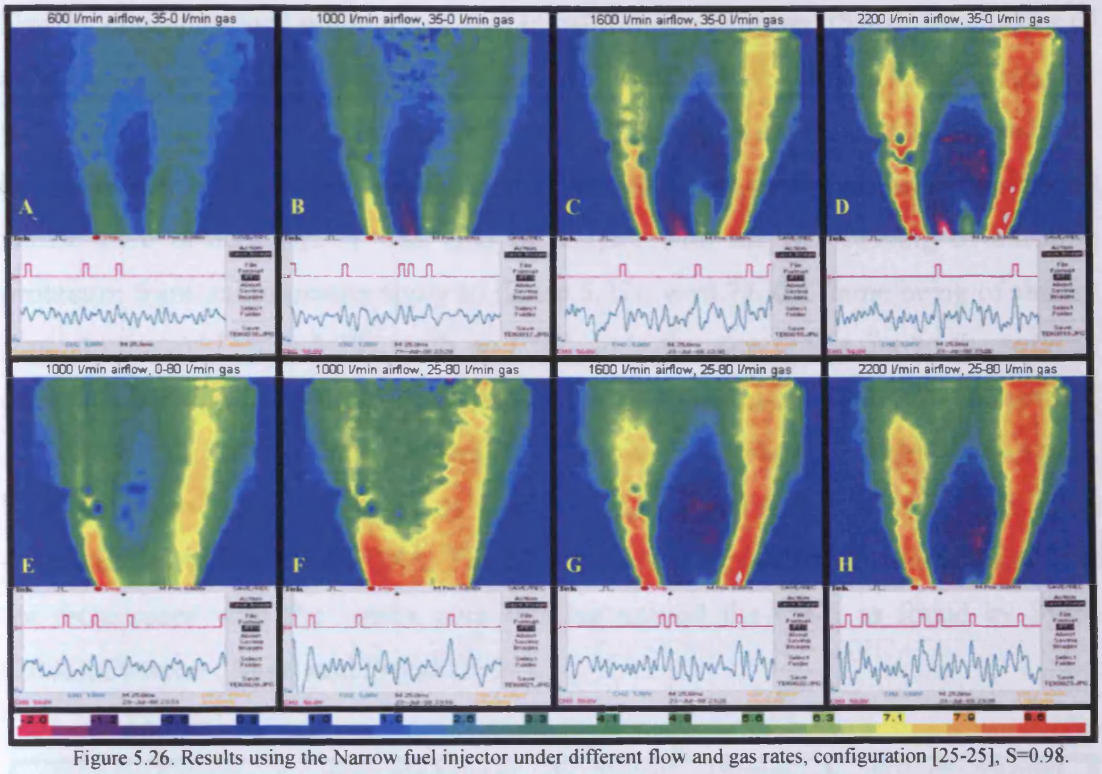

Figure 5.26. Results using the Narrow fuel injector under different flow and gas rates, configuration [25-25], S=0.98. The conditions for these experiments were: A) Re~11,100, φ=0.55; B) Re~18,200, φ=0.33; C) Re~28,800, φ=0.21; D) Re~39,300, φ=0.15; E) Re~19,000, φ=0.77; F) Re~19,400, φ=0.99; G) Re~30,000, φ=0.62; H) Re~40,500, φ=0.45.

At low air flowrates and φ=0.55 the fuel jet has pushed the CRZ slightly downstream, whilst aligning itself in a side by side position; this continues with an air flowrate of 1000 l/min, φ=0.34, but here the CRZ has strengthened, extending back to the burner exhaust. Finally at higher air flowrates, figure 5.26c, φ=0.21, 24d, φ=0.15 the strengthening CRZ starts to overwhelm the central fuel jet as the reducing temperature allows the swirl number to increase.

The solely premixed case, figure 5.26e, φ=0.77 showed a small, wobbling, CRZ located downstream of the injector and burner exhaust as in the previous case. Again this flow regime seems to be close to that of the Vortex Breakdown with combustion inside the rig, in and around the narrow injector, reducing the swirl number.

Diffusive natural gas injection into the premixed flame showed similar patterns to those observed with the 23.4 mm diameter wide injector, figure 5.26f, φ=0.99 to h, φ=0.45, although the CRZs produced are somewhat larger, giving more stable flames.

Finally, configurations without any fuel injectors were analyzed that showed traces of complex flames, PVCs or abnormal behavior, figure 5.27. All the flames extended back through the rig to the baseplate. Figure 5.27a shows the flow patterns produced by a blue flame, φ=0.55, at low Re. The flame stabilizes because of the low velocities, whilst there is no CRZ. It was also in contact with the rig, causing overheating problems. Similar comments apply to figure 5.27c, φ=0.77, the flame being of similar shape to that of Figure 5.23c, with no CRZ. In both cases this is due to the reduced swirl number due to combustion inside of the rig. Two cases, figure 5.27b, φ=0.24, 5.27d, φ=0.44, showed the presence of a wobbling lifted recirculation zones. Different from other the cases of figure 5.27, the flame was shorter, and small vortices were visible in the CRZ. The HSP analysis showed some traces of the PVC for these cases with the vortex core rotating around the CRZ, as found by Syred (2006), Dawson (2000) and Froud (1995).

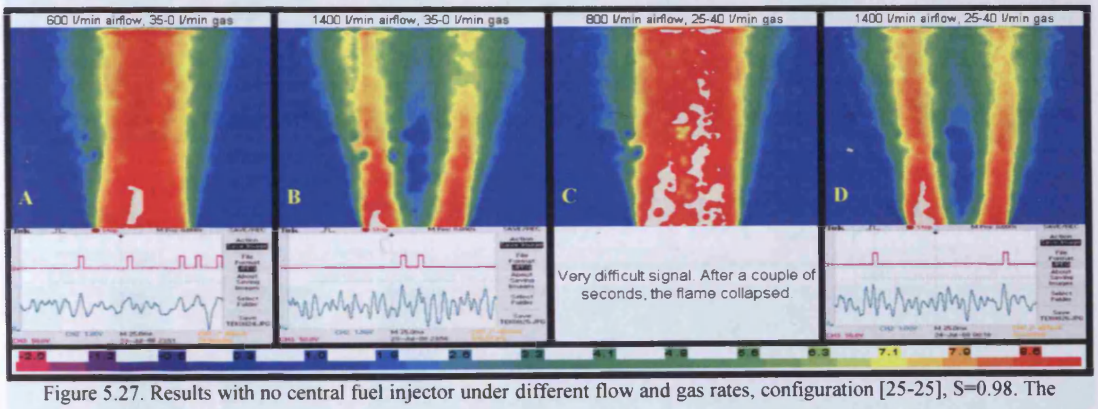

Figure 5.27. Results with no central fuel injector under different flow and gas rates, configuration [25-25], S=0.98. The conditions for the experiments were: A) Re~11,100, φ=0.55; B) Re~25,200, φ=0.24; C) Re~15,200, φ=0.77; D) Re~25,700, φ=0.44.

Next the effect of higher S was investigated for comparison purposes as well as cases where strong PVCs were observed, Figure 5.28 and 5.29.

For the [50-0] case a stronger CRZ than the [25-25] cases developed, Figure 5.28. The CRZ structures, figure 5.28, a to f and h, show that the CRZ extends upwards far beyond the bulbous section located next to the rig nozzle. This has been observed with other systems (Syred, 2006). Especially with the perforated injector the CRZ appears to divide into 2 lobes, possibly indicative of 2 interrelated CRZs as found during the isothermal cases. The results from the 23.4 mm and perforated injector are

similar, although the CRZs are slightly weaker for the wide injector, figure 5.28a and b, compared to 5.28c and d. The narrow 9.9mm injector, figure 5.28e and f, again shows the influence of the central fuel jet upon the CRZ close to the rig nozzle, although further downstream the CRZ is relatively unaffected. With no central fuel injector, and axial fuel entry through the baseplate, figure 5.28 g and h, the CRZ is more columnar in shape at higher air flowrates, with the flow being close to vortex breakdown at lower air flowrates.

This is in agreement with other authors (Lieuwen and Yange, 2005; Vaniershot et al., 2008). Figure 5.28g and h also show those experiment where a strong PVC was observed using HSP. The image at 600 l/min of air and 25-0 l/min of natural gas, figure 5.28g matches the bifurcated structure observed in figure 5.9.

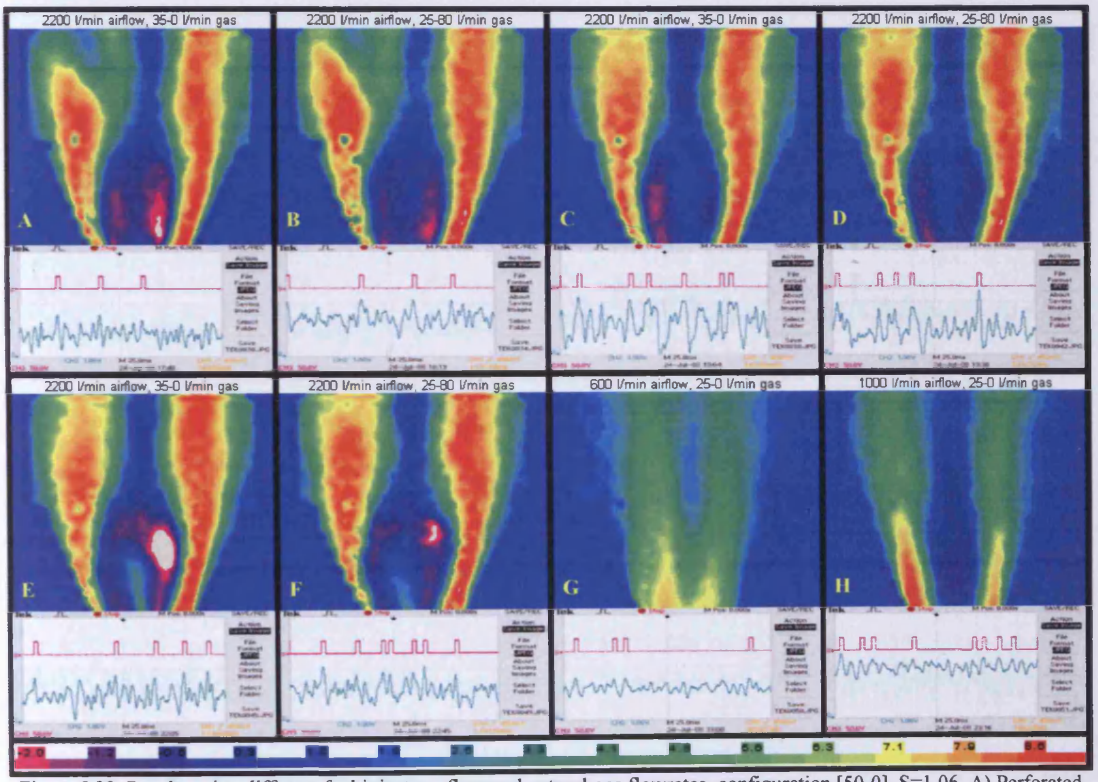

Figure 5.28. Results using different fuel injectors, flow and natural gas flowrates, configuration [50-0], S=1.06. A) Perforated injector, Diffusive, Re~39,300, φ=0.15; B) Perforated injector, Diffusive-Premixed, Re~40,500, φ=0.45; C) Wide injector, Diffusive, Re~39,300, φ=0.15; D) Wide injector, Diffusive-Premixed, Re~40,500, φ=0.45; E) Narrow injector, Diffusive, Re~39,300, φ=0.15; F) Narrow injector, Diffusive-Premixed, Re~40,500, φ=0.45; G) No injector, Diffusive, Re~11,000, φ=0.40; H) No Injector, Diffusive, Re~18,000, φ=0.24.

It is confirmed that the PVC is rotating around a lifted CRZ which has formed just after vortex breakdown. It is likely that the PVC encounters the latter before downstream collapse. Low velocities and the entrainment of the fuel entering through

the centre of baseplate into the central vortex (which then precesses) allows the flame to initially develop inside of the rig.

Increasing the air flowrate, figure 5.28h, causes the columnar CRZ to form, which extends down inside the rig to the baseplate. This flow pattern also hosts a single PVC whose coherence was observed using HSP. Single PVCs seem to appear when a strong CRZ has developed, initially forming well inside of the rig.

Configuration [50-50] was also examined at high flow rates and also for those configurations that showed traces of the Precessing Vortex Core, figure 5.29a to h. All high flowrate cases, figure 5.29a to f, show a strong bulbous CRZ close to the nozzle with long downstream columnar extensions.

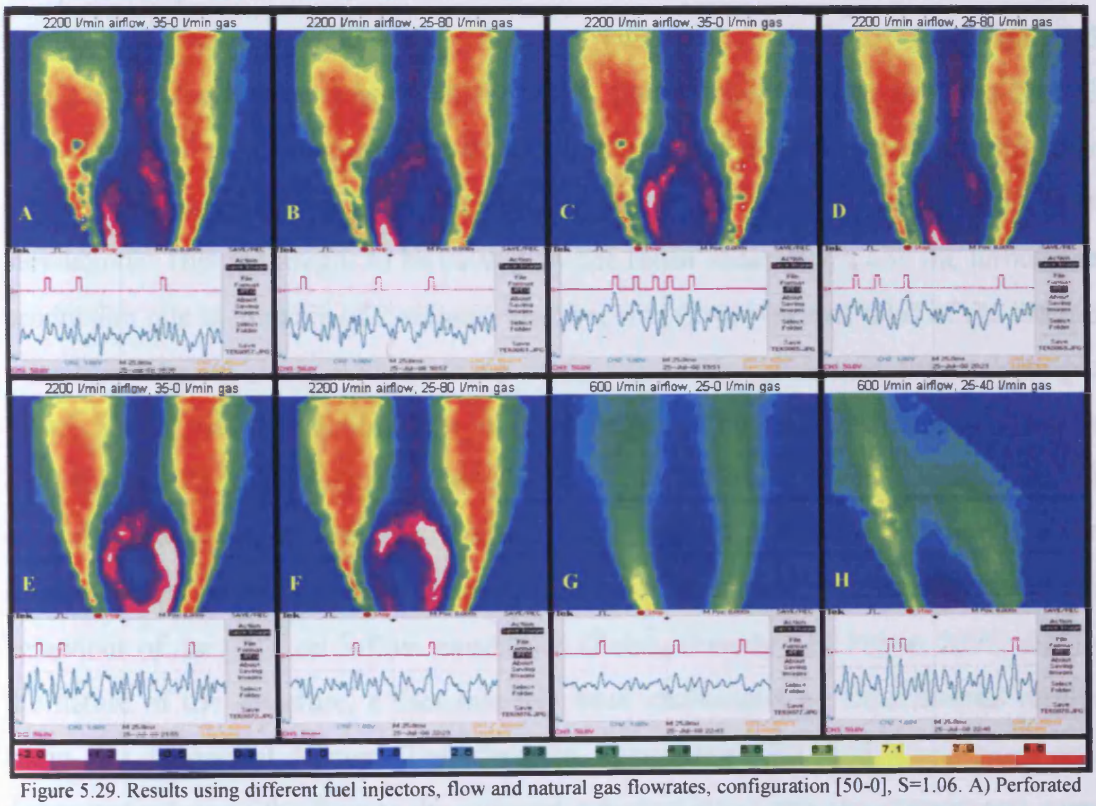

Figure 5.29. Results using different fuel injectors, flow and natural gas flowrates, configuration [50-0], S=1.06. A) Perforated injector, Diffusive, Re~39,300, φ=0.15; B) Perforated injector, Diffusive-Premixed, Re~40,500, φ=0.45; C) Wide injector, Diffusive, Re~39,300, φ=0.15; D) Wide injector, Diffusive-Premixed, Re~40,500, φ=0.45; E) Narrow injector, Diffusive, Re~39,300, φ=0.15; F) Narrow injector, Diffusive-Premixed, Re~40,500, φ=0.45; G) No injector, Diffusive, Re~11,000, φ=0.40; H) No Injector, Diffusive, Re~11,700, φ=1.03.

All these CRZs appear to be stronger than previous cases, doubtless a function of the increased level of swirl from ~1 to ~2.

Figure 5.29g and h show cases without any fuel injector, the natural gas just entering through the centre of the baseplate, being entrained into the vortex core, and forming a double PVC. The PIV results show the Precessing vortex is moving around the CRZ in the burner exhaust as found isothermally. It is thus confirmed that PVC-CRZ systems appear during combustion conditions. Finally, the case with diffusive and premixed natural gas, figure 5.29h, showed a lifted flame which apparently is shifted to the left side of the rig, there still being an inner CRZ at the burner exit. The asymmetry seems to be a problem caused by the fact that the flame was extremely unstable.

5.3. Experimental Approach. Confined Combustion

As previously mentioned, simulations of real conditions have shown a great advantage in the study of swirling flows. However, their difficulty to be modeled leaves room for improvement. Jakirlic et al. (2002) have studied low and high S scenarios. High swirl intensities create a free vortex, this then evolves to a solid-body rotation due to swirl decay downstream, a transition not well modelled in their simulations. This is thought to be caused by the mean shear $\partial U/\partial r$ and the turbulence production rate at the axis of symmetry that become zero, whereas most of the models were calibrated in flows with a strong mean shear. This yields an almost isotropic stress field, under predicting the normal Reynolds stress components. This is accompanied by the inadequate modelling of the pressure scrambling process in second-moment closures models, and the lack of specific terms accounting for the swirling effect in κ-ε models. Other simulations mention the independence of the behaviour of the CRZ on inflow conditions (Baba-Ahmady and Tabor, 2008) due to the nature of the structure, a fact that has been challenged by experimental results using this tangential burner. Therefore, to demonstrate the high importance and dependant nature of the flow to the inherent coherent structures, the experiments were expanded to the use of confined combustion conditions.

5.3.1. Combustion at different flow and gas rates. Same geometry.

First experiments were performed at low gas rates (entirely Diffusive and Weak Diffusive-Premixed). The system was analyzed with the Wide Injector fitted, due to the way it mixed the fuel with the air in comparison to the perforated and narrow

injectors, respectively. The results showed high correlation to those obtained under isothermal confined conditions, figure 5.30, not surprising seeing the very weak values of φ used in the initial tests, <0.4. The position of the CRZ2 and the region of intense recirculation near the left side of the burner are very similar to the isothermal state. The appearance of this region is a consequence of the reduced velocity of the flow in the zone of the burner which is opposite to the high momentum crescent shaped region. Flow velocities are very low compared to the latter, reducing the pressure and allowing the movement of particles from the main recirculation zone into this area, creating this eddy. However, it could not be confirmed that a secondary Central Recirculation Zone had formed, since there was no bifurcation with the main CRZ, as observed in the isothermal case where the separation was caused by the PVC. Contrary to the latter, the PVC was never observed, although its presence and intermittency was confirmed by the erratic Harmonics observed. Combustion thus suppresses the strength and coherence of the Precessing Vortex core, without eradicating it, even at the weak values of φ used.

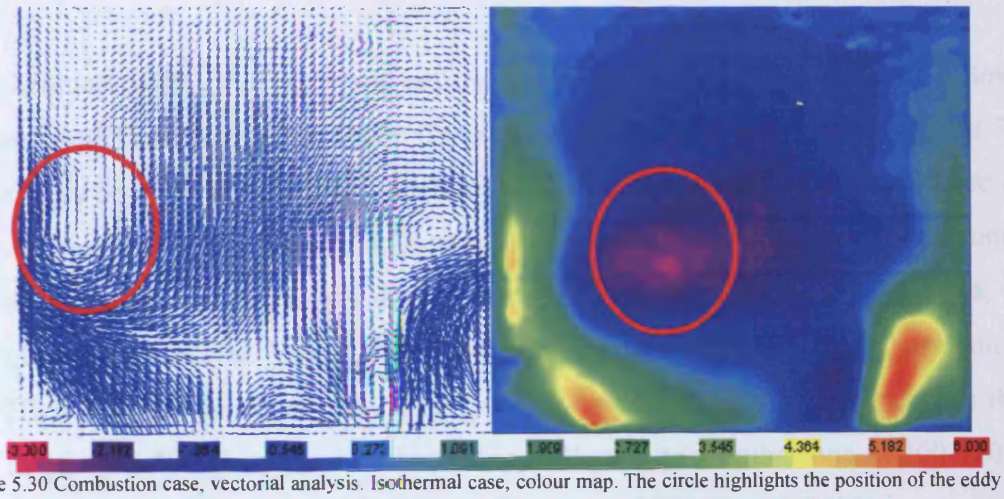

Figure 5.30 Combustion case, vectorial analysis. Isothermal case, colour map. The circle highlights the position of the eddy and the CRZ2, respectively. Colour scale in [m/s].

Further experiments were performed in order to obtain more insights into the system at different fuel ratios and regimes. Figure 5.31 shows a diffusive weak flame at different air flowrates. It is observed that the condition creates a coherent stable recirculation zone even at low air flowrates. This appears to be a consequence of the weak equivalence ratios. Only the fastest flows show what seems to be a harmonic related to the PVC/High Momentum Region (HM), but it is not as clear as under isothermal conditions, confirming the suppression of the PVC amplitude. The strength of the CRZ has increased with the flowrate and reduction of φ, as expected.

Moreover, the shape of the Recirculation Zone maintains an irregular, lobbed pattern, as observed by Syred (2006) and Dawson (2000).

More diffusive gas was injected to observe the flame pattern, figure 5.32. A coherent stable recirculation zone occurs for air flowrates greater than 1000 l/min, with a very weak CRZ at low flowrates, probably a structure recently formed after the Vortex Breakdown as the swirl number is reduced by combustion due to the increased axial flux of axial momentum, the effect being greatest for higher equivalence ratios (up to $\varphi \sim 1$). Unclear harmonics were observed at moderate and high flowrates in the range of 0-100 Hz, representative of cold flows. Again, at higher flowrates the strength of the CRZ increased, keeping the lobbed shape, figure 5.32.c and 5.32.d. It is interesting to note that the system develops weaker CRZs than the case at lower gas injection rates. The system at 40 l/min did not reach the strength of the case at 25 l/min until an air flowrate of 1600 l/min, clearly due to axial momentum flux and reduction of swirl number considerations.

The addition of 40 l/min premixed natural gas for a diffusive-premixed case followed. These conditions showed stronger flames with weaker inner structures, figure 5.33. This is to be expected as the overall equivalence ratios are higher with more heat release, increased axial flux of axial momentum and more reduction of swirl number. A coherent stable Recirculation Zone developed at moderate-high air flowrates, with a wobbling unattached Vortex Breakdown at low air flowrates. Clear harmonics of the High Momentum shear flow Region were observed at moderate and high Re in the range of 0-100 Hz for a first harmonic, followed by another one at 200-250 Hz, the latter being characteristic of hot flows (Dawson, 2000; Syred, 2006).

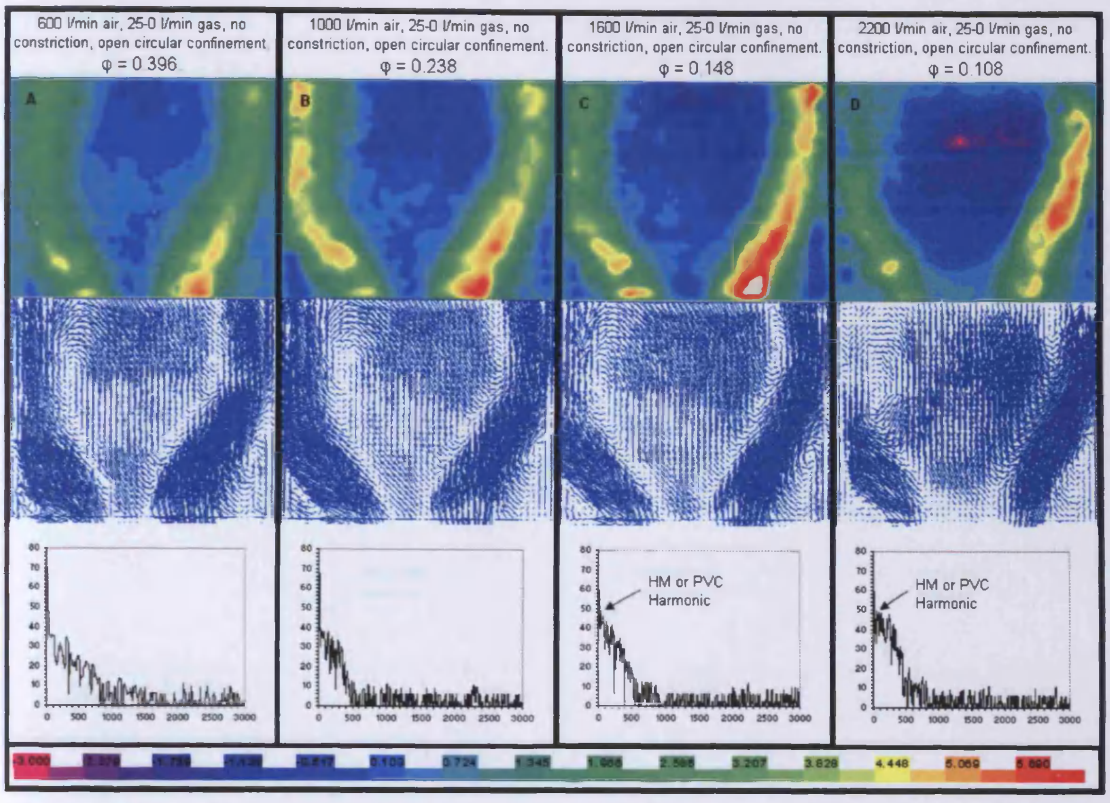

Figure 5.31. Confined flame analysis at low diffusive gas injection at different flowrates and equivalence ratios with their vectorial map and frequency analysis. Colour scale in [m/s].

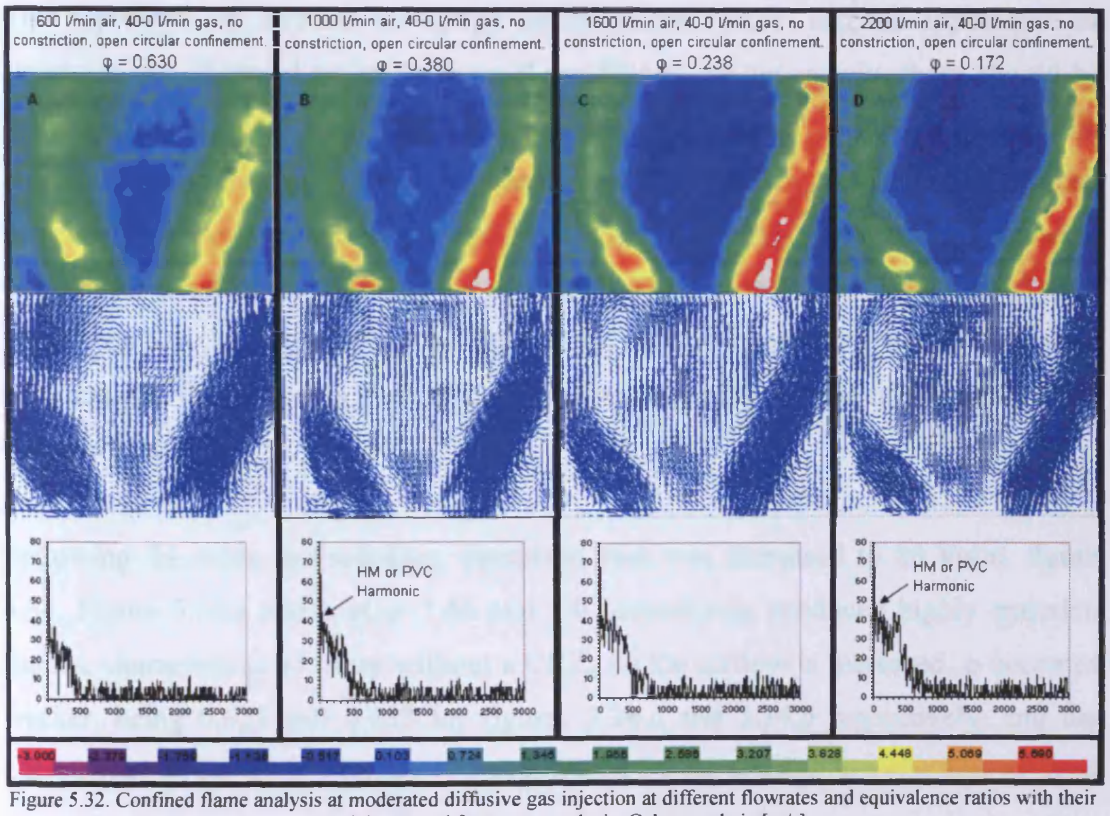

Figure 5.32. Confined flame analysis at moderated diffusive gas injection at different flowrates and equivalence ratios with their vectorial map and frequency analysis. Colour scale in [m/s].

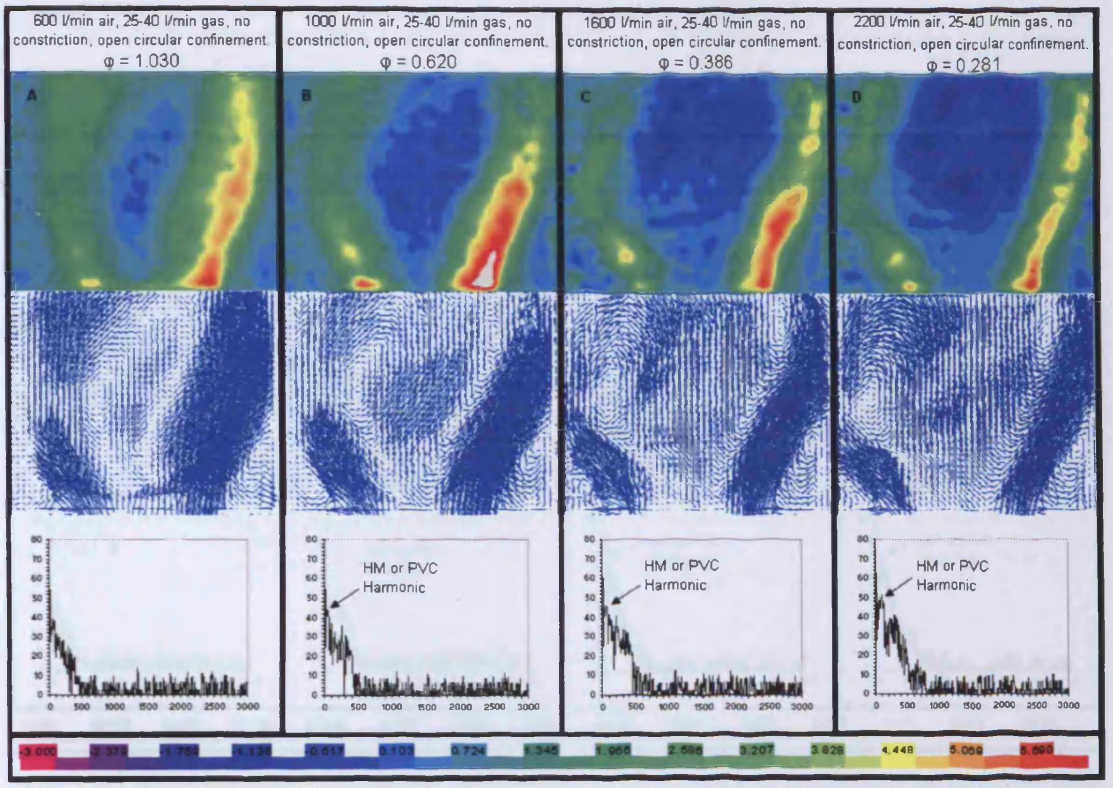

Figure 5.33. Confined flame analysis at low diffusive-premixed gas injection at different flowrates and equivalence ratios with their vectorial map and frequency analysis. Colour scale in [m/s].

This represents an increase in energy inside of the system and the appearance of structures not observed under isothermal conditions. Unfortunately, these should be studied at higher repetition rates, as discussed by Boxx et al. (2009). At 600 l/min airflow, figure 5.33.a.φ=1.030, heat release is near its maximum, axial flux of axial momentum is near its maximum and the swirl number has been reduced to being close to the point of vortex breakdown. At φ=0.620, figure 5.33.b. reduction of swirl number is not so high and a stronger CRZ has re-established itself, the effect continuing as the airflow is increased and equivalence ratio decreases to figure 5.33.d. where φ= 0.281.

Following the same methodology, premixed fuel was increased to 80 l/min, figure 5.34. Figure 5.34.a and b at φ=1.66 and 1.0 respectively produced highly emissive flames, characteristic of those without a CRZ. As the airflow is increased, φ becomes weaker, being 0.623 and 0.453 for figures 5.34.c and 5.34.d respectively, and the CRZ grows as the swirl number is less affected by the change in axial flux of axial momentum.

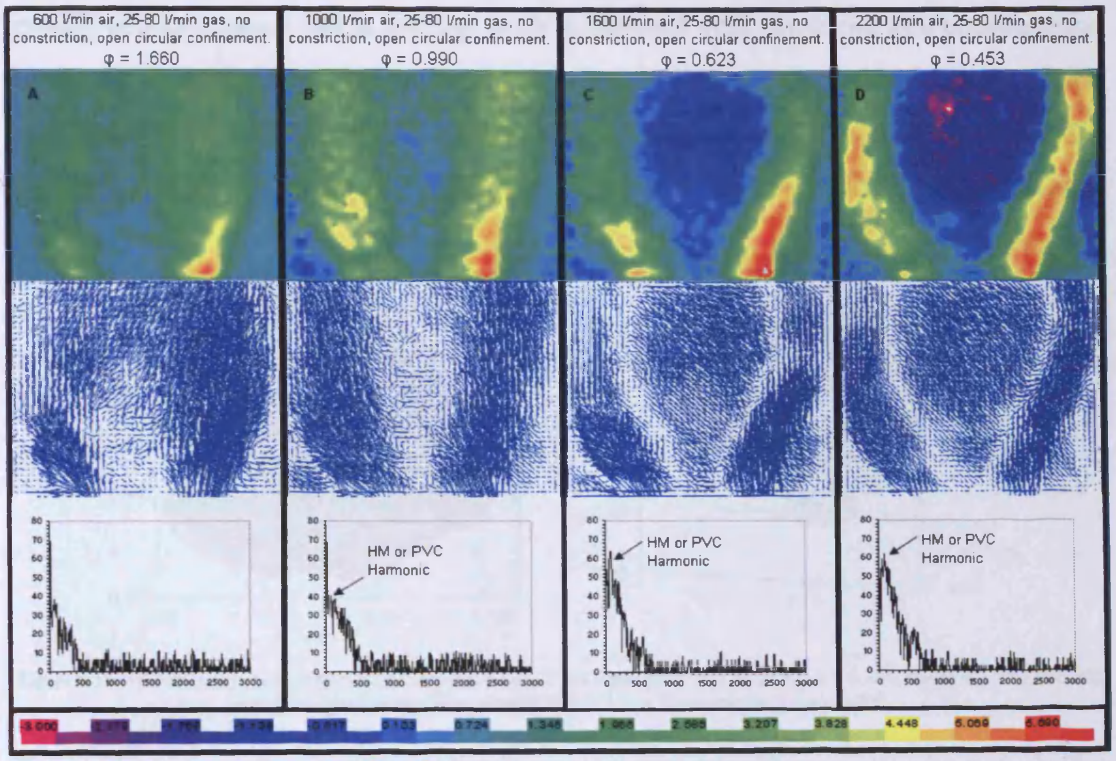

Figure 5.34. Confined flame analysis at moderated diffusive-premixed gas injection at different flowrates and equivalence ratios with their vectorial map and frequency analysis. Colour scale in [m/s].

Clear harmonics were observed at in the range of 0-100 and 200-250 Hz for cases without CRZ, figures 5.34.a and 5.34.b, possibly due to some form of acoustic coupling or natural frequency of the vortex breakdown.

At higher air flowrates with a well established CRZ, figures 5.34.c and 5.34.d, a clear harmonic was found at ~100 Hz, with unclear appearance of other harmonics. Possibly the noise spectrum from the combustion process overwhelmed all the other frequencies, a consequence of the increased energy input to the system, figures 5.34.

5.3.2. Combustion at fixed flow and gas rates. Different geometries.

The study was expanded to the recognition of coherent structures in a 3D analysis using different geometries, as in figure 5.4. First analyses were performed using geometry 5.4.a. The conditions were set at 25-40 l/min of methane, with an airflow of 1600 l/min (φ=0.386). This configuration was selected due to the strong CRZ produced and the stable flame observed, which was easier to follow for visualization. Isosurfaces were created at 0.273 m/s, where the boundaries of the CRZ seemed more coherent between planes. The results can be observed in figure 5.35. Since the recirculation zone extended upstream the visualization area, the three-dimensional

reconstruction appears flat at the top, with an internal void produced as a consequence of the used isosurfaces. However, it is easy to observe the lobbed shape of the structure at the left side corroborating previous asseverations. The zone appears as an asymmetric body whose shape depends on the localized pressure inside of the system.

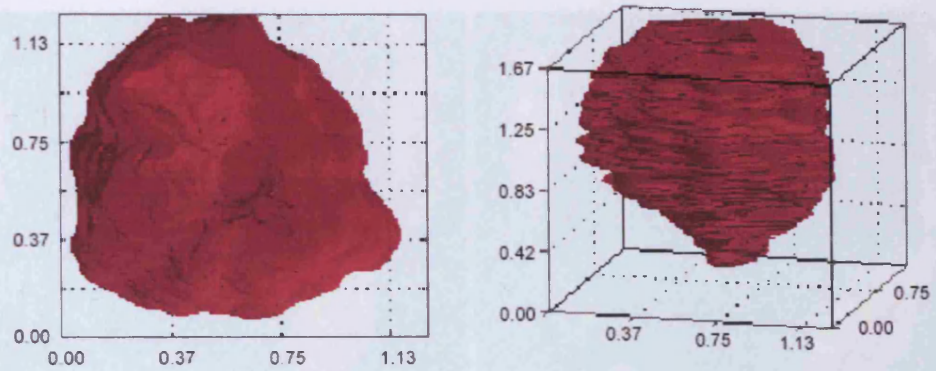

Figure 5.35. 3D Reconstruction of the Open Confined Case, 25-40 l/min gas, 1600 l/min air, φ = 0.386, figure 4.a. The left side appears lobbed. Isosurfaces created at 0.273 m/s. Dimensionless scale [x/D].

The analysis was then performed using geometry 4.b. The results showed similar trends to the open case, figure 5.36. The lobbed shape is conserved even at different conditions.

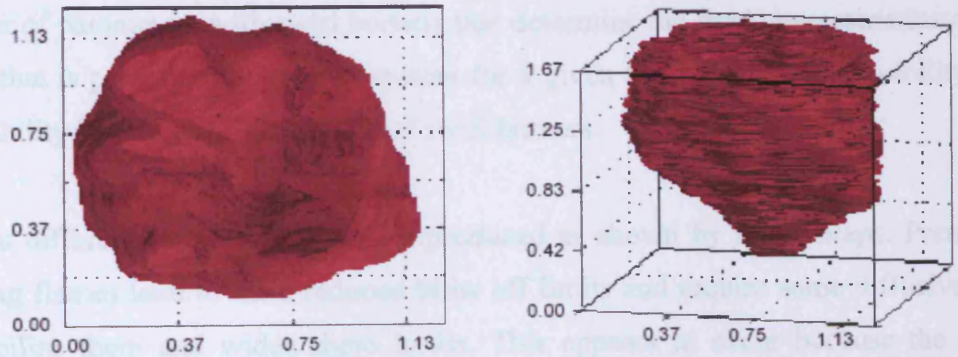

Figure 5.36. 3D Reconstruction of the Conical Confined Case, 25-40 l/min gas, 1600 l/min air, φ = 0.386, figure 4.b. The left side appears lobbed. Isosurfaces created at 0.273 m/s. Dimensionless scale [x/D].

Moreover, it was noticed in various planes the existence of an anchored vortex which bifurcated the CRZ. This same vortex was previously observed under isothermal conditions (Agustin Valera-Medina et al., 2009), where the swirling movement of the flow through the reduced exhaust is creating the vortex, which may be responsible for an increase mixing rate after O'Doherty et al. (2005). Figure 5.37 shows two planes located at 67.50° from the triggering point for the conical and open configurations, respectively. However, this vortex is not visible in the 3D reconstruction because it

only appeared in 4 planes as a strong structure and in 5 planes as a weak structure. The rest of the planes did not show signs of the vortical structure. Since the programme is designed to avoid gaps between consecutive planes, the simulation did not show the irregular appearance of the body. Nevertheless, it is clear that the structure exists.

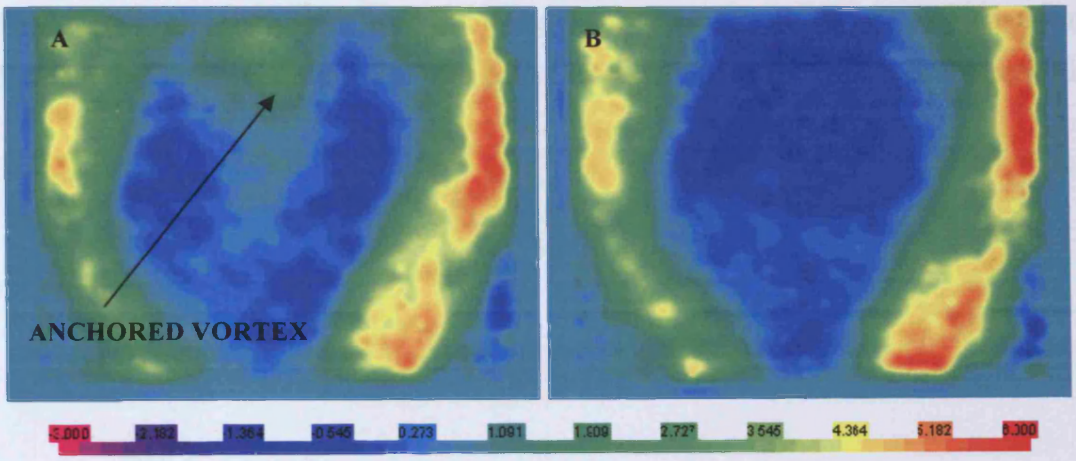

Figure 5.37. Two planes at 67.50° from the triggering point. A) Conical Obstruction; B) Open (No) Obstruction.

5.4. Summary

What this work clearly shows is that there is considerable interaction between a number of parameters with swirl burners that determine the final characteristics of the flame that is produced by a given system for a given fuel. Indeed this flexibility and adaptability is one of the attractions of swirl burners.

Several different flame types may be produced as shown by flame maps. Premixed swirling flames tend to have reduced blow off limits and require some diffusive fuel to stabilize them and widen these limits. This appears to occur because the outer region of initial flame stabilization occurs in the high velocity shear layer. The quantities of diffusive fuel required are generally quite small to alleviate this phenomenon.

Coherent structures such as the PVC are well known to occur in these systems, especially with premixed and partially premixed burners. At low Re interesting double PVC structures occur as well as vortex bifurcations of PVCs.

Confined conditions demonstrated the asymmetric, lobbed shape of the CRZ structure whose geometrical patterns were dictated by the localized pressure inside of the system. This corroborates previous experiments. Moreover, the usage of different exhaust constrictions allowed the visualization of intermittent vortices which were anchored to the tip of the constriction. However, due to the reduced field of view, these were not clearly visualized in all the planes of interest, emphasizing the use of different and improved setups for the correct recognition of the former in future work.

CHAPTER 6

FLASHBACK ANALYSIS

6. FLASHBACK ANALYSIS

"If we knew what it was we were doing, it would not be called research, would it?."

Albert Einstein, physicist (1879-1955)

Large scale coherent structures have demonstrated to be crucial for the development of stable and unstable regimes under combustion conditions when swirling flows are applied. However, the entire complexity of the latter is not only concerned with the stability of the flame by means of recirculating flow, but also by the interaction of the species and chemical reactions that act on the system. One of these interactions is flashback produced by back propagation of premixed flames through regions of low velocity where the (normally) turbulent flame speed exceeds the local velocity (Kroner et al., 2003). Here two main forms of flashback occur. The first type (Type 1) is associated with the CRZ which can (depending on Swirl Number, φ, fuel injector configuration, exhaust geometry, etc.) surround the central fuel injector and often extend back to the baseplate, allowing the flame to also extend backwards on the CRZ boundary, often causing damage to sensitive areas, especially the fuel injector. The second type of flashback (Type 2) can be quite violent and occurs when the flame flashes back through the swirl generator to the premixing region, where even more damage can occur (Syred et al., 1984; Coghe et al., 2004; Vanoverberghe, 2004). Carbon deposits produced by the high content of carbon radicals generated during the combustion process cause problems as the increased residence time augments soot growth nucleation, potentially leaving thick layers of deposit on the injector surfaces with Type 1 flashback, reducing the efficiency and increasing maintenance requirements when Type 1 occurs. These products also tend to form hydrocarbon species such as C_2H_2, C_2H_4, etc., which play an important role in the formation of aromatics, soot nucleation and particle growth (Barmina et al., 2007).

Flashback has been studied in relation to the development of new fuels based on biofuels, syngas or hydrogen to tackle climate change. Hydrogen/hydrogen enrichment is considered as one of the best options for energy carriers of the future. Current technologies have focused on the development of blends and prototypes

capable of burning such fuels under stable conditions (Ilbas et al., 2006). Moreover, fuel security in Europe has increased the interest on the area, and prototypes based on biomass and coal gasification are already functioning in order to test the feasibility of using the former industrially (Arias et al., 2008). These fuels contain high quantities of hydrogen, augmenting the need for technologies capable of using it efficiently and effectively.

It has also been experimentally and numerically found that the release of high pressurized hydrogen could lead to spontaneous ignition with unstable flames dependent on the configuration of the system, reducing the probabilities of using the element in very rich quantities in current devices (Xu et al., 2007). Moreover, the enrichment of fuels by hydrogen also increases the burning velocity and cell number during the flame wrinkling, making more difficult the flame stabilization (Coppens and Konnov, 2008). If this is added to the problem of flashback using premixed swirled flows, new or modified industrial systems need considerable development to overcome the various problems likely to be encountered.

The use of different fuels may also cause potential reduction in compressor stall margin in gas turbines due to different mass flow rates. Different transport properties and flame velocities also obviously occur with different fuels, diluents and hence flames (Lieuwen et al., 2008). Many different diluents such as N_2, CO_2, H_2O, have been studied (OMEGA, 2008). Even when large N_2 dilution levels are used to reduce NO_x, they tend to promote flashback, contrary to the intuitive assumption that higher levels are safer (Lenze and Carroni, 2007). CO_2 can lower flame temperature and laminar flame speed, whilst fuels with similar laminar flame speed may have different turbulent flame speed (Lieuwen et al., 2008). Air temperature is also a concern, since it has been found that the onset of flashback shifts to higher air temperatures with higher velocities and small injector diameters (Markides and Mastorakos, 2008). Clearly flashback depends on factors such as pilot fuelling rate and geometry. Other researchers (Lamnaouer et al., 2007) have studied the effects of flashback using the Wobbe number [MJ/m3], which gives the energetic characteristics of the gas used. The Damkoler number (Da), a parameter that relates residence and chemical times, has also been used for the study of the phenomenon.

Mixtures with lower Wo tend to flashback easier than those with higher values (Lamnaouer et al., 2007), the result for any nozzle was only valid for a limited Wo range. When Wo is varied greatly from the original fuel specification, system modifications are necessary to avoid failure. Moreover, recent experiments show that fuels with similar Wo but with diverse mixes of heavy hydrocarbons may respond differently during the combustion process, producing more or less NOx (Nag et al., 2007). High LHV fuel blends tend to have less resistance to flashback. Turbulent flame speed is not especially dependent on pressure, and only heat transfer produced by wrinkled flames was linked to Da dependence (Lamnaouer et al., 2007), Da having an inverse dependency with increasing pressure. Thus, it is not only the Wobbe Number, Da number, heating value, Turbulent and Laminar Flame Speed or autoignition temperature, but a combination of parameters that define the resistance to flashback in a system. While a significant amount of fundamental understanding of flame propagation has been gained in natural gas systems, little is known about alternate gaseous fuels (Lieuwen et al., 2008; Bagdanavicius et al., 2009).

It has been recognized that the shape of the CRZ can influence the final stability of the system. Some authors have observed how it progresses into the mixing chamber as a Combustion Induced Vortex Breakdown (CIVB) (Kroner et al., 2003; Umemura and Tomita, 2001), where they attribute the appearance of the vortex as a consequence of the combustion and air entrance, linking the phenomenon to the CRZ. Moreover, vortical structures can be modified by geometrical factors and flow conditions, as well as by the interaction of unburned gases and the reaction zone, complicating even more their part in flashback occurrence and avoidance. It has been recognized that this structure plays a crucial role in the propagation of the flame, creating low velocity paths for flame propagation similar to that occurring with the CRZ.

Thus, passive methods need to be developed to cope with new demands and necessary configurations for burning improvement and alternative fuels. Flashback must be avoided and thermal stability accomplished. The most promising way to extend the thermoacoustic stable operation condition of the combustor is to change the burner outlet conditions. According to some authors (Krebs et al., 2002) this

influences the time lag of a fluid element from the moment that this leaves the burner exit to the instant that it crosses the flame front. The increase of this value is thought to balance out thermoacoustical instabilities. The principle states that the velocity fluctuation at the burner exit induces a fluctuation of mass flux of reacting species which is convected to the flame front where it generates heat release fluctuations. Therefore, the velocity fluctuation can be damped by increasing the momentum exchange between gases in the CRZ, which can be accomplished by changing the burner outlet, such as mounting a cylindrical extension capable of enlarging the recirculation zones. This has proved to allow a higher thermal released by contact with the shearing flows -flame envelope, also increasing the time lag (Berenbrink and Hoffmann, 2000). Therefore, promising technologies make use of new configurations based on nozzle modifications.

Numerical Simulations have been used extensively to increase the understanding of such type of flows and reduce the time and cost of physical prototypes. However, Direct Numerical Simulations (DNS) are limited to small computational domains and low Re, since the smallest scales must be resolved on the grid, requiring larger computer resources. On the other hand, Large Eddy Scales (LES) methodologies are used for practical purposes, but the representation of the flame on a course grid always is a problem (Candel, 2002), thus leaving much to be desired for highly complicated flows.

Nevertheless, various numerical simulations have been successful when accompanied by extensive experimentation for optimization (Brundish et al., 2007; Freitag et al., 2006; Selle et al., 2006; Jochmann, 2006; Roux et al., 2005; Zimont et al., 1998), allowing a close interpretation of the inner physical events with enough accuracy for the development of larger scale prototypes, permitting more complex analysis.

Therefore, this chapter is intended to analyze passive modes of flame stabilization by geometrical changes in order to improve the thermal stability of the system using natural gas and allow wider operational ranges for their future usage with alternative fuels. Experimental techniques were used to characterize a swirling flow under combustion conditions at atmospheric conditions under a variety of equivalence ratios.

6.1. Experimental Setup

Experiments were performed in the same burner specified in Chapter 5. Only configuration [25-25] was used in order to obtain an isothermal swirl number of 0.98, the most stable as previously specified.

The diffusive and premixed modes of fuel injection were utilized. Premixed gas injectors, extending across the inlet ducts, were located just before the inlets. The diffusive injector had a 23.4 mm diameter, positioned 47.5 mm upstream of the burner nozzle (wide injector). Overall equivalence ratio φ is reported as well as the fuel proportion injected diffusively by the fuel injectors mounted along the axis followed by that injected as premixed in the tangential inlets. The format (25-80) here refers to 25 l/min diffusive natural gas injection, the 80 to that injected as premixed. Due to the high temperature variation, the Re is defined from the rig nozzle diameter and isothermal condition. Pressure fluctuation measurement was made with a EM-1 Yoga Electret Condenser Microphone, as mentioned elsewhere. Experiments were undertaken using a Phase Locked PIV system as specified in the previous chapter.

Four swirl rig nozzle constrictions were used at the burner outlet with the aim of characterizing the flame and its behaviour under a variety of geometrical cases. Circular constrictions of 0%, e.g. no constriction, 10% and 20% (both cylindrical sections with a total length of 35 mm and sharp, square inlet/outlet) of the outlet diameter were utilized. Thus, nozzle geometries of 1.00 D, 0.90 D and 0.80 D were characterized. A last case was used with a quarl modification initially 0.80 D expanding to 1.00 D, with a geometrical slope of 1.25 (a length of 8 mm). An entire diagram of the inserts and configuration used is shown in figure 6.1.

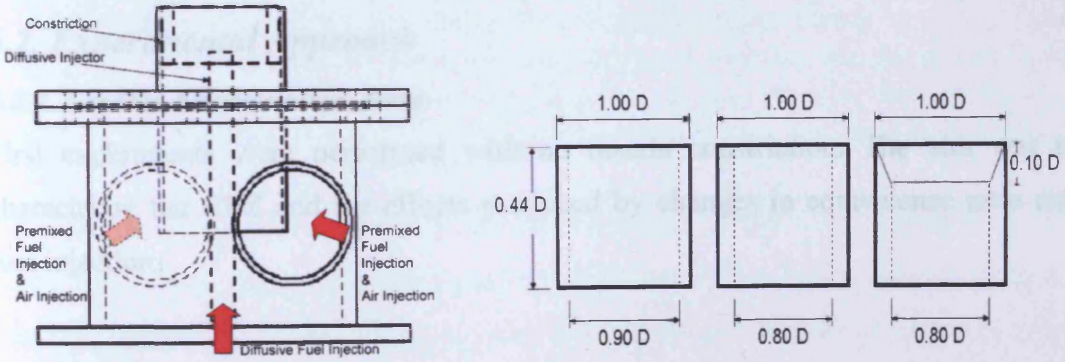

Figure 6.1. Diagram of Rig and Constrictions used (35 mm total length of all constrictions; the length of the slope is 8 mm; diagrams not at scale).

A Kodak M753 Digital Camera in Speed Mode was used to capture colour images of the lifted flames to find the position of initial flame stabilization and the characteristic of the CRZ and surrounding flame envelope. Acquisitions were performed at the same flow rates for comparison purposes. In order to observe the flashback phenomenon occurring inside of the rig, the steel baseplate was replaced by a quartz crystal plate. When diffusive fuel injection was required to allow observation of the phenomenon, a new support structure and bottom cage were designed with a horizontal pipe residing close to the rig baseplate, allowing the injection of fuel into the chamber at the same position as in previous experiments. The quartz plate was placed at the bottom of the cage (130 mm length), permitting the visualization of the phenomenon and the positioning of the quartz far any violent flashback, figure 6.2. 500 frames per second were obtained for a great variety of fuel conditions and the various rig nozzles using the High Speed Camera. In order to achieve best visualization, two mirrors were positioned above and beneath the rig, respectively. With a distance of 0.50 m from the rig, the mirrors were angled at 45° to permit a proper recognition and recording of the phenomenon as it occurs in the system at different flows and geometrical conditions. The system was analyzed using the circular confinements utilized in chapter 5, section 5.3.2, which are more representative of industrial conditions.

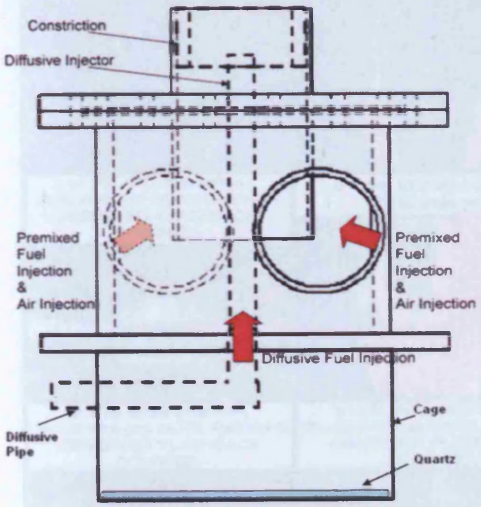

Figure 6.2. Modified Flashback Setup Array with Quartz Plate moved away from exhaust sleeve and tangential inlets.

6.2. Experimental Approach

6.2.1. Central Recirculation Zone

First experiments were performed with no nozzle constriction. The aim was to characterize the CRZ and the effects produced by changes in equivalence ratio and fuel injection.

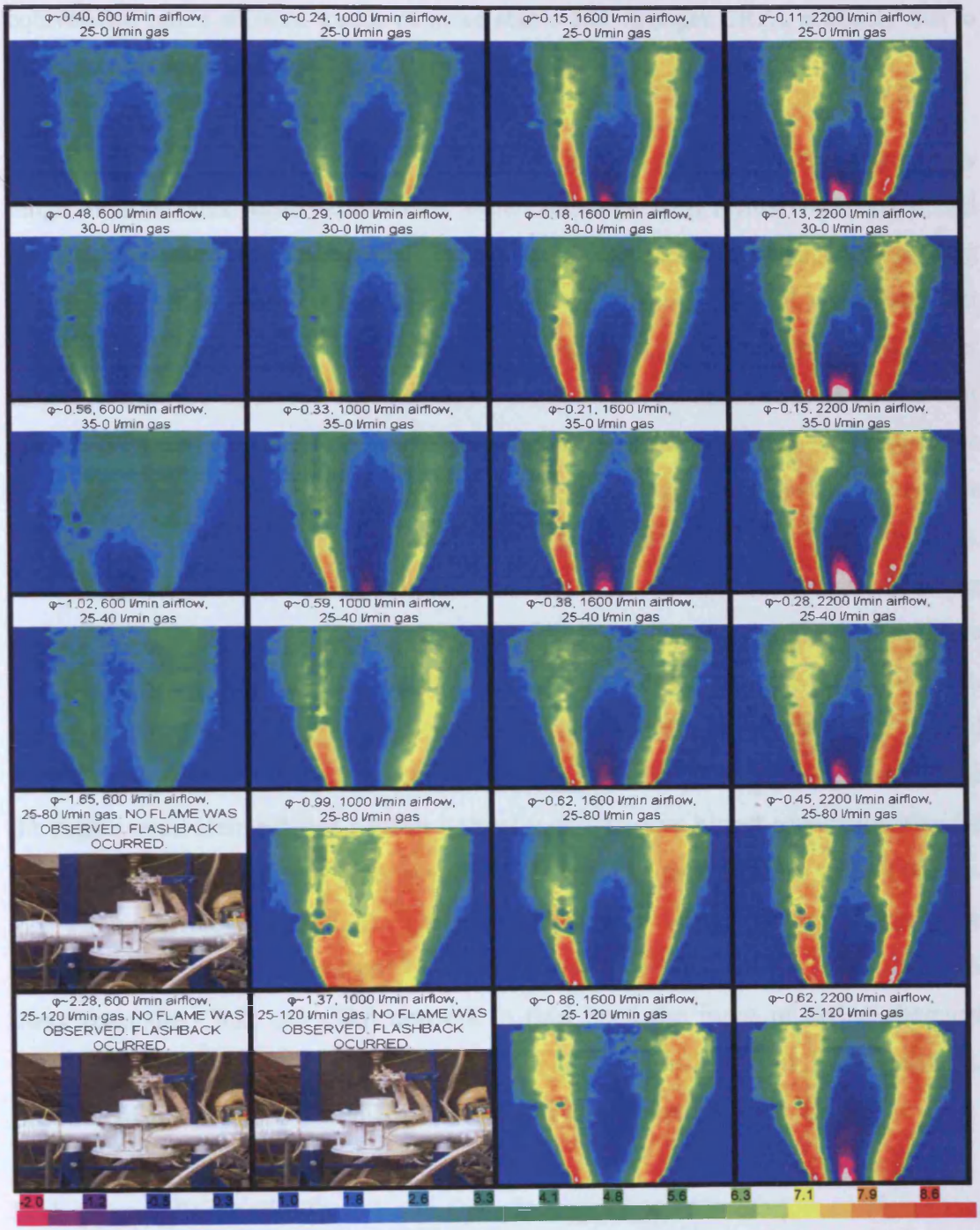

Figure 6.3. Fixed air flow rates, different modes of gas injection and gas flowrate rates. Wide Injector Used. Colour bar in [m/s]. Vortex Breakdown appears as a wobbling unattached weak (blue) region, very difficult to visualize. The CRZ is completely attached, very coherent and strong (purple), being very easy to follow for visualization.

Equivalence ratio plays a decisive role in the shape of the CRZ, figure 6.3. First experiments were carried out using entirely diffusive fuel injection, which showed a coherent structure whose strength was dependent on the Re number. Higher

equivalence ratios showed trends of more stable and stronger CRZs, probably due to the higher velocities and general stability of the flow.

Experiments using entirely premixed injection showed stability over a very narrow range of flow rates, thus experiments were continued with diffusive-premixed fuel entry. A small amount of diffusive fuel proved sufficient to allow the stable anchoring of the flame, increasing considerably the stability of the system. It was found that these systems developed strong recirculation zones past the Vortex Breakdown faster than their entirely diffusive counterparts. This is visible in the case at 1600 l/min air and 25-120 l/min gas, which is still wobbling and unstable since it has only passed the Vortex Breakdown threshold (remember combustion reduces the swirl number, see figure 6.3, φ=0.99, 1000 l/min, 25-80 l/min of gas where the CRZ has disappeared). The following case at 2200 l/min air and 25-120 l/min gas depicts very strong recirculation, whose length surpasses those of its predecessors. Comparison with the entirely diffusive flames is difficult as the equivalence ratios are very different. Visual observation and figure 6.3 shows that the diffusive-premixed flames are spread over a larger area at the swirl nozzle and hence show lower axial velocities, despite the higher equivalence ratios (which normally should give higher axial velocities for the same flame shape), compare φ=0.15, 35-0 l/min (pure diffusive) to φ=0.62, 25-120 l/min (diffusive-premixed). This also appears to be the reason for the poor stability of the entirely premixed flame as the outer flame boundary is located well away from the CRZ; the CRZ appears to thus need the input of active chemical species from the initial flame reactions, not just recirculated hot burnt products. Injection of small amounts of diffusive fuel into this region achieves this aim.

Both types of flashback (Type 1 and Type 2) were observed with this configuration, flame propagation around the fuel injector to the baseplate followed by radial flashback to the tangential inlets, obviously depending on equivalence ratio and flowrate.

6.2.2. Axial Flashback. Use of Nozzle Constrictions.

To analyze the axial flashback, different geometries were used to push the flame upwards and avoid contact with the injector. With no confinement or combustion can

to fire into, the open flames proved to be dirty at low airflow rates, with a very thin envelope and very rich inner core. Figure 6.4 shows the flames obtained for a fixed fuel flowrate of 25-40 l/min and varying airflow hence φ. The flame can be seen to strengthen and become more stable as the airflow is increased and φ reduces. Again this is due to the reducing value of φ, higher swirl number and stronger CRZ. The initial dirty flames at low air flowrates and highest vales of φ are thus due to the flow being located around the point of Vortex Breakdown with a very weak CRZ.

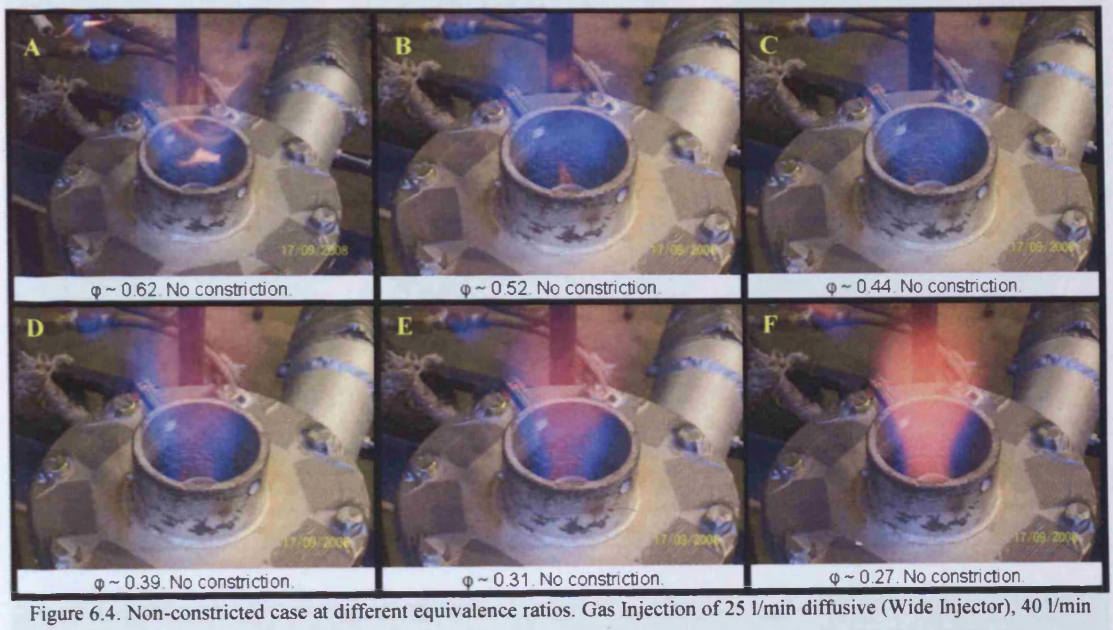

Figure 6.4. Non-constricted case at different equivalence ratios. Gas Injection of 25 l/min diffusive (Wide Injector), 40 l/min premixed. Airflows used: A) 1000 l/min. B) 1200 l/min. C) 1400 l/min. D) 1600 l/min. E) 2000 l/min. F) 2200 l/min.

Changing to a nozzle constriction of 0.90 D, figure 6.1, the flame showed considerable improvement, figure 6.5, for a constant fuel flowrate of 25-40 l/min. Initially, the flame was pushed up enough to avoid touching the injector at low flowrates. This flame was cleaner and of more stable shape than the previous case. Contrary to the entirely open case where the flame touched the injector at 1000 l/min of air, this was delayed until 1600 l/min. Higher air flowrates, hence lower values of φ, allowed the CRZ to increase in size and length and extend back undesirably over the fuel injector. This again is a swirl number effect. This nozzle constriction alters the swirl number to 0.88 (Syred, 2006) and this work shows the associated importance of nozzle geometry.

The nozzle constriction of 0.80 D, figure 6.1, gave a cleaner flame at low flowrates, figure 6.6. This flame never touches the injector and remains always blue, showing a

higher degree of mixing and reaction, despite the slightly lower value of S at 0.78. Possibly this is due to the higher Re. As the airflowrate is increased φ overall decreases from 0.62 (1000 l/min) to 0.27 (2200 l/min) when the flame is now only a few millimeters long and the CRZ has enlarged in size as the swirl number is not reduced so much by the effects of combustion.

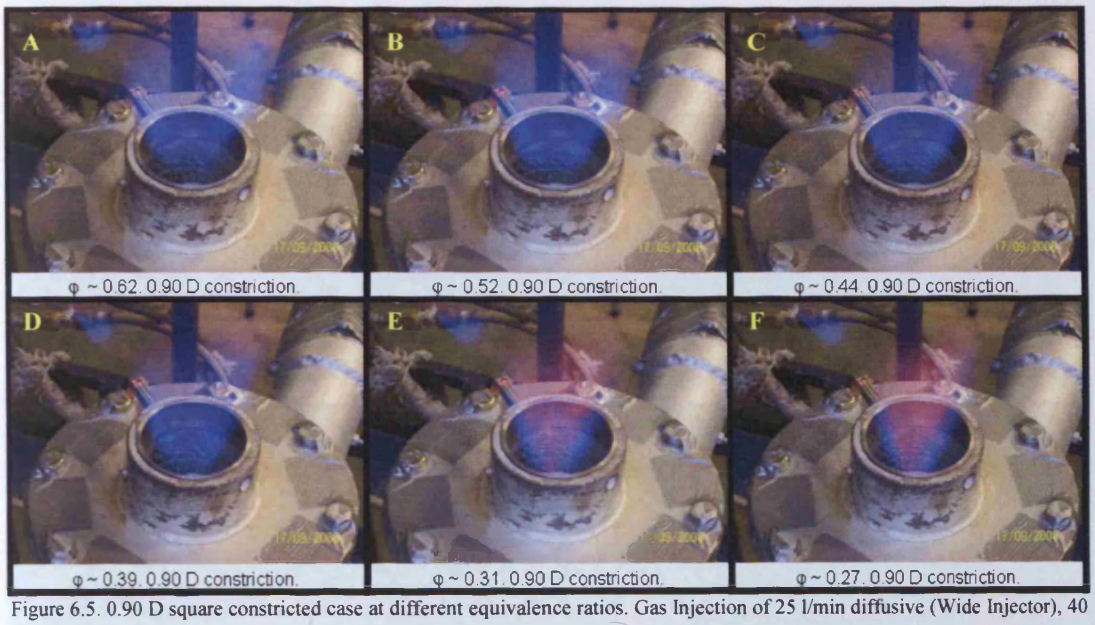

Figure 6.5. 0.90 D square constricted case at different equivalence ratios. Gas Injection of 25 l/min diffusive (Wide Injector), 40 l/min premixed Airflows used: A) 1000 l/min. B) 1200 l/min. C) 1400 l/min. D) 1600 l/min. E) 2000 l/min. F) 2200 l/min.

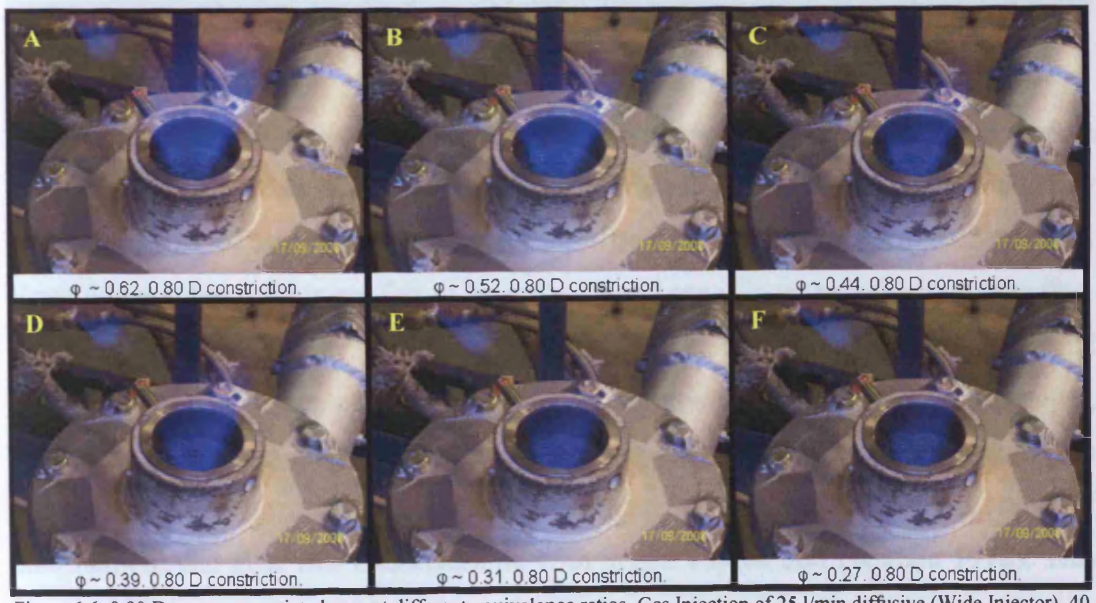

Figure 6.6. 0.80 D square constricted case at different equivalence ratios. Gas Injection of 25 l/min diffusive (Wide Injector), 40 l/min premixed. Airflows used: A) 1000 l/min. B) 1200 l/min. C) 1400 l/min. D) 1600 l/min. E) 2000 l/min. F) 2200 l/min.

Finally, a short quarl constriction was used, figure 6.1, with a cylindrical base of 0.80D expanding to 1.00D at the nozzle in 8 mm length, flames are shown in figure

6.7. This configuration proved to be the most effective in terms of flame stabilization. The flame never touched the injector and the expansion caused by the radial movement of the shearing flow allowed a wider stronger flame at high Re. It appears that the effect of the quarl to expand the diameter of the CRZ (due to changed radial and axial pressure gradients) gives a better match between the initial flame front, the expanding shear flow and the CRZ boundary.

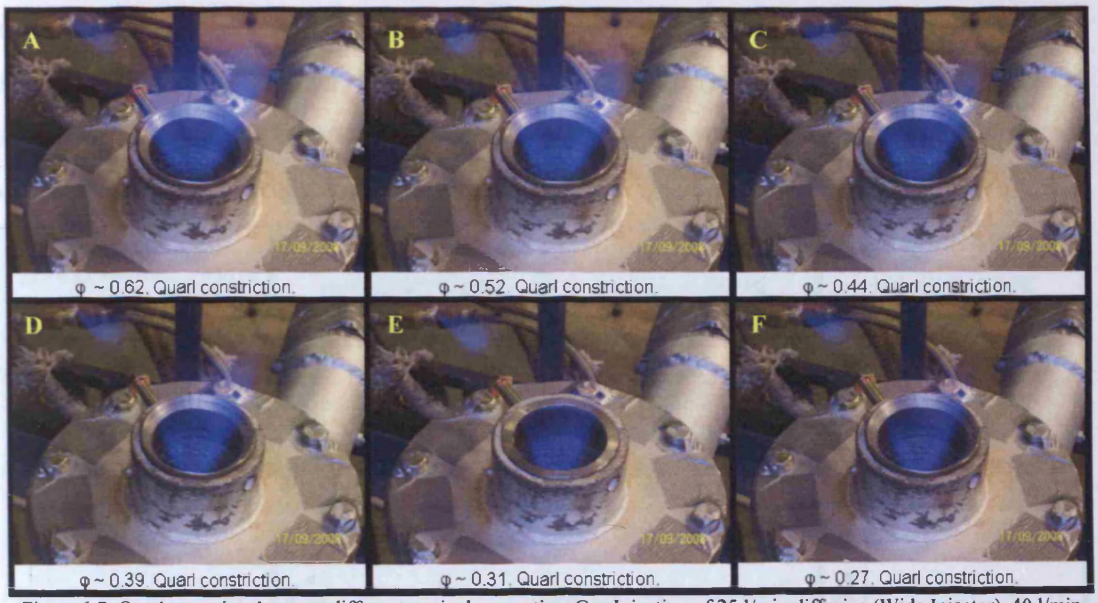

Figure 6.7. Quarl constricted case at different equivalence ratios. Gas Injection of 25 l/min diffusive (Wide Injector), 40 l/min premixed. Airflows used: A) 1000 l/min. B) 1200 l/min. C) 1400 l/min. D) 1600 l/min. E) 2000 l/min. F) 2200 l/min.

This configuration increases the stability of the flame in terms of efficiency with a more defined and stable envelope while maintaining the flame out of contact with any surface or part of the burner, despite the large variation in φ from 0.62 to 0.28. Reynolds number effects are felt to be quite small here. Since the velocity of the flow has increased considerably, Type 2 flashback is reduced (Type 1 does not exist) and the flame remains located at a couple of centimeters from the injector outlet, increasing the system efficiency and reducing the risk of damage and soot nucleation with particle growth on cooler surfaces. It must be noted here that high levels of confinement can alter this characteristic with quarls (Syred and Dahmen 1978). This is usually taken to occur when the ratio of the confinement diameter to the burner throat diameter is less than ~3.

6.2.2.1. Particle Image Velocimetry

A Phase Locked PIV analysis was then carried out to determine the size and shape of the CRZ with these nozzles, figure 6.1, at high air and fuel flow rates more representative of gas turbine combustion. These were 2250 l/min air and 25-125 l/min gas, results are shown in figure 6.8.

The length of CRZ has decreased in comparison to the case with no nozzle constriction, whilst the strength appears to have increased somewhat, especially with figures 6.8C and 6.8D with the 80% square and quarl nozzles. The CRZ has become wider allowing more extensive mixing, matching the premixed flame front with that of the CRZ better, producing better combustion.

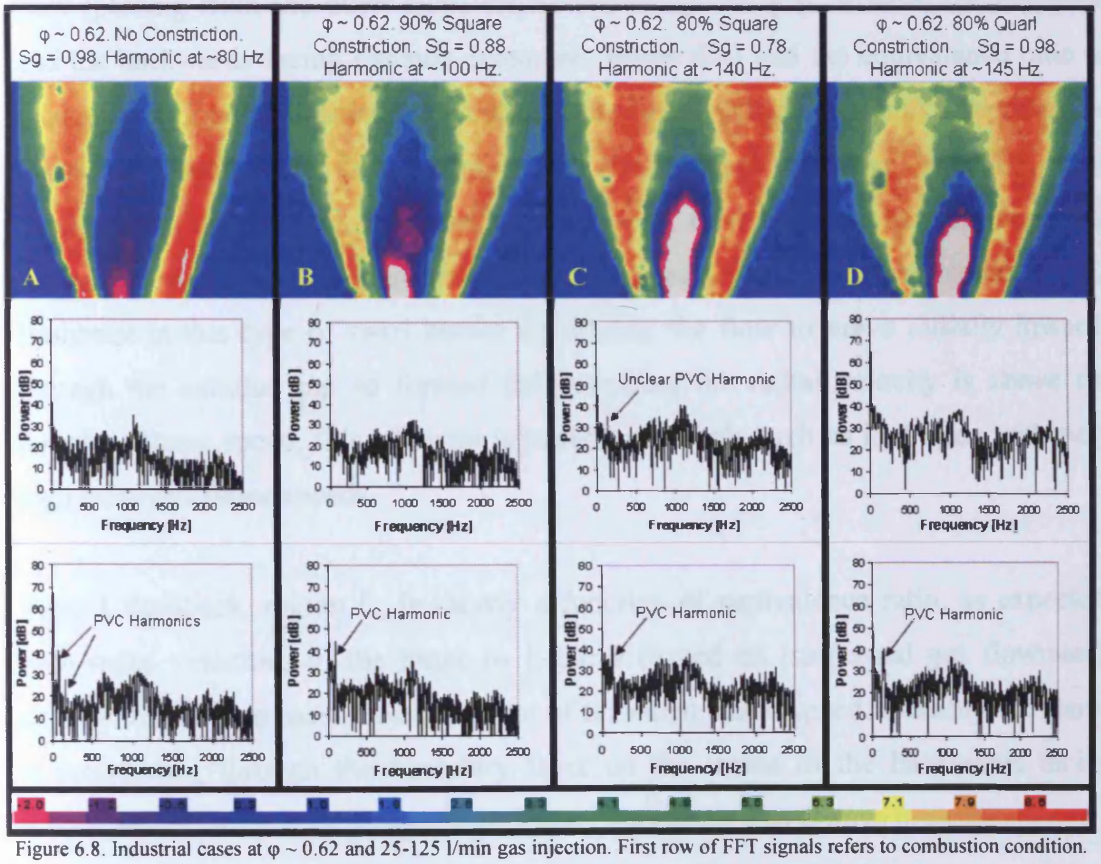

Figure 6.8. Industrial cases at φ ~ 0.62 and 25-125 l/min gas injection. First row of FFT signals refers to combustion condition. Second row is the Isothermal condition. A) Non-constriction. B) 0.90D square constriction. C) 0.80D Square constriction. D) Quarl constriction. The colour bar represents the flow velocity [m/s], with colour white being out of the range (extremely strong negative velocity for these cases).

Isothermal and Combustion conditions were also characterized using FFT Analyses, to depict the harmonics of the Precessing Vortex Core (PVC) (Valera-Medina 2006; Syred, 2006). This structure is highly attenuated when using higher thermal input conditions such as these. Although the structure has been observed under combustion

with high coherence and interaction with the CRZ in the previous experiments, chapter 5, the FFT analysis did not show as high a level of coherence as in the isothermal and lower thermal input cases, possibly as combustion generated noise starts to overwhelm the signal. Thus, it was considered that such kind of flow could be at least partially simulated using a commercial software such as FLUENT in time averaged mode to permit a better characterization under pressurized conditions before final assembly of a full scale prototype (Valera-Medina et al., 2009). Although some results were obtained, the simulation is part of another project.

6.2.2.2. Stability Maps

Comparison between cases was performed using the average radial velocity of the flow (passing from the outer swirl chamber through the gap between the baseplate and the backwards facing exhaust extension, figure 6.1) and the equivalence ratio to recognize regions of flashback for both premixed and diffusive-premixed conditions. Figure 6.9 shows the first results with and without diffusive injection. This configuration did not have any nozzle constriction. Here it should be mentioned that the backwards facing nozzle extension has been used for many years to reduce Type 2 flashback in this type of swirl burner by forcing the flow to move radially inwards through the annular gap so formed thus ensuring the radial velocity is above the turbulent flame speed, this is easily adjustable for fuels such as hydrogen with very high turbulent flame speeds.

Type 2 flashback, region C, is clearly a function of equivalence ratio, as expected, with radial velocities in the range to 1-2 m/s (based on isothermal gas flowrates), slightly higher than most measurements of turbulent flame speed. Possibly the flame is propagating through the boundary layer on the inside of the backwards facing nozzle where lower velocities prevail. Type 1 flashback was always present.

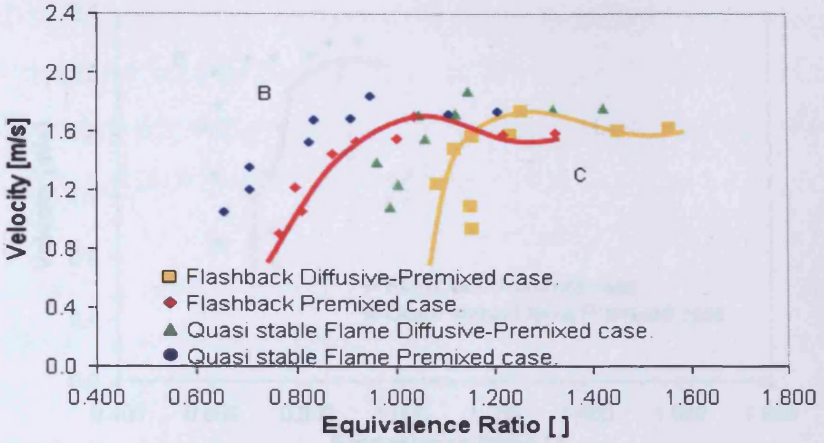

Figure 6.9. Different regions recognised in the Type 2 flashback map at atmospheric conditions. Blow-off region (A) does not appear in this graph. B) Region of quasi stability for the flame, with different flame shapes. C) Flashback region. Region A) of blowout is at much lower φ and equivalence ratios and not visible here.

The Type 2 flashback curves for fully premixed and diffusion-premixed combustion can be made to match almost exactly if the equivalence ratio solely based on the premixed equivalence ratio is used. Thus flashback limits can be readily altered by using partially premixed combustion. Configurations at high equivalence ratios showed very long and emissive flames before flashback up to φ~1.2. After this, flames have an unstable elongated shape that pulsates before flashing back.

Experiments were expanded to the use of configurations with nozzle constrictions, figure 6.1. Since the Quarl proved to be the most efficient geometry, this was evaluated for flashback analysis. It was found that the system using diffusive injection never flashbacked under the conditions analyzed. The flame only retouched the quarl with an elongated emissive pattern. Higher equivalence ratios and Re could not be tested due to equipment limitations, thus limiting the investigations of flashback for this configuration.

Experiments in the premixed case without diffusive injection were investigated. For the case without the fuel injector, no diffusive gas and quarl constriction, the flashback limit peaked at φ~0.875 and ~2.1 m/s, figure 6.10. The case without constriction, figure 6.9, peaked at φ~1.03 and ~1.7 m/s, showing a considerable reduction in the flashback limit using the quarl with this configuration.

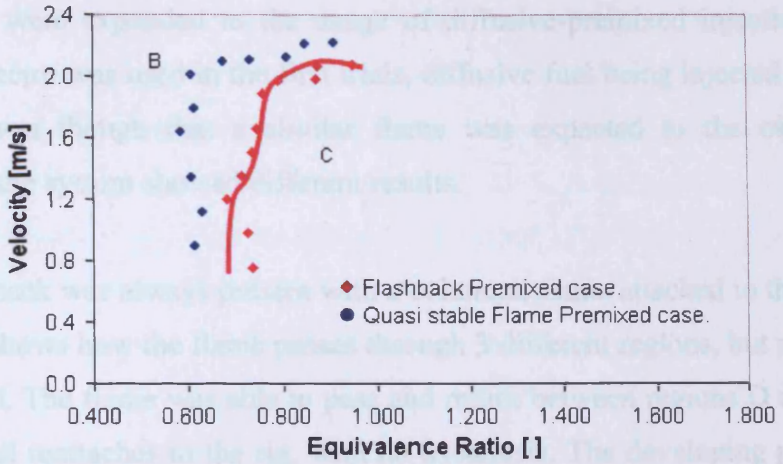

Figure 6.10. Different regions recognised in the flashback map at atmospheric conditions using the Quarl Constriction without injector. B) Region of quasi stability for the flame, with different flame shapes. C) Flashback region. The flashback curve peaks faster than the non-constricted case.

When the fuel injector was re-placed into the rig, but not used, leaving an entirely premixed condition, the resistance to flashback increased considerably, peaking at φ~1.09 and ~1.17 m/s, figure 6.11. This is a velocity reduction of almost twice that observed without the injector. The nozzle suffers a constriction of ~50% of its diameter due to the injector, increasing the Re number in this area, and pushing the flame out of the nozzle. Figure 6.11 also shows the different flame regions found, illustrating the position of the lifted flame and regions where the flame touches the quarl at high equivalence ratios, probably due to the low flow velocities.

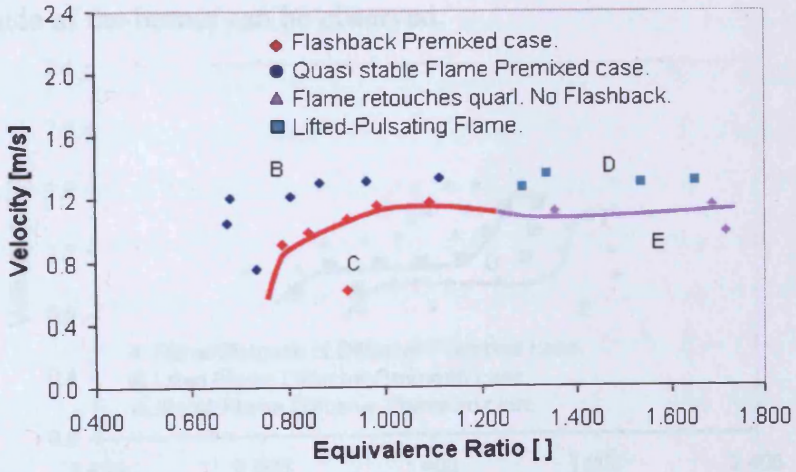

Figure 6.11. Different regions recognised in the flashback map at atmospheric conditions using the Quarl Constriction with injector. B) Region of quasi stability for the flame, with different shapes and emissions. C) Flashback region. D) Lifted flame. E) The flame retouches the quarl.

Experiments were expanded to the usage of diffusive-premixed injection with the quarl. No injector was used in the first trials, diffusive fuel being injected through the baseplate. Even though that a similar flame was expected to the case with no constriction, the system showed different results.

Type 1 flashback was always present with a columnar flame attached to the baseplate. Figure 6.12 shows how the flame passes through 3 different regions, but no flashback was observed. The flame was able to pass and return between regions D and E where it touched and reattaches to the rig, with no hysteresis. The developing process is as follows: a stable flame would form at high flowrates giving traces of being partially lifted from the tip of the injector, with a conical shape and high stability for this type of nozzle constriction. At lower flowrates and higher equivalence ratios, the flame would lift forming just in and around the end of the recirculation zone, this being caused by the lack of oxygen and the higher value of equivalence ratio. Reducing the airflow even more would allow the upstream movement of the flame inside of the rig, but the flame only just retouches the nozzle. Although the rig temperature increases (as observed in the plastic joints close to the air inlets), the flame never goes into the noisy, powerful Type 2 flashback observed with other configurations. Moreover, it is possible to recover the first stable flame with no problem. Type 2 flashback seems to be avoided by the increase in velocity caused by the nozzle constriction (a reduction of 36%). Other flame modes can be easily recovered. Other experiments are needed where the inside of the burner can be observed.

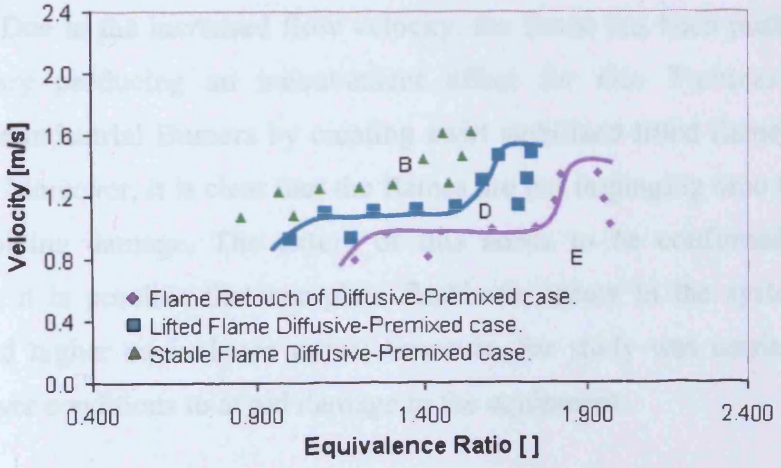

Figure 6.12. No flashback observed when the Quarl is used with diffusive-premixed injection and No Injector. B) region of quasi stability for the flame, with different shapes and emissions. D) Lifted flame. E) The flame retouches the Quarl. 25-40 l/min diffusive-premixed injection.

The use of a diffusive injector showed the similar trends, with no flashback. However, the threshold between regions moved as a function of velocity and equivalence ratio, figure 6.13. Since Re has changed and increased due to the nozzle reduction caused by the injector, the flame may be pushed upwards for a longer velocity range. It is not until the equivalence ratio has increased considerably that the flame retouches the nozzle. The reason for this behaviour must be that velocities around the injector are sufficiently high to prevent Type 2 flashback into the rig (by the extra 14% reduction in outlet area).

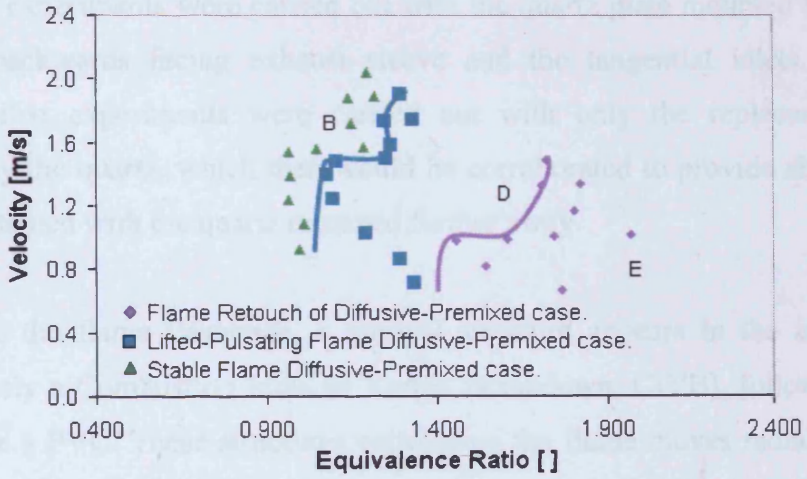

Figure 6.13. No flashback observed when the quarl is used with diffusive-premixed injection and Injector. B) region of quasi stability for the flame, with different shapes and emissions. D) Lifted flame. E) The flame retouches the quarl. 25-40 l/min diffusive-premixed injection.

Thus, it is experimentally confirmed that the flame can be kept away from the nozzle and the injector tip of the burner for a wider range of equivalence ratios than without the injector. Due to the increased flow velocity, the flame has been pushed up more than necessary producing an inconvenient effect for Gas Turbines but useful behaviour for Industrial Burners by creating swirl stabilized lifted flames (region D, figure 6.13). Moreover, it is clear that the flames are not impinging onto the diffusive injector, avoiding damage. The extent of this needs to be confirmed by further experiments. It is possible that complete flashback occurs in the system at lower flowrates and higher equivalence ratios; however, the study was carried out under safe-low power conditions to avoid damage to the equipment.

6.2.3.Type 2 Internal Flashback. High Speed Photography.

The experimental analysis was expanded to recognize the Type 2 flashback in the region formed by the backwards facing exhaust sleeve, the baseplate and the outer section of the swirl burner where the tangential inlets meet the main swirl chamber.

6.2.3.1. Type 2 Flashback using Nozzle Constriction. Quarl.

The phenomenon was successfully visualized, figure 6.14, here the quartz plate was used to replace the steel baseplate. Owing to concerns about damage to the quartz plate many experiments were carried out with the quartz plate mounted further away from the backwards facing exhaust sleeve and the tangential inlets, figure 6.2. However, first experiments were carried out with only the replacement of the baseplate by the quartz, which then would be corroborated to provide similar results as those obtained with the quartz mounted further away.

Previous to the flame flashback, a vortical structure appears in the centre of the system (likely a Combustion Induced Vortex Breakdown, CIVB), followed by what seems to be a PVC. These structures collapse as the flame moves radially outwards into the swirl chamber. The flame accesses the chamber with high radial-tangential velocity, starting the process near the wall of the rig exhaust sleeve (possibly via boundary layer propagation).

Then the flame reaches the first inlet, igniting the supplying jet. The flame keeps moving to the other inlet, with its subsequent ignition. However, the flashback is not violent, and remains stable inside of the swirl chamber of the burner. A vortex appears at the centre of the body, engulfing both flames and producing 2 regions of intense burning in the centre. This behaviour is sustained until the system is shut down. The flame does not propagate completely inside of the swirl chamber, with only these two jets maintaining the flame. Several eddies developed as a consequence of the contact between the flame and the wall of the chamber.

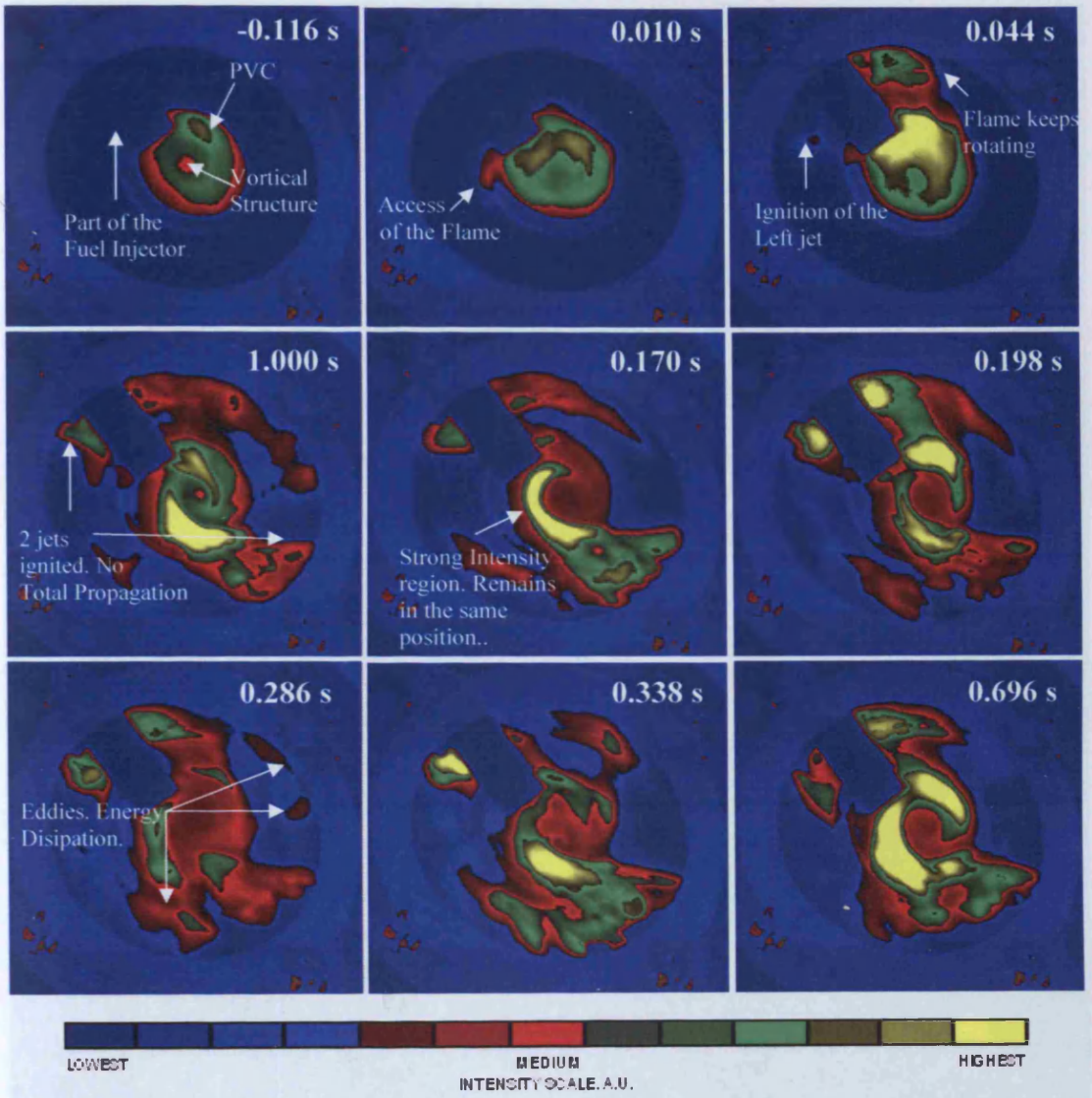

Figure 6.14. Flashback under Confined Conditions. Open Exhaust. Quarl Nozzle Constriction. No. Injector. Quartz positioned at baseplate. 700 l/min air, 0-40 l/min gas (100% premixed, $\varphi = 0.54$). The time is measured starting from the first image with a flame that passes the sleeve threshold. Configuration as Figure 6.1 where the quartz plate replaces the steel baseplate. Note: The presence of part of the fuel injector was unavoidable.

A close look at the initial process was performed, figure 6.15. Flashback commences due to the backwards propagation of the flame in the swirl chamber. However, the positioning of the flame and its shape are consistent with flame propagation back along a swirl spiral or stream tube formed by the incoming swirling flow. The effect is highly 3 dimensional. The speed of radial propagation of the flame is ~1.91 m/s, typical tangential inlet velocities are ~1.83 m/s giving a combined flashback velocity of ~2.64 m/s. The same behaviour remained invariant even at higher equivalence ratios and using the Conical Exhaust, figure 6.16.

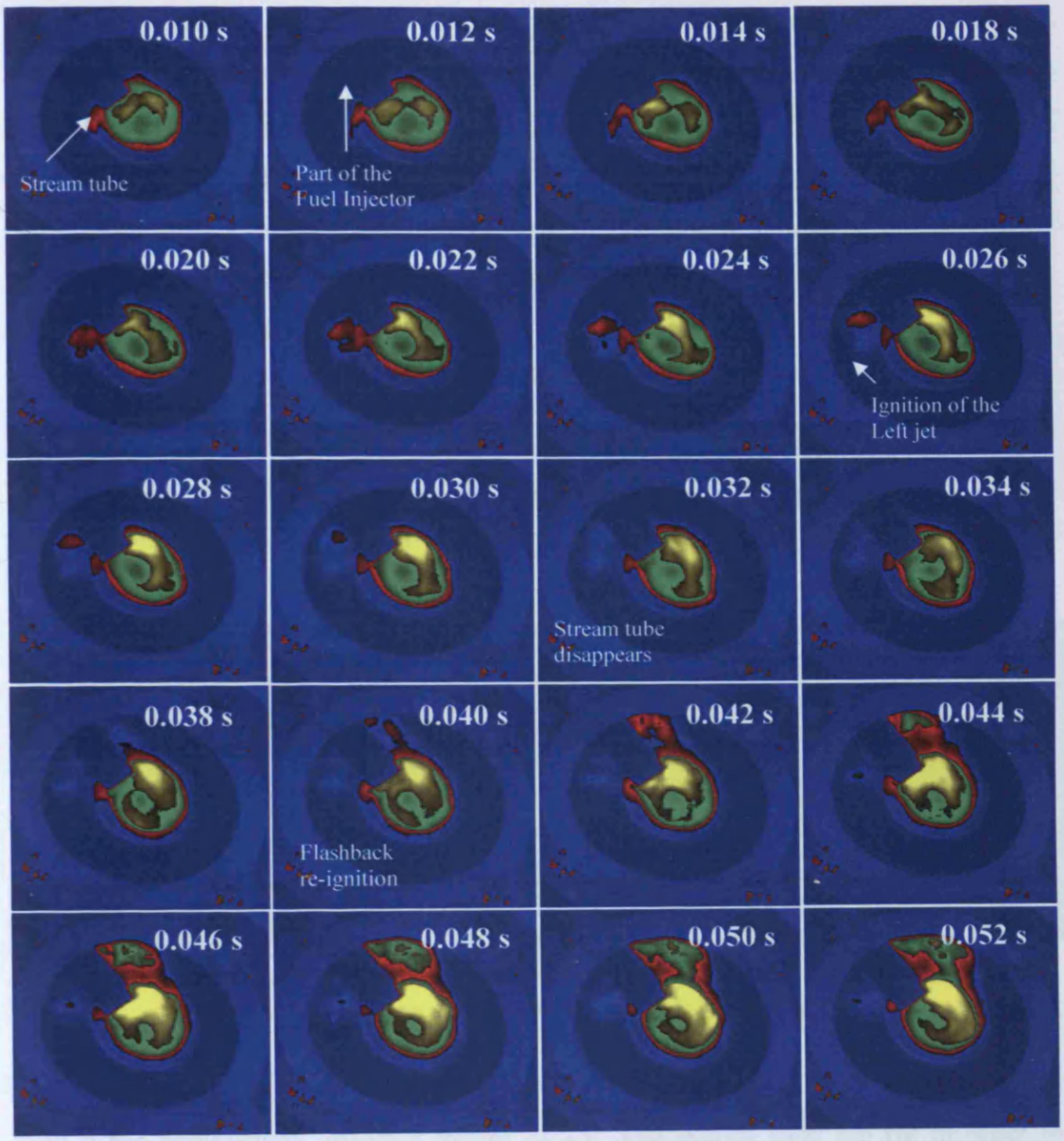

Figure 6.15. Flashback in the system commences due to the entrance of the flame in the swirl chamber as a Stream Tube. Probably another stream tube traps the flame afterwards during its movement to the right jet. Configuration as figure 6.1 where the quartz plate replaces the steel baseplate.

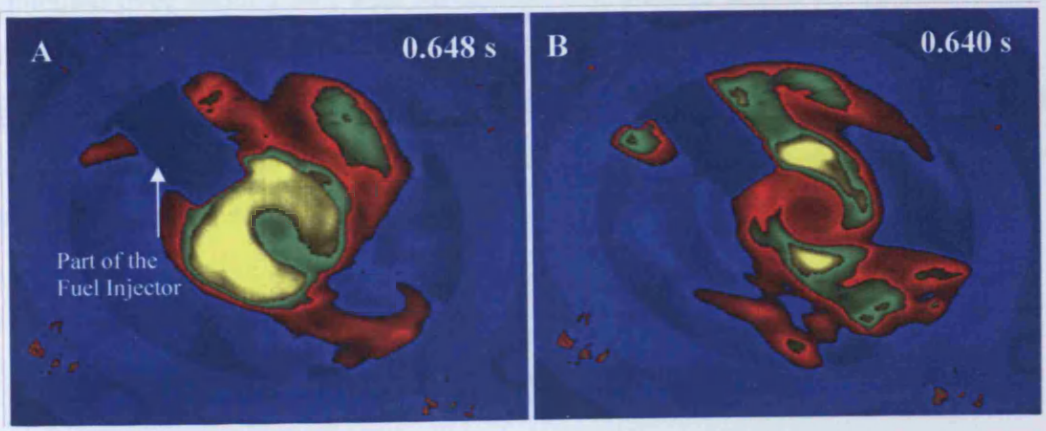

Figure 6.16. Same behaviour observed at A) Different Exhaust Geometry (Conical) and B) Different Equivalence Ratio $\varphi = 0.71$. Intensity scale as in Figure 6.14. Configuration as figure 6.1 where quartz plate replaces steel baseplate.

The configuration of figure 6.2 when compared to figure 6.1 could create a different flow pattern and flashback pattern owing to the large volume of gas below the backwards facing exhaust sleeve. Thus when analyzing the diffusive-premixed case experiments were performed to corroborate the similitude between results from the two configurations. Figure 6.17 shows how the pattern is similar to the previously analyzed case, with two jets propagating outwards into the swirl chamber at a quasi-stable rate with similar strength.

Neither fast flame propagation nor enlarged eddies near the quartz baseplate were observed during the trials, confirming that the primary development of the phenomenon is not influenced by this change in geometry for most cases.

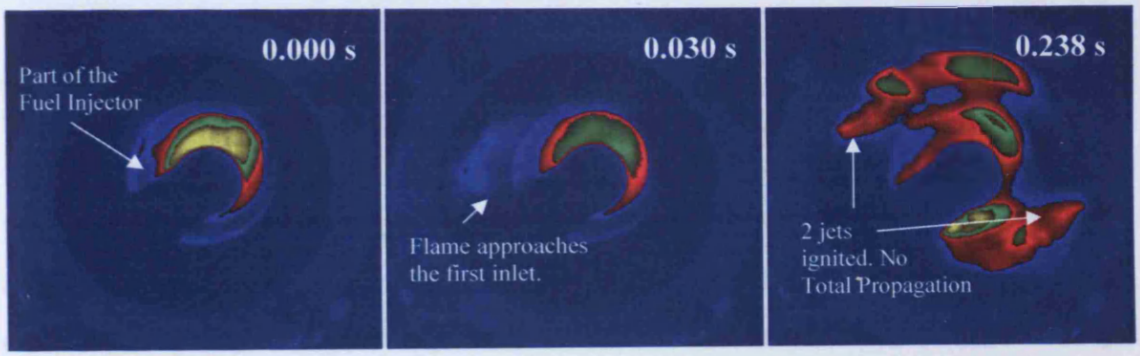

Figure 6.17. Same behaviour observed between the case with the Quartz replacing the normal baseplate (figure 6.14) and the Quartz at the bottom of the cage, see figure 6.2. Same conditions as in figure 6.14.

The analysis was then carried out to observe the development of the phenomenon from a top perspective. Another mirror at 45° was placed over the rig in order to observe the flashback using the High Speed Camera. Initially the flame is well established over about 270°, with an intense combustion region in the central vortex core, figure 6.18. Combustion is well established completely around the periphery of the sleeve. At ~0.014s the flame starts to propagate backwards up the sleeve and the central flame core starts to collapse as the flame moves radially outwards in the swirl chamber beneath it, starving it of fuel.

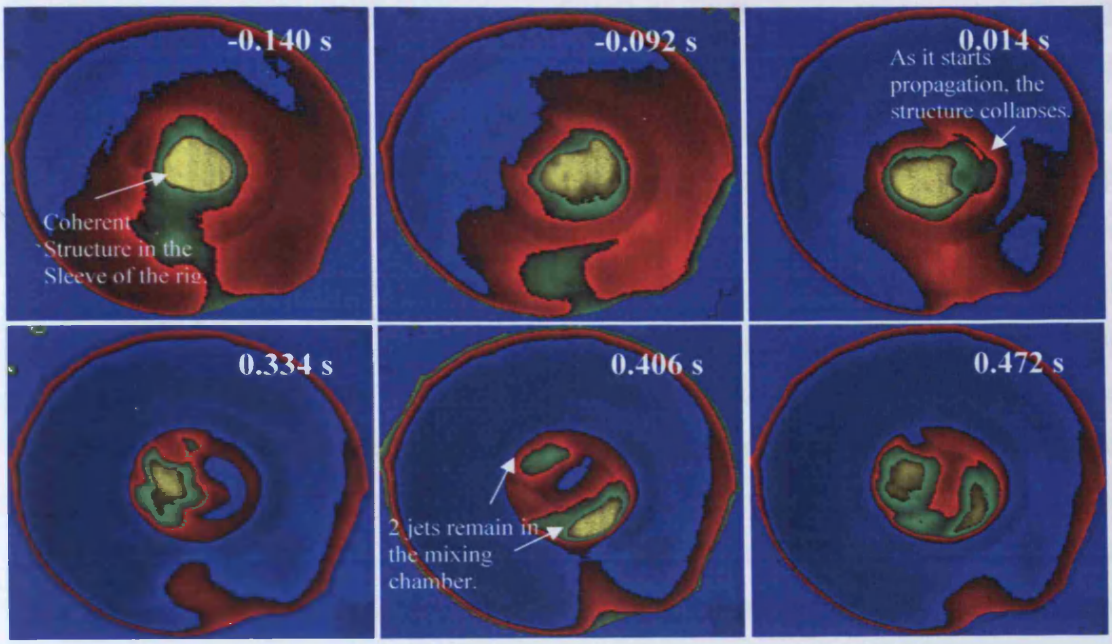

Figure 6.18. Top View of the nozzle and sleeve only, same conditions as in figure 6.14. The flame moves up the exhaust sleeve towards the swirl chamber with high coherence. When it reaches the end of the sleeve, the flame collapses and moves radially outwards, igniting the supplying jets. Numerical simulations (Valera-Medina et al., 2009) present the same localized position of the last remnants of the flame in the combustion chamber.

Finally combustion is well established in the swirl chamber reducing downstream combustion as fuel is consumed upstream. Owing to the flow patterns in the swirl chamber caused by the two inlet jets (which can act as flame stabilisers by generating small recirculation zones close to the outer wall of the swirl chamber) the flame stabilises here and is not easily blown downstream to its original position by higher velocities.

This scenario would change drastically if hydrogen would be used. The mass diffusion coefficient of the molecule is three times faster than the coefficient of methane, oxygen and nitrogen (Kroner et al., 2007), whilst turbulent flame speeds are also augmented. According to Kroner et al. (2007) criterion, intense local heat release can avoid local flame extinction and enable fast enough propagation to ignite unburned gases. Otherwise, the local disturbances produced by turbulent flame quenching –turbulent vortex structures- could penetrate the reaction layer, feeding the system with cold unburned mixtures, producing a quenching effect and avoiding flashback. It is generally accepted that flashback will be worse with hydrogen fuels. In this burner one solution to reduce flashback is to move the sleeve downwards towards the baseplate so as to increase the radial velocity.

When analysing the system with injector but no diffusive injection, the Type 2 flashback phenomenon observed was completely different. With the expectation of having similar results as in the original prototype, the system was fed with premixed gas only. Although first experiments at low equivalence ratios did not show any flashback, an increment to $\varphi = 0.95$ permitted the visualization of the phenomenon and its propagation into the mixing chamber, figure 6.19. Contrary to the case with no injector, the primary flame in the sleeve region is stronger and more coherent. As it moves upstream, the flame remains strong with a uniform expansion inside of the sleeve, and no visible coherent structures moving downwards, hence a reduced quenching factor by the appearance of vortical structures. When the propagation of the flame starts inside of the swirl chamber, this is more radial than tangential. The flame does not collapse as in the previous case, but remains strong. The propagation only takes place initially via boundary layer propagation along the sleeve walls, not along the injector. Although the first projections of the flashback flame are tangential as in the case with no injector, the fast propagation of the flame inside of the swirl chamber starts a violent explosion. The propagating flames reach both tangential inlets where the flows ignite. A second explosion follows, probably a consequence of the cage which contains a large reservoir of fuel/air mixture. As the flame stabilized inside of the swirl chamber, it was evident that both inlet jets produced a more intense flame which expanded completely into the rig. It is recognised that the equivalence ratio is considerably higher than the results observed with no injector.

The reduced outlet area increases internal pressure, thus also reduces available vent area for explosion relief so flashback tends to be more violent under these conditions. Moreover, the lack of the central vortex that appears during the phenomenon with no injector is suppressing the quenching effect that the vortical structure can produce, allowing a more uniform movement of the propagating flame front into the swirl chamber. It has been demonstrated that the lack of the CIVB due to the presence of a central fuel injector is completely changing the stability of the flame and increasing the resistance to flashback.

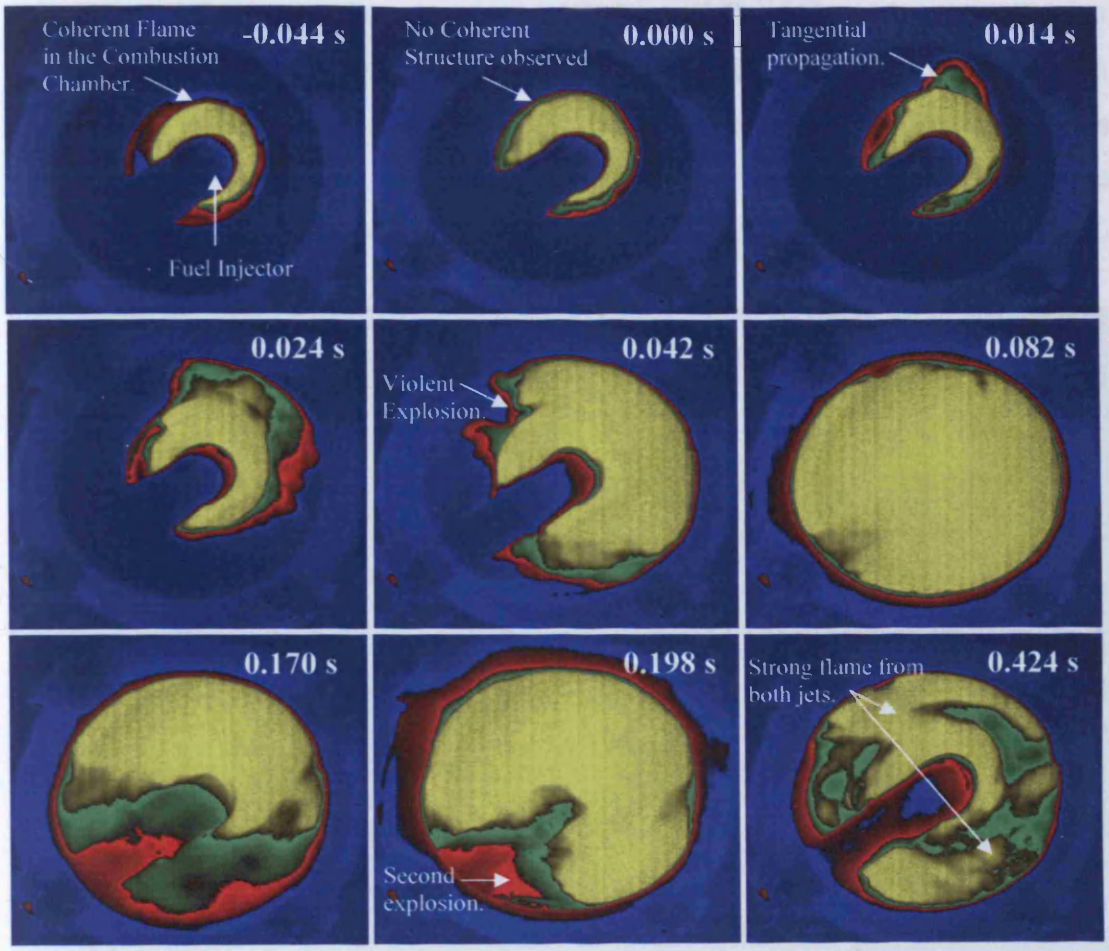

Figure 6.19. Bottom view with injector. Air flow injection of 600 l/min, 0-60 l/mi gas (100% Premixed injection, $\varphi = 0.95$). The intensity scale as in figure 6.13.

This phenomenon was observed by Yazdabadi (1996), who studying cyclone separators used central bodies to mitigate the appearance of undesirable vortical structures. The resistance to flashback has been corroborated, with the latter being observed at higher equivalence ratios. Nevertheless, the reduced outlet area has also reduced the relief vent area in case of explosion whilst the injector has reduced or eliminated the vortical structures which can produce quenching processes on the flames which are attempting to flashback. Thus more damaging effects can be produced. Therefore, it seems that better flashback resistance is obtained with the addition of the injector (or a central body), with the inconvenience that if flashback occurs, this would be more devastating.

Unfortunately, the high coherence of the flame and its emissive pattern did not allow the visualization of the top view. A closer analysis was performed for the first moments of flame propagation inside the swirl chamber, figure 6.20. Contrary to the

case with no injector, the flame moves practically radially, with minimum movement in the tangential direction. Although the speed of propagation is almost the same as in the case with no injector, ~1.9 m/s radially, the lack of tangential movement suggests that the propagation is occurring at a different section where tangential velocities are low, maybe well inside the 'cage' region, figure 6.2. This needs further investigation.

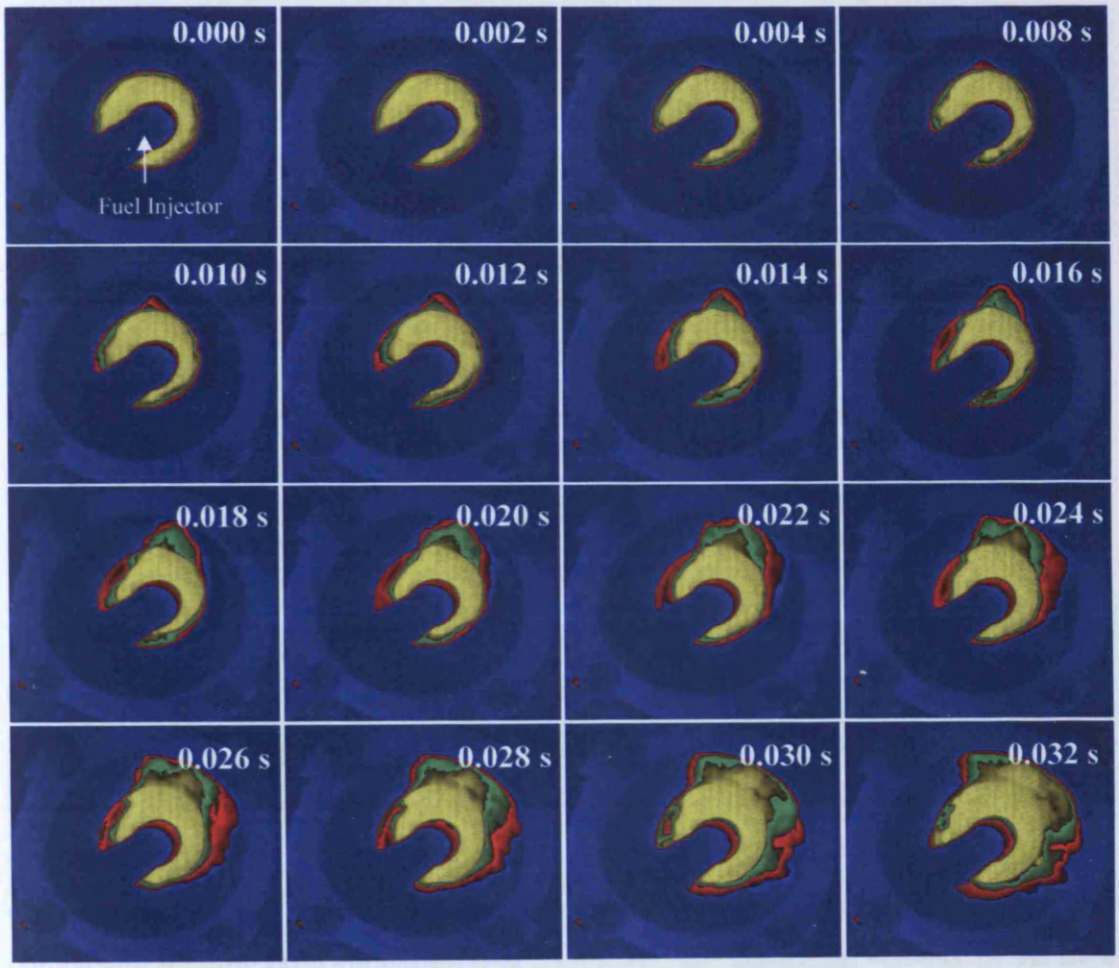

Figure 6.20. First moments of propagation. The flame moves practically radially, with slower motion in the tangential direction. Air flow injection of 600 l/min, 0-60 l/mi gas (100% Premixed injection, $\varphi = 0.95$). The intensity scale as in figure 6.13.

Higher gas flow rate and hence equivalence ratios were next investigated, figure 5.38, for both configurations with exhaust confinements, figure 5.4; both confinements were cylindrical, but one with an open exhaust, the other with a conical one. The case with no injector showed a reduction in flashback resistance compared to the unconfined case, doubtless produced by the circular confinement, which now produces a stronger CRZ due to the changed radial pressure gradients, as observed under isothermal and combustion conditions. The strengthened CRZ reduces

flashback resistance as it aids backwards flame propagation. Figure 6.21 shows the plot for this case, with a line that is even steeper than its unconfined counterpart. Although a maximum equivalence ratio as in the case with the fuel injector was attained, $\varphi = 0.95$, the reduced resistance to flashback for this case did not allow reaching value.

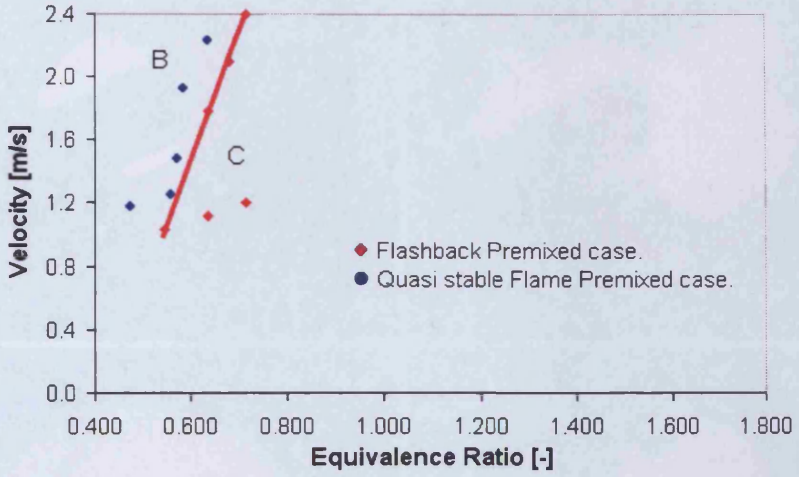

Figure 6.21. Confined Case, Figure 5.4a, with Cylindrical Open Exhaust. No Injector and Quarl Nozzle Constriction. The flashback resistance is even worse than its unconfined counterpart, figure 6.10.

The High Speed Photography analyses showed a similar behaviour for the case with no injector and higher air flow rates as in the low equivalence ratio-low Re scenario, figure 6.14. The only difference observed was the velocity of propagation of the flashback inside of the system. Due to the higher flow and gas rates, the chamber operates at a higher pressure due to the higher mass and faster mixing ratio as a consequence of the smaller length scales, producing a single explosion before completely igniting both supplying jets. Moreover, the tangential velocity of the flow has considerably increased due to the air flowrate, and appears to encourage the faster movement of the flame in this direction.

The flame has already accessed the swirl chamber, swirling until the explosion takes place. Once the jets are ignited, these create faster and stronger flames whose intensity can be observed in figure 6.22 at 0.272 s. The flame covers the entire chamber in only 0.030s, faster than 0.082s observed at low flow rates, with a radial velocity similar to all the cases, ~2.01 m/s, but a tangential velocity considerably

higher of ~6.28 m/s, figure 6.19, a consequence of the higher turbulent flame speed, a function of many variables.

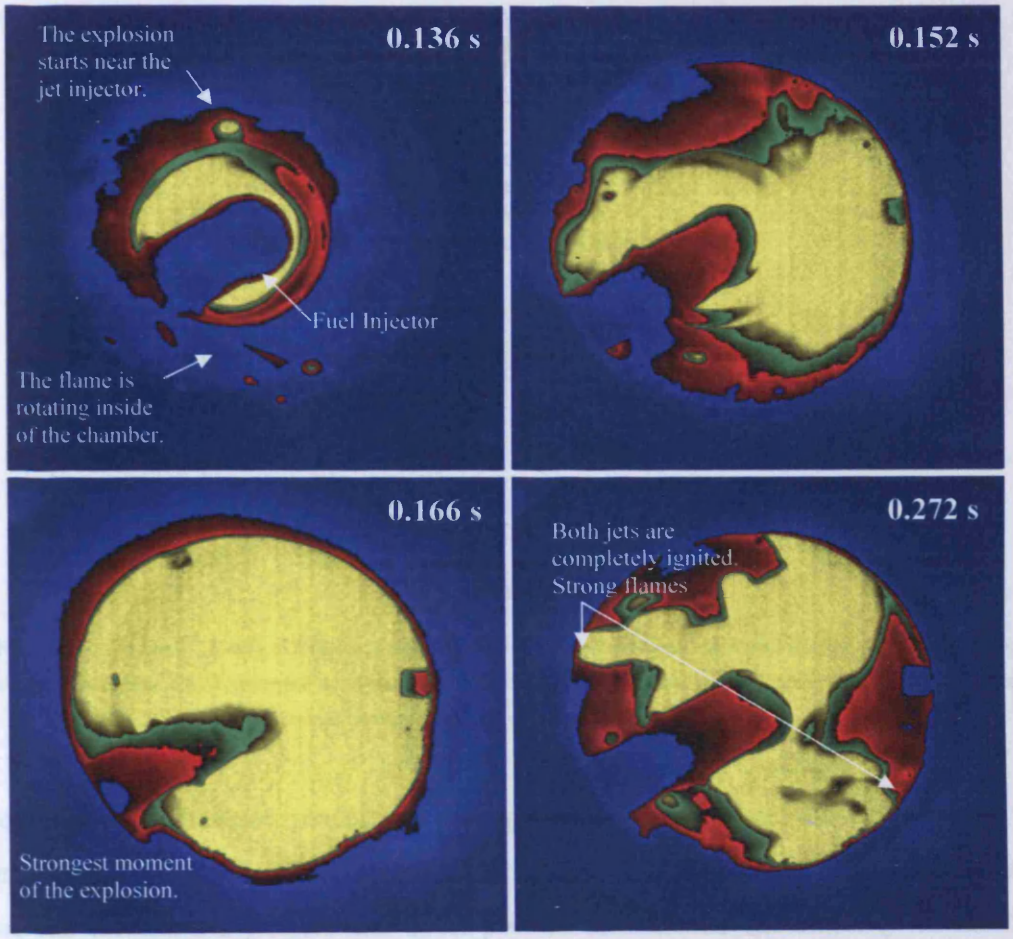

Figure 6.22. The higher gas injection (140 l/min, premixed injection) and higher flowrate (1800 l/min) produced an explosion of less damaging effects than its counterpart with injector. Confined conditions, Figure 5.4a. However, the speed of tangential propagation is considerably higher due to the higher flowrate and thermal input. The equivalence ratio for this experiment was only 0.73. Intensity as in figure 6.13.

Nevertheless, the flame never entirely fills the chamber, contrary to the case with injector. It has to be noted that the equivalence ratios are still very different, a probable cause for the more violent explosion inside of the chamber with injector.

Experiments with the injector at higher gas rates were also performed. The results were similar to those observed with the unconfined case, figure 6.23. It seems that the peak value for the flashback resistance is practically the same, and the reattaching of the flame to the burner was also observed. Although it was impossible to see the lifting of the flame inside of the combustion chamber, the phenomenon is likely to repeat. Thus, it can be confirmed that in this case the suppression of the CIVB by

means of a bluff central body -wide injector- is increasing the flashback resistance considerably, and the latter is only produced as a consequence of boundary layer propagation and turbulent flame speed. Numerical simulations (Valera-Medina et al., 2009) have confirmed the lack of this structure, corroborating these results.

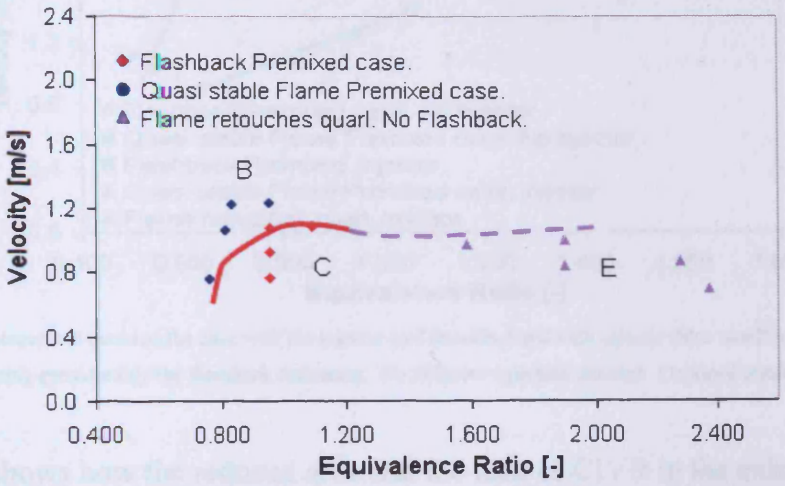

Figure 6.23. Confined Cylindrical Exhaust, Open condition. Quarl nozzle constriction with injector. Similar plot to the unconfined case, Figure 6.11, using the quarl constriction with injector. Due to the lack of lifted results, the dotted line only resembles the limit obtained under unconfined conditions.

Other experiments were performed using diffusive injection. However, as it was observed previously, the flame only reattaches to the burner at high equivalence ratios. Thus, the diffusive injection has been proved to increase the stability of the final flame. Thus stable premixed flames can be produced with anchoring via small quantities of diffusive gas. Thus, lower diffusive fuel flow rates need to be analyzed in future experiments for a proper understanding of the phenomenon.

6.2.3.2. Flashback with No Nozzle Constriction.

First experiments were performed using a No Injector configuration, with entirely premixed injection, figure 6.1. The results showed a steeper trend to that observed in the case with the quarl with no injector, figure 6.24, compare to figure 6.9.

However, when the injector was used the system regained a considerable resistance to the flashback effect, with a smaller slope trend, as observed in figure 6.24. A

reattachment effect to the quarl was also observed using the injector, a phenomenon already associated with the incoming air-gas flow rate and the weakened CRZ.

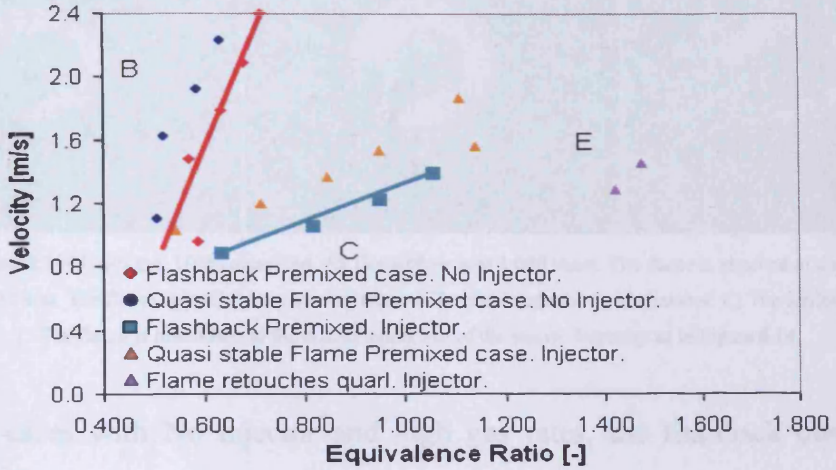

Figure 6.24. Comparison between the case with No injector (red trendline) and with injector (blue trendline). The case with injector is increasing considerably the flashback resistance. No diffusive injection attained. Confined conditions, Figure 5.4a.

This effect shows how the reduced area and the lack of CIVB in the exhaust sleeve of the rig are improving the final resistance to Type 2 flashback. Although it seems that the case with the quarl is even better with a lower peak velocity, the suppression of this central vortex core structure located along the sleeve centreline has left a low velocity boundary layer with flame propagation governed by turbulent speed propagation. At low air flowrates boundary layer propagation is the leading mechanism of flashback. However, if the air-gas flow rate is high enough to overcome the propagation in the boundary layers of the sleeve and injector, flashback will not occur and the flame will be pushed up to the nozzle, with a phenomenon of reattachment to the lip of the burner. This was corroborated using the HSP, figure 6.25. Here is shown how the flame propagates downwards at certain flowrates, and then starts to move back to the nozzle at lower Re. This phenomenon was observed in swirling experiments by Kronner et al. (2007), but the experiments were performed looking at the quenching of the CIVB caused by an excessive entrance of cold air in the system, allowing the flame to recover into the combustion chamber. Nevertheless, the present experiments lack the presence of this structure, leaving the boundary propagation as being responsible for the upstream propagation of the flame. It is recognised that the case with the quarl and No injector could be affected by the quenching of the CIVB at the narrowest part of the nozzle constriction. However, this is a parameter that needs further analysis via PIV or numerical simulation.

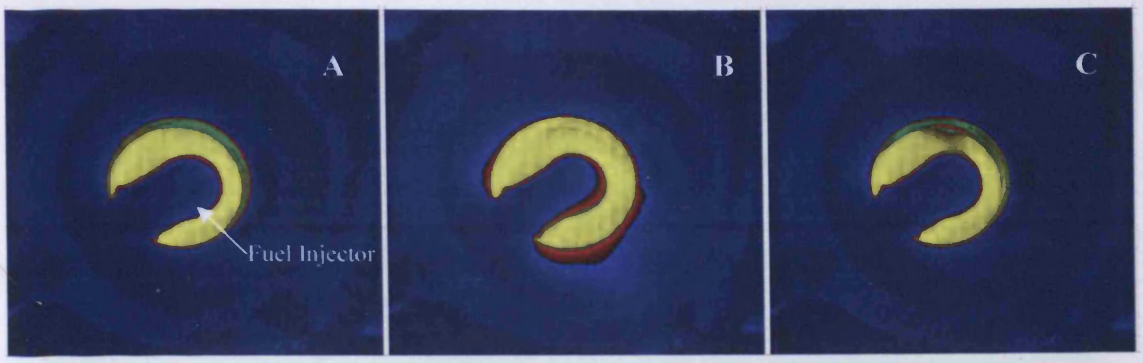

Figure 6.25. Case at 100 l/min gas, 100% premixed. A) The airflow is at 1,000 l/min. The flame is attached to the nozzle. B) The airflow is at 900 l/min. The flame is inside of the sleeve, close to flashback into the swirl chamber. C) The airflow is at 800 l/min. The flame is reattached to the nozzle again, out of the sleeve. Intensity as in Figure 6.14.

For those cases with No injector and high gas rates, the flashback observed was similar to the cases with the quarl and No injector, figure 6.26. The flame moves along the sleeve, and tangentially-radially flashes into the swirl chamber. The primary flame collapses and propagates into the entire volume, igniting a couple of seconds latter both tangential inlet jets. These cases also show how the flame moves faster into the chamber due to the increased flow rate. The time of ignition of the jets is longer with flames that are weaker and pulsating. This phenomenon is doubtless related to the turbulent flame speed.

When the injector was re-placed, apart from the higher resistance to flashback, an increase in equivalence ratio caused a similar explosion in the swirl chamber, figure 6.27. This is related to the increased equivalence ratio, the reduce relief vent area and altered flow dynamics produced by this geometry, as was observed with the quarl. Therefore, it is not the quarl but the injector (bluff body) that is responsible for the stronger explosion of the mixture in the chamber. The quarl seems beneficial for reduction of the Type 1 and 2 flashback propagation, with no major contribution to the negative effects of the explosion produced by the parameters dependent on the injector used.

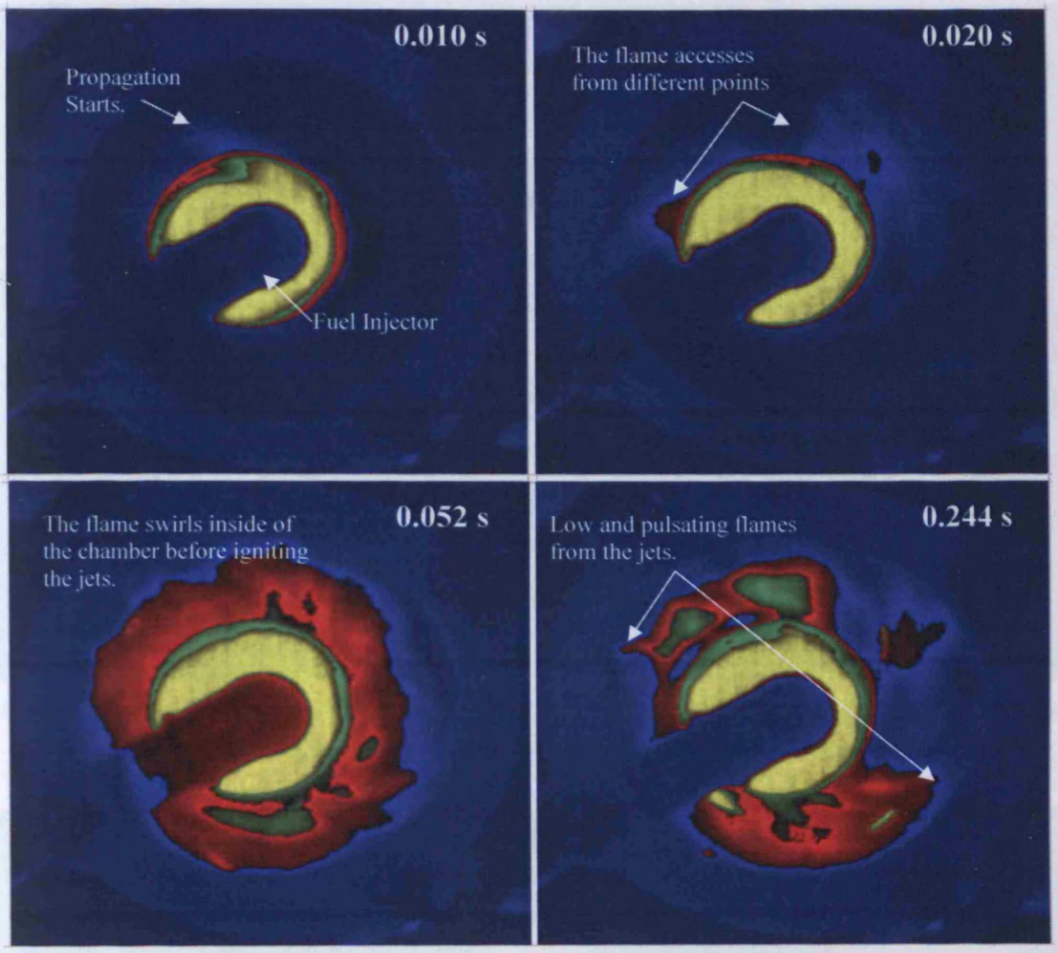

Figure 6.26. Flashback under Confined Open Exhaust, Figure 5.4a, No Nozzle Constriction and No Injector. Quartz positioned at baseplate. 100% premixed, $\varphi \sim 0.74$. The time measured from the first sign of flashback. Intensity as in Figure 6.14. Flowrate 1800 l/min.

Finally, experiments were performed using some diffusive fuel injection with the injector in place. The system showed Type 2 flashback at very rich conditions when the airflow and the gas flow were relatively low (500 l/min air, 25-40 l/min gas). The turbulent velocity of flashback propagation remains almost the same. When the flow and gas values were increased, only the reattachment phenomenon was observed. There seems to be a balance between the turbulent flame speed and the air-gas flow speed when the flame stops propagating down and reaches its lowest position along the sleeve. Higher or lower flowrate values will only move the flame upwards, primarily by the increased flow velocity or by the changed turbulent flame speed caused by fundamental flow changes such as vortex breakdown. The Type 2 flashback observed with the injector and high equivalence ratios occurred as a explosion in the swirl chamber, figure 6.28.

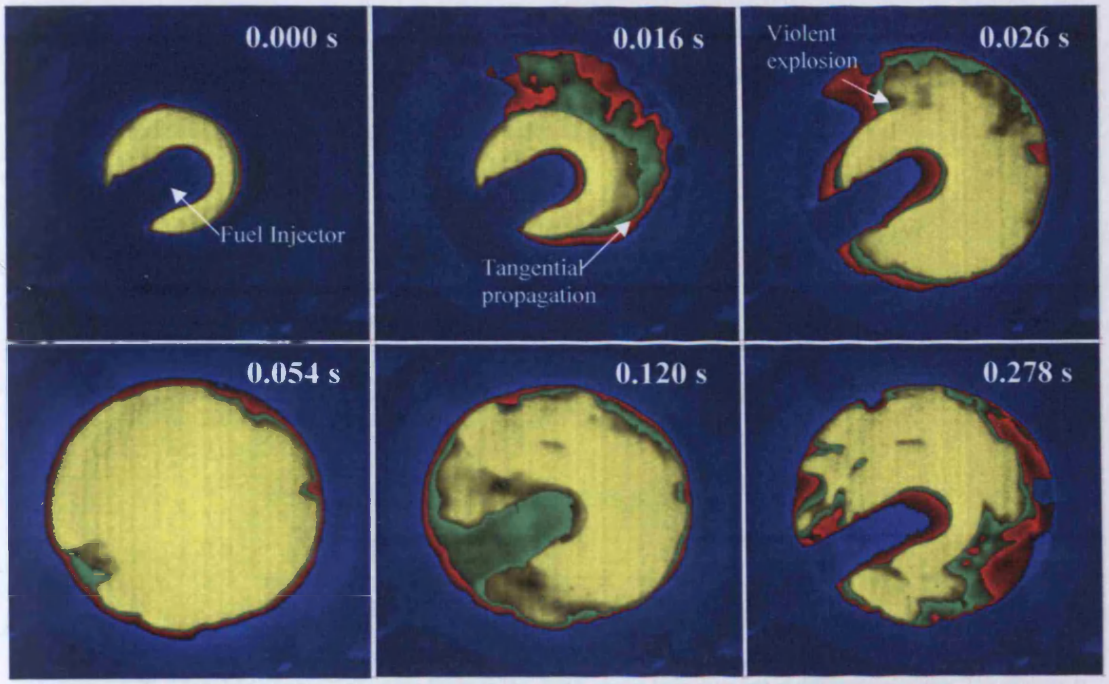

Figure 6.27. Bottom view with the geometry with injector and No Constriction. Flow injection of 900 l/min, 0-100 l/min gas (100% Premixed injection, φ ~ 1.06). The explosion is as intense as with the quarl. The intensity scale as in Figure 6.14.

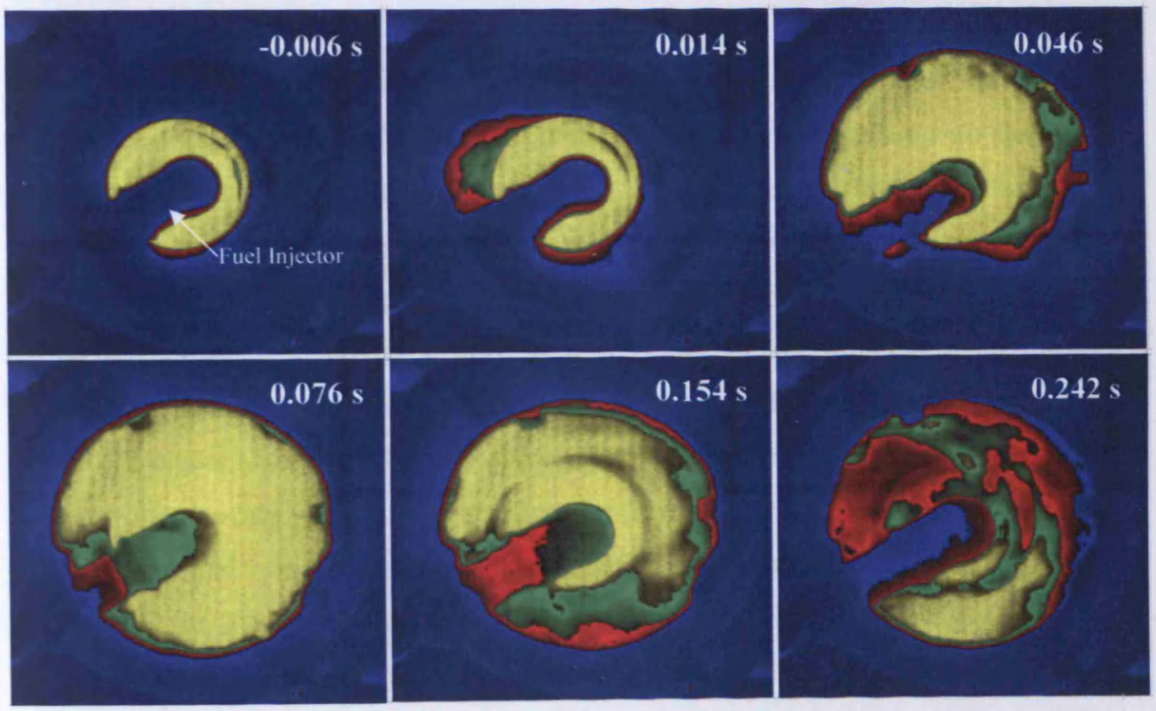

Figure 6.28. Bottom view with the geometry with injector and No Constriction. Flow injection of 500 l/min, 25-40 l/mi gas (100% Premixed injection, φ ~ 1.24). The explosion is as intense as with the quarl and the open case without diffusive injection. The intensity scale as in Figure 6.14.

Another interesting phenomenon observed was the balance point for the lowest location of the flame in the exhaust sleeve of the burner, figure 6.29, lying in the equivalence ratio range $1.15<\varphi<1.25$, irrespective of velocity or effectively air

flowrate. Different flowrates were used with different gas rates, and the minimum position of the flame was always reached within this range. The flame usually reached a position of 10-20 mm above the edge of the sleeve.

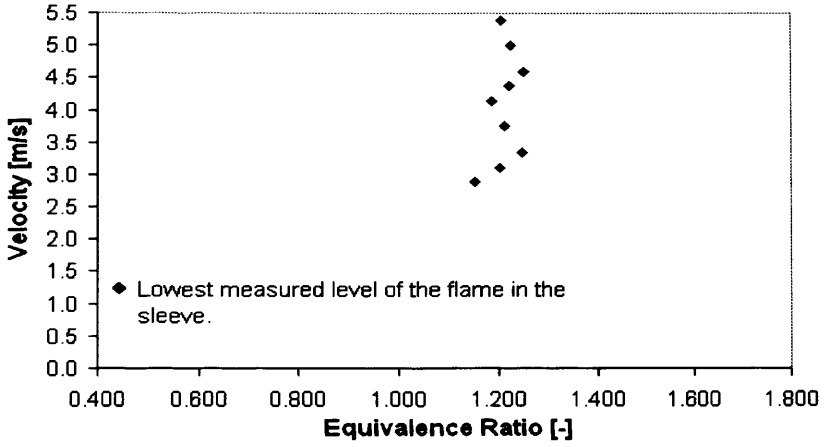

Figure 6.29. The minimum position of the flame in the sleeve seems to be constant at different velocities. The velocity is measured with the transversal area of the sleeve (80 mm nozzle diameter and 25.4 mm diameter diffusive injector).

6.3. Summary

Two types of flashback occur; that due to the backwards propagation of the CRZ to the rig baseplate, Type 1 flashback, and that due to radial propagation into the outer swirl chamber from the exhaust sleeve, Type 2. Diffusive fuel injection eliminates Type 2 flashback as to be expected but not Type 1 where certain conditions allow CRZs to form which can extend over the fuel injector, a problem well known Industrially. Type 2 flashback occurs as a consequence of turbulent flame speed, boundary layer flame propagation and Combustion Induced Vortex Breakdown (CIVB). Tangential and radial propagation of the flame to the walls of the swirl chamber often occurs with entirely premixed injection with an asymmetric movement of the flame and with a tangential radial velocity of propagation being a direct function of the Re, temperature and equivalence ratio. Radial flame propagation velocity remains the same at a great variety of conditions and geometries, ~1.9 m/s. There are strikingly different effects when a central fuel injector is present as the often large vortical structures formed in the middle of the flow significantly change the ways in which the flame starts to propagate outwards as it flashes back.

The use of a quarl nozzle constriction helped to increase the resistance to flashback at high Re, Type 1 propagation, pushing up the flame and avoiding any contact with the hardware. Negative effects appear under Confined conditions as a consequence of the increase strength of the CRZ formed at the tip of the injector, reducing the resistance at low Re, Type 2 propagation. It was demonstrated that the quarl improves the resistance for both types of propagation, whilst the presence of the injector gives a stronger Type 2 flashback. The use of an injector (bluff body) increases considerably the resistance in both open and constricted cases, with better response using the quarl constriction. Unconfined and confined cases showed the same trend using this injector; numerical analysis (Valera-Medina, et al., 2009) gave the same trends as the experimental result for the entire suppression of the CIVB, hence leaving Type 2 flashback only dependent on the turbulent flame speed and boundary layer propagation.

Due to the increased pressure inside of the swirl chamber, the reduced flow rate and the augmentation of the equivalence ratio, the cases with an injector, but no diffusive fuel, showed a violent explosion, whilst the cases with no injector showed a smoother transition to flashback. A combination of increased equivalence ratio, combustion temperature and changed turbulence parameters are probably responsible for the phenomenon. The flame tends to impinge on the fuel injector tip at certain air flow and gas flow rates, showing a balance between velocities where the flame reaches its minimum position along the sleeve of the rig.

CHAPTER 7

DISCUSSION

7. DISCUSSION

"Scientific principles and laws do not lie on the surface of nature. They are hidden, and must be wrested from nature by an active and elaborate technique of inquiry."

John Dewey, Western Philosopher (1859-1952)

After series of experiments, it was confirmed that the Precessing Vortex Core and the Central Recirculation Zone co-exist under a great variety of conditions. Phase Locked PIV, Hot Wire Anemometry and High Speed Photography demonstrated that under several conditions the system not only co-exists, but there is also a great correlation between structures that define the entire flow field.

7.1. Isothermal Conditions

The shape of the CRZ was found to be highly dependent on the Re since the radial pressure is altered due to the increased flowrate and non-linearities in the associated pressure field. Higher Re reduce the length of the Recirculation Zone, compressing and pushing it down into the rig. This has an important effect under combustion conditions. This is in agreement with the theory of the appearance of the CRZ (Syred, 2006) as a phenomenon caused by the decay in radial pressure gradients, which in turn cause reverse centreline axial pressure gradients, thus forming the CRZ.

Close to the point of Vortex Breakdown, the CRZ wobbles with unstable behaviour and the formation of a very weak PVC whose traces were difficult to locate. However, higher swirl numbers allowed the formation of a stronger structure. Thus, it seems that the wobbling nature of the Vortex Breakdown (VB) has created an intermittent PVC whose energy exchange with the VB has been decreased by its unstable nature. Since the Vortex Breakdown is often not coherent, the levels of energy dissipation to the exterior are greater than those observed in more coherent structures. The appearance of vortical structures and wrinkled shapes of the latter confirm this. Therefore, the energy exchange with the PVC in the upper part of the structure is very weak, not allowing the strong interactions observed with other cases. On the other hand, the coherent shape of both the PVC and the CRZ increases as a consequence of

the increased swirl and Re. Therefore, it is the CRZ that influences the coherent formation of the PVC with a very well defined shape in the upper region of the flow field.

Nevertheless, the CRZ does not seem to influence the first part of the PVC at the rig nozzle. If figures 4.11 to 4.14 are meticulously studied, the first 10 planes denote a very strong structure, whose shape will be defined by the following planes and shape of the CRZ. All the vortex cores are very well defined near to the rig nozzle, with a similar initial twist or helical shape between all of the cases no matter the case studied. Thus, it is clear that the PVC is independent from the CRZ for the first planes where it twists, losing strength as the flow progresses, and finally being defined by the energy exchange between it and the Central Recirculation Zone. The system proves to be a combination of Strong PVC-Weak CRZ in the first planes, followed by a Weak PVC-Strong CRZ. Momentum exchange between structures may occur during the entire process, as observed in the planes where the high level of variance between bodies suggests a high exchange in energy probably aiding to the preservation of the CRZ-PVC system, figure 4.35.

The interrelation between structures has also been confirmed for intermediate sections due to the formation of a canal on the side of the CRZ created by the movement and interaction with the PVC, which spirals for 70-90 degrees up to 0.6D from the nozzle. The results show clearly the movement of the structure along this path with high correlation between axial sections. Afterwards, the Vortex Core reattaches to another vortex which seems to form inside of the CRZ, a secondary structure previously observed by other authors with the use of filtration techniques (Cala et al., 2006). The new structure then passes downstream as an enlarged, decaying, wobbling central vortex core. The lack of direct interaction between structures at this position is also a proof of the weak momentum exchange that drives the coherence of the PVC in this region.

Thus, it is confirmed that this swirl burner creates a semi-helical PVC under isothermal conditions, produced as a consequence of energy exchange between structures. Even when the PVC is well defined and strong, it still follows a helical

shape defined by the CRZ just passed the rig nozzle. Both structures are caused by the sudden expansion of flow as it leaves the rig nozzle and the consequent pressure gradients generated.

When the system was confined, the appearance of a secondary recirculation zone (CRZ2) was evident. Doubtless this new body forms as a consequence of the reduced rate of decay of tangential velocity arising from the use of the confinement. Pressure inside of the system plays an important role in the deformation of the body, and the movement of flow into the reduced pressure region enhances the formation of secondary recirculatory bodies. However, it is the presence of the PVC that allows the recognition and partition of this new structure from the main recirculatory body. Both entities share a common section where they join again, but due to the vortex core the new body appears very well defined, and with the circular confinement, as an extremely strong region. With mixing reactors this configuration could prove to be of benefit due to the high levels of recirculation occurring next to the exhaust nozzle. However, the appearance of an anchored vortex with the conical and sudden exhausts can lead to a second vortex breakdown and formation of another system (Fick, 1998). The shape change of the main recirculation zone CRZ1 proved to be a consequence of the confinement used, which directly affects the internal pressure of the system and its changed decay rates. The conical exhaust results showed the presence of CRZ2 with a toroidal shape. This time the attachment between recirculatory structures was weaker and only a mild region of interaction occurred with CRZ1. CRZ2 was suppressed considerably and the shape of CRZ1 was more homogeneous. The PVC is of a similar size and extent to that of the square confinement case in the lowest regions of the flow near the burner exit. A corner recirculation zone (ERZ) appeared as a consequence of the expansion of the shear flow from the burner passing into the confinement in all cases. This has not been extensively quantified in this project.

It was proved that the PVC can be considerably distorted and suppressed by changes to the exhaust nozzle of the confinement. Studies using the circular confinement with a sudden exhaust under isothermal conditions demonstrated that the axisymmetric geometry of the confinement creates an anchored vortical structure extending back to the end of and through the recirculation zone, then precessing and forming the PVC

passing into and through the rig nozzle finally. Despite the substantially increased pressure loss caused by the sudden exhaust constriction to the confinement, the amplitude of the PVC has been suppressed considerably with no high Harmonics in the FFT study of this configuration. As previously, the pressure and flow movement affect the final shape of the field, an effect also illustrated by other work (Dawson, 2005; Fick, 1998), which showed that with a swirl burner furnace arrangement the crescent shaped region of high velocity in the shear flow leaving the swirl burner was smeared circumferentially, thus clearly altering the signal received from the PVC, especially the amplitude.

Focusing on combustors, the usage of better mixing technologies can provide confidence in the usage of alternative fuels since the reactants are well stirred, reducing instabilities caused by pockets of fuel. Moreover, the control of the CRZ can be achieved with the combined use of confinement, exhaust constrictions and mode of flow injection. Other authors (Mongia et al., 2007) have presented work about reduced NOx observed in counter-rotating multi swirl equipments. The importance of the isothermal work is that it shows for the first time:

- In detail the interaction of the PVC and CRZ for freely expanding flows. Here the PVC appears to decay rapidly after about 1 diameter, with some indications of return to a very weak central vortex core;
- The presence of at least 2 completely separate CRZs which may or may not mutually interact, when the exhaust flow from the swirl burner is confined (confinement ratio 2 here). The central vortex core then normally exists with high swirl beyond the vortex breakdown, leaving the rig nozzle often with some precession, then mutually interacting with the CRZ(s) before stabilizing and forming a central stabilized anchored vortex.

Although these structures will obviously be modified by combustion, where the main effect will be the reduction of the swirl number due to increased axial flux of axial momentum. The structures (CRZs and PVC) are likely to stay similar giving valuable insight into the combustion conditions which are much more difficult to quantify in detail as discussed in Chapter 5 in the context of using phase locked PIV to create

three dimensional representations of CRZs. Different techniques and faster equipment are recommended for better resolution and demonstration of the previous hypothesis.

7.2. Combustion Conditions.

7.2.1. Coherence between structures.

During combustion, one of the most important effects arising with premixed and partially premixed injection is the appearance of the PVC at high equivalence ratios. The presence of the structure was confirmed using High Speed Photography. However, it was found that only fuel rich combustion using asymmetric configurations showed traces of the structure. It is possible that the PVC is still in the system, especially in the isothermal region prior to the flame. Nevertheless, experiments carried out using configurations with weaker equivalence ratios did not show visible traces of the body, with only some harmonics associated to the periodic movement of the high momentum crescent shape structure (which still existed). The latter probably appears immersed in the PVC-High Momentum Region system as observed at high equivalence ratios in this work and by other authors (Dawson, 2000; Syred, 2006). Unfortunately, this was impossible to confirm with the current equipment and lack of internal access to the rig.

It was found that the presence of large coherent structures, especially the three dimensional CRZs and the region of high momentum will considerably affect the Damkohler, Karlovitz and turbulent Reynolds numbers, hence turbulent flame speed in regions where flame stabilization occurs, as well as initial flame location relative to the rig nozzle. Due to the large velocity fluctuation caused by the presence of coherent structures, the CRZ boundary acts as a point of high heat and mass transfer, especially towards the base of the structure where the PVC interaction is expected to be stronger. Moreover, the wobbling nature of some recirculatory zones under elevated equivalence ratios and low Re produce traces of inconsistent/intermittent bodies whose interaction with the field may cause irregular pockets of fuel and air to form, with the associated unbalanced level of heat production and velocity fluctuations.

Therefore, the propensity to excite combustion driven oscillations via the Rayleigh criterion is high. Unfortunately, these flows are well known to cause combustion driven oscillations that can couple with the natural frequencies of some devices in the combustion system. Examination of the periodic signals of such oscillations can allow the proper recognition of damaging harmonics which can be altered or suppressed by passive or/and active mechanisms. The PVC can be a body whose high coherence permits a localized interaction with the frame of the burner, hitting walls and buff bodies in its periodic movement.

Experiments with combustion showed the existence of the PVC with a well defined shape at high equivalence ratios and low Re. There are cases that show the existence of two internal vortices or double PVCs, a phenomenon studied before by other authors (Syred, 2006; Cala et al., 2007) but with clear visualization obtained during this project. This seems to be caused by centrifugal forces created as the mass of the precessing vortex core increases and can not be maintained stable by the precessing motion of the structure, bifurcating and producing a vortical body of similar length and strength. Contrary to models that only characterize the field as a single PVC system, the existence of this double system confirms that the PVC keeps its energy as a consequence of its interaction with the CRZ, which under these high equivalence ratio-low Re conditions has not entirely formed yet. Thus, the precessing energy of the body is weak enough to impede a better coherence of the vortex, allowing its bifurcation as a consequence of external forces. According to Aleseenko et al. (1999), the PVC remains coherent as a consequence of internal forces that due to the precessing motion try to compact the vortical structure, and when the vortex is compressed enough the system will try to expand to regain balance. This seems to be correct with the inclusion that this precessing movement is obtained from the interaction of the PVC with the CRZ. Due to the repetition rate of the laser used and the shape of the swirl burner, the results did not show the formation of the PVC. Nevertheless, since the vortex appears to readily attach to other vortical structures, the suppositions of other authors (Lieuwen and Yang, 2005) seem to be confirmed as they present a paper where the numerical analysis concludes that the former is comprised by smaller vortices which find each other during the swirl flow process, merging into a strong structure that will create the PVC.

Another important point is that the PVC structure was only visualized under fuel rich conditions with a yellow flame on the PVC boundary. However in the weaker equivalence ratio systems with blue flames the PVC could not be easily visualized. Other experiments denoted the existence of the vortex core with bifurcations which spiraled around the principal body. This is probably the system that modellers have followed, as the secondary vortex is extremely weak compared to the main PVC. Therefore, the new structure is caught in the precessing movement of the latter, and following the tangential movement of the swirling flow appears as a spiraling body which completes more than two cycles around the strongest structure, normally the CRZ.

Another important structure is the High Momentum Crescent Shape region, capable of producing the low-frequency modes, known to produce "combustor" instabilities (Yuang and Yang, 2004). This region lies next to the PVC and arises from the PVC squeezing the flow leaving the rig nozzle, thus often confirming its existence upstream of the flame. This must also affect the size, shape and the length of the CRZ and hence the PVC in the correlation between bodies. The PVC has a well known susceptibility to small perturbations (Syred et al., 1984) which can cause large scale instabilities to develop. This is possibly the initial mechanism of excitation and arises from natural PVC fluctuations which couples through into the CRZ. The position of flame stabilization, dependent on the CRZ, will then naturally follow this movement. When the oscillation of the CRZ occurs, any natural frequency of the system can then act to further excite this process and lead to increased oscillatory behaviour. Dawson et al. (2005) showed that for a geometrically similar swirl burner with attached circular furnace and conical exhaust a 250Hz oscillation could be generated with partially premixed natural gas combustion. Phase locked Laser Doppler Anemometry measurements showed that the oscillation was causing a sinusoidal variation in flow into the burner, thus giving a large variation in swirl number, correspondingly the strength of the CRZ varied considerably over the limit cycle, reflecting the variation in swirl number. Other authors (Schildmacher et al., 2002) have also performed experiment work observing this oscillatory behaviour at 250 Hz.

These coherent structures were initially created because of stable burning swirling flow, forming a flame located in the shear flow. Natural fluctuations in the shape and location of the CRZ due to the PVC cause variations in heat release (both extent and position) which can then couple with an axial acoustic (i.e.Helmholtz) oscillation. The CRZ (1 and 2) as well as the PVC respond to this coupling, the change in swirl number not only alters the size and shape of the CRZs but also that of the PVC, accentuating the effect further. The PVC may well disappear if the swirl Numbers drops to 0.2 as indicated by Schildmacher et al. (2002).

Experiments were performed using a great variety of equivalence ratios. The utilization of diffusive-premixed mixtures allowed the recognition of different patterns and shapes of the coherent structures. Although it was impossible to visualize the PVC with this study which was performed using the 25-25 configuration, (the most stable of all of the configurations analyzed) the existence of a strong periodic structure was measured and quantified via FFT analysis (essentially the crescent shaped region of high momentum flux).

First analyses focused on defining the combustion conditions and stability of the system based on the shape and strength of the flame. It was recognized that the use of diffusive injection changed the stability of the system considerably, especially if it was run under a diffusive-premixed condition. Cases when only diffusive injection was used showed higher pressure fluctuations, which according to the Raleigh criterion could be amplified as a consequence of the variable heat release and flow velocity. This behaviour was a direct function of diffusive fuel injection flow rate. The more gas diffusively injected, the higher the pressure variations registered. This arises because extra momentum is being injected on the centre line and is interacting with the radial and axial pressure gradients generated by the swirling flow and can for instance cause the CRZ to oscillate axially (Dawson et al 2005). With premixed combustion the pressure fluctuations observed are high but similar to those at lower diffusive injection rates, Lieuwen and Yang (2005). However, the pressure fluctuation is not linear and shows polynomial characteristics, suggesting the presence of non-linearities in the combustion processes, including flame location and anchorage. Due to the lack of diffusive gas, the flame tends to move upwards,

influenced by the presence and shape of coherent structures. These may be strong enough to fix the flame to the rig nozzle if high Re are used. However, if these are weak flashback can occur at relatively high flow rates. On the other hand, if these are high enough the flame is pushed up until blow off occurs. Therefore, the flame suffers of a certain degree of unsteadiness without diffusive injection, which helps anchoring the flame to the injector (if any) or baseplate of the rig. Thus, it is recognized that the use of a small quantity of diffusive gas is essential for the stability of premixed systems in order to anchor the flame and avoid lifting by feeding active radicals into the CRZ. Also, the results with only one premixing inlet clearly showed greater irregularity and the importance of proper, symmetric premixing. Because flames tended to develop inside of the burner without the fuel injector, three extended fuel injectors were used to try to push the flame past the burner exhaust. This also allowed identification of the positions of the different coherent structures that interact in the system and the effects of these diffusive injectors.

Maps for each condition were developed in order to recognize regions of stability. Four regions were noticed, with the first region being of high instability with flashback into the rig. Although the rest of the regions were defined on each map by the swirl number used, this region of instability was always constant for the same type of injector, independent of the swirl number. The regions of quasi-stability, stability and flame compression, respectively, depended on the type of confinement used, which as observed during the isothermal experiments is capable of enlarging or shortening the CRZ, which dictates the flow stability of the flow field. If the air flow rate is low and vortex breakdown has not occurred, the flame is wrinkled and is yellow in colour, being columnar in nature, the yellow colour being caused by reduced momentum exchange on the boundary (Beer and Chigier, 1972). On the other hand, if the flowrate is high enough with elevated Re, the CRZ forms after vortex breakdown and the flame changes completely in nature, widening and in the limit becoming blue. It was found that the best scenario for these flames is located at the point where a stable, conical flame forms (region C). Systems with air flowrates between 1,400 to 1,600 l/min give results similar to others (Fick, 1998; Syred, 2006).

The length of the flame was also analyzed in order to study the effect of various geometries, looking for the fuel injector that reached these stable conditions faster with a stable flame. Trials with a Narrow injector demonstrated that the flame reached this point of equilibrium slower than with a Wide or a Perforated injector. The slope of the curves decays slower due to the high levels of kinetic energy injected into the system as a consequence of the low outlet area of the injector. The gas leaves the latter with enough energy to push the flame further downstream than its counterparts. Moreover, it was found in the system that the increased length of the flame is also caused by the forced injection of gas into the recirculation zone at higher Re, the gas expanding the CRZ.

On the other hand, the Wide injector produced long columnar flames only at low Re before vortex breakdown and the formation of a CRZ. However, at higher Re around 20,000 (flowrates around 1,200 l/min) the system quickly reaches its stable length, hence increasing the stability of the system. This high stability was found for all cases run with the Perforated injector, as the diffusive injection anchors the flame whilst the distributed fuel mixes better than the other cases.

The analysis using different swirl numbers showed that the cases with symmetric swirl are more stable than those with asymmetric configurations. Although the point of high efficiency is reached faster, this point appears in a very narrow range, since the flame immediately enters in a region of compression (region D). This again suggests that a moderate, symmetric swirl is the best manner of achieving high burning efficiencies useful for Gas Turbine Combustors. This is also corroborated by a relative pressure analysis which shows that the pressure of the system is kept low when symmetry exists. This is also in accordance with the previous assertions about fuel pockets, which are also created by the unmixidness caused by the different level of injection and velocity in each inlet.

Further analysis showed the existence of lifted flames whose stability was doubtless achieved by their interaction with coherent structures. This was put to the test using Particle Image Velocimetry, and it was found that it was only the Central Recirculation Zone which was stabilizing the lifted flames. This was expected, since

External Recirculation Zones (ERZ) were not expected as a consequence of the lack of confinement. Confinement may create secondary recirculatory regions that would increase the stability of the flame in the same manner as Corner Eddies (ERZ) anchor the flames in other experiments (Lieuwen and Yang, 2005).

Similar experiments using PIV showed that the coherent structures were created using the Perforated injector. However, it was not only a phenomenon produced by the swirl, but recirculation arising from the bluff body effect of the injector. Higher airflow rates for the same equivalence ratio produced much more intense flames. The Wide injector was demonstrated to be a reliable mode of injection, producing a recirculation zone with similar strength over a wide range of flowrates. It is also evident that the recirculation zone is suffering an expansion downstream, confirmed by the long blue flame tail on top of the structure. When compared to the case with the perforated injector, this behaviour is less pronounced. The CRZ readjusts itself (often changing shape) to balance with the negative pressure gradients generated by the expanding swirling flow (and any bluff body effects), also being affected by the shear flow influences on its outer boundaries, especially in terms of turbulent exchange and flame stabilization capability. The CRZ may move axially in accord with changes in swirl number, burner exhaust geometry, level of confinement, equivalence ratio etc.

Diffusive fuel injection with the narrow injector also produced a blue flame tail. Combustion of this gas in the CRZ appears to expand the body from the inside; this may go too far and increase recirculation to such an extent that cool products are recirculated, reducing combustion efficiency, an effect observed during the experiments.

Therefore, it can be said that the CRZ is an entity that can be altered via geometrical changes and that behaves like a bubble, being an active structure with the ability to be distorted according to the pressure and flow situations inside and outside of it. This structure is not stable unless the conditions are well developed with an asymmetric field that has been well investigated as to its propensity to excite natural modes of oscillation. Some diffusive fuel injection is essential for the proper anchoring of the

flame. Nevertheless, the mode of injection is crucial for the stability of the flame, with the perforated injection being the most efficient due to the better mixing. The Wide injector gave also traces of good stability at moderate flow rates, although it was noticed by the shape, colour and CRZ in the system that the perforated injection was even better for the burning process in gas turbine combustors.

The confinement of the flame was also analyzed. This was performed using the Wide injector, since this gave a better variety of flames for the study of instabilities in the combustion system. This injector supplies diffusive fuel entirely axially through a centrally located orifice, in contrast to the perforated injector that inject fuel radially into the inner part of the shear flow as it passes by the injector and around the CRZ.

The results showed that the system tends to produce CRZs at low Re when the burning intensity is low, as observed when entirely diffusive fuel injection was used. For these cases, the CRZ is observed at high equivalence ratios, this being a function of the location of the flame front and main burning zone which are inevitably further downstream than the premixed or partially premixed combustion cases and thus have reduced effect on the CRZ. The strength of the CRZ increases as the air flow is increased, and behavior somewhat similar to the isothermal state was found.

With the addition of premixed gas, a Vortex Breakdown appeared in the velocity maps at low Re and high equivalence ratios. It is recognized that the equivalence ratios for these experiments are almost double those for purely diffusive injection at similar flowrates. As expected if comparison is made between cases at similar equivalence ratios, figures 5.32 and 5.33, the strength of the CRZ in the diffusive fuel injection cases is higher than for the diffusive-premixed scenarios. Even though the flow rate has increased for the latter which may had increased the radial pressure gradients of the system and thus the strength of the CRZ, the structures are actually weaker, as observed by the darker colours in the diffusive cases. Because of the more intense combustion close to the nozzle the flame produces more heat upstream and radiates more energy (as observed in the plastic joints of the rig, which started melting after a couple of minutes running under those conditions), reducing the density of the surrounding air and decreasing the radial pressure gradients necessary

for the appearance of stronger recirculatory flows, showing the higher burning intensity of partially premixed cases.

As the rate of injection of premixed fuel is doubled, the system experiences another change of behaviour. In this case, the flame starts behaving at low Re and high equivalence ratios just like its predecessor at lower premixed fuel injection rates, with no structures in the system at the lowest Re cases. However, at high Re, the strength of the system CRZ reaches its highest levels: this can be observed by the purple dots in the inner area of the CRZ, figure 5.34D. Since the heat input into the system has increased, the field suffers a density reduction produced by the heat release and radiative nature of the flame at low Re, with wrinkled emissive flames. As the flowrate increases, the flame is compressed by the increasing size of the CRZ, caused by increasing pressure gradients. This has been observed by other authors (Kroner et al., 2003; Kiesewetter et al., 2007). Due to the increased energy inside of the structure, active radicals provided via diffusive injection and better burning efficiencies by the premixed injection, the CRZ is considerably stronger than any other case. It is demonstrated with these experiments that the combustion in the system is not solely responsible for the appearance of strong recirculatory coherent structures, but also the application of increased flowrates. These produce strong radial and axial pressure gradients, which combined with the field energy and reactants inside of the structures can aid to the development of stronger recirculatory bodies. Here the non linearity of the response of the pressure field to flow rate increments must be noted. The radial pressure gradients are given approximately by the term (Syred et al., 1984): $\partial P/\partial r = -\rho w^2/r$ (where P is the pressure, r the radius, w the tangential velocity and ρ the density). Thus pressure and pressure gradients do not respond linearly to flowrate changes.

Clearly for future experiments the utilization of PLIF techniques or similar are needed so as to be able to locate the position of the reaction field relative to the velocity field.

The shape of the combustion CRZ was confirmed by 3D analyses, which showed the existence of a lobbed body, as observed by Syred (2006) and Dawson et al. (2005), but in two dimensional planes. The use of conical exhaust constrictions to the

confinement after the burner exhaust also showed a lobbed CRZ similar to the open case. This is as a consequence of the asymmetric flow in the system which creates regions of variable pressure, with the position of the lobbed region opposite to the triggering from the High Momentum Crescent shape region. It was also noted that the conical geometry produced a strong central vortex core after the CRZ which passed through the confinement to the exhaust (anchored vortex); this was previously observed during the isothermal trials. This vortex arises because the confinement reduces the rate of decay of swirling flow. Other work has shown that this vortex can create another vortex breakdown in the confinement exhaust (Syred, 2006). The positioning and configuration of the confinement exhaust outlet can reduce both effects if this is located further from the rig nozzle, as observed by Dawson (2000).

However, the CRZ can cause the flame to propagate upstream, creating what is called a Combustion Induced Vortex Breakdown (CIVB) starting with reattachment to the tip of the fuel injector to Type 1 flashback to the baseplate, followed by Type 2 flashback to the tangential inlets. Thus, the following part of the project was to recognize some of these effects and use passive mechanisms of suppression to try to reduce their damaging properties.

7.2.2. Unstable Effects during Combustion. Flashback.

Different conditions can produce Type 1 and 2 flashback. In essence, four of them are critical to the occurrence of this phenomenon, (i) boundary layer flame propagation, (ii) turbulent flame propagation in core flow and other low velocity flow regions, (iii) combustion instabilities and (iv) upstream flame propagation by means of coherent recirculatory structures.

During the analysis of the coherent structures under combustion it was observed that the flame tends to lift at low Re numbers, followed by Type 2 flashback into the rig. It was also observed that an increase in flowrate could produce another form of flashback or flame reattachment to the tip of the injector, with a soot growth that not only augmented the temperature of the latter, but also stained it and reduced considerably the efficiency of the combustion process with a yellow rich flame. Thus, it was noticed that both conditions could affect the final system efficiency with a

damaging effect to the hardware. Type 2 flashback at low Re was able to propagate into the swirl chamber, and the temperatures reached a point of causing serious damage to the supply hoses which started to melt. On the other hand, the high Re situation showed that the flame was weak and produced an isothermal like behaviour under low gas injection flowrate conditions, with substantial soot growth at the tip of the fuel injector. It was assumed that both phenomena were related to the presence of coherent structures in the system. Although it is recognized that the internal flashback is also propagated by boundary layer flame movement, as will be discussed later, the presence of the Recirculation Zone is increasing the propensity to suffer this problem.

One of the main objectives of this project was to develop ideas to reduce instabilities in the system caused by coherent structures. Due to the high interest of the research community in the usage of alternative fuels for the reduction of CO_2 footprint, it was considered that the analysis could focus on the resistance increment to flashback, a problem observed in current technologies where premixed injection is used with hydrogen enriched fuels (Lamnaouer, 2007; Lenze and Carroni, 2007; OMEGA, 2008). Thus, the interesting case of region A observed in the flame maps of chapter 5, figures 5.13 and 5.14, where flashback does not seem to be highly influenced by the swirl number but by the injector was chosen to be investigated.

Some authors have analyzed the use of passive technologies (Paschereit and Gutmark, 2008; Lacarelle et al., 2009; Thornton et al. 2007) such as a change in the rig nozzle in order to analyze the flashback and increase the efficiency via changing the delay time of the reactants to the burning region. Thornton et al. (2007) talked about an expansion angle of the jet as a momentum balance of the axial and tangential momentums, thus the increase in axial velocity caused a decrease in the expansion angle of the flame. Therefore, different nozzle constrictions were designed for a coherent structure analysis using Particle Image Velocimetry.

The use of different nozzle constrictions agreed with the change in velocity and jet angle proposed by Thornton et al. (2007). The change in velocity not only changed the jet flow, but it also changed the shape and strength of the CRZ, figure 6.7. However, an interesting result was found when an angled quarl was used with the

same outlet diameter as with no nozzle constriction. First tests showed that the flame was pushed upwards due to the increment of velocity, avoiding the flame touching the tip of the injector or reattaching to the burner exhaust. This was also noticed with other configurations where the constriction was over 80% of the main rig nozzle diameter. Different to other cases, the PIV analysis showed a compressed wider CRZ structure than with cylindrical constrictions. Moreover, the flame was considerably more stable at high Re and lean equivalence ratios, with no traces of rich regions or carbonaceous deposits produced by the sooting phenomenon. As shown by Thornton et al., the jet angle changes according to the axial and tangential momentums. When using a cylindrical constriction of 0.80 D, the axial velocity was suddenly increased, whilst the tangential component decayed somewhat, leaving a final flow with more axial momentum and slightly lower swirl number. This reduced the jet angle, increasing the length of the CRZ, elongating its shape upstream and downstream of the nozzle, reattaching to the tip of the injector. Although this only occurs partially, the extra length of the CRZ is sufficient to move the flame upstream and change the heat release distribution. On the other hand, the use of the quarl constriction gave the well known result of a wider CRZ due to the change in axial and radial pressure gradients, beneficially locating the CRZ close to the shear flow and the main reaction zone. This is shown in both by the PIV and imaging of the flame, which show a coherent compressed flame with a spinning top shape. The flame was pushed up aided by the increased flow rate, whilst the coherence and stability of the structure was maintained by the re-balance of axial and tangential momentums, hence pressure gradients. Therefore, the presence of this coherent structure and its location are essential for the avoidance of the flashback at high Re, Type 1.

The analysis of flashback at low Re, Type 2, was also investigated, with several results and configurations showing the importance of coherent structures in flame propagation back into the rig. As mentioned in the last paragraph, the coherence of the CRZ obtained with the quarl was higher. This would cause, as expected, a lower resistance to flashback due to the improved and stronger structure. First experiments with no quarl showed Type 2 flashback occurring around 1.60 m/s radial velocity. When the quarl was used with no injector this rose to 2.0 m/s radial velocity, an increase of 25%. Since the stability of the burning process has improved and the

strength of the CRZ is higher, the propagation of the structure in the system is faster and stronger, with less resistance to the phenomenon.

However, when the wide injector was used the resistance to flashback increased with a radial velocity of 1.2 m/s, an increment of 25% compared to the open case. This is caused by the disappearance of the CRZ in the exhaust sleeve of the burner (CIVB). Numerical simulations gave similar results of the disappearance of the CIVB in this region (Valera-Medina et al., 2009), flashback occurring merely due to the flame propagating with the local turbulent flame velocity in this part of the burner. Figure 7.1 shows one of the simulated conditions where flashback was observed, with no CIVB in the sleeve.

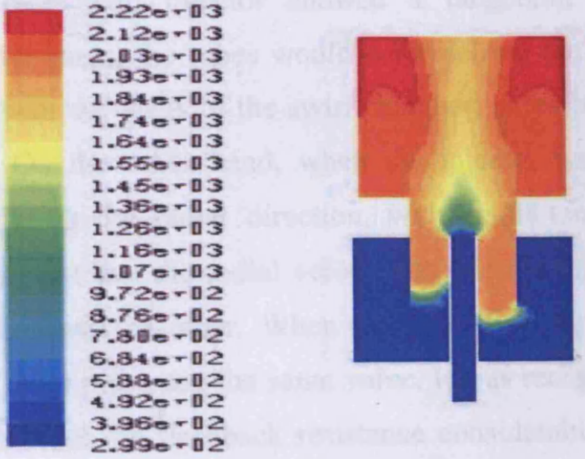

Figure 7.1. Asymmetric flashback in the rig. No CRZ is observed during the phenomenon (Valera-Medina et al., 2009). Colour bar in m/s.

Therefore, the system is suffering of flashback caused by a boundary layer flame propagation and turbulent flame propagation in the tip of the flame front (as observed in the concave shape of both sides of the flame). The disappearance of the CIVB in the system is increasing the resistance of the arrangement to flashback.

When diffusive injection was used, the system showed that the flame tends to anchor, not unexpectedly, past or at the fuel injector with obviously no Type 2 flashback. Although emissions will be higher than with premixed fuel and air, it does establish a region of stability that allows the flame to find a continuous supply of reactants for the combustion process.

During the internal analysis of the Type 2 flashback, it was observed how the cases with no injector showed lower resistance to leaner mixtures. Although the propagation is less aggressive, this could be related to the fact of less fuel in the mixture and the reduced relief vent area. It was found that the system produces a very damaging explosion when using the Wide injector. Since the flashback resistance has increased, the equivalence ratio has also increased and the higher quantities of fuel causes a stronger effect that is also augmented by the reduced area throughout which the pressure wave can escape.

When leaner conditions were analyzed, it was found that the cases with no injector had a primary flame propagation caused by stream tubes in the swirl chamber, which in contrast to case with injector showed a tangential movement over some milliseconds. Afterwards, the tubes would collapse and the remaining flame would reignite the fuel near the walls of the swirl chamber, aided by the still incoming fuel from the inlets. On the other hand, when the injector was used the propagation occurred primarily in the radial direction, with small tangential movement. The mixture ignites so fast that the radial velocity overcomes all the others, propagating through the entire swirl chamber. When the velocities of radial propagation were measured, all of them presented the same value. It was recognised that the use of the injector could increase the flashback resistance considerably, but if this occurs the potential for explosion was greater.

The use of Confined Exhaust conditions showed that the cases with no injector did suffer the presence of the stronger CRZ, which as noted during chapter 4 has increased its recirculatory effect considerably due to an increment in radial and axial pressure gradients. However, when the injector was used, the system regained its high resistance to flashback, a fact that doubtless is related to the suppression of the Combustion Induced Vortex Breakdown by this centred body.

Finally, some parameters that were left for further study are those related to the constant equivalence ratio at which the flame moves upstream when no flashback is observed in the mixing chamber. As stated previously, this may be a phenomenon

caused by the balance between the outgoing flow, the flame burning velocity and the strength of the CRZ.

7.3. Summary

It was found during the entire project that the coherent structures in both cold and hot swirling flows are essential for the stabilization of the system. The correlation between structures is crucial for the proper development of stable or unstable systems. The shapes of the CRZ and PVC seem to be affected by the conditions used, with the visualization of the PVC as a semi-helical body, contrary to previous assertions done by other authors. It seems that the point where both structures meet suffers higher velocity fluctuations, suggesting the high exchange in momentum between the CRZ and PVC.

The usage of different geometries, equivalence ratios, swirling flows and injection parameters showed that the structures behave accordingly to the situation and conditions imposed in the system, thus giving an numerous number of states for the development of any variety of flames. It was demonstrated that the flames can be distorted to a certain degree. Although these changes may interfere with the reduction of emissions, this topic has to be analyzed elsewhere. The equivalence ratio combined with the Re used showed different CRZs which were more coherent at higher fuel injection values. However, these were also less resistant to Type 2 flashback with no fuel injector. On the other hand, high Re showed the impingement of the flame on the diffusive injection system with its inherent growth nucleation and damage of injectors. Thus, two types of flashback were defined.

The flashback analysis showed that geometrical passive constrictions at the nozzle can alter the resistance for natural gas. A quarl design was the most beneficial for minimizing Type 1 and 2 flashback, at high and low Re respectively. The use of an injector at the centre of the system has demonstrated to be beneficial for the increase in resistance, with the negative effect of having a Type 2 flashback at higher equivalence ratios. However, since lean premixed blends are the current trend of fuel injection, this is a minor drawback that can be avoided with higher Re numbers.

CHAPTER 8

CONCLUSIONS

8. CONCLUSIONS

"I was taught that the way of progress was neither swift nor easy."

Marie Curie (1867-1934)

Throughout all this work is has been demonstrated the importance of various coherent structures in the burning system in Swirl Gas Turbine Combustors. The coexistence of these structures and their interaction change the entire field and stability of the combustion process. Therefore, their analysis requires extensive work and experiments in order to understand their characteristics with the aim of being able to control them in the near future. Development of techniques, equipments and design processes will be key factors in the stabilization of the PVC and CRZ to increase the efficiency of future combustors, with the avoidance of damaging effects such as flashback at high and low flowrates and equivalence ratios.

Some of the most interesting points that were found during this project are listed below to give an overview of the final conclusions.

- Previous results on the shape and relationship between structures in tangential swirl burners have been challenged, leading to a clear argument as to their extremely high importance in the stability of swirl combustion systems.
- The PVC-CRZ system co-exists under isothermal conditions, with high coherence of the structures.
- The CRZ is highly dependent on S_g and Re, being compacted at higher Re and thinned at high S_g.
- Low S_g demonstrated the wobbling behaviour of the Vortex Breakdown, appearing as a lifted CRZ structure not always attached to the burner.
- The PVC is a semi-helical structure, rapidly straightening towards the end of the CRZ. Contrary to previous experiments, the body does not behave as a complete helix.
- CRZ and PVC were demonstrated to be very coherent structures. Standard deviation velocity analysis of the boundary of the CRZ showed highest levels in

and around the CRZ base and at the end of the CRZ. This result supports the idea of energy interaction between structures that drives such a coherent field.

- The CRZ appears as a highly 3 dimensional time dependent structure. When confined, the zone is highly asymmetric and rotates with the same frequency as the high momentum crescent shaped velocity region.
- CRZ2 was observed under confined and rapid pressure decay conditions. The system showed strong second and third harmonics. Overall CRZ1 and CRZ2 increased the extent of the recirculation regions.
- Slow pressure decay destroys CRZ2, creating a more compacted recirculation region. Vortex core precession almost disappears as well. This result confirmed the high importance of the pressure in the development and shape of the inner structures in such type of flows.
- The PVC length is suppressed by 30% under slow pressure decay confined condition, (with sudden exhaust outlets to the confinement).
- This work clearly shows that there is considerable interaction between a number of parameters with swirl burners that determine the final characteristics of the flame that is produced by a given system for a given fuel. Indeed this flexibility and adaptability is one of the attractions of swirl burners.
- Under combustion, the level of swirl as defined by the swirl number is of primary importance. For swirl numbers greater than ~ 0.5 a CRZ forms which increases in strength and stability with increasing swirl number and has very desirable flame stabilization characteristics.
- The equivalence ratio, φ, is very important and can strongly interact with swirl to alter the size and strength of CRZs.
- Reynolds numbers effects are also important and can seriously affect smaller systems. The high kinematic viscosity of high temperature gases can affect the vortex breakdown phenomena and the size and shape of CRZs.
- The mode of fuel injection is important, whether premixed or diffusive or partially premixed with contributions from both modes. The configuration of the fuel injectors as well as the configuration of the swirl burner are also important.
- These assertions confirm the complexity of the swirl phenomenon under combustion conditions, making extremely difficult the numerical study of such type of flows, without taking into consideration different fuels which would

considerably increase the level of difficulty. Several different flame types may be produced as shown by flame maps, which are dependent on all these parameters.

- Premixed swirling flames tend to have reduced blow off limits and require some diffusive fuel to stabilize them and widen the blow off limits. This appears to occur because the outer region of initial flame stabilization occurs in the high velocity shear layer. The quantities of diffusive fuel required are generally quite small to alleviate this phenomenon.
- The small amounts of diffusive injection introduce active radicals into the CRZ, anchoring the flame and increasing stability. Not only hot products are necessary in this region if stable conditions are required.
- Coherent structures such as the PVC are well known to occur in these systems, especially with premixed and partially premixed burners. At low Re interesting double PVC structures occur as well as vortex bifurcations of PVCs. The existence of interacting PVCs and CRZs has also been indicated for the combustion state, corroborating other work in the area.
- Although stable PVCs may be produced there is also evidence that the PVC can be transient and intermittent in nature, periodically forming and being extinguished. This has considerable ramifications for the stability of the associated CRZ.
- Confinement has denoted the asymmetric shape of the final CRZ, a problem not observed in numerical results. This is primary caused by the difference in pressure produced by the asymmetric flow. The variance may change the efficiency of the system as specified by the Rayleigh Criterion.
- The CRZ experiences an increase of strength as a consequence of increased flowrate and heat and active chemical species liberation inside of the system. However, the latter can only provide energy to the recirculatory hot products if a CRZ has formed as a consequence of axial and radial pressure gradients. If this does not happen, the system created an elongated, wrinkled flame with no traces of a recirculation Zone. If this does appear, then the heat transfer to the products increases incrementing the strength of the coherent structure with its benefits.
- Two flashback mechanisms were observed: at high Re impinging on the tip of the injector, Type 1, and at low Re with the entire entrance of the flame inside of the swirl chamber, Type 2.

- Passive rig nozzle constrictions to the burner produce flames that do not impinge onto rig nozzle surfaces or extend back to and around the central fuel injector.
- Partial premixing of fuel and air is shown to have significant advantages, as is well known industrially. Velocities at which flashback occurs are characterised and certain rig nozzle configurations are shown to have advantages in reducing the flashback limits from ~1.6 to ~1.2 m/s.
- The quarl constriction with a 0.80D nozzle constriction showed the best improvement in flame stabilization, whilst minimizing flame impingement on the fuel injector. Here the shear flow expands to follow the quarl whilst giving some pressure recovery due to the diffuser effect. The shape of the CRZ was affected, compressing, strengthening and widening the structure to a spinning top shape. For premixed combustion the CRZ was now located much closer to the reacting shear flow giving the significant improvements mentioned above
- Flashback velocities matched well those found experimentally in the other systems. Four different nozzle configurations are studied and advantages found in two of them in minimising partial flashback around the fuel injector.
- Flashback resistance was shown to be dependent on the coherence of the CRZ. When the structure exists with its strongest features and extends down to the burner baseplate, the flashback limit decreases by up to 25%. When the former is eliminated via passive bodies such as fuel injectors, the limit is increased considerably.
- The radial velocity at which Type 2 flashback propagates inside of the swirl chamber remains constant for a great variety of conditions, ~ 2.0 m/s.
- The use of bluff bodies (fuel injectors) gave an increased resistance to Type 1 and 2 flashbacks, with higher equivalence ratios for the propagation of the flame inside of the swirl chamber for Type 2 flashback. However, due to this fact and the increased internal pressure of the system (reduced burner nozzle outlet area), if flashback occurs it is more violent with a considerable reduction of tangential flame movement.
- The use of confinements did change the flashback resistance when no fuel injector was used. However, a similar tendency to the unconfined cases was observed when the injector was re-placed in the burner baseplate. This, in conjunction, with the previous results demonstrates that the flashback resistance has been influenced

by the presence of the CIVB. When the CIVB is stronger (causing Type 1 flashback), Type 2 flashback propagates faster into swirl mixing chamber. However, if the CIVB is suppressed, the propagation will occur as a consequence of boundary layer and turbulent flame speed propagation, which essentially are similar in all the cases and are weaker than when the CIVB is present.

- At leaner conditions, the flame propagation occurs by means of vortical bodies which are located on or near to the central axis and extend to the baseplate. They then collapse inside of the swirl chamber. The remaining flame in the chamber ignites the mixture close to the walls, propagating to the supplying jets (tangential inlets) that ignite the entire chamber. This flashback was quite mild.
- A balance between effects is achieved with certain geometries, certain equivalence ratios and operating conditions, with a flame that does not flashback. Flow velocity, turbulent flame speed and CRZ strength reach a point of equilibrium. If this point is reached low down the exhaust sleeve, the flame will flashback.

8.1. Further Work

As mentioned earlier in the project, the advantages of using swirl flows in gas turbines and furnaces are remarkable. This project is directed at looking at the characteristics of swirl burners in the context of the next generation of fuels. Some of these future fuels contemplate the use of biomass, synthetics (Fischer-Tropsch process), pulverized coal with Carbon Capture and Sequestration (CCS) technologies, enriched hydrogen blends, etc. (OMEGA, 2008; Briones et al., 2009).

However these new fuels produce problems for the gas turbines. The main problems are associated with the change of stability, burning rate and heat capacity of the fuel of concern, which may cause flame speed changes, increase of temperature in mechanical components, increase of NO_x due to higher flame temperatures, increment of noise and stabilities, etc.

For that reason, one of the proposals of this project is to continue with the investigations on Swirling flows in new commissioned equipments in Port Talbot, the Gas Turbine Research Centre, so the structures can be studied with more detail under

pressurized and preheated conditions. Moreover, the system needs to be run with different fuels such as hydrogen-enriched mixtures, CO_2 blended fuels that alter heat transfer, chemical reactions and increases flashback resistance (Valera-Medina et al., 2009). Other fuels included methanol used to reduce NO_x and carbon dioxide emissions, and a range other liquid bio-fuels.

New designs can be tested utilizing passive nozzle constrictions, measuring the advantages of the designs, with modifications in the burner to alter the pressure decay so as to be able to alter the characteristics of the CRZs. Moreover, different methods of generating swirl need to be investigated as this clearly has a considerable effect on the results. Vaned type swirlers are especially favoured in gas turbines owing to their compactness and this is an area needing considerable study. Complete analysis for isothermal and combustion conditions is required as demonstrated by this work.

Another important issue to be consider is the usage of other methods of visualization, such as Planar Laser Induced Fluorescence (PLIF), which various authors (Venkataraman et al. 1999; Hubschmid et al., 2008; Schneiders et al., 2001; Giezendanner et al., 2003; Bellows et al., 2007; Meulen, 2008) have successfully used in the analysis of swirling flames and the propagation of CH* and OH* radicals, which according to the theory are related to the burning region and temperature intensity. These experiments can be supplemented by the analysis of aldehydes formed during the process, which are correlated to the inner region consistent to the CRZ (Giezendanner et al., 2003) allowing the location of the boundary zone of the flame. Cardiff University has the potential to run experiments under atmospheric conditions, with the possibility of getting results under pressurized conditions in Port Talbot.

The use of Proper Orthogonal Decomposition (POD) software can provide evidence of other structures inside of the burning region based on their level of energy. Secondary modes can be obtained with the latter and the current PIV systems used at the University. Moreover, the acquisition of a high rate laser could also give results of the shape of the structures in real time, with the instantaneous correlation between planes.

The balance point between parameters during flashback has to be analyzed more depth. It is interesting to see that this balance occurs at the same equivalence ratio, probably a phenomenon caused by the geometry of the system.

Flashback analysis can be studied numerically allowing risk safe trials with low energy systems at high pressure and different fuel blends. These may give details about the process and propagation of the flame in the inner region of premixing required for good stability in Gas Turbine Combustors. Some research centres (Lenze et al., 2007) have started experiments that due to the high energy input conditions have proved to be very damaging to the hardware. However, these can be modelled via simulation codes after these have been confirmed under less serious situations (Valera-Medina et al., 2009). The usage of hydrogen and CO_2 fuel blends will doubtless show different patterns of combustion which combined with an improved geometrical design of passive components could be demonstrated at industrial scales.

On the existing system different inserts for the tangential inlets have to be tested in order to investigate the effect of different swirl numbers. According to the flow maps obtained during the combustion analysis, the flashback region threshold seems to remain unchanged using different inserts. Since the flashback limit is highly dependent on the geometry of the exhaust sleeve and fuel injector, probably the swirl is of lesser importance when the CIVB has been destroyed (although not with respect to the CRZ), leaving the system to cope with only boundary layer and turbulent flame speed propagation, as discussed in this project. However, this has to be confirmed.

Another interesting point observed was the presence of this constant trend of the flame to reach its lowest position in the exhaust sleeve at $\varphi \sim 1.2$ when no flashback was observed. This could be linked to the quenching values proposed by Kronner et al (2007), who argues that these are characteristic of each burner. Nevertheless, this has to be analyzed further.

The study can be widen using Flame Transfer Functions (FTF) that compare the heat variance in the system and the flow velocity or pressure variations. Several authors (Lieuwen and Yang, 2005; Lacarelle et al., 2009; Schneiders et al., 2001) have

successfully characterized the system by these means, with a complete analysis of combustion instabilities which primarily have focused on active methods of suppression of unstable modes and passive methods for the avoidance of fuel pockets and change in the delay time of emission and combustion of the reactants.

Finally, there is room for the design of new diffusive injection systems. As mentioned during chapter 7, the shape and constriction of the rig nozzle allowed the avoidance of propagation of the flame to the tip of the injector used. However, the injector of interest created different structures based on the method of injection, giving a vast number of cases and flames. Therefore, more research should be focused on the development of new injectors in conjunction with appropriate rig nozzles which can increase stability by anchoring the flame, reducing Type 1 flashback. Reduction of diffusive fuel usage is important, as especially with the quarl the gas velocities can push the flame upwards away from the main body of the CRZ. Liquid fuel injection could be implemented to increase the anchorage and stability, a topic that requires deeper experimentation.

Swirl Combustors are being used for many years as the best candidate for energy and propulsion for flame stabilization. However, there is still plenty of room to improve these devices, making clear that there are subjects such as the Coherent Structures and their associated instabilities which need to be more fundamentally understood.

ANNEX 1

VORTICITY DYNAMICS

A1.1. Fluid Dynamics

A1.1.1. Mathematical Models

Before establishing the parameters that contribute to the formation and study of vortices, some details about fluid dynamics must be presented in order to have a better understanding of the equations used to solve these problems.

Claude-Louis Navier and Gabriel Strokes derived their equations assuming that a change in momentum is simply the product of changes in pressure and dissipative viscous forces (friction) in the fluid (Shames, 1992).

Suppose a constant volume of analysis. The particles that cross the boundaries of this volume can be analyzed in particular point or through a streamline. The first case is known as the spatial derivative, since the second is the substantive derivative. The latest is defined as,

$$\frac{D}{Dt}(x) \equiv \frac{\partial(x)}{\partial t} + u_i \cdot \nabla(x) \tag{A1.1}$$

The first term on the right side is the variation of the "x" property through the time in a fixed frame, whereas the second parameter is the variation due to the moving fluid (Shames, 1992). From here, an equation of conservation of mass derived by Navier-Stokes may be written as,

$$\frac{\partial \rho}{\partial t} + \nabla \cdot (\rho u_i) = \frac{D\rho}{Dt} + \rho \nabla \cdot u_i = 0 \tag{A1.2}$$

In the same way, the conservation of momentum can be expressed as follows,

$$\frac{\partial(\rho u_i)}{\partial t} + \nabla \cdot (\rho u_i u_j) = \rho f_i \tag{A1.3}$$

ρf_i is the force acting on the fluid. Simplifying it with equation 2.17,

$$\rho \frac{Du_i}{Dt} = \rho f_i \tag{A1.4}$$

Here, F=ma can be recognised. The general form of Navier-Stokes equations for conservation of momentum is,

$$\rho \frac{Du_i}{Dt} = \nabla \cdot P^* + \rho f_i \tag{A1.5}$$

In this case, P^* is a tensor that represents the surface forces applied on a fluid particle. Thus it is shown in figure A1.1.

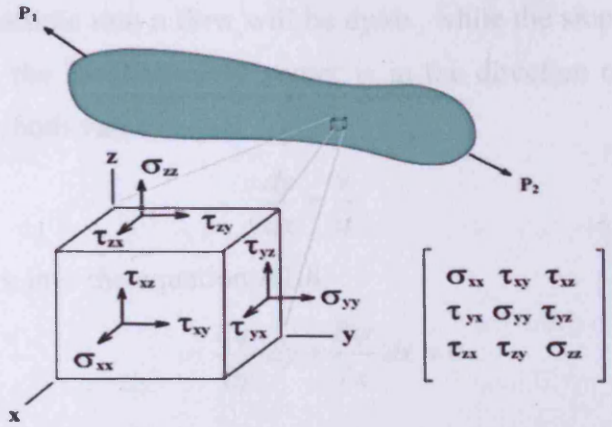

Figure A1.1. Stress Tensor (Wikipedia, 2006)

Nevertheless, the solution to these equations is very complicated, so the Reynolds average Navier-Stokes (RANS) calculation is a very good approach in engineering problems (Liu, 2006). These equations include the equation of mass continuity and the use of some simplifications in the momentum equation as follows,

$$\frac{\partial(\rho u_i)}{\partial t}+\frac{\partial(\rho u_i u_j)}{\partial x_j}=-\frac{\partial p}{\partial x_i}+\frac{\partial}{\partial x_j}\left[\mu\left(\frac{\partial u_i}{\partial x_j}+\frac{\partial u_j}{\partial x_i}-\frac{2}{3}\delta_{ij}\frac{\partial u_i}{\partial x_i}\right)\right]+\frac{\partial(-\rho u_i' u_j')}{\partial x_j} \quad \text{(A1.6)}$$

Where $\rho u_i' u_j'$ is known as the Reynolds stress tensor, which represents the effects of turbulence and can be seen in the Swirl equation.

A1.1.2. Vortex Properties

Before continuing with the description of the phenomenon, it is important to describe the average behaviour of different vortices in order to recognise some patterns that could lead to the development of equations that describe the precessing core.

A vortex is a mass of whirling fluid, especially a whirlpool or whirlwind, which possesses vorticity or any flow that has closed streamlines around a centre. In order to understand this concept, two functions must be defined,

- Stream function, designated by ψ(x,y), so

$$u=\frac{\partial\psi}{\partial y} \qquad \text{and} \qquad v=-\frac{\partial\psi}{\partial x} \quad \text{(A1.7)}$$

Where the components u and v are the velocities of the flow in x and y, respectively. The slope of any particle into a flow will be dy/dx, while the slope of the velocities is v/u. By definition, the local velocity vector is in the direction of the tangent of the streamline, making both values equal. Thus,

$$\frac{dy}{dx} = \frac{v}{u} \tag{A1.8}$$

Substituting u and v into the equation A1.8,

$$\frac{\partial \psi}{\partial y} dy + \frac{\partial \psi}{\partial x} dx = 0 \tag{A1.9}$$

As defined in calculus,

$$d\psi = \frac{\partial \psi}{\partial x} dx + \frac{\partial \psi}{\partial y} dy \tag{A1.10}$$

Therefore, $d\psi = 0$ along a streamline. So, the stream function remains constant along a streamline. In other words, the equation for a streamline in a flow field can be obtained from the expression for the stream function by setting the stream function equal to a constant, which has different constant values defined by a reference point (John et al., 1980). See the following example,

$$\psi = Uy$$

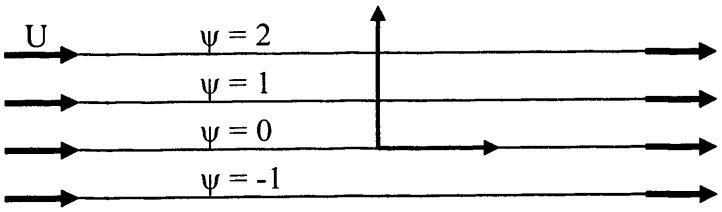

Figure A1.2. Streamlines in uniform flow (John et al., 1980)

- The velocity potential function, defined as $\phi(x,y)$, thus

$$u = \frac{\partial \phi}{\partial x} \qquad \text{and} \qquad v = \frac{\partial \phi}{\partial y} \tag{A1.11}$$

A flow for which the potential function exists is called potential flow. As an example, consider a uniform flow along x (figure A1.3),

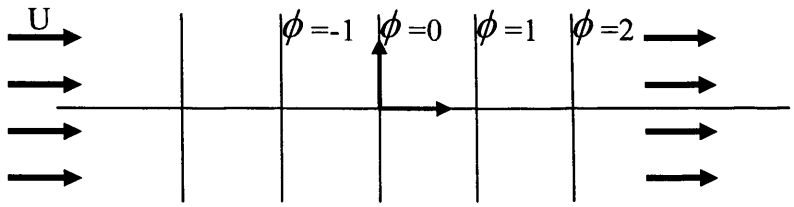

Figure A1.3. Equipotential lines for uniform flow (John et al., 1980)

These equations are perpendicular one to each other. This statement is true in general. Now, examining the properties of velocities, it can be seen that,

$$\frac{\partial u}{\partial y} = \frac{\partial v}{\partial x} = \frac{\partial^2 \phi}{\partial x \partial y} \tag{A1.12}$$

or

$$\frac{\partial u}{\partial y} - \frac{\partial v}{\partial x} = 0 \tag{A1.13}$$

This expression signifies that the fluid elements do not rotate during the course of their movement, which refers to an *irrotationality* condition for 2D flow. This is demonstrated in figure A1.4,

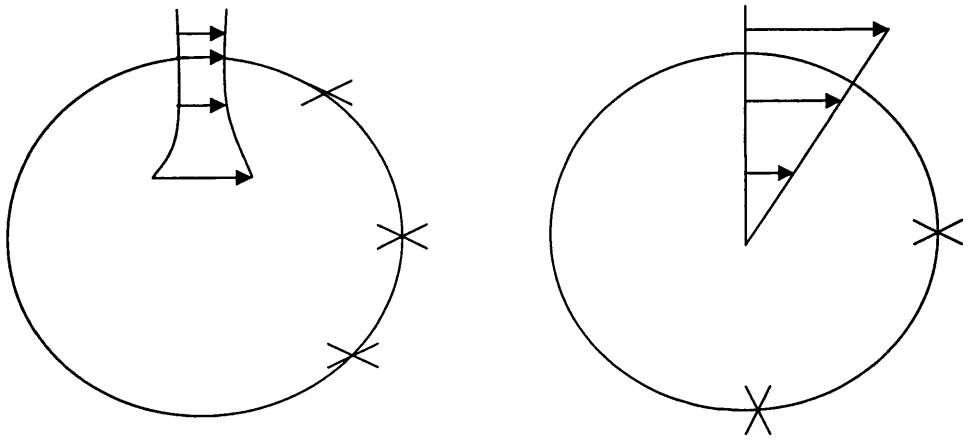

Figure A1.4. Irrotational (free) vortex and rotational (solid body) vortex (John et al., 1980)

The elements move in circular paths without changing their orientation. However, to achieve this, the inner side of the element must move faster than the outer side, so it can handle the element speed plus the velocity required to keep its orientation. Thus, the tangential velocity is proportional to the inverse of the radial distance from the centre of the circle.

An example of rotational flow occurs when the element move in a circular trajectory changing its orientation, as if it was a rigid body. Here, the tangential velocity is proportional to the radial distance from the centre.

Another function that must be defined is the rotation of the fluid, which is the average of the rotation of all the sides of the fluid element. Therefore, in a 2D analysis, the rotation ω is given by

$$\omega = \frac{1}{2}\left(\frac{\partial v}{\partial x} - \frac{\partial u}{\partial y}\right) \tag{A1.14}$$

Which must be equal to zero for irrotational flows. If a continuity equation is included, then the sum of the partial velocities must be zero. Knowing the values of u and v from equation A1.8, it is obtained the *Laplace's* equation as follows,

$$\frac{\partial}{\partial x}\left(\frac{\partial \phi}{\partial x}\right) + \frac{\partial}{\partial y}\left(\frac{\partial \phi}{\partial y}\right) = \frac{\partial^2 \phi}{\partial x^2} + \frac{\partial^2 \phi}{\partial y^2} = 0 \tag{A1.15}$$

This equation can be converted to polar coordinates using the chain rule of partial differentiation, so flows from sources or to sinks can be analyzed. Laplace's equation in polar coordinates is,

$$\frac{\partial^2 \phi}{\partial r^2} + \frac{1}{r}\frac{\partial \phi}{\partial r} + \frac{1}{r^2}\frac{\partial^2 \phi}{\partial \theta^2} = 0 \tag{A1.16}$$

In axisymetric flows u = v = 0. The only existent component is the tangential (swirl) velocity, w, which is a function of the radius, r,

$$w = f(r) \tag{2.32}$$

Therefore, in this flows,

$$\omega = \left(\frac{1}{r}\frac{\partial}{\partial r}(rw), 0, 0\right) \tag{2.33}$$

This is just an example to obtain the values for an irrotational element. Values of rotation can be specified knowing the velocity functions for a certain flow field. Table A1.1 shows some of the principal characteristics of different vortices,

Table A1.1. Vortex Characteristics (Gupta , 1984; Dawson, 2000)

	Forced vortex (solid body rotation)	Free vortex (irrotational)	Rankine vortex (combined)
Tangential velocity, w	$w = c'r$	$w = \frac{C}{r}$	$w = \frac{C'}{r}\left[1 - \exp\left(-\frac{r^2}{r_0^2}\right)\right]$
Angular velocity, Ω	c' (constant)	$\frac{C}{r^2}$	Function of radius
Circulation, Γ	$2\pi \cdot \Omega r^2$	$2\pi \cdot C$	$2\pi C'\left[1 - \exp\left(-\frac{r^2}{r_o^2}\right)\right]$
Vorticity, ω	$4\pi \cdot \Omega$	0	$\frac{4\pi C'}{r_o^2}\left[\exp\left(-\frac{r^2}{r_o^2}\right)\right]$

ANNEX 2

AVERAGE FRAME

```
global Base_file
global First_number Last_number total_pictures
save_averages = cell(1,51);
second_save_average = cell(1,6);


disp('Type the name of the base file:');      % Gets the name of the
Base_file = input('Base_file: ','s');         % root file.

disp('First picture number:');                % Gets the first picture
First_number = input('First_number: ');       % to be processed.

disp('Last picture number (the total number of pictures must be
500):');
Last_number = input ('Last_number: ');        % Gets the last picture in
                                              % the analysis. 500 frames
                                              % are processed.

total_pictures = Last_number - First_number; % Total number of pictures.

if total_pictures~=500                         % If the number of frames
                                               % is different to 500 the
    disp('You need a multiple of 10');         % program breaks.
    break;
end

k = 0;
first_value = 1;

for i = 1:50
    for j = 1:10
        numero = num2str(j+k);                 % No. of image of interest.
        sort_file = '.jpg';                      % Type of file.
        picture = [Base_file,numero,sort_file]; % Image of interest to
                                                 % be analyzed.
        read_picture = imread(picture);          % Reads picture.

        if first_value==1    % Creates averages of 10 frames, that then
                             % uses with other 50 average results.
            sequence = zeros([size(read_picture)10],class(read_picture));
            sequence(:,:,j) = read_picture;
            first_value = 0;
        else
            sequence(:,:,j) = imread(picture);
        end
    end

    A1 = sequence(:,:,1);              % This part of the command gets the
    A2 = sequence(:,:,2);              % values of 10 consecutive frames.
    A3 = sequence(:,:,3);              % Then weights each of them at 10%
    A4 = sequence(:,:,4);              % of the final average result.
    A5 = sequence(:,:,5);              % This is repeated 50 times to get
    A6 = sequence(:,:,6);              % 50 batches of 10 frames each.
    A7 = sequence(:,:,7);
    A8 = sequence(:,:,8);
```

```
    A9 = sequence(:,:,9);
    A10 = sequence(:,:,10);

    average = imlincomb(.1,A1,.1,A2,.1,A3,.1,A4,.1,A5,.1,A6,.1,A7,.1,A8,.1,A9,.1,A10);
    save_averages(1,i) = {average};
    k = k+10;
end

j = 0;

for i = 1:5

    A1 = save_averages{1,1+j};      % After the average of batches
    A2 = save_averages{1,2+j};      % of 10 frames has been
    A3 = save_averages{1,3+j};      % performed batches of 10 average
    A4 = save_averages{1,4+j};      % results are weighted
    A5 = save_averages{1,5+j};      % again, with a 10% contribution
    A6 = save_averages{1,6+j};      % to the average of 100 frames.
    A7 = save_averages{1,7+j};
    A8 = save_averages{1,8+j};
    A9 = save_averages{1,9+j};
    A10 = save_averages{1,10+j};

    average = imlincomb(.1,A1,.1,A2,.1,A3,.1,A4,.1,A5,.1,A6,.1,A7,.1,A8,.1,A9,.1,A10);
    second_save_average(1,i) = {average};
    j = j+10;
end

A1 = second_save_average{1,1}; % Finally, the batches of 100 frames are
A2 = second_save_average{1,2}; % weighted a final time, each at 20%
A3 = second_save_average{1,3}; % of the final result, final_average.
A4 = second_save_average{1,4};
A5 = second_save_average{1,5};

final_average = imlincomb(.2,A1,.2,A2,.2,A3,.2,A4,.2,A5);
imtool(final_average);
```

APPENDIX 1

TURBINE DESIGN

Ap1.1. Introduction

This appendix may help new students to learn about Gas Turbine designs and the most important parameters taken into consideration for this purpose. This is a summary of "The Design of High Efficiency Turbomachinery and Gas Turbines" (Gordon and Karakianitis, 1998) and "Aerothermodynamics of Gas Turbine and Rocket Propulsion" (Gordon, 1997).

Nomenclature

a: Constant for Carmichael and Lewis eq. [-]

A : Characteristic area [m^2]

A_h: Area of the wall where the mass flow rate occurs [m^2]

A_{an}: Area through which the flow passes [m^2]

b: Constant for Carmichael and Lewis eq. [-]

C: Absolute velocity [m/s]

C_{ex}: Outlet velocity [m/s]

C_{in}: Inlet velocity [m/s]

$C_{u,x}$: Tangential velocity [m/s]

C_p: Specific Heat Capacity [J/kgK]

C_{pr}: Real pressure rise coefficient [-]

$C_{pr,tl}$: Theoretical pressure rise coefficient [-]

C_{ra}: Ratio of the smaller heat capacity rate to the larger [-]

d_{hb}: Inner diameter [m]

d_{sh}: Outer diameter [m]

ds: Derivate of Entropy [J/kg.s.K]

du: Derivate of internal energy [J/kg.s]

dv: Derivate of Specific Volume [m^3/kg]

d_b: Combustor diameter [m]

g: Gravity [9.81 m/s^2]

g_c: Newton's constant (in the SI is equal to 1)

h_0: Stagnation Enthalpy [J/kg.s]

h_{st}: Static Enthalpy [J/kg.s]

$\hat{h}$: Molal enthalpy [J/kg.s.mol]

h_t: Heat transfer coefficient [W/m^2K]

k: Thermal conductivity [W/mK]

K: Constant valued [W/kg.s.K]

L: Characteristic length [m]

l_b: Combustor length [m]

M: Mach number [-]

$\dot{m}$: Mass flow [kg/s]

N: Angular speed [rev/min]

n: Polytropic constant [-] or constant for Carmichael and Lewis eq. (section A3.6.)

n': Constant value (n-1)/n [-]

$\hat{n}$: Number of moles [mol]

Nu: Nusset number [-]

N_{tu}: Number of transfer units [-]

p: Pressure [N/m^2]

p_0: Stagnation Pressure [N/m^2]

p_{st}: Static Pressure [N/m^2]

$p_{st,in}$: Static Inlet Pressure [N/m^2]

$p_{st,ex}$: Static Outlet Pressure [N/m^2]

$p_{0,in}$: Stagnation Inlet pressure [N/m^2]

$p_{o,ex}^{\otimes}$: Stagnation Outlet pressure in an isentropic process [N/m^2]

Pr: Prandtl number [-]

$\dot{Q}$: Heat that gets in (in) or out (ex) from the control volume [J/kg/s]

$\dot{Q}_b$: Heat released in the combustor [J/kg/s]

$\dot{Q}_{mx}$: Maximum heat transferred [J/kg/s]

R: Gas constant [J/kg/K]

R_n: Reaction [-]

Re: Reynolds number [-]

r: Pressure ratio [-] or radius (section 1.5.) [m]

r_c: Compressor pressure ratio [-]

r_e: Turbine pressure ratio [-]

S: Entropy [W/kg.s.K]

St: Stanton number [-]

T: Temperature [K]

T_0: Stagnation Temperature [K]

$T_{0,ex}$: Stagnation Outlet Temperature [K]

$T_{0,in}$: Stagnation Inlet Temperature [K]

T_{bm}: Maximum temperature resistance of blading material [K]

T_{st}: Static Temperature [K]

$\overline{U}$: Mean heat transfer coefficient [W/m^{2}K]

u_{st}: Static internal energy [J/kg.s]

v: Especific Volume [m^3/kg]

v_0: Stagnation specific volume [m^3/kg]

v_{st}: Static specific volume of the fluid [m^3/kg]

V_b: Combustor volume [m^3]

W: Relative velocity [m/s]

$\dot{W}$: Work that gets in (in) or out (ex) from the control volume [J/kg/s]

$\dot{W}_{ex,ie}$: Specific work obtained from an ideal process [J/kg/s]

$\dot{W}_{ex,ac}$: Specific work obtained from the actual process [J/kg/s]

$\dot{W}_{in,ie}$: Specific work added from an ideal process [J/kg/s]

$\dot{W}_{in,ac}$: Specific work added from the actual process [J/kg/s]

y: Position in the vertical plane [m]

z: Vertical distance from datum to calculate Potential energy [m]

α: Angle between the velocity and the vertical line [rad]

β: Blade angle [rad]

ϵ_{hx}: Heat Exchanger effectiveness [-]

γ: Ratio of specific heats for T_{st} [-]

ΔE: Increase of energy level into a control volume [J]

Δp_0: Difference in pressure, relative to losses [N/m^2]

δq: Heat transferred in the process [J]

δw: Work transferred out of the control volume [J]

Λ: Hug-shroud ratio [-]

μ: Viscosity [kg/m.s]

η_{df}: Diffuser Effectiveness [-]

η_e: Efficiency, Expander [-]

$\eta_{p,e}$: Polytropic efficiency, Expander [-]

$\eta_{s,e}$: Isentropic efficiency, Expander [-]

η_c: Efficiency, Compressor [-]

$\eta_{p,c}$: Polytropic efficiency, Compressor [-]

$\eta_{s,c}$: Isentropic efficiency, Compressor [-]

ρ: Average Density [kg/m^3]

ρ_0: Stagnation density [kg/m^3]

$\rho_{0,ex}$: Stagnation Outlet density [kg/m^3]

$\rho_{0,in}$: Stagnation Inlet density [kg/m^3]

ρ_{st}: Static density [kg/m^3]

σ_ω: Weiner's correlation of velocities [-]

τ_ω: Skin friction tangential stress at the wall [N/m^2]

ω: Angular velocity [1/s]

ψ: Work coefficient [-]

θ: Variable for the temperature difference ($T-T_{wall}$) [K]

θ_m: Mean temperature difference [K]

θ_0: Maximum temperature difference [K]

Φ: Flow coefficient [-]

Ω: Number of microstates in which the particles can be arranged [-]

Ap1.2. A brief history

During the beginnings of humanity, the energy has been always one of the most important issues. Its importance is based on the fact that without energy neither human nor machines could work. Therefore, the study of it and the different ways to transform it has always been part of the most advanced discoveries.

During the Roman age, they introduce one of the most important equipments to transform one type of energy to another, the water wheels. Even though Hero of Alexandria was the first one to report the use of a steam powered engine (a curios toy at that moment), the use of the former was not practical until 1629, when Giovanni Branca proposed its usage.

The term "Turbine" was coined by Claude Burdin. The latin word means "that which spins". Therefore, the later applies not only to gas or steam equipments, but also to any device that spins.

During the first years of research, several engineers tried to create different equipments based on the properties and behaviour of different fluids. At the beginning, people such as James B. Francis designed high efficiency water turbines, which were promptly characterised by the discoveries of Osborne Raynolds in 1883 and Rayleigh in 1892.

However, major problems appeared when trying to develop a new type of equipment run by gases. One of these was the design of compressors, since the lack of resistant materials made impossible higher temperatures and pressures, leaving everything to the reduction of leakages of gas.

Several years passed before the invention of a turbine that would change the world. Charles Parson was the one who created a multistage axial-flow reaction turbine in 1884. His discoveries and proposals took him to create propulsion machineries capable of pushing large navies, such as the Mauritania, powered by a turbine driver of 70,000 hp.

Other names appeared in the list of celebrities who shared a podium for the creation of the actual gas turbine. Amongst them, Charles Curtis patented in 1896 the velocity stage turbine, similar to one created by Patrik de Laval. Most of these designs were used for the Navy, especially during the Victorian years and the beginning of the century.

In the case of the gas turbine, as its name implicates, this is referred to the gas turbine engine and for the gas expander. In comparison to the steam engine, the gas turbine presented several problems of vibrations and efficiency, since the materials used were not as resistant as they are nowadays. Franz Stolze, led by different books of previous designers, was able to create a "fire turbine", which was exactly the principle and configuration of today's gas turbines. Some other researchers and engineers, including Aegidius Elling, Charles Lemale, Hans Holzwarth, etc., participated in the improvement of these machineries.

These discoveries led to the design of the first turbojets, which were developed during the WWII. The use of new alloys and combustible conditions made possible their use in commercial aviation of today. The use of alloy sheets made of manganese, excluding nickel and using just a little bit of other metals, led to the design of bigger equipments and higher efficiencies, reaching more than 45 kN in thrust at the end of the previous century.

In terms of commercial power generation, the rising of energy prices in 1970 ceased the high production of gas turbines. However, the introduction of combined cycles, cogeneration and new advanced cycles, gave a new thrust to these equipments, that now can exceed 500 MW of output. Several experts used to say that the gas turbines would fail in a world governed by Diesel and Gasoline engines. However, the reality is that these devices gain day to day more fields in the area of production and generation.

Ap1.3. Basic Concepts

A turbomachine is an equipment that changes the enthalpy in a stream of a fluid that passes through it, transferring work through a rotation shaft. This can be done by heat transfer, even though its contribution in such type of engines is negligible.

There are different types of turbomachines:

- Those that work on liquids (pumps) or gases (fans and compressors).
- Those that are full admission, where the fluid flow through the blading is axisymetric, and the partial admission ones, which have nozzles in specific points to push and move the blades. In the later, all the pressure drop takes place in the nozzles and the rotor converts only kinetic energy to shaft power.

Let's consider an airfoil. The forces produced can be split in those that are normal to the relative movement of the former, or Lift, and those that are along it, or Drag. However, some classes of machines use shaped channels. Therefore, these important forces may be defined with reference to the normal and tangential directions of the channel walls. These concepts will be required later.

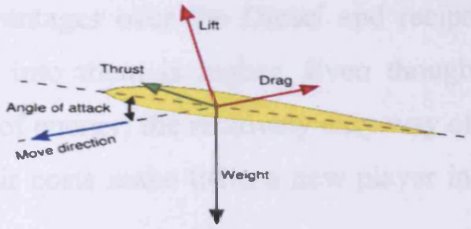

Figure Ap1.1. Lift and Drag forces.

The total equipment is formed by the stator, which can be as simple as the "snail-shell" volute of a centrifugal blower, and the rotor, which combined are known as a "stage". Therefore, machines can be categorized as being just rotors, single stage or multiple stages.

Ap1.3.1. Gas Turbines

This is the abbreviation of gas-turbine engine, which accepts and rejects heat and produces work. The heat input is usually in the form of fuel that is burned, and the rejected one is done via a heat exchanger. The work may be given as output torque in a turning shaft or as velocity and pressure energy in a jet.

A gas turbine consists in a compressor, which compresses air to a higher pressure; heaters in which the temperature of the compressed gas is raised; an expander, which expands the hot gas to a lower pressure; and a cooling system, where the heat can be recovered or "regenerated". There are different types of cycles, depending on the final place of the expanded gas and the type of regenerator or cooling system. Therefore, a closed cycle system uses the expanded gas in a new cycle; in an open cycle the gases leave the expander to the atmosphere, which performs as the cooling system. The new air is taken from the surroundings.

In an internal combustion gas turbine engine, the gas is heated by combustion of fuel, where the gas must be either atmospheric air or oxygen. The exhausted gases can be regenerated, or recuperated, so the heat can be exchanged with the heaters to increase the efficiency and reduce the losses.

These equipments can be split into different expanders, so the high pressure turbine produces the energy required to operate the compressor, and lower turbines are used to obtain the desired output power.

Turbines have great advantages over the Diesel and reciprocate devices, since the amount of air that gets into them is higher. Even though the steam engines can produce higher amounts of energy, the relatively easy way of running the gas turbines, their small sizes and their costs make them a new player into the energy production field.

If we compare them with a Diesel engine, the amount of air that the turbine suctions is 68 times the one of the diesel engine. Also, the price for unit made is cheaper at production rates over 1,000 hp. However, there are some production problems that can increase the final price, and have made these machineries more reluctant to take their place in the production system.

Ap1.3.2. Thermodynamic Principles and Fundamental Equations

Ap1.3.2.1. First Law of Thermodynamics

Several equations rule over these types of mechanisms. However, some are fundamental for their understanding and prediction of properties. One of them is the *First Law of Thermodynamics*, which dictates,

$$\delta q = dE + \delta w \tag{Ap.1}$$

When we talk about a control volume, imagine a hermetic volume which can be analyzed and studied as a separate body from the entire world. Figure Ap1.2 gives an idea of the former, with all the possible energies that get in and out of it, with the properties of concern. With this overview, the equation Ap.2 becomes into a more general equation that will lead us to important results,

$$\begin{aligned} \dot{W}_{ex} + \dot{Q}_{ex} + \dot{m}_2\left(u_{st,2} + p_{st,2}v_{st,2} + \frac{C^2{}_2}{2g_c} + \frac{gz_2}{g_c}\right) = \\ \dot{W}_{in} + \dot{Q}_{in} + \dot{m}_1\left(u_{st,1} + p_{st,1}v_{st,1} + \frac{C^2{}_1}{2g_c} + \frac{gz_1}{g_c}\right) \end{aligned} \tag{Ap.2}$$

This is known as the "steady flow energy equation". Another important parameter is known as *Enthalpy*, which can be defined as,

$$h_{st} \equiv u_{st} + p_{st}v_{st} \tag{Ap.3}$$

In air and gas turbomachineries the changes of height are negligible. Knowing that the stagnation enthalpy (that includes the velocity effects, h_0) is,

$$h_0 \equiv h_{st} + \frac{C^2}{2} \tag{Ap.4}$$

And substituting this value in equation A3.2, what we have is,

$$\frac{\dot{Q}_{in} + \dot{W}_{in} - \dot{Q}_{ex} - \dot{W}_{ex}}{\dot{m}} = h_{0,2} - h_{0,1} \qquad \text{(Ap.5)}$$

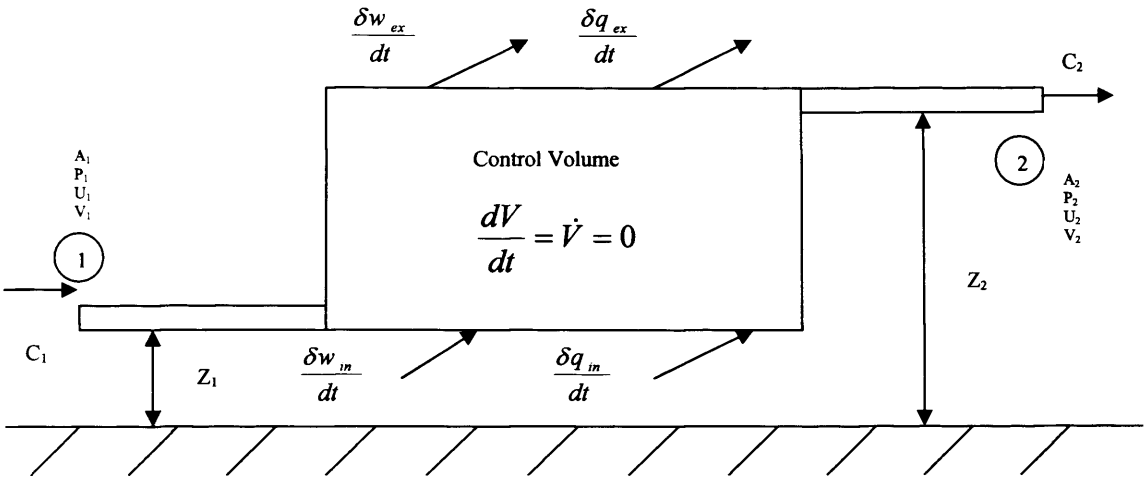

Figure Ap1.2. Control Volume (Gordon, 1997).

Some of the machines incorporated in the turbines are thermally isolated (compressors, pumps, turbines, etc.) or do not produce work (exchangers, ducts, nozzles, etc). Thus, the equation can be simplified according to the case.

Ap1.3.2.2. Second Law of Thermodynamics

The most popular expression for it is "*Heat cannot pass from a cooler to a warmer body without the expenditure of work*" (Gordon, 1997). This law simply states that a state that is in order will pass to a disordered one, or at least, it will maintain its degree of "order". The later concept is known as *Entropy*, which is defined as,

$$S \equiv K \ln \Omega \qquad \text{(Ap.6)}$$

Knowing that S is a function of u and v as well a summation of various collections of assemblies of particles (S_A and S_B), the substitution in the previous equation of some defined values such as temperature and difference in internal energies, gives one of the most important equations in the analysis of turbomachineries, *Gibb's equation,*

$$Tds = du + pdv \qquad \text{(Ap.7)}$$

Ap1.3.2.3. Perfect gas and semi-perfect gas models

By definition, a perfect gas has constant values of specific heat capacities at constant volume and constant pressure, C_v and C_p respectively. By definition, a semi-perfect gas has specific heat capacities that are function only of temperature. An important parameter is the *Ideal Gas Equation,*

$$pv = RT \tag{Ap.8}$$

The specific internal energy and the specific enthalpy can be written in the following form, which obey the previous equation.

$$\begin{aligned} dh &= C_p dT \\ du &= C_v dT \end{aligned} \tag{Ap.9}$$

These equations, mixed with the Gibb's and Ideal Gas ones, lead to the following results that are very important in the resolution of thermodynamic problems related to turbines and turbomachines, as well as the creation of T-s diagrams used for graphic resolution,

$$C_v + R = C_p \tag{Ap.10}$$

$$\gamma \equiv \frac{C_p}{C_v} \tag{Ap.11}$$

$$u_2 - u_1 = C_v(T_2 - T_1) \tag{Ap.12}$$

$$h_2 - h_1 = C_p(T_2 - T_1) \tag{A3.13}$$

Also, if the second law is derived for flow processes, and based on Gibb's equation, some isentropic (that the entropy does not change) relations can be obtained as follows,

$$\frac{T_1}{T_2} = \left(\frac{p_2}{p_1}\right)^{\frac{R}{C_P}} = \left(\frac{\rho_2}{\rho_1}\right)^{\frac{R}{C_V}} = \left(\frac{v_1}{v_2}\right)^{\gamma-1} \tag{Ap.14}$$

These relations can be applied for perfect gases and as an approximation for semi-perfect ones. Also, many flow problems in the design of turbomachinery involve the specification of the stagnation pressure and temperature, as well as the absolute velocity or the mass flow rate or characteristic area. Therefore, they are linked to the dimensions of the equipment. If the Mach number (M, the ration between the flow speed and the sound speed) is known, all the actual, static, properties are immediately calculable. These can be obtained from the following equations and their correspondent graphs, equation that can be represented in maps for their easy use, figure Ap1.3. and Ap1.4.

$$\frac{T_0}{T_{st}} = 1 + \left(\frac{\gamma - 1}{2}\right) M^2 \tag{Ap.15}$$

$$\frac{p_0}{p_{st}} = \left[1 + \left(\frac{\gamma - 1}{2}\right) M^2\right]^{\frac{\gamma}{\gamma-1}} \tag{Ap.16}$$

$$\frac{\rho_0}{\rho_{st}} = \frac{v_{st}}{v_0} = \left[1+\left(\frac{\gamma-1}{2}\right)M^2\right]^{\frac{1}{\gamma-1}} \qquad \text{(Ap.17)}$$

$$\frac{\dot{m}\sqrt{RT_0}}{Ap_0} = M\sqrt{\gamma}\left[1+\left(\frac{\gamma-1}{2}\right)M^2\right]^{-\frac{\gamma+1}{2(\gamma-1)}} \qquad \text{(Ap.18)}$$

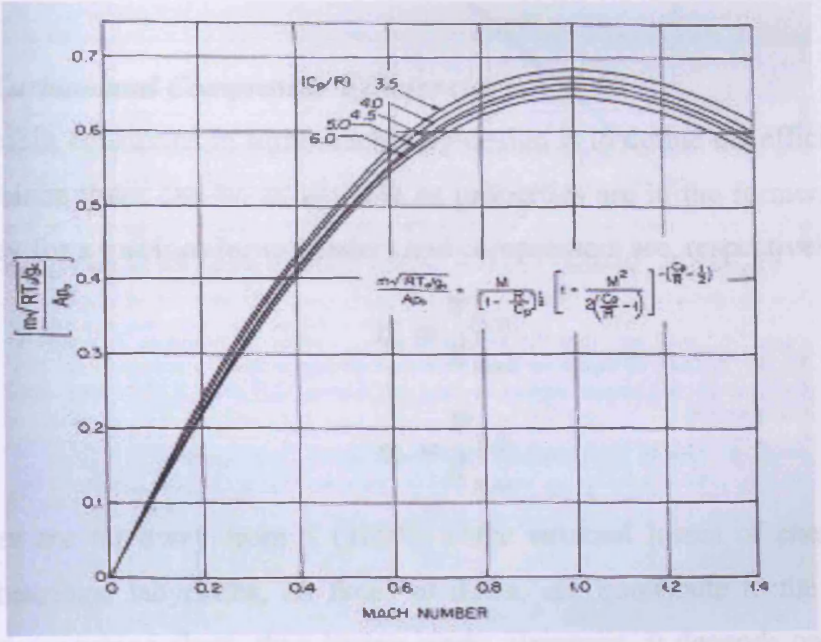

Figure Ap1.3. Mach Number versus eq. Ap3.18 (Gordon, 1997)

$$\frac{C}{\sqrt{RT_0}} = \sqrt{2\left(\frac{\gamma}{\gamma-1}\right)\left[1-\left(1+\frac{\gamma-1}{2}M^2\right)^{-1}\right]} \qquad \text{(Ap.19)}$$

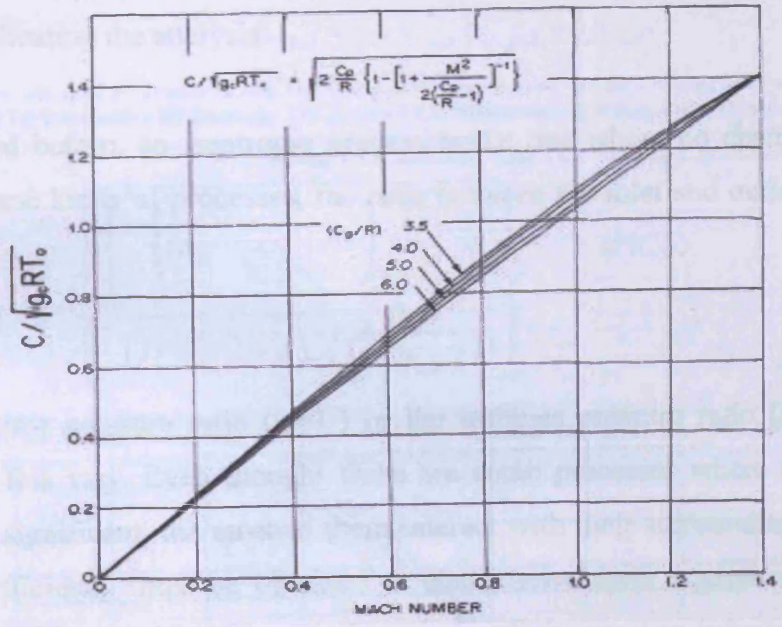

Figure Ap1.4. Mach number versus eq. Ap3.19 (Gordon et al., 1998)

Another important point to take into consideration is that the actual movement of the flow is not parallel to the axis of the equipment. Therefore, to calculate the real value of A we must include the angle that the flow makes with the axial direction, α, so it can be calculate as A_{act} =A cos α. All these parameters may help to obtain the characteristic dimensions of the turbine.

Ap1.3.2.4. Turbine and Compressor Efficiencies

One of the main constrains in turbomachinery design is to define the efficiency of the equipment, since these can be as variable as properties are in the former. Therefore, the efficiency for a turbines (or expander) and compressors are, respectively,

$$\eta_e \equiv \frac{\dot{W}_{ex,ac}}{\dot{W}_{ex,ie}} \qquad \text{(Ap.20)}$$

$$\eta_c \equiv \frac{\dot{W}_{in,ie}}{\dot{W}_{in,ac}} \qquad \text{(Ap.21)}$$

These values are far away from 1 (100%) since external losses of energy such as friction in bearings, labyrinths, on faces of disks, etc. contribute to the increase of entropy in the working fluid, thus losing work. However, it depends on the system analyzed and the interactions of the former the final evaluation of efficiency. It is very important to take into consideration a polytropic (that the system interacts with its surroundings) equation, since an isentropic approach depends on the pressure and losses, complicating the analysis.

As mentioned before, an isentropic process is the one where no change in entropy occurs. In these kinds of processes, the ratio between the inlet and outlet pressures is defined as,

$$r \equiv \frac{p_{0,ex}^{\otimes}}{p_{0,in}} \qquad \text{(Ap.22)}$$

The compressor pressure ratio (r_c>1) or the turbines pressure ratio (r_e<1) are also specified in this way. Even thought there are some processes where the change in entropy is insignificant, the most of them interact with their surroundings. Therefore, polytropic efficiency must be obtained to characterise these equipments. The term "polytropic efficiency" is equal to the isentropic efficiency of an infinitesimally small

process. These kind of processes are represented by the polytropic relation pv^n = constant, so this leads to the relation,

$$r \equiv \frac{p_{0,ex}\otimes}{p_{o,in}} = \left(\frac{\rho_{o,ex}}{\rho_{o,in}}\right)^n \qquad \text{(Ap.23)}$$

And for any process,

$$r = \frac{\rho_{0,ex}}{\rho_{0,in}}\frac{T_{0,ex}}{T_{0,in}} \qquad \text{(Ap.24)}$$

Therefore,

$$\left(\frac{T_{0,ex}}{T_{0,in}}\right) = r^{\left(\frac{n-1}{n}\right)} = r^{n'} \qquad \text{(Ap.25)}$$

Knowing the isentropic efficiencies of the processes as,

$$\eta_{s,c} = \frac{r^{R/C_p} - 1}{r^{n'} - 1} \qquad \text{(Ap.26)}$$

Its expansion using the binomial theorem (Gordon, 1998) and the knowledge that we are dealing with infinitesimally small steps (which tend to 0), gives the following isentropic efficiencies for compressors and turbines, respectively,

$$\eta_{p,c} \equiv \left(\eta_{s,c}\right)_{r\to 1.0} = \frac{R/C_p}{n'} \qquad \text{(Ap.27)}$$

$$\eta_{p,e} \equiv \left(\eta_{s,e}\right)_{r\to 1.0} = \frac{n'}{R/C_p} \qquad \text{(Ap.28)}$$

This leads to the useful relation,

$$\frac{T_{0,ex}}{T_{0,in}} = r_c^{\left[\left(\frac{R}{C_p}\right)\frac{1}{\eta_{p,c}}\right]} \qquad \text{(Ap.29)}$$

For compressors, and

$$\frac{T_{0,ex}}{T_{0,in}} = r_e^{\left[\left(\frac{R}{C_p}\right)\eta_{p,e}\right]} \qquad \text{(Ap.30)}$$

For turbines.

From now on, the shape of polytropic lines will depend on the values of these efficiencies.

Ap1.4. Gas Turbine Cycles

As mentioned before, the gas turbine cycles are composed by different steps, which can categorised them in a variety of different processes. In this case, the performance of simple cycles (compressor, burner, expander, CBE) and the incorporation to the former of heat exchangers (CBEX) or intercooled compressors (CICBEX) will be mentioned in this section. As it is logical, the final work obtained will depend on the efficiency of the components of the turbine.

Some technical reports claim that the higher the inlet pressure, the greater the gas turbine efficiency. This is true for aircraft engines, but false for power cycles. In fact, the higher the inlet temperature (linked to the high pressure), the greater the net output and the cycle efficiency are. Also, some other constrains about the design of turbines are the operative temperature, the atmospheric and inlet pressures, the exchanged heat, etc. For example, if a low pressure expander is used, the low blade speed will lead to low stress and the possibility of using a higher gas temperature for a given blade life. However, many times the designer can play only with one or two of these parameters.

Depending on the type of cycle, the previous efficiencies and specific powers will vary. Their performance is a function of the inlet and outlet temperatures, pressures and equipment efficiencies. The specific power is a useful way to compare different cycles, and it is defined as,

$$\dot{W} \equiv \frac{\dot{W}}{\dot{m}\overline{C}_{p,c}T_{0,1}} \tag{Ap.31}$$

And the thermal efficiency, which is the ratio of the specific power to the specific heat addition,

$$\eta_{th} = \frac{\left[\dot{W}\left(\dot{m}\overline{C}_{p,c}T_{0,1}\right)\right]}{\left[\dot{Q}\left(\dot{m}\overline{C}_{p,c}T_{0,1}\right)\right]} \tag{Ap.32}$$

As logic, different cycles have different vales, which are based on the recuperation of heat, losses, working pressures and temperatures.

Also, the type of equipment used gives different efficiency values. For example, the radial ones are more suitable for processes where the typical output energy does not exceeds 200 kW, while the axial ones are more used for more powerful cycles.

Another important factor that must be taken into consideration is the use of cooling technologies for the blades and stators. In previous years, the lack of resistant materials made impossible the design of more powerful cycles. However, nowadays the use of coated zirconia and other alloys have allowed the performance of specific power and efficiency in different cycles, as well as the design of new methods to obtain energy.

Ap1.4.1. Other Components

In advanced cycles, the inlet turbines temperature is lower than the maximum temperature flame, and higher than the maximum temperature of the blading material, T_{bm}. For this reason, a cooling system must be incorporated to the entire cycle. Sometimes, a portion of the compressor exit flow is used to dilute the flow around the flame, reducing the temperature. A second portion is used to cool the first turbine stator. A third one is used to cool the turbine rotors and subsequent stators in order to drop the final temperature below the blading material temperature limit. Obviously, this contributes with the final losses of the cycle. The frontier of cooling technologies is to design more resistant materials to minimize the losses due to cooling air.

Other important components are the heat exchangers or recuperators, which are used to recover energy from the outlet turbine gases. Therefore, less combustible is used and the final efficiency increased. Consider the following cycle, figure Ap1.5,

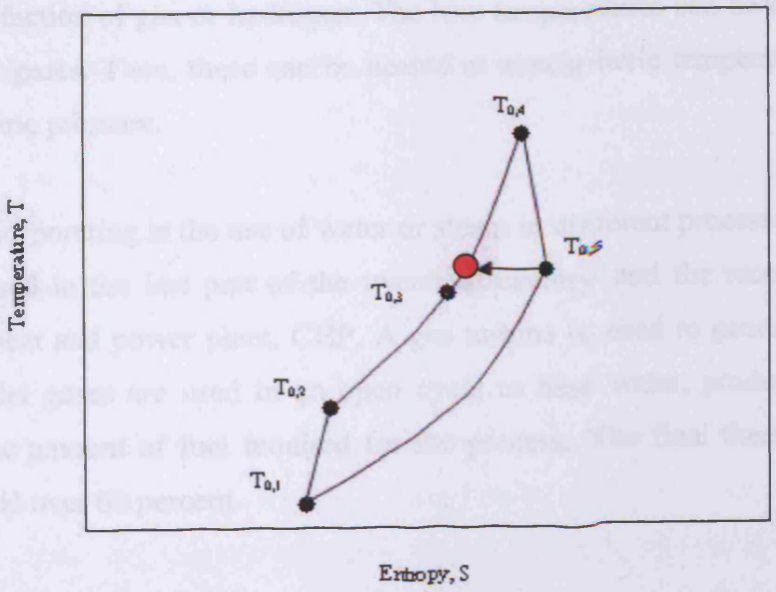

Figure Ap1.5. Diagram T-s representing a heat exchanger process

If the cycle has a heat exchanger where the outlet gases circulate, the maximum temperature rise that can be obtained from the outlet turbine gases is where the red point is. Since this would require 100% efficiency, this is not possible. Thus, the real value rises until the $T_{0,3}$ point. So, the transfer temperatures characterise the heat-exchange effectiveness, ϵ_{hx} defined as,

$$\epsilon_{hx} \equiv \frac{T_{0,3} - T_{0,2}}{T_{0,5} - T_{0,2}} \qquad \text{(Ap.33)}$$

The energy required to reach the point $T_{0,4}$ will come from burning fuels. So, the better the heat exchanger, the less combustible is required for the process.

The use of intercoolers to reduce the temperature of gases at different steps of compression is another way of increasing the final efficiency and the final shaft work. If we reduce the temperature of the compressed gases, the work required for another compression is less. However, the cost of intercoolers must be analysed before acquiring them, considering the work gains.

Ap1.4.2. Alternative Cycles

In addition to the equipments required to increase the efficiency, advanced cycles include other alternatives that can increase this factor. One of them is the use of engines that can produce power from cold, while absorbing heat. This requires the use of cryogenic liquids, and can be very useful in recovering energy from processes such as the liquefaction of gas or hydrogen. The low temperatures can be used to cool the compressed gases. Then, these can be heated at atmospheric temperature, expanding at atmospheric pressure.

Another incorporating is the use of water or steam in different processes. One of them, the most used in the last part of the twentieth century and the recent years, is the combined heat and power plant, CHP. A gas turbine is used to generate power. The turbine outlet gases are used in an open cycle to heat water, producing steam and reducing the amount of fuel required for the process. The final thermal efficiencies have reached over 60 percent.

Another advance is the use of steam directly into the gas turbine. This increases the pressures and reduces the high cost of a steam turbine. However, the steam must be dry. To assure this, the use of moisture removals in wet steam turbines can be very useful, since this can reduce the amount of drops that get in contact with the blades, increasing the life expectancy of the rotor. Also, the mixture with superheated steam before the combustion chambers has increased the expected efficiency of these cycles.

One of the most promising cycles is the one which uses the heat for residential purposes. The outlet gases are used to heat water for houses and building, "co-generating" energy. The high efficiencies reported have been verified by different governments who are supporting construction projects over 200 MW.

A chemical recuperation is another way of making the best of the energy of the cycle. The reformation of gas due to the high outlet temperatures is another way of producing useful methane and reducing NO_x emissions.

There are other cycles which incorporate other equipments to storage energy. This can be done with the use of inlet cooling cycles (where the shaft energy is used to generate ice which will decrease the compressed air temperature later), the injection of compressed air in deep caverns, or the producing of liquefied gas that can be used in a closed cryogenic cycle.

Another approach is the used of more than 1 burner. However, more than one can use biomass or coal as fuel. These can be used after the expansion, so the flue gases can be heated. Then, the former are passed through heat exchangers that will interact with the compressed air, increasing the final temperature of the working fluid. The slag can be recovered easily, and the dirty gases can be washed in order to being processed.

New ideas consider the inclusion of the so-called "wave rotors". When the compressor flow is admitted, the outlet is closed by a wall, and the flow comes to rest, reaching its stagnation pressure, with a compression wave reflected. By the time this reaches the intake end, this is also closed. Fuel is injected and ignited and the pressure rises in constant volume combustion. The rotor reaches a port opening to the turbine and the port empties at higher pressure. Also, the use of closed cycle plants for

nuclear and other applications is one of the best alternatives for the use of these fuels, since the behaviour of the hydrogen and helium, working fluids, will not vary due to their stability. However, the use of difficult designs and the reduced efficiency (in comparison to open cycles) make this a challenge for future research.

Ap1.5. Diffusers

The design of turbomachines is dominated by diffusion, or the conversion of velocity into static pressure. In fact, every blade row in a typical axial compressor is a collection of parallel diffusers.

Diffusion can occur on isolated surfaces or in ducts, due to the change in area or the flow curvature. However, the boundary layer (which is in contact with the walls) must remain attached, if not, dissipation can occur with its correspondent turbulences. Indeed, separation can occur due to the increase of pressure in the diffuser outlet, causing a flow reversal since the kinetic energy is overwhelmed by the static pressure. This can occur due to the increment in the diffuser angle or the diffuser length.

Flows with laminar boundary layers at inlet, or thick turbulent layers, will not withstand as much diffusion without separation as will thin turbulent layers. This is because the thin turbulent layers can "help" the boundary layers to face the increment in pressure, while the laminar ones have not the same energy to withstand this effect. To characterise these equipments, the pressure-rise coefficient is used and defined as,

$$C_{pr} \equiv \frac{p_{st,ex} - p_{st,in}}{p_{0,in} - p_{st,in}} \qquad \text{(Ap.34)}$$

Where the denominator is the velocity and the numerator the pressure increment. In fact, the static pressure can be obtained as the actual velocity minus the stagnation pressure. Even though this is an approximation, it can be very useful for the analysis of such equipments.

Also, a design guide to the value of outlet relative velocity can be obtained from the next equation,

$$C_{ex} = C_{in}\sqrt{1 - C_{pr,tl}} \qquad \text{(Ap.35)}$$

The ratio between the actual, C_{pr}, and theoretical, $C_{pr,tl}$, pressure rise is known as the diffuser effectiveness, η_{df}. This value depends on a variety of different parameters, which include the diffuser cross section, the ratio of length to the inlet, size and shape of inlet boundary layers, Mach number, flow direction and characteristics, smooth walls or rough, downstream conditions, etc.

Nevertheless, different performances have been recorded, experimentally, from different types of diffusers. There are 4 different types that are the most common used: conical, square, rectangular and annular. Depending on the final velocity value and the pressure rise wanted, the type of diffuser may change. Also, other shapes such as the ribbed diffuser, the bell-shaped, the splitter vanes one, etc. have been analysed and reported (Gordon, 1997).

There are some axial diffusers that generate a swirl flow, which can generate turbulences and breakdowns if the flow pressure is not well analysed. There is some evidence that swirl up to the point of flow breakdown in flow in a conical diffuser actually improves pressure recovery, but it can also reduce the pressure rise.

The radial diffusers are also important when the diffusion requires large amounts of swirl. They are used typically downstream of radial flow compressor and pump rotors. These can be characterised by experimental charts of efficiency, and their variety is considerable. However, the risk of using diffusers is the greed of converting more pressure than the allowed by the system. In this case, a flow reversal may occur, causing big damages and losses in energy and efficiency.

Ap1.6 Energy Transfer

When a fluid gets into a rotor, it changes its radial, axial and tangential velocities due to the energy transfer. However, only the tangential component of the force can produce a change in enthalpy through a work transfer. So, there will be a change in the net torque of the fluid from point 1 to 2 due to the action of the rotor. So,

$$T_q = F_1 r_1 - F_2 r_2 = \dot{m} C_{u,1} r_1 - \dot{m} C_{u,2} r_2 = \dot{m}\left(C_{u,1} r_1 - C_{u,2} r_2\right) \qquad \text{(Ap.36)}$$

Thus, knowing that the net energy transfer is $T_q\omega$ and $\omega r = u$,

$$\dot{W}_{ex} - \dot{W}_{in} = T_q \omega = \omega \dot{m}(C_{u,1} r_1 - C_{2u,} r_2) = \dot{m}(u_1 C_{u,1} - u_2 C_{u,2}) \quad \text{(Ap.37)}$$

Or,

$$\frac{\dot{W}_{ex} - \dot{W}_{in}}{\dot{m}} = (u_1 C_{u,1} - u_2 C_{u,2}) \quad \text{(Ap.38)}$$

Known as the Euler's equation that is universally applicable for any turbomachine. This is the energy transferred in the rotor of these kinds of equipments. It can be reduced for adiabatic processes, giving

$$(h_{0,2} - h_{0,1}) = u_2 C_{u,2} - u_1 C_{u,1} \quad \text{(Ap.39)}$$

Another useful relation is for the preliminary design of axial flow machines, where "u" remains constant since the change in radius is negligible. Also, for radial flow equipment the inlet fluid arrives without any "swirl", so the tangential component velocity is zero. These equations can be written as follows,

$$\Delta_1^2 h_0 = u \Delta_1^2 C_u \quad \text{(Ap.40)}$$

$$\Delta_1^2 h_0 = u_2 C_{u,2} \quad \text{(Ap.41)}$$

To obtain the final power, one must deduct the losses due to bearings, seals and disk friction that sometimes can be negligible.

Ap1.6.1. Velocity Diagrams. Axial Designs.

In order to analyse the effect of blades and change of energy in the flow, velocity diagrams have been developed, so an easier analysis of the phenomenon can be done. In these diagrams, the use of absolute velocities (C, in reference of immobile parts) and relative velocities (W, relative to moving surfaces) helps to aim this purpose. An example for compressors and turbines is shown, figures Ap1.6 and Ap1.7.

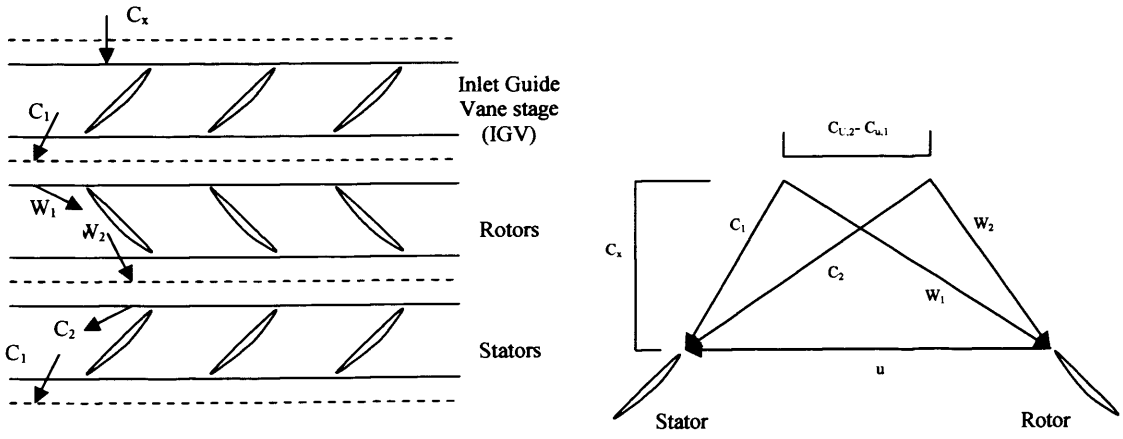

Figure Ap1.6. Axial compressor velocity diagram (Gordon et al., 1998)

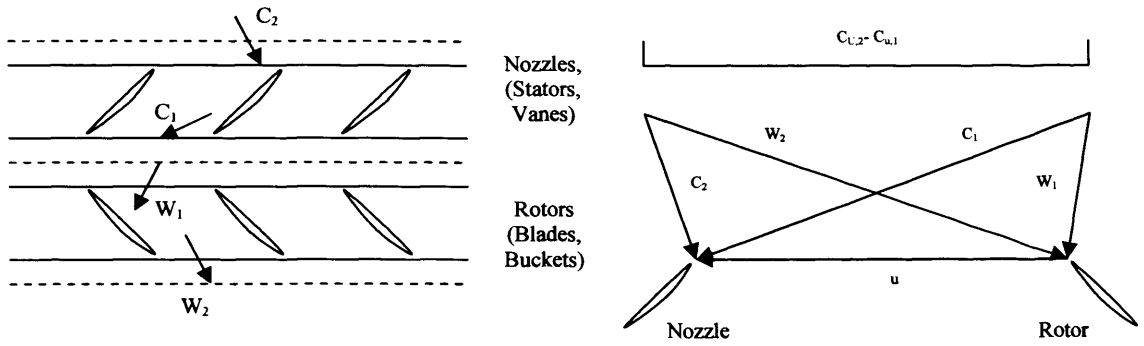

Figure Ap1.7. Axial turbine velocity diagram (Gordon et al., 1998)

α represents the angle between the velocity and the vertical line. To specify a stage velocity diagram there are 3 parameters. These are,

1. The work or loading coefficient, ψ, which specifies if the turbomachine is highly loaded (high work produced) or lightly loaded (low work produced).

$$\varphi \equiv \frac{-\Delta_1^2 h_0}{u^2} = -\left[\frac{\Delta_1^2 (uC_u)}{u^2}\right] \qquad \text{(Ap.42)}$$

2. C_u depends on the angle of the blades. Thus, the loading coefficient is a function of the attack angles. However, with the same value of ψ and a high or low value of C_x, the required flow deflection through any blade row could be low or high, respectively. So, the second parameter is known as the flow coefficient, Φ, which is constant in simple cases, and varies with the radius in more complexes ones,

$$\Phi \equiv \frac{C_x}{u} \qquad \text{(Ap.43)}$$

3. Finally, the geometric relationship of the difference of tangential velocity to the blade peripheral speed is known as the "reaction", R_n, defined as,

$$R_n \equiv \left[\frac{\Delta h_{st}}{\Delta h_0}\right]_{rr} \qquad \text{(Ap.44)}$$

Which can be equal to $1-[(C_{u,2}+C_{u,1})/2u]$ for simple velocity diagrams. This value specifies the "percentage of reaction" in a turbine or compressor, which is the change in kinetic energy to pressure.

These three parameters allow several geometric equations that can be used to study the velocity diagrams, which represent, at the same time, the shape of blades and nozzles.

Indeed, there are some concepts that apply for high swirls or efficiencies. One of them is the Zero reaction turbine, where $(C_{u,1}+C_{u,2})/2$ is equal to u. In this case, the swirl produced after the rotor is very high. These are known as zero reaction turbines because there is no expansion or acceleration of the flow and the rotor torque comes wholly from the impulse of the stream. The flow leaves the rotor with the same angle with which it enters, but with negative value for compressors. Thus, pressure seals are unnecessary. Other are the fifty percent reaction diagram (when the diagram is symmetric, due to its mirror image similarity between the blade shapes), where the polytropic efficiency of the turbine reaches its peak, with low losses. Here, the first angle and the third one are equal, as well as the second and the forth (0) ones; and the high reaction diagrams, where $C_{u,2}=-C_{u,1}$, which in compressors make the machine less sensitive to dirt. In the later case, the flow is having acceleration, losing some of the static pressure rise produced by the rotor row. In this case, the stator has a constant area with no change in velocity in compressors, and an attack angle or 0 in turbines.

Finally, the election of one or other value of these parameters has to be with the diffusion velocity ratio above which the equipment is stable. Also, the angles of the blades, or staggers, must be defined based on the performance of the turbomachine.

Ap1.6.2. Velocity Diagrams. Radial Designs

Another important consideration is the degree of freedom that can be chosen to shape the velocity diagrams, which is based strongly on the hub-shroud diameter ratio, Λ, or the ratio of the inner to the outer diameters of the blade row,

$$\Lambda \equiv \frac{d_{hb}}{d_{sh}} \qquad \text{(Ap.45)}$$

However, its value must be carefully decided, since if it approaches to 1 the total work will be done in a very thin laminar layer, reducing the efficiency of the equipment. On the other hand, a very low value could contribute to the change in velocity of the outer layer in a considerable way, reaching Mach numbers that can damage the entire system.

This value can be correlated to the peak stage efficiency through the following equation,

$$1-\Lambda^2 = 1-\left(\frac{d_{hb}}{d_{sh}}\right)^2 = \frac{d^2{}_{sh}-d^2{}_{hb}}{d^2{}_{sh}} = \frac{A_{an}}{\pi d^2{}_{sh}/4} = \frac{\dot{V}}{C_x \pi d^2{}_{sh}/4} \qquad \text{(Ap.46)}$$

$$1-\Lambda^2 = \frac{\dot{V}N^2}{\Phi u_2 (\pi d^2{}_{sh}/4)(60\omega/2\pi)^2} \qquad \text{(Ap.47)}$$

Substituting some parameters, the final equation is,

$$\sqrt{1-\Lambda^2} = \sqrt{1-\left(\frac{d_{hb}}{d_{sh}}\right)^2} = \frac{\sqrt{\pi}}{30}\frac{|\varphi|^{3/4}}{\sqrt{\Phi}}\frac{N\sqrt{\dot{V}}}{\Delta h_0{}^{3/4}} \qquad \text{(Ap.48)}$$

The most important property of the diagram is the ratio of $C_{u,2,ac}/u_2$. This ratio can be found in terms of the blades angle, β,

$$\tan\beta_2 = \frac{u_2 - C_{u,2,tl}}{C_{r,2}} \qquad \text{(Ap.49)}$$

$$\tan\alpha_{C,2} = \frac{C_{u,2,ac}}{C_{r,2}} \qquad \text{(Ap.50)}$$

Defining $\sigma_\omega \equiv \frac{C_{u,2,ac}}{C_{u,2,tl}}$ and substituting this value with the previous equations gives,

$$\left[\frac{C_{u,2,ac}}{u_2}\right] = \left\{\left[\frac{\tan\beta_2}{\tan\alpha_{C,2}}\right] + \frac{1}{\sigma_\omega}\right\}^{-1} \qquad \text{(Ap.51)}$$

At this point, the designer has to make a choice of the number of blades on the rotor and the blade angle. All these parameters will contribute to the final design of axial, or radial, turbomachines. The best selection of angles, diffusers, heat exchangers and combustors will be highly dependant on the type of work required from the mechanism. For instance, the number of stages must be based on the pressure ratio, diffusion limits, the velocities, the type of fluid, the reduction of noises, etc.

It must be remembered that the relative velocity is always measured with respect to the rotating part (the absolute moving part velocity is always added to the relative velocity).

Ap1.7. Design Facts

In the preliminary design of turbomachines, the variation of stagnation enthalpy, Δh_0, should be the same for all the stages. In more sophisticated cases this is not the case.

But let's consider a constant change. Knowing the definition of φ from eq. Ap.42, u can be changed in terms of ω and r, so the loading coefficient can be expressed as,

$$\varphi = \frac{-\Delta h_0}{\omega^2 r^2} \qquad \text{(Ap.52)}$$

This gives the maximum permissible work coefficient at the hub radius, with a lightly loaded work at the shroud.

However, every fluid with a tangential velocity will have a pressure gradient dependant on the radius, and therefore a variation of enthalpy. To avoid this, some equations must be mixed. Knowing that $C^2 = C_x^2 + C_u^2 + C_r^2$, and taking into consideration equations Ap.3, Ap.4 and Ap.7, the final formula to eliminate this degree of freedom, known as Simple Radial Equilibrium (SRE), is

$$\frac{1}{r^2}\frac{d}{dr}(r^2 C_u^2) + \frac{d}{dr}C_x^2 = 0 \qquad \text{(Ap.53)}$$

The use of this equation gives freedom to the designer to set up one of these velocity values, determining the other one. Using Euler's equation, the velocities in a second plane can be calculated, fixing the whole system and the correct drawing of velocity diagrams. A particular case is when rC_u = constant, which is related to a free vortex, making C_x = constant.

There are some prescribed criterions in the design of turbines. One is that W_2/W_1 (Haller ratio) must stay above 0.7 for axial compressors. Also, the relative Mach number must stay below 0.9 for the stator hub radius and 1.4 for the rotor shroud. Other parameters, such as the change in reaction at different points of the blade, must be taken into consideration.

Another important parameter is the swirl produced. A general form studied by Carmichael and Lewis is,

$$C_{u,1} = ar^n - b/r \qquad \text{(Ap.54)}$$

$$C_{u,2} = ar^n + b/r \qquad \text{(Ap.55)}$$

Where a, b and n are constants for any one type of swirl distribution. It is desirable to use a swirl pattern that produces and increases axial velocity towards the hub, because the loading coefficient is higher in this part. Also, it will reduce losses caused by the

flow turning required in the blading. In terms of manufacture, a nozzle blade with little twist is easier to produce. Indeed, it was found that the swirl distribution that gave nearly constant nozzle flow outlet angles also gave increased axial velocities at the hub, confirming in that way the previous assertion.

Until at least the 70's, the cost of manufacturing special blades for each stage was very high. However, the introduction of numerically controlled machining reduced the final prices, making possible the design of more efficient equipments. The use of 3D twisted blades reduced the losses in 10% (Gordon et al., 1998), introducing the radial equilibrium into axial turbomachineries. The use of complex software and programmes to design these blades has made easier this task.

Ap1.7.1. Mechanical Considerations

There are several considerations when choosing the materials and specifications of a turbomachine. In the case of gas turbines, the election of the cycle to be used is the most important. From there, there are some others that will contribute with the final cost and efficiency of the equipment.

One of them is the use of a single shaft or more. The advantages of using 2 are that the gasifier (compressor and high pressure turbine) can be separated from the "power turbine", which can work at high-torque low-speed or zero-torque high-speed. However, the price increases as well as the losses.

The number of spools and their design is another point. The use of 2 or more spools depends on the final pressure and the energy required to start up the whole system. Also, the rotor design depends on the size of the engine, with radial or axial characteristics based on the required output and the shaft speed.

The selection of the stator and the casings is based on the pressure ratios. So, the higher the pressure, the thicker the flange will be. Double casings are used for many industrial gas turbines. Also, leaving axial and radial gaps between components is a very usual custom, since the expansions and small vibrations must be mitigated in this way.

Ap1.7.1.1. Materials

A very important fact is the selection of the materials. Gas turbine designers must set the thermal parameters in accordance to the maximum temperature that the materials can resist. Almost all surfaces of modern gas turbines are coated, creating a barrier against corrosion and temperature. Casings can be made of nodular cast iron, steel or stainless steel (aluminium or titanium for aircrafts).

Other materials include stainless steel "custom 450" (stronger than AISI 403), AISI 403 with columbium, "plasmaguard" alloys, chromium (as coating), M152 alloy (12CrNiMoV steel), CrMoV steels, SA516 carbon steel, titanium blading, nickel alloys, ceramic materials such as magnesium and lithium aluminium silicates (MAS and LAS), copper graphite, flame-sprayed NiO-$BaTiO_3$, silicon nitride, whisker toughened ceramics, carbon fibre in a graphite matrix, INCO alloy 907, etc.

These materials must resist all the fatigue cycles (stress or thermal), which may vary according to the work required from the equipments. These parameters can be combined, so the final resistance and life of the material will depend on the temperature and the suffered fatigue. Large industrial engines are designed to live over 100,000 hours. Accompanied by a good material, the reduction of these unpleasant vibrations must be vital for any designer.

Another criterion in the selection is the oxidation-corrosion phenomenon. The coating is also designed to prevent this chemical reaction. If the coating is removed by dust or an abrasive process, the blade will be exposed to a hostile environment, reducing its life expectancy.

Ap1.7.2. Other Components

Ap1.7.2.1. Control Systems

The use of control systems is to safeguard the integrity of the machinery; to reduce the operator's workload and to choose optimum working points to optimize the process.

One of the most important parts is the Starting equipment, which is used to start the engines. When a single shaft machine is used, the system is started completely.

However, when a multi spool machine is activated, the starting engines will be coupled to the high pressure equipment, which is comprised by the compressor and the high pressure turbine, so the gas exhausted by the former will start the low pressure turbine recovering the work produced.

Some of these equipments use compressed air, while others use electrical motors. However, the designer must be aware that the starting (and shutting down) process requires fluids at variable temperatures, so the equipments must resist the former. In fact, some turbines are run at very low speed but high temperatures to prepare them for the load. These temperatures can be coped thanks to the low speed and the materials used.

Another mechanism is the ignition system, which used to be a "torch", but nowadays is an igniter plug that generates enough energy to start the combustion process. This plug works using a high energy spark (4-20 Joules) which is close to the primary zone of combustion.

The use of other control systems to maintain the shaft speed constant, to avoid compressor surges and to keep the turbine temperature stable has received great support in the previous years, especially because of the inclusion of electronic devices in this area, which now are capable of controlling more complex equipments.

Ap1.7.2.2. Combustion Systems

The fuel that is burned in the combustion systems usually is relative to kerosene, diesel or methane (natural gas). The latest has being used for decades and is gaining field to the other fuels due to its relative cleanliness. Natural gas produces less contaminant than other fossil fuels. However, the imposition of new laws related to environmental issues has opened the research for new combustibles capable of reducing even more the greenhouse gases and increase the efficiencies of the machineries.

Different fuels produce different flames. Nevertheless, the average speed of turbulent flames goes from 2 to 15 m/s, while the laminar ones are in the range of 0.1 to 2 m/s. If we think about the average speed of the fluid inside of the compressor and the

turbine, the average value is between 125 m/s – 200 m/s. Even though the speed will be reduced because of diffusion in the nozzle, the reduction will only achieve a sixth of the required one. Therefore, to produce a 10 m/s flame, the fluid must be stopped using baffles, which represents an inefficient process. Also, part of the air will be used to decrease the temperature in the second zone of the combustor.

One type of combustion system is the "Standard", due to its widespread use, with effective performance. However, it produces a lot of contaminants, especially NOx. The use of water or steam injection to trap the impurities can decrease the former. In these systems the fuel is mixed with part of the upstream air in a stoichiometric way. Other part of the air is used to produce a swirl which will mix the reactants, as well as reducing the contact of the products with the fuselage. The rest of this flow is used to cool the casing and decrease the gases temperatures to the inlet turbine temperature. Thus, the control of emissions is achieved thanks to the increase of time of the reactants in the flame and the reduction of nitrates due to the incoming air.

Another way to control the emission is to use an "staged" combustion, in which multiple fuel burners within a combustion chamber are brought into action successively as the temperature rises above that for rapid NOx production.

The use of lean pre-mixed systems is another alternative, which also increases the efficiency of the equipment. However, a flash back could occur due to the previous mixing of oxygen and combustible.

It is worth to mention the use of catalytic combustors, where alloys are used to produce the reaction. Nevertheless, the incoming gas must be at least at 725 K. Therefore, the use of pre-burners is essential. So, the production of contaminants takes place in this area.

Finally, the use of fluidized beds is another option. Recycled materials, bio-waste, coal, etc. can be utilised in this equipments. The bed is heated at temperatures where the bed decomposes into gases, which comprises contaminants and fuels such as methane and hydrogen. The contaminants are removed and the cleaned gas feed the combustor. Water scrubs the flue gases, which then is disposed in an ecological form.

The use of swirl equipments is another option that is taking more importance nowadays. These machines produce a swirl which mixes the air in a more effective way, reducing contaminants and increasing the fuel mixing. Therefore, the reduction in combustible is achieved and the gases produced have an adequate temperature to ingress into the turbine.

To calculate the quantities of fuel required for a process, a stoichiometric analysis must be done. According to the analysis done, the Brayton cycle is one of the more efficient, since the temperatures are high enough to produce exhaust gases that can be "recycled" to reheat the compressed ones.

In these kinds of analyses the use of the "adiabatic flame temperature" gives more details about the process. Imagine the following condition. If we have a combustor which ignites a fuel, and there is not contact or exchange with the surroundings, then the total work done and the heat transfer is equal to zero. So, the total energy exchange from the reactants to the products is equal. Thus,

$$\sum\left(\hat{n}\hat{h}\right)_{rc} = \sum\left(\hat{n}\hat{h}\right)_{pd} \qquad \text{(Ap.56)}$$

This equation must be iterated between 2 different temperatures, so the final values must be equal, giving the flame adiabatic temperature in which all the process took place. Some of the equations used to calculate the energy released by a combustor include the following formula,

$$\frac{\dot{Q}_b}{V_b} \propto \frac{p_{0,in}\sqrt{T_{0,in}}\sqrt{(\Delta p_0 / p_{0,in}}}{(l_b / d_b)d_b} \qquad \text{(Ap.57)}$$

Notwithstanding, the designer must have in mind that the final flow must be as homogeneous as possible, because the existence of great gradients of temperature can create big stresses in the blades and the shaft. Actually, the fluid gets into the turbine with a gradient, where the highest temperature is at the tip of the vanes. Therefore, the stress in the base is reduced, increasing the life of the equipment. If the case is reversed, a cooling system must be employed to prevent the failure of the rotor.

Ap1.7.2.3. Heat Exchangers

As previously mentioned, heat exchangers can increase the final efficiency of the entire cycle. Therefore, these equipments are very important in the design of new

cycles. Their behaviour is based on different analysis, where the conclusions and results of Osborne Reynolds are essential. In essence, he said that the heat transfer coefficient in certain classes of fluid flow is a simple multiple of the skin friction coefficient. Therefore, several dimensionless equations were derived from his assertions. The one that has his name is defined as,

$$\mathrm{Re} = \frac{InertiaForces}{ViscousForces} = \frac{\frac{\rho C^2}{L}}{\frac{\mu C}{L^2}} = \frac{\rho C L}{\mu} \qquad \text{(Ap.58)}$$

This number can be interpreted as the ratio of 2 forces that influence the behaviour of a fluid in its boundary layer, which is a microscopical zone close to the surface of interaction where the complicated phenomena of heat transfer take place.

It is essential to define some parameters before getting to other dimensionless parameters. First, the viscosity which is defined as,

$$\mu \equiv \frac{\tau_\omega}{(\partial C / \partial y)_\omega} \qquad \text{(Ap.59)}$$

Other parameter is the thermal conductivity coefficient, which can be inferred from the equations of thermal conductivity,

$$k \equiv \frac{\dot{Q} / A_h}{(\partial \theta / \partial y)_\omega} \qquad \text{(Ap.60)}$$

From these values, one of the dimensionless numbers is known as the Prandtl number, defined as,

$$\mathrm{Pr} \equiv \frac{C_p \mu}{k} \qquad \text{(Ap.61)}$$

It can be related to the thickness of the thermal and velocity boundary layers. It is actually the ratio of velocity boundary layer to thermal boundary layer. Another useful number is the Nusselt. Thus,

$$Nu \equiv \frac{h_t L}{k} \qquad \text{(Ap.62)}$$

The Nu can be viewed as the ratio of convection and conduction heat transfer for a layer fluid.

Finally, another non dimensional number that will be helpful for the design of heat exchangers is the Stanton Number, S_t, formed by the previous ones,

$$S_t \equiv \frac{Nu}{\mathrm{Re}\,x\,\mathrm{Pr}} \equiv \frac{h_t}{\rho C_p C} \qquad \text{(Ap.63}$$

These numbers can be expressed in terms of other non dimensional numbers. The use of the former is to characterise the exchanger and the flow in it. As a reference number, the thermal performance is always used, and it refers to the ratio of actual transferred heat to the maximum transferred heat,

$$\in_{hx} \equiv \frac{\dot{Q}}{\dot{Q}_{mx}} \qquad \text{(Ap.64)}$$

The maximum heat depends on the fluid with the smaller heat capacity, $(\dot{m}C_p)_{mn}$. Therefore, it is equal to,

$$\dot{Q}_{mx} = (\dot{m}C_p)_{mn}\theta_0 \qquad \text{(Ap.65)}$$

The actual heat transferred can be used to define an overall mean heat transfer coefficient, $\overline{U}$, a mean temperature difference, θ_m, and a mean heat transfer area $\overline{A}_h$. So,

$$\dot{Q} = \overline{U}\overline{A}_h\theta_m \qquad \text{(Ap.66)}$$

Therefore,

$$\in \equiv \frac{\dot{Q}}{\dot{Q}_{mx}} = \left[\frac{\overline{U}\overline{A}_h}{(\dot{m}C_p)_{mn}}\right]\left(\frac{\theta_m}{\theta_0}\right) \equiv N_{tu}\frac{\theta_m}{\theta_0} \qquad \text{(Ap.67)}$$

The ratio of the mean to the overall temperature difference is a function of the heat exchange flow arrangement, the N_{tu} (known as the Number of transfer units), and the ratio of the smaller heat capacity to the larger, C_{ra},

$$C_{ra} \equiv \frac{(\dot{m}C_p)_{mn}}{(\dot{m}C_p)_{mx}} \qquad \text{(Ap.68)}$$

These parameters are used to identify in different tables and graphs the effectiveness of different equipments, given the designer a better idea of the best selection. Finally, the exchanger must have the minor transversal area for the flow and the major perimeter in the tubes in order to increase the heat transfer. However, much of this work is done in previous experience, since various factors such as the flow rates and the configurations must be defined by the designer. Also, factors such as pressure

losses and materials must be specified after defining the basic parameters of the equipment of interest.

In order to increase the heat transfer, some configurations have emerged from crimped sheets to increase the surface area and reduce the transversal one. Nevertheless, the use of the more common shapes for the tubes, such as triangles, squares, rectangles and circles, has predominated in the recently years designs.

Ap1.7.2.4. Turbine Blade Cooling

As mentioned previously, one of the major problems in the current design of turbines is the resistance of the materials in the expander. Higher temperatures would give greater efficiencies, but the thermal resistance of the blades can not support temperatures over 1500 – 1700 K alone.

For this reason, the use of cooling inside of the blades has given the advantage of constructing more powerful equipments, since these devices help to reduce thermal stresses and the superficial temperature of the blades. The increase of temperature in the cycles during the last 40 years has been of 20 K per year thanks to the use of these cooling systems.

These can be designed to use air with a mass exchange. In this case, pressurised air at relative low temperature is injected into a web of labyrinths inside of the blade. Small perforated holes are placed in strategic positions of the blade where the temperatures reach a peak. Then, the air is released from these holes, which are parallel to the surface to avoid the generation of great turbulences. Thus, the surface is cooled, while the blade transfers heat to the incoming air that is in the labyrinths. The use of water has not been successful since the temperatures convert it into its critical state. Heat has been another solution because this vapour has better characteristics than air. Research has been done in this field during the last years in order to improve the heat exchange.

APPENDIX 2

PUBLICATIONS, CONFERENCES

AP2. 1. List of Publication and Conferences done as an outcome of this thesis.

Ap2.1.1. Conferences

- Valera-Medina A., Syred N., Griffiths A. "Characterisation of Large Coherent Structures in a Swirl Burner". 46th AIAA Aerospace Sciences Meeting 2008, 6th-10th January, Reno, USA Ref. AIAA 2008-1019.
- Valera-Medina A., Syred N., Griffiths A. "Visualization of Large Coherent Structures in a Swirl Burner", 14th International Symposium in Laser Techniques in Fluids Mechanics, 2008, 7th-10th July, Lisbon, Portugal.
- Valera-Medina A., Syred N., Griffiths A. "Recognition of Large Coherent Structures in a Tangential Swirl Burner", 3rd International Conference on Heat and mass transfer and hydrodynamics in swirling flows, 21-23 October 2008, Moscow, Russia.
- Valera-Medina A., Syred N., Griffiths A. "Characterization of Large Coherent Structures in a Swirl Burner under Combustion Conditions", 47th AIAA Aerospace Sciences Meeting 2009, 5th-9th January, Orlando, USA, Ref. AIAA 2009-646.
- Valera-Medina A., Abdulsada M., Syred N., Griffiths A. "Flashback Avoidance Analysis using Geometrical Constrictions in a Tangential Swirl Burner", British-French Flame Joint Meeting, 2009, 9th-10th March, Lille, France.
- Valera-Medina A., Abdulsada M., Shelil N., Syred N., Griffiths A. "Flashback Analysis in Swirl Burners using Passive Nozzle Constrictions and Different Fuels" for the IFRF International Meeting, 2009, 8th-10th June, Boston, USA.

Ap2.1.2. Publications

- Final Submission (3rd Version) of the paper "Visualization of Isothermal Large Coherent Structures in a Swirl Burner" to the journal 'Combustion and Flame', February 2009. Ref. CNF-D-08-00301R1.
- Submission of the paper "Effects of Swirl Number, Reynolds Number, Geometry and Equivalence Ratio upon Large Coherent Structures in a Swirl Burner" to the journal 'Fuel', September 2008. Ref. JFUE-D-08-00734.

- Submission of the paper "Flame Stabilization and Flashback Avoidance using Passive Nozzle Constrictions" to the 'International Journal of Hydrogen Energy', June 2009.
- Submission of the paper "Numerical and Experimental Study of Large Coherent Structures in a Swirl Burner under Combustion" to the journal 'Combustion and Flame', June 2009.
- Preparation of the paper "Numerical and Experimental Analysis of Flashback in Swirling Combustors" for the journal 'Combustion and Flame' or 'Fuel', 2009.

REFERENCES

American Institute of Aeronautics and Astronautics. 2007. *Air and Space, Year in Review*. Aerospace America 45 (12), pp. 11-12.

Al-Abdeli, Y. and Masri, A. 2007. Turbulent swirling natural gas flames: stability characteristics, unsteady behaviour and vortex breakdown. *Combustion Science and Technology* 179, p.p. 207-225.

Albrecht, P., Bade, S., Paschereit, C. and Gutmark, E. 2008. Avoidance Strategy for NO_x emissions and Flame Instabilities in a Swirl-stabilized combustor. *46th AIAA Aerospace Sciences Meeting and Exhibit.* January 5th-9th, Reno, USA, ref. AIAA-2008-1059.

Aleseenko, S., Kuibin, P., Okulov, V. and Shtork, S. 1999. Helical vortex in swirl flow. *Journal of Fluid Mechanics* 382, p.p. 195-243.

ALSTOM. 2006. *EU OPEC Roundtable* [Online]. Available at: http://www.opec.org/home/Press%20Room/EU-OPEC%20presentations/David%20Pollard%20-%20Presentation.pdf [Accessed: 31 October 2006]

Andover Corporation. 2008. *Quality Optical Filters* [Online]. Available at: http://www.andovercorp.com/Web_store/pdf/Andover_catalog.pdf [Accessed: 21 August 2008]

Angello, L. and Castaldini, C. 2004. Combustion Tuning Guidelines: understanding and mitigating dynamic instabilities in modern gas turbine combustors. *Proceedings of the ASME Turbo Expo 2004* 5A, p.p. 81-85.

Arias, B., Fermoso, J., Plaza, M., Pevida, C., Rubiera, F., Pis, J., Garcia-Pena, F. and Casero P., 2008. Production of H2 by Co-gasification of Coal with biomass and petroleum coke. *Proceedings of 7th European Conference on Coal Research and Its Applications*. September 3rd-5th, Wales, UK.

Avenell, C., Sainz-Diaz, I., Griffiths, A. 1996. Solid waste pyrolysis in a pilot scale batch pyrolyser. *Fuel* 75 (10), pp. 1167-1174.

Baba-Ahmady, H. and Tabor, G. 2008. Inlet Conditions for Large Eddy Simulation of Gas-Turbine Swirl Injectors. *AIAA Journal* 46 (7), pp. 1782-1790.

Badeshia, H. 2006. *University of Cambridge. Nickel Based Superalloys* [Online]. Available at: http://www.msm.cam.ac.uk/phase-trans/2003/Superalloys/superalloys.html [Accessed: 26 October 2006]

Bagdanavicius, A., Bowen, P., Syred, N., Kay, P., Crayford, A. and Wood, J. 2009. Burning Velocities of Alternative Gaseous Fuels at Elevated Temperature and Pressure. *47th AIAA Aerospace Sciences Meeting.* 6th-10th January, Orlando, USA, ref. AIAA-2009-0229.

Balsone, S. 2004. Nickel superalloy material technology for advanced IGT applications. *Proceedings of the International Symposium on Niobium for High Temperature Applications*, January, Warrendale, USA, pp. 3-9.

Barmina, I., Desnickis, A., Meijere, A. and Zake, M. 2007. Active Electric Control of Emissions from Swirling Combustion. *Advanced Combustion and Aerothermal Technologies, NATO Science for Peace and Security Series*, Springer, pp. 405-412.

Baukal, C. 1998. *Oxygen-Enhanced Combustion*, Air Products, U.S.A., p.p. 350.

Beer, J. and Chigier, N.A., 1972. *Combustion Aerodynamics*. Applied Science Publishers LTD, London.

Beer, J. and Syred, N. 1974. Combustion in Swirling Flows: a Review, *Combustion and Flame* 23, pp.143-201.

Belzer, D., Scott, M. and Sands, R. 1996. Climate change impacts on U.S. commercial building energy consumption: An analysis using sample survey data. *Energy Sources* 18 (2), pp. 177-201.

Bellows, B., Bobba, M., Forte, A., Seitzman, M. and Lieuwen, T. 2007. Flame Transfer Function saturation mechanisms in a swirl stabilized combustor. *Proceeding of the Combustion Institute* 31, pp. 3181-3188.

Berenbrink, D. and Hoffmann, S. 2000. Suppression of Combustion Dynamics by Active and Passive Means. *ASME Gas Turbine Expo*, May 8th-11th May, Munich, Germany, ref. 2000-GT-0079.

Bouremel, Y., Yianneskis, M. and Ducci, A. 2008. Vorticity and Strain Dynamics for Vortex Ring Mixing Process. *Proceedings 14th Int. Symp. on Applications of Laser Techniques to Fluid Mechanics*, July, Lisbon, Portugal.

Boxx, I., Blumenthal, R., Stohr, M. and Meier, W. 2009. Investigation of a Gas Turbine Model Combustor by means of High-Speed Laser Imaging. *47th AIAA Aerospace Sciences Meeting*. 6th-10th January, Orlando, USA, ref. AIAA-2009-0644.

Bradley, D., Gaskell, P., Gu, X., Lawes, M. and Scott, M. 1998. Premixed turbulent flame instability and no formation in a Lean Burn Swirl Burner. *Combustion and Flame* 115, pp. 515-538.

Briones, A., Mukhopadhyay, A. and Aggarwal, S. 2009. Analysis of Entropy Generation in Hydrogen-Enriched Methane-Air Propagation Triple Flame. *47th AIAA Aerospace Sciences Meeting*. 6th-10th January, Orlando, USA, ref. AIAA 2009-1394.

Brundish, K., Miller, M., Morgan, L. and Wheatley, A. 2007. Variable Fuel Placement Injector Development. *Advanced Combustion and Aerothermal Technologies, NATO Science for Peace and Security Series*, Springer, pp. 425-444.

Buzek, J. 2006. *The European Technology Platform for Zero Emission Fossil Fuel Power Plants (ZEP)*, Brussels, pp. 17.

CAME-GT. 2005. *EC RTD Framework Programme FP7* [Online]. Available at: http://www.came-gt.com/docs/EC%20FP7%20Consultation.pdf
[Accessed: 23 October 2006]

Cala, E., Fernandes, C., Heitor, M. and Shtork, S. 2006. Coherent Structures in unsteady swirling jet flow. *Experiments in Fluids* 40, pp. 267-276.

Candel, S. 2002. Combustion Dynamics and Control: Progress and Challenges. *Proceedings of the Combustion Institute* 29, USA, pp. 1-28.

Channel 4, BBC. 2007. *The Great Global Warming Swindle* [Online]. Available at: http://www.channel4.com/science/microsites/G/great_global_warming_swindle/inde.html [Accessed: 09 March 2007].

Chen, Z., Li, Z., Wang, F., Jing, J., Chen, L. and Wu, S. 2008. Gas/Particle flow characteristics of a centrally fuel rich swirl coal combustion burner. *Fuel* 87, pp. 2102-2110.

Claypole, C. 1980. *Pollutant Formation in Swirling Jets.* PhD Thesis, Cardiff University, Wales, UK.

Claypole, T. and Syred, N. 1981. Integration of swirl burners with furnaces for the combustion of Low Calorific Value gases. *IMechE Conference publications, International Conference on Combustion in Engineering* 2, 19th-20th May, Birmingham, UK, pp. 139-145.

Claypole, T. and Syred, N. 1984. Optimisation of a swirl burner/furnace system for Low Calorific Value fuels. *Energy Conservation in Industry, Proceeding of the International Seminar* 1, Duesseldorf, West Germany, pp. 316-324.

Coghe, A., Solero, G. and Scribano G. 2004. Recirculation phenomena in a natural gas swirl combustor. *Experimental Thermal and Fluid Science* 28, pp. 709–714.

Commission of European Communities. 2005. Framework *Directive in the field of water policy.* [Online]. Available at: http://europa.eu/scadplus/leg/en/lvb/l28002b.htm [Accessed: 26 October 2006]

Commission of European Communities. 2005. Proposal for a Directive of the European Parliament and of the Council on ambient air quality and cleaner air for Europe [Online]. Available at: http://ec.europa.eu/environment/air/cafe/pdf/cafe_dir_en.pdf [Accessed: 26 October 2005]

Coppens, F.H.V. and Konnov, A.A. 2008. The effects of enrichment by H_2 on propagation speeds in adiabatic flat and cellular premixed flames of $CH_4 + O_2 + CO_2$. *Fuel* 87, pp. 2866-2870.

Dam, N.J. 2008. *Laser Diagnostics in Flames, Course of Advanced Combustion.* Netherlands, Technische Universiteit Eindhoven, pp. 235-280.

DANTEC. 2005. *LIF Application Guide in Gas and Combustion Processes.* Dantec Dynamics Publications, pp. 81.

DANTEC. 2006. *Measurement Principles of PIV.* [Online]. Available at: http://www.dantecdynamics.com/piv/princip/index.html [Accessed: 30 October 2006]

Davidson, P. 2004. *Turbulence: an introduction for Scientists and Engineers.* Oxford University Press, United Kingdom.

Dawson, J. 2000. *An investigation into naturally excited Helmholtz oscillations in a swirl burner/furnace system.* PhD Thesis, Cardiff University, Wales, UK.

Dawson, J., Rodriquez-Martinez, V., Syred, N. and O'Doherty, T. 2005. The Effect of Combustion Instability on the Structure of Recirculation Zones in Confined Swirling Flames. *Combustion Science and Technology Journal* 177 (12), pp. 2341-2371.

DEFRA. 1999. *Climate Change and its Impacts.* Hadley Centre, Met Office, UK.

DISA. 1995. Type 55M10 Instruction Manual. DISA Information Department, pp. 23.

DTI. 2003. *Energy White Paper "Our Energy future – creating a low carbon economy"*. The Stationary Office, UK.

Emiris, I. and Whitelaw, J. 2003. Control of Combustion Oscillations. *Combustion Science and Technology* 175 (1), pp. 157-184.

Escudier, M. and Keller, J. 1985. Recirculation in Swirling Flow: A manifestation of Vortex Breakdown. *American Institute of Aeronautics and Astronautics Journal* 23 (1), pp. 111-116.

ETUC. 2006. *Resolution adopted by the ETUC Executive Committee.* [Online]. Available at: http://www.etuc.org/a/2964 [Accessed: 25 October 2005].

European Commission. 2006. *Research Themes in FP7.* [Online]. Available at: http://ec.europa.eu/research/future/themes/index_en.cfm [Accessed: 25 October 2005].

European Parliament and the Council of the European Union. 2001. Directive 2001/77/EC. *Official Journal of the European Communities* L 283/33, 27.10.2001.

Fang, A. 2005. Experimental investigation of air humidified combustion gas turbine combustor. *Journal of Engineering Thermophysics* 26 (4), pp. 713-716.

Farber, J., Koch, R., Bauer, H., Krebs, W. and Hase, M. 2008. The Effects of Piloting and Liner Boundary Conditions on Flame Locations and Stability Margins of an Industrial Size Premixed Flame. *Proceedings 8th European Conference on Industrial Furnaces and Boilers*, 25th-28th March, Estoril, Portugal.

Fick, W. 1998. *Characterisation and Effects of the Precessing Vortex Core.* PhD Thesis, Cardiff University, Wales, UK.

Fick, W., Griffiths, A. and O'Doherty, T. 1997. Visualization of the precessing vortex core in an unconfined swirling flow. *Optical Diagnostics in Engineering* 2 (1), pp. 19-31.

Fick, W., Syred, N., Klinge, T., Griffiths, A., O'Doherty, T. 1998. Clean and efficient combustion of simulated low-calorific-value gases in swirl burner/furnace systems. *Journal of the Institute of Energy* 71 (486), pp. 12-20

Free Patents Online. 2006. *Swozzle*. [Online]. Available at: http://www.freepatentsonline.com/6438961.html [Accessed: 05 January 2007]

Freitag, M., Kleina, M., Gregora, M., Geyera, D., Schneidera, C., Dreizlera, A. and Janicka, J. 2006. Mixing analysis of a swirling recirculating flow using DNS and experimental data. *International Journal of Heat and Fluid Flow* 27 (4), pp. 636-643.

Froud, D. 1992. *An investigation of the Flow Patterns in a 2MW Swirl Burner*. MSc Dissertation, University of Wales, Wales, UK.

Froud, D., O'Doherty, T. and Syred, N. 1995. Phase Averaging of the Precessing Vortex Core in a Swirl Burner under Piloted and Premixed Combustion Conditions. *Combustion and Flame* 100 (3), pp. 407-412.

GE Aviation. 2006. *Engines.* [Online]. Available at: http://www.geae.com/engines/index.html [Accessed: 14 December 2006].

General Electric. 2006a. *GE10-1 Gas Turbine*. [Online]. Available at: http://www.gepower.com/businesses/ge_oilandgas/en/prod_serv/prod/gas_turbine/en/ge10_1.htm [Accessed: 17 October 2006].

General Electric. 2006b. *Oil and Gas.* [Online]. Available at: http://www.gepower.com/businesses/ge_oilandgas/en/downloads/gas_turb_cat.pdf [Accessed: 17 October 2006].

General Electric. 2006c. *H System, the most advanced combined cycle technology* [Online]. Available at: http://www.gepower.com [Accessed: 24 October 2006].

Georgia Institute of Technology, Research News. 2006. *Pulse Combustion.* [Online]. Available at: http://gtresearchnews.gatech.edu/reshor/rh-sf99/t-pulse.html [Accessed: 30 October 2006].

Giezendanner, R., Keck, O., Weigand, P., Meier ,W., Meier, U., Stricker ,W. and Aigner M. 2003. Periodic Combustion Instabilities in a Swirl Burner Studied by Phase Locked Planar Laser Induced Fluorescence. *Combustion Science and Technology* 175, pp. 721-741.

Global Energy Equipt. 2006. *GE Frame 5 Dual Fuel Combined Cycle.* [Online]. Available at: http://www.globalenergyequipment.com/global2.nsf/WebAllByNumber/29318?Open document [Accessed: 30 October 2006].

Goldmeer, J., Sanderson, S., Myers, G., Stewart, J. and D'Ercole, M. 2005. Passive control of dynamic pressure in a dry, low NOx combustion system using fuel gas circuit impedance optimization. *Proceedings of the ASME Turbo Expo* 2, 6th-9th June, Reno, USA, ref. GT2005-68605, pp. 453-460.

Gordon, D. and Karakianitis, T. 1998. *The Design of High efficiency Turbomachinery and Gas Turbines*, 2nd edition, Prentice Hall.

Gordon, O. 1997. *Aerothermodynamics of Gas Turbine and Rocket Propulsion.* 3rd Edition, AIAA Series, USA.

Greenberg, S., McDonald, N.K., Weakley, C.K. and Kendall, R.M. 2005. Surface Stabilized Fuel Injectors with Sub three ppm NO_x Emissions for a 5.5 MW Gas Turbine Engine. *Journal of Engineering for Gas Turbines and Power* 127 (2), pp. 276-285.

Griebel, P., Boschek, E. and Jansohn, P. 2007. Lean blowout limits and NOx emissions of turbulent, lean premixed, hydrogen-enriched methane/air flames at high pressure. *Journal of Engineering for Gas Turbines and Power* 129, pp. 404-410.

Griffiths, D., Stirling, W.D. and Weldon, L. 1998. *Understanding Data: principles and practice of statistics*, Wiley..

Grossmann, F., Monkhouse, P., Ridder, M. and Wolfrum, J. 1996. Temperature and Pressure dependences of the Laser-Induced Fluorescence of gas phase acetone and 3-pentone, *Applied Physics B* 62, pp. 249-253.

Gupta, A. 1979. Combustion instabilities in swirling flames, *Gas Waerme GmbH International* 28, pp. 55-66.

Gupta, K., Beer, J. and Swithenbank, J. 1976. Concentric multi-annular swirl burner - Stability limits and emission characteristics. *16th Symposium on Combustion (International)*, 15th-20th August, Massachusetts, USA, pp. 79-91.

Gupta, A., Ramavajjala, M., Marchionna, N. and Chomiak, J. 1991. Burner geometry effects on combustion and NO_x emission characteristics using a variable geometry swirl combustor. *Journal of Propulsion and Power* 7, pp. 473-480.

Guyot, D., Borgia, P.T., Paschereit, C. and Raghu, S. 2008. Active Control of Combustion Instabilities Using a Fluid Actuator, *46th AIAA Aerospace Sciences Meeting and Exhibit*. January 5th-9th, Reno, USA, ref. 2008, AIAA 2008-1058.

Harman, R. *Gas Turbine Engineering, Applications, Cycles and Characteristics*. The Macmillan Press, Hong Kong.

Herzog, R., Warnken, N. and Slembach, I. 2006. Integrated approach for the development of advanced, coated gas turbine blades. *Advanced Engineering Materials* 8 (6), pp. 535-562.

Hsu, K. and Goss, P. 1998. Characteristics of a Trapped-Vortex Combustor. *Journal of Propulsion and Power* 14 (1), pp. 57-65

Huang, Y. and Yang, V. 2005. Modelling and Control of Combustion Dynamics in Lean Premixed Swirl Stabilized Combustors. *Proceeding of 6th Symposium on Smart Control of Turbulence*. Japan, pp. 1-21.

Hubschmid, W., Bombach, R., Inauen, A. and Guther, F. 2008. Thermoacoustically driven flame motion and heat release variation in a swirl sabilized gas turbine burner investigated by LIF and Chemiluminescence. *Experiments in Fluids* 45, pp. 167-182.

Ilbas, M., Crayford, P.A., Yilmaz, I., Bowen, P. and Syred, N. 2006. Laminar-burning velocities of hydrogen-air and hydrogen-methane-air mixtures: An experimental study. *International Journal of Hydrogen Energy* 31 (12), pp. 1768-1779.

International Energy Agency. 2006. *Optimising Russian Natural Gas.* [Online]. Available at: http://www.iea.org/textbase/npsum/opt_russ_gas.pdf [Accessed: 13 December 2006].

International Power Generation. 2006. *Baglan Bay Begins.* [Online]. Available at: http://www.gepower.com/about/press/en/articles/ipg_article_baglan_bay.pdf [Accessed: 24 October 2006]

IPCC. 2006a. *Climate Change 2001: Synthesis Report.* [Online]. Available at: http://www.ipcc.ch/pub/SYRspm.pdf [Accessed: 23 October 2006].

IPCC. 2006b. *Carbon Dioxide Capture and Storage, Special Report.* [Online]. Available at: http://arch.rivm.nl/env/int/ipcc/pages_media/SRCCS-final/ccsspm.pdf [Accessed: 12 October 2006].

IPCC. 2007. *Climate Change 2007: The physical science basis. Summary for Policymakers*. Switzerland, pp. 18.

IPCS INCHEM, 2006. *Carbon Monoxide.* [Online]. Available at: http://www.inchem.org/documents/ehc/ehc/ehc013.htm [Accessed: 2 January 2007].

Jakirlic, S., Hanjalic, K. and Tropea, C. 2002. Modelling Rotating and Swirling Turbulent Flows, A Perpetual Challenge. *AIAA Journal* 40 (10), pp. 1984-1997.

Jochmann, P. 2006. Numerical simulation of a precessing vortex breakdown. *International Journal of Heat and Fluid Flow* 27, pp. 192-203.

Jones, B. 2006. *Gas Turbine Fuel Flexibility for a Carbon Constrained World,* General Electric, Workshop on Gasification Technologies, Bismarck, ND, pp. 29.

John, J. and Haberman, W. 1980. Introduction to Fluid Mechanics, 2nd editions, Prentice Hall, USA.

Jorgensen, E. 2005. *How to measure turbulence with Hot Wire Anemometers-a practical guide*. Dantec Dynamics, Denmark.

Keller, J. and Hongo, I. 1990. Pulse Combustion: the mechanisms of NO_x production. *Combustion and Flame* 80 (3-4), pp. 219-237.

Kiesewetter, F., Konle, M. and Sattelmayer, T. 2007. Analysis of Combustion Induced Vortex Breakdown Driven Flame Flashback in a Premix Burner with Cylindrical Mixing Zone. *Journal of Engineering for Gas Turbines and Power* 129, pp. 929-236

Khalatov, A. and Syred, N. 2006. Generation and alleviation of combustion instabilities in Swirling Flow. *Advanced Combustion and Aerothermal Technologies, Proceedings of the NATO*, pp. 3-20.

Koeneke, C. 2004. Keeping the dry Low NO_x flame alive. *Turbomachinery International* 45 (4), pp. 20-22.

Krebs, W., Flohr, P., Prade, B. and Hoffmann, S. 2002. Thermoacoustic stability chart for high intensity gas turbine combustion systems. *Combustion Science and Technology* 174 (7), pp. 99-128.

Kroner, M., Fritz, J. and Sattelmayer, T. 2003. Flashback Limits for Combustion Induced Vortex Breakdown in a Swirl Burner. *Journal of Engineering for Gas Turbines and Power* 125, pp. 693-700.

Kroner, M., Sattelmayer, T., Fritz, J., Keisewetter, F. and Hirsch, C. 2007. Flame propagation in Swirling Flows-Effects of Local extinction on the Combustion Induced Vortex Breakdown. *Combustion Science and Technology* 179, pp. 1385-1416.

Kuhn, S., Wagner, C. and von Rohr, P. 2006. Influence in wavy surfaces on coherent structures in a turbulent flow, *Experiments in fluids* 43 (2), pp. 20-28.

Kuper, W. 1999. Catalytic combustion concept for gas turbines, *Catalysis Today* 47 (1), pp. 377-389.

La Vision. 2006. *FlowMaster, Advanced PIV systems for Quantitative Flow Field Analysis.* [Online]. Available at: www.lavisioninc.com
[Accessed: 12 December 2006].

Lacarelle, A., Moeck, J. and Paschereit, C.O. 2009. Dynamic Mixing Model of a Premixed Combustor and Validation with Flame Transfer Fuction Measurement. *47th AIAA Aerospace Sciences Meeting.* 6th-10th January, Orlando, USA, ref. AIAA-2009-0986.

Lafay, Y., Taupin, B., Martins, G., Cabot, G., Renou, B. and Boukhalfa, A. 2006. Experimental study of biogas combustion using a gas turbine configuration. *Experiments in fluids* 43 (2-3), pp. 112-128.

Lamnaouer, M., Petersen, E. and Laster, R. 2007. *Flashback Analysis for ULN Hydrogen Enriched Natural Gas Mixtures.* Department of Mechanical Engineering, University of Central Orlando. [Online]. Available at:
www.clemson.edu/scies/UTSR/FellowLamnaouerSUM.pdf
[Accessed: 01 November 2008].

Lang, W., Poinsot, T., Bourienne, F., Candel, S. and Esposito, E. 1987. Active Control of Combustion Instabilities. *Combustion and Flame* 70 (3), pp. 281-289.

Lavoie, P., Avallone, G., De Gregorio, F., Romano, G. and Antonia, R. 2007. Spatial resolution of PIV for the measurement of turbulence. *Experiments in Fluids* 43 (1), pp. 39-51.

Layne, A. 2000. *Advanced Turbine Systems*. 1st edition, National Energy Technology Laboratory, USA.

Law, C.K. 1989. Dynamics of Stretched Flames, *22nd Symposium (International) on Combustion*, Pittsburgh, USA, pp.1381-1402.

Lee, S., Seo, S., Broda, J., Pal, S. and Santoro, R. 2000. An experimental estimation of mean reaction rate and flame structure during combustion instability in a lean premixed gas turbine combustor. *Proceedings of the Combustion Institute* 28, pp. 775–782.

Lenze, M. and Carroni, R. 2007. *Public Summary Report of ENCAP deliverable D.23.3 Report on limits of current burner using H2-rich fuel mixtures*. [Online]. Available at: www.encapco2.org [Accessed: 01 December 2008].

Lieuwen, T., McDonell, V., Petersern, E. and Santavicca, D. 2008. Fuel Flexibility Influences on Premixed Combustor Blowout Flashback, Autoignition and Stability. *Journal of Engineering for Gas Turbines and Power* 130, ref. 011506.

Lieuwen, T. and Yang, V. 2005. *Combustion Instabilities in Gas Turbine Engines*, AIAA, Progress in Astronautics and Aeronautics, vol. 210, USA.

Lieuwen, T. and Zinn, B. 1998. The role of equivalence Ratio Oscillations in Driving Combustion Instabilities in Low NO_x Gas Turbines. *27th Symposium (International) on Combustion* 2, Pittsburgh, USA, pp. 1809-1816.

Liu, Z., Jiao, J., Zheng, Y., Zhang, Q. and Jia, L. 2006. Investigation of Turbulence Characteristics in a Gas Cyclone by Stereoscopic PIV, *AIChE Journal* 52 (12), pp. 4150-4160.

Malalasekera, W., Ranga-Dinesh, K.K.J., Ibrahim, S.S. and Masri, A.R. 2008. LES of Recirculation and Vortex Breakdown in Swirling Flames. *Combustion Science and Technology* 180, pp. 809-832.

Mansour, A., Benjamin, M., Straub, D. L. and Richards, G. A. 2001. Application of Macrolamination technology to lean, premixed combustion. *Journal of Engineering for Gas Turbines and Power* 123 (4), pp. 796-802.

Markides, C. and Mastorakos, E. 2008. Flame Propagation following the Autoignition of Axisymmetric Hydrogen, Acetylene and Normal Heptane Plumes in Turbulent Coflows of Hot Air. *Journal of Engineering of Gas Turbine and Power* 130, ref. 011502.

Matta, R., Mercer, G. and Tuthill, R. 2000. *Power Systems for the 21st Century-"H" gas turbines for combined cycles. General Electric Power Systems.* [Online]. Available at: http://www.gepower.com/prod_serv/products/tech_docs/en/downloads/ger3935b.pdf [Accessed: 24 October 2006].

Meier, W., Weigand, P., Duan, X.R. and Giezendanner-Thoben, R. 2007. Detailed characterization of the dynamics of thermoacoustic pulsations in a lean premixed swirl flame. *Combustion and Flame* 150, pp. 2-26.

Miller, S. 2004. Next Generation combustors achieve sub 9-ppm NO_x, *Diesel and Gas Turbine Worldwide* 36 (5), pp. 50-51.

Mongia, H., Cai, J., Fu, Y. and Flohren, N. 2007. Experimental Study on coherent structures of a counter-rotating multi-swirler cup. *Collection of technical papers 43rd AIAA/ASME/SAE/ASEE* 7, pp. 6594-6604.

Morgan, D. J., Woycenko, D. M. and Van de Kamp, W. L. 1995. Effect of scale and scaling criteria on the Performance of Swirl Stabilised Pulverised Coal Burners in the Thermal Input range 2.5-12 MW: results of the AP25 investigations. *International flame Research Foundation Document IFRF F37/y/34.*

Mourtazin, D. and Cohen, J. 2007. The effect of buoyancy on vortex breakdown in a swirling jet. *Journal of Fluid Mechanics* 571, pp. 177-189.

Nag, P., Wu, J., Abou-Jaoude, K., LaGrow, M., Rising, B., Mumford, S. and Engel, J. 2007. LNG Interchangeability in Land Based Gas Turbines: The Siemens Approach. *Proceedings of Power 2007*, ref. POWER2007-22094.

Nave R. 2008. *Interference Filters, Hyperphysics.* [Online]. Available at: http://hyperphysics.phy-astr.gsu.edu/Hbase/phyopt/intfilt.html [Accessed: 21 August 2008].

Nori, V. and Seitzman, J. 2008. Evaluation of Chemiluminescence as a Combustion Diagnostic under Varying Operation Conditions, *46th AIAA Aerospace Sciences Meeting and Exhibit.* January 5th-9th, Reno, USA, ref. AIAA 2008-953.

Oak Ridge National Laboratory. 2006. *ATS Materials Manufacturing.* [Online]. Available at: http://www.ms.ornl.gov/programs/energyeff/ats/matman.htm [Accessed: 26 October 2006].

O'Doherty, T., Biffin, M. and Syred, N. 1992. The use of tangential off takes for energy savings in process industries. *Proc. Institute Mech. Engineers Part E: Journal of Process Mechanical Engineering* 206, pp. 99-109.

O'Doherty, T. and Gardner, R. 2005. Turbulent Length Scales in an Isothermal Swirling Flow, *The 8th Symposium on Fluid Control, Measurement and Visualization,* 22nd-25th August, Chengdu, China, pp. 6.

Ogawa, K., Gotoh, N. and Shoji, T. 2002. Growth Kinetics of thermally grown oxide in thermal barrier coatings. *Advanced Materials and Processed for Gas Turbines 2002*, pp. 187-195.

OMEGA Aviation in a sustainable World. 2008. *International Conference on Alternative Fuels, 24-26 November*. [Online]. Available at: http://www.omega.mmu.ac.uk/international-conference-on-alternative-fuels.htm [Accessed: 27 November 2008].

Panduranga, A., Sujith, R. and Chakravarthy, S. 2006. Swirler Flow Field Characteristics in a Sudden Expansion Combustor Geometry. *Journal of Propulsion and Power* 22 (4), pp. 800-808.

Paschereit, C. and Gutmark, E. 2006. Control of high-frequency thermo-acoustic pulsations by distributed vortex generators. *AIAA Journal* 44 (3), pp. 550-557.

Paschereit, C. and Gutmark, E. 2008. Enhanced Stability and Reduced Emissions in an Elliptic Swirl-Stabilized Burner. *AIAA Journal* 46(5), pp. 1063-1071.

Paul Schrrer Institut, Switzerland. 2002. *Combustion Research: Combustion Diagnostics.* [Online]. Available at: http://cdg.web.psi.ch/ [Accessed: 21 August 2008].

Paulonis, D.F. 2001. Alloy 718 at Pratt & Whitney – Historical perspective and future challenges. *Proceedings of the International Symposium on Superalloys and Various Derivatives* 1, June 17th-20th, Canada, pp. 13-23.

Pendley, G. 2002. High Speed Imaging Technology Yesterday, Today and Tomorrow. *Proceedings of the SPIE - The International Society for Optical Engineering* 4948, pp. 110-113.

PEW Center, Global Climate Change. 2006a. *The Greenhouse Effect.* [Online]. Available at: http://www.pewclimate.org/global-warming-basics/facts_and_figures/greenhouse.cfm [Accessed: 12 October 2006].

PEW Center, Global Climate Change. 2006b. *CO2 emissions from fossil fuel combustion and land use change.* [Online]. Available at: http://www.pewclimate.org/global-warming-basics/facts_and_figures/co2_emissions.cfm [Accessed: 12 October 2006].

Pope, S. 2000. *Turbulent Flows*. Cambridge University Press, UK.

Power Clean, CO2NET and CAME-GT. 2004. *Strategy for Sustainable power generation from fossil fuels*. [Online]. Available at: http://www.co2net.eu/public/brochures/EC%20Network%20Common%20Strategy%20FINAL%2020Nov04.pdf [Accessed: 17 November 2006].

PowerNet. 2006. *The European Technology Platform for Zero Emission Fossil Fuel Power Plants (ZEP)*. Strategic Research Agenda, pp. 46.

Raffel, M., Willert, C.E. and Kompenhans, J. 1998. *Particle Image Velocimetry: a practical guide.* Spinger-Verlag, Berling, Heidelberg.

Regunath, G. 2008. *Measurement and Investigation of Helicity in Turbulent Swirling Flow*. PhD Thesis, University of Sheffield, England, UK.

Roux, S., Lartigue, G., Poinsot, T., Meier, U. and Bérat, C. 2005. Studies of mean and unsteady flow in a swirled combustor using experiments, acoustic analysis and large eddy simulations. *Combustion Flame* 141, pp. 40–54.

Sadanandan, R., Stohr, M. and Meier, W. 2008. Simultaneous OH-PLIF and PIV measurements in a gas Turbine model Combustor. *Applied Physics B* 90, pp. 609-618.

Sadiki, A., Maltseva, A., Wegnera, B., Flemminga, F., Kempfa, A. and Janickaa, J. 2006. Unsteady Methods (URANS and LES) for simulation of combustion systems. *International Journal of Thermal Sciences* 45 (8), pp. 760-773.

Schildmacher, K.U., Koch, R., Krebs, W., Hoffmann, S. and Willig, S. 2002. Experimental Investigation of Unsteady Flow Phenomena in High Intense Combustion Systems, *Proceedings of the 6th European Conference on Industrial Furnaces and Boilers*, Estoril, Portugal, 2002.

Schneiders, T., Hoeren, A., Michalski, B., Pfost, H. and Sherer, V. 2001. Investigation of Unsteady Gas Mixing Processes in Gas Turbine Burners Applying a Tracer-LIF method, *Proceedings of the ASME Turbo Expo 2001*, June 4th-7th, New Orleans, USA, ref. 2001-GT-49.

Schreel, K.R.A.M. 2008. *Laser Velocimetry Techniques: LDV, PTV, PIV, Course of Advanced Combustion.* Netherlands, Technische Universiteit Eindhoven, pp. 287-314.

Schorr, M. and Chalfin, J. 1999. *Gas Turbine NO_x Emissions approaching Zero – is it worth the price?*. General Electric, USA, pp. 12.

Schuermans, B., Bellucci, V., Guethe, F., Meili, F., Flohr, P., Paschereit, CO. 2004. A detailed analysis of thermoacoustic interaction mechanisms in a turbulent premixed flame. *Proceeding of ASME Turbo Expo 2004*, Vienna, Austria, pp. 539-551.

Selle, L., Benoit, L., Poinsot, T., Nicoud, F., Krebs, W. 2006. Joint use of compressible large-eddy simulation and Helmholtz solvers for the analysis of rotating modes in an industrial swirled burner. *Combustion and Flame* 145 (1-2), pp. 194-205.

Serre, E. and Bontoux, P. 2002. Vortex breakdown in a three dimensional swirling flow. *Journal of Fluid Mechanics* 459, pp. 347-370.

Shames, I. 1992. *Mechanics of Fluids*, McGraw Hill, USA.

Shelly, S. 2006. The quest for lower emissions. *Turbomachinery International* 47 (3), pp. 10-13.

Shtork, S., Cala, C. and Fernandes, E. 2007. Experimental characterization of rotating flow field in a model vortex burner. *Experimental Thermal and Fluid Science* 31 (7), pp. 779-788.

Shtork, S., Viera, N. and Fernandes, E. 2008. On the Identification of helical instabilities in a reacting swirling flow. *Fuel* 87, pp. 2314-2321.

Smith, L., Karim H., Castaldi M. J., Etemad S., Pfefferle W. C. 2006. Rich Catalytic Lean Burn combustion for fuel flexible operation with ultra low emissions. *Catalysis Today* 117 (4), pp. 438-446.

Soo, S. L. and Zhou, L. 1990. Gas- Solid flow and collection of solids in a cyclone separator. *Powder Technology* 63 (1), pp. 45-53.

Stohr, M., Sadanandan, R. and Meier, W. 2008. Experimental Study of Unsteady Flame Structures of an Oscillating Swirl Flam in a Gas Turbine Model Combustor. *32nd International Symposium Combustion Institute*, 3rd-8th August, Toronto, Canada, 2008.

Syred, N. 2005. *Hot Wire Anemometry, Special Notes*. Cardiff University, Wales, UK, pp. 20.

Syred, N. 2006. A review of oscillation mechanisms and the role of the PVC in swirl combustion systems. *Progress in Energy and Combustion Science* 32 (2), p.p. 93-161.

Syred, N. and Dahmen, K. 1978. The Effect of High Levels of Confinement upon the Aerodynamics of Swirl Burners, *AIAA Journal of Energy* 2 (1), pp. 8-15.

Syred, N. Dahmen, K., Styles, A. and Najin, S. 1974. A review of combustion problems associated with low calorific value gases. *Journal of Institute of Fuel* 50, pp. 195-207.

Syred N., Gupta A. and Lilley D. 1984. *Swirl Flows*. Abacus Press, UK.

Thornton, J., Chorpening, B., Sidwell, T., Strakey, A., Huckaby, E. and Benson, K. 2007. Flashback detection sensor for Hydrogen augmented Natural Gas Combustion. *Proceedings of the ASME Turbo Expo 2007*, Montreal, Canada, ref. GT2007-27865, pp. 739-746.

Thumuluru, S. and Lieuwen, T. 2008. Characterization of Acoustically forced swirl flame dynamics. *32nd International Symposium Combustion Institute*, 3rd-8th August, Toronto, Canada, 2008.

Tran, N., Ducruix, S. and Schuller, T. Acoustic Control of the Inlet Boundary Conditions of a Turbulent Swirled Burner, *32nd International Symposium Combustion Institute*, 3rd-8th August, Toronto, Canada, 2008.

Tuthill, S., Bechtel, W., Benoit, J., Deleonardo, G., Meyer, S., Taura, J., Battaglioni, J. 2002. *Swozzle based burner tube premixer including inlet air conditioner for low emission combustion.* [Online]. Available at: http://www.freepatentsonline.com/6438961.html [Accessed: 20 November 2006].

Umemura, A. and Tomita, K. 2001. Rapid Flame Propagation in a Vortex Tube in Perspective of Vortex Breakdown Phenomenon. *Combustion and Flame* 125 (1-2), pp. 820-838

United Nations. 1998. *Kyoto Protocol to the United Nations Framework Convention on Climate Change*. [Online]. Available at: http://unfccc.int/resource/docs/convkp/kpeng.pdf [Accessed: 25 October 2005]

University of Cambridge. 2005. *Hot Wire Anemometers.* [Online]. Available at: http://www-g.eng.cam.ac.uk/whittle/current-research/hph/hot-wire/hot-wire.html [Accessed: 17 March 2008].

Van der Meer, H. 2008. *Application of Laser Diagnostics in Turbulent Flame Analysis, Course of Advanced Combustion*, Netherlands, Technische Universiteit Eindhoven, pp. 315-330.

Valera-Medina, A. 2006. *Precessing Vortex Core and its impacts on NO_x reduction.* MSc Dissertation, Cardiff University, Wales, UK.

Valera-Medina A., Abdulsada M., Shelil N., Syred N., Griffiths A. 2009. Flashback Analysis in Swirl Burners using Passive Nozzle Constrictions and Different Fuels, *16th International IFRF Member's Conference*, 8th-10th June, Boston, USA.

Vaniershot, M. 2007. *Fluid Mechanics and Control of Annular Jets with and without Swirl.* PhD Thesis, Faculty of Engineering, Katholieke Universiteit Leuven, Belgium.

Vaniershot, M., Persoons, T., Van den Bulck, E. 2008. An Eulerian Time Filtering Technique to Study Large Scale Transient Flow Phenomena. *Proceedings 14th Int. Simp. on Laser Techniques to Fluid Mechanics*, July, Lisbon, Portugal.
Vanoverberghe, K. 2004. *Flow, Turbulence and Combustion of Premixed Swirling Jet Flame.* PhD Thesis, Faculty of Engineering, Katholieke Universiteit Leuven, Belgium.

Venkataraman, K., Preston, L.H., Simons, D., Lee, B. and Santavica, D. 1999. Mechanism of Combustion Instability in a Lean Premixed Dump Combustor. *Journal of Propulsion and Power* 15 (6), pp. 909-918.

Walston, S., Cetel, A., MacKay, R., O'Hara, K., Duhl, D. and Dreshfield, R. 2004. *Joint Development of a fourth generation single crystal superalloy*, NASA Glenn Research Centre Technical Reports, NASA TM-2004-213062, p. 16.

Warhaft, Z. 2000. Passive Scalars in Turbulent Flows. *Annual Review Fluid Mech.* 32, pp. 203-240.

Wayu, Y., Nakagawa, N., Kobayashi, K., Kinoshita, Y. and Yokoi, S. 2005. Fabrication and characterization of MGC components for ultra high efficiency gas turbine. *Ceramic Engineering and Science Proceedings* 26 (2), pp. 197-204.

Wikipedia. 2006. *Stress Physics.* [Online]. Available at: http://en.wikipedia.org/wiki/Stress_(physics) [Accessed: 4 January 2007].

William, R. 2005. *Turbulent Length Scales in Isothermal Swirling Flows.* MPhil Dissertation, Cardiff University, Wales, UK.

World Energy Council. 2006a. *WEC Survey of Energy Sources 2004.* [Online]. Available at: http://www.worldenergy.org [Accessed: 13 December 2006].

World Energy Council. 2006b. *Integracion Energetica en Latinoamerica y el Caribe.* [Online]. Available at: http://www.worldenergy.org/wec-geis/global/downloads/lac/lacbiregional0606fb.pdf [Accessed: 13 December 2006].

Xu, B., El Hima, L., Wen, J., Dembele, S. and Tam, V. 2007. Spontaneous Ignition of Pressurized Hydrogen Release. *40th United Kingdom Explosion Liaison Group Meeting*, 19th-20th September, Cardiff, Wales, U.K.

Yazdabadi, P. 1996. *A study of the Precesssing Vortex Core in Cyclone dust separators and a method of Prevention.* PhD thesis, Cardiff University, Wales, UK.

Zhou, J. 2004. Influence of humidity on the swirl diffusion combustion characteristics in a humid air turbine (HAT) cycle combustor. *Journal of Engineering for Thermal Energy and Power* 19 (4), pp. 363-366.

Zimont, V., Polifke, W., Bettelini, M., and Weisenstein, W. 1998. An Efficient Computational Model for Premixed Turbulent Combustion at High Reynolds Numbers Based on a Turbulent Flame Speed Closure. *Journal of Gas Turbines Power* 120, pp. 526- 532.